



DEVELOPMENTS IN SEDIMENTOLOGY 59

# THE GREAT SAND SEA IN EGYPT

FORMATION, DYNAMICS AND  
ENVIRONMENTAL CHANGE –  
A SEDIMENT-ANALYTICAL APPROACH

H. BESLER



SERIES EDITOR: A.J. VAN LOON

*Developments in Sedimentology, 59*

# THE GREAT SAND SEA IN EGYPT

FORMATION, DYNAMICS AND ENVIRONMENTAL  
CHANGE – A SEDIMENT-ANALYTICAL APPROACH

---

**Cover photo:** Looking NNW from a sinuous longitudinal dune in the eastern Great Sand Sea towards Ammonite-Hill Escarpment rising in the background at the right. A Pleistocene megadune formed by strong trade winds with superimposed Holocene dunes runs along the western horizon at a distance of approximately 3 km. The parallel eastern megadune ends farther north and starts again below the dune in front because the escarpment caused a disturbance in the Pleistocene formation dynamics. The symmetrical shape of the lower part of the dune (both slope angles around 20°) indicates a bimodal modern wind regime causing oscillating crests. The last effective wind blew from the west. [Photo: 03.03.1996]

*Developments in Sedimentology, 59*

# THE GREAT SAND SEA IN EGYPT

FORMATION, DYNAMICS AND ENVIRONMENTAL  
CHANGE – A SEDIMENT-ANALYTICAL APPROACH

*by*

**Helga Besler**

Geographisches Institut, Universität Köln, Germany

*with contributions from*

A. Bolten, O. Bubenzer, A. Hilgers and A.J. Van Loon



Amsterdam • Boston • Heidelberg • London • New York • Oxford  
Paris • San Diego • San Francisco • Singapore • Sydney • Tokyo

Elsevier

Radarweg 29, PO Box 211, 1000 AE Amsterdam, The Netherlands  
Linacre House, Jordan Hill, Oxford OX2 8DP, UK

First edition 2008

Copyright © 2008 Elsevier B.V. All rights reserved

No part of this publication may be reproduced, stored in a retrieval system or transmitted in any form or by any means electronic, mechanical, photocopying, recording or otherwise without the prior written permission of the publisher

Permissions may be sought directly from Elsevier's Science & Technology Rights Department in Oxford, UK: phone (+44) (0) 1865 843830; fax (+44) (0) 1865 853333; email: [permissions@elsevier.com](mailto:permissions@elsevier.com). Alternatively you can submit your request online by visiting the Elsevier web site at <http://www.elsevier.com/locate/permissions>, and selecting *Obtaining permission to use Elsevier material*

Notice

No responsibility is assumed by the publisher for any injury and/or damage to persons or property as a matter of products liability, negligence or otherwise, or from any use or operation of any methods, products, instructions or ideas contained in the material herein. Because of rapid advances in the medical sciences, in particular, independent verification of diagnoses and drug dosages should be made

**British Library Cataloguing in Publication Data**

A catalogue record for this book is available from the British Library

**Library of Congress Cataloguing-in-Publication Data**

A catalogue record for this book is available from the Library of Congress

ISBN: 978-0-444-52941-1

For information on all Elsevier publications  
visit our website at [books.elsevier.com](http://books.elsevier.com)

Printed and bound in Hungary

08 09 10 11 12 10 9 8 7 6 5 4 3 2 1

Working together to grow  
libraries in developing countries

[www.elsevier.com](http://www.elsevier.com) | [www.bookaid.org](http://www.bookaid.org) | [www.sabre.org](http://www.sabre.org)

ELSEVIER

BOOK AID  
International

Sabre Foundation

# TABLE OF CONTENTS

<i>List of Figures</i>	ix
<i>List of Tables</i>	xi
<i>Preface</i>	xiii
<b>1 Introduction to the Great Sand Sea</b>	<b>1</b>
<b>2 Methods of Investigation</b>	<b>5</b>
2.1. The Main Objectives	5
2.2. Selection of Suitable Methods	6
2.3. Brief Description of the Procedures	8
2.3.1. Digital elevation models and watershed analysis on the basis of satellite and radar data (A. Bolten and O. Bubenzer)	8
2.3.1.1. Introduction	8
2.3.1.2. Digital elevation data	8
2.3.1.2.1. ASTER elevation data	10
2.3.1.2.2. Elevation data from the Shuttle Radar Topography Mission	12
2.3.1.2.3. Quality and accuracy of the digital elevation models used	14
2.3.1.3. Generating a uniform elevation database for the Western Desert of Egypt	17
2.3.2. The topographic surveys	19
2.3.3. Sedimentological analysis	24
2.3.3.1. Granulometry	24
2.3.3.2. Morphoscopic analysis	25
2.3.3.3. Heavy-mineral analysis	26
2.3.3.4. Scanning-electron microscopy	26
2.3.4. Salinity measurements	27
2.3.5. Luminescence dating of sand deposits (A. Hilgers and A.J. van Loon)	27
2.3.6. Meteorological observations	30
<b>3 Topography of the Great Sand Sea</b>	<b>33</b>
3.1. Geological Setting and Bedrock Topography	33
3.1.1. Geological formations and their spatial pattern	33
3.1.2. Bedrock landforms	34
3.1.3. Reconstruction of palaeo-drainage systems by digital elevation data (O. Bubenzer and A. Bolten)	39
3.1.3.1. Introduction	39
3.1.3.2. The potential bedrock relief and the hypothetical palaeo-drainage system	41
3.1.3.3. Conclusions	46

3.2.	The Pleistocene Draa	46
3.2.1.	The southern longitudinal draa of the trades	49
3.2.2.	The northern transverse draa of the westerlies	52
3.3.	The Holocene Dunes	58
3.3.1.	Dunes on the transverse draa	59
3.3.2.	Dunes on the longitudinal draa	60
3.3.3.	The southward progradation and the northern extension of dunes	67
3.3.4.	Comparison with modern winds	68
3.4.	The Sand Budget	71
<b>4</b>	<b>The Granulometric Analysis</b>	<b>73</b>
4.1.	Historical Developments	73
4.2.	Grain-Size Parameters	75
4.2.1.	Mean grain size ( $Mz$ )	76
4.2.2.	Sorting ( $So$ )	79
4.2.3.	Skewness ( $Sk$ )	80
4.2.4.	Kurtosis ( $K$ )	81
4.3.	The System of Granulometric Sand Types	82
4.3.1.	Granulometric sand types of the draa	85
4.3.2.	Granulometric sand types of the dunes	88
4.3.3.	Granulometric types of the sandstones	94
4.4.	The Response Diagram	95
<b>5</b>	<b>Luminescence Dating</b>	<b>99</b>
5.1.	The Sampling Sites	99
5.2.	Laboratory Procedures and Results (A. Hilgers)	105
5.2.1.	Equivalent-dose determination	106
5.2.1.1.	Sampling, sample preparation and measurement facilities	106
5.2.1.2.	Measurement procedures for $D_e$ estimation	106
5.2.1.3.	$D_e$ determination for the Great Sand Sea samples	110
5.2.2.	Dose-rate determination	112
5.2.2.1.	Uncertainty about the state of equilibrium of the radioactive-decay chains	114
5.2.2.2.	Impact of varying overburden thickness on the cosmic-dose contribution	115
5.2.2.3.	Influence of uncertainty in water-content variations	115
5.3.	Interpretation of Dating Results	118
5.3.1.	OSL ages of the draa	118
5.3.2.	Growth rates of the draa	119
5.3.3.	Younger aeolian reworking of draa	121
5.4.	Comparative Discussion of Regional Datings: Time Slices in the Great Sand Sea	123

<b>6</b>	<b>Quartz Sand as an Indicator of Humid Periods</b>	<b>129</b>
6.1.	The Salinity of Sands	129
6.1.1.	Water in dunes	129
6.1.2.	Interpretation and discussion of the salinity	130
6.2.	The Rubification of Sands	135
6.2.1.	Introductory discussion of red dune sands	135
6.2.2.	Reddened sands in the Great Sand Sea	138
6.2.2.1.	The western transection	139
6.2.2.2.	The middle transection	139
6.2.2.3.	The eastern transection	141
6.2.2.4.	Colour observations during the topographic surveys	143
<b>7</b>	<b>Heavy-Mineral Analysis</b>	<b>145</b>
7.1.	The Total Heavy-Mineral Content	145
7.2.	The Heavy-Mineral Assemblages	148
<b>8</b>	<b>Scanning Electron Microscopy</b>	<b>153</b>
8.1.	Brief History of the Development	153
8.2.	How to Prevent a Biased Interpretation	154
8.3.	General Properties of the Quartz Grains	155
8.4.	Correlations with Dating	156
8.5.	The Most Frequent Microstructures: Controversial Phenomena	160
8.6.	Discussion of the Environmental Developments	164
8.6.1.	Processes in the Holocene	164
8.6.1.1.	The more common features	164
8.6.1.2.	The environments at the dating sites	170
8.6.1.2.1.	The eastern sites	170
8.6.1.2.2.	The sites in the middle	172
8.6.1.2.3.	The western sites	174
8.6.1.3.	The spatial pattern	175
8.6.2.	Pre-Holocene processes in the Great Sand Sea	176
8.6.3.	Major sand sources	181
8.6.3.1.	Environments outside the Great Sand Sea	181
8.6.3.2.	Major differences	186
8.6.3.3.	The southwestern sand source	186
8.6.3.4.	The eastern sand source	189
8.6.3.5.	The western sand source	190
8.6.3.6.	Sand sources for the southern middle sand sea	192
8.7.	The Question of Earlier Cycles of Draa/Dune Formation	193
<b>9</b>	<b>The History of the Great Sand Sea Compared to that of Other Active Ergs</b>	<b>195</b>
9.1.	Sand Sources and Their Influence	195
9.2.	Draa Patterns and Draa Formation	197
9.3.	Time Slices of Draa Formation and Reworking	202
9.4.	Conditions During the Holocene Climatic Optimum	206
9.5.	The Final Aridization	208



<i>Appendix 1: List of Samples and Their Investigated Parameters</i>	211
<i>Appendix 2: Procedure of SEM Feature Analysis and Environmental Composition Exemplified for Sample No. 35/96</i>	219
<i>References</i>	225
<i>Index</i>	243

## LIST OF FIGURES

1. The Great Sand Sea in Egypt – an overview.	2
2. Routes of investigation in the Great Sand Sea.	7
3. ASTER spectral bands compared to Landsat ETM+.	10
4. Comparison using drainage-system mapping.	14
5. Derivation of flow direction and flow accumulation.	17
6. Situation of SRTM-3 and ASTER models for the Western Desert.	19
7. Cross-section sequence along eastern transection.	21
8. Cross-section sequence along middle transection.	22
9. Cross-section sequence along western transection.	23
10. Basic principles of luminescence dating.	29
11. Methods of luminescence measurements.	30
12. Typical lee (shadow) dune behind a sandstone hill.	36
13. Playa surface with desiccation cracks below blown sands.	36
14. Test dig at Willmann's Camp.	38
15. Prehistoric working site in the Desert Glass Area.	39
16. Gilf Kebir and Abu Ras Plateaus.	40
17. New elevation data set of potential bedrock relief.	42
18. Map of the potential drainage system.	43
19. Latitudinal profiles along 25°N, 26°N and 27°N.	45
20. Longitudinal profiles along 26°E and 27°E.	45
21. Typical secondary flow in the Planetary Boundary Layer.	47
22. Dunes below the Ammonite Hill Escarpment.	52
23. Wavelength change between longitudinal and transverse draa.	53
24. Silk dune on transverse draa.	59
25. Silk dune on longitudinal draa.	61
26. Silk dune with cock's-comb crest on longitudinal draa.	62
27. Silk dune and transverse dunes on draa at Willmann's Camp.	64
28. Silk dunes crossing draa diagonally.	66
29. Barchan dune at southern end of eastern transection.	67
30. Aerodynamic stream-flow charts above western Egypt.	70
31. Granulometric sequences of aeolian sand evolution.	83
32. Characteristic frequency distributions of granulometric sand types.	83
33. Comparison of frequency distributions in 2000 and 2006.	88
34. Grain-size frequency distribution of eastern dune sands.	89
35. Grain-size distributions of western dune sands (south).	90
36. Grain-size distributions of western dune sands (north).	91
37. Grain-size distributions of dune sands in the middle (on transverse draa).	92
38. Grain-size distributions of dune sands in the middle (on longitudinal draa).	93
39. Grain-size frequency distributions of sandstones.	94
40. The response diagram.	96
41. Drilling sites for dating in the Great Sand Sea.	100

---

42. Drilling at Regenfeld.	102
43. Detail of drilling profile at Regenfeld.	102
44. Methods of luminescence measurements.	109
45. Impact of varying overburden thickness.	116
46. Impact of the water-content variation.	117
47. Proposed history of longitudinal draa.	122
48. Probability density curves of OSL data.	128
49. Saline horizons in the drilling profiles.	132
50. Colours of sands.	137
51. Stratigraphic profile at Regenfeld.	142
52. Knobby quartz grain.	161
53. Quartz grain with smoothing.	162
54. Quartz grain with early chemical weathering.	168
55. Untreated quartz grains with coatings.	169
56. Detail of Fig. 55 with X-ray spectrum.	169
57. Detail of quartz grain with silica spalling.	171
58. Detail with NaCl crystal and X-ray spectrum.	172
59. Detail of quartz grain with silica scaling.	173
60. Detail with calcite and X-ray spectrum.	174
61. Detail of quartz grain with feldspar moulds.	182
62. Detail of quartz grain with healing of moulds.	183
63. Details of quartz grain with healing structures.	183
64. Quartz grain with different conchoidal fractures.	184
65. Quartz grain with Fe–Cr–Ni flakes and X-ray spectrum.	185
66. Tentative reconstruction of alluvial fans.	188

# LIST OF TABLES

1. Specifications of ASTER and SRTM-3 models	11
2. Additional information on the catchments presented in Fig. 18	44
3. Sand budget of draa	72
4. Comparative grain-size parameters	77
5. Granulometric types in draa sands	87
6. Spatial distribution of OSL data	101
7. Luminescence-dating results	107
8. Net-accumulation rates in the draa	119
9. Comparative total heavy-mineral contents	146
10. Heavy-mineral assemblages	149
11. Mean heavy-mineral assemblages at drilling sites	151
12. Summarized environmental developments: eastern transection	157
13. Summarized environmental developments: middle transection	158
14. Summarized environmental developments: western transection	159
15. Holocene developments along the eastern transection	165
16. Holocene developments along the middle transection	166
17. Holocene developments along the western transection	167
18. Pre-Holocene developments along eastern transection	177
19. Pre-Holocene developments along middle transection	178
20. Pre-Holocene developments along western transection	179
21. Time slices of draa formation and reworking in active ergs	203

This page intentionally left blank

## PREFACE

In 1995, the Collaborative Research Centre 389 ACACIA (Arid Climate, Adaptation, and Cultural Innovation in Africa; subtitle: Developmental Processes under Ecologically Limiting Conditions) – initiated by the archaeologist Rudolph Kuper – was established at the University of Cologne. A main objective was the comparison between northeastern Africa (mainly Egypt and Sudan) and southwestern Africa (mainly Namibia) with regard to the title. Together with R. Kuper, I was leading the sub-project A1 “Regional Climate Development and Human Settlement between the Nile Valley and the Central Sahara”. Apart from investigations in Sudan and Namibia, many archaeological sites in Egypt (e.g. palaeo-pans) were studied by our team, which consisted of archaeologists, botanists and geoscientists and always included a specialized vehicle mechanic.

The idea of studying the Great Sand Sea entered our mind since this very uniform landscape, with a large meridional extent and with – today – very homogeneous climatic conditions, could offer the chance to find the northern boundary of the palaeo-monsoonal influence. Outside of the sand sea, the very differentiated topography and the occurrence of artesian groundwater provided so many niches favourable for human occupation that a possible north–south gradient in the palaeo-environment was blurred.

Three south–north transections through the Great Sand Sea were accomplished in 1996, 1999 and 2000, and a diagonal crossing in 2006 (see Fig. 2). Numerous difficulties were encountered during these expeditions, including long detours due to impassable dunes, heavy sandstorms, break-down of vehicles, shortage of petrol and/or water, not to mention the freezing cold nights during February and March. The “base camp” for these and for comparative investigations (e.g. of the Farafra Sand Sea: Bubbenzer and Besler, 2005) was a traditional Egyptian homestead at Balat in the Dakhla Oasis, that had been built as a dependency of the Heinrich-Barth-Institut, established at the University of Cologne in 1989.

Since in most sand seas there is little more than sand to use for the reconstruction of the developmental history, they are an ideal subject of sedimentological analysis. Therefore – apart from field observations – this book mainly focuses on the importance and the scope of the sedimentary analysis. It is also one of the objectives to highlight the role of sand as an archive of environmental change. Traditional methods were developed further and adapted to the various objectives. It is surprising how much of the history can be deduced from the analysis of sands. It has to be taken into account, however, that many results from the application of different methods do not individually provide evidence in a strict sense but only support each other, thus presenting evidence by a cumulation of facts. Among the methods applied, scanning electron microscopy (SEM) is most labour- and time-consuming and involves a great amount of effort. Therefore – apart from several atlases – relatively few applications exist in literature, particularly with regard to the developmental synthesis of different environments. The interpretation of several

microfeatures of quartz grains is still debated and far from being well understood and established. Although a wealth of information may be drawn from the SEM analysis, Chapter 8 at the research frontier still includes uncertainties.

In the account of the development of methods and concepts, the importance of older literature is stressed for various reasons. First, the numerous books and articles about Saharan regions by French (and also German) authors have often been neglected in later English literature. Second, it is important – and sometimes surprising – to learn how many facts that had already been known a long time ago have not been considered in later contexts (e.g. the essential differences between megadunes and dunes, or the changing granulometry of barchans). A third reason lies in the fact that it becomes more and more a custom to quote only the latest literature, without regarding the primary text; this favours the propagation of errors once established (see, for instance, Section 4.3.1). This does not mean that the text in this book is free of errors and misunderstandings. It is hoped, however, that they will not be passed on.

During the last years, considerable progress in our research subjects was particularly achieved within two fields: dating of sediments, and the use of satellite data for reconstructing palaeo-environments. The new luminescence-dating techniques use quartz grains that are abundantly present in sand seas. In order to get reliable results, however, the sampling sites have to be chosen carefully and systematically after the morphogenetic history of the area has been understood (Munyikwa, 2005). The advancement of techniques in remote sensing and the availability of digital elevation data with increasing spatial resolution allow the modelling of palaeo-surfaces and palaeo-drainage systems. Both fields have contributed considerably to this book. For a better understanding, these recently developed methods – particularly the use of digital elevation data – are more extensively described and explained in the methods chapter (Chapter 2), compared to the brief descriptions of the well-established methods.

Of all Saharan ergs, the Great Sand Sea in Egypt is most probably best understood, although more luminescence data are needed to support the formation history and to gain a higher resolution. All methods applied here are suitable and promising for the investigation of other ergs, which is recommended since our knowledge on sand seas is still rather limited. With the new dating possibilities, however, they become increasingly important as a source of terrestrial proxy data that help to understand the changing climatic conditions of the past. The records from polar glaciers and marine sediments alone are not sufficient to reconstruct the terrestrial history: the data from sand seas are urgently needed and asked for by scientists modelling prognostic climatic scenarios of the future on the basis of palaeo-environmental developments.

The final chapter attempts to compare the history of the Great Sand Sea to that of other active ergs. I did, however, not use the scarce data that are known for a global comparison with the more abundant data from outside the sand seas, since diverse environments need a different approach.

It is self-evident from the above that this book represents just one of the manyfold results of the ACACIA project, and that many institutions and persons have assisted in the course of ACACIA's 12 years of existence (terminated in 2007).

ACACIA was funded by the Deutsche Forschungsgemeinschaft (DFG) and supported by the University of Cologne. We like to thank all members of ACACIA for their discussions, and particularly all colleagues working with us in the field for their good cooperation. Personally, I'm particularly grateful to Rudolph Kuper and to Olaf Bubenzer (who followed me in leadership) and, in addition, to the archaeologists Karin Kindermann and Heiko Riemer who always joined our field work. Special thanks are due to Wolfgang Mackowiak, who not only accompanied several investigations as a skilled mechanic but also mastered the SEM at the Department of Geology and Palaeontology.

Numerous students have accompanied parts of our investigations, helping in the field as well as in the laboratory or with the sand database, and achieving important additional results in their diploma/master theses. Special thanks go to the persons who produced the electronic form of the text, graphs, tables and photos. As I myself – due to an interior eye failure – cannot read a computer screen, the senior students Andreas Arnolds and David Spiesser carried a heavy load. Andreas Bolten provided the maps and satellite images. Lothar Pfeiffer accomplished the heavy-mineral analysis. At last, I thank Tom van Loon for his great support and critical comments, which were appreciated very much.



This page intentionally left blank

## INTRODUCTION TO THE GREAT SAND SEA

With an area of more than 100 000 km<sup>2</sup>, the Great Sand Sea holds the seventh rank among the sand seas of Africa (Embabi, 2000, 2004). It is situated in westernmost Egypt (Fig. 1), where its northwestern edge extends across the border into Libya. This Libyan part could not be investigated. The sand sea does not lie in a distinct depression, but covers weakly sculptured ground sloping from more than 500 m a.s.l. in the south to less than 100 m a.s.l. near the Siwa Depression (−16 m) in the north. The Qattara Depression northeast of Siwa even descends to 133 m below sea level. Consistent with the northward gradient, the surrounding escarpments and plateaus, that are strongly dissected in the east, rise towards the south. The highest part, above 1000 m a.s.l., is reached in the more massive Gilf Kebir Plateau south of the Great Sand Sea. There is no mountainous border in the west, where the low terrain, including gravel plains, extends into Libya.

The climate in this part of the Sahara is hyper-arid with a precipitation of <5 mm/year. Meteorological stations, however, are either far away or located in depressions (e.g. Siwa) and therefore do not provide reliable records of the climatic conditions in the sand sea. This is particularly problematic with regard to the wind field, because in a sand sea the wind is the most important agent for landform development and morphodynamics.

The descriptive term “sand sea” is often used because the (mega)dunes resemble the waves of an ocean. The Great Sand Sea acquired its name from Rohlfs, who mentioned a “great sand sea to the west of Dakhla and Farafra” (Ball, 1927). On the other hand, the term sand sea is also used for large sandy plains without dunes, e.g. the Selima Sand Sea in southern Egypt (a.o. Stokes et al., 1998).

A more geoscientific term for sand sea is “erg”, which is used in this book as well. According to the glossary by Capot-Rey et al. (1963), the Arabic term “erg” means massive dunefields independent of their dimensions. Therefore, it is applied to large megadune areas like the Erg Chech in Algeria as well as to small younger dunefields like the Erg Zmilet (only about 10 km<sup>2</sup>) in southern Tunisia (Besler, 1977b). According to Wilson (1973), “an erg is an area where windlaid deposits cover at least 20% of the ground and which is large enough to contain draas” (= megadunes; the term draa is extensively discussed in Chapter 3). In accordance with this definition, the Great Sand Sea is a true erg, because (mega)dunes cover 74.6% of its area (Embabi, 2000, 2004).

A first crossing of the northernmost Great Sand Sea was already accomplished by the German medical doctor and explorer Rohlfs in 1869. Starting from the Jalu Oasis in Libya, he hoped to reach the oases of Al Khufrah in the south, but was

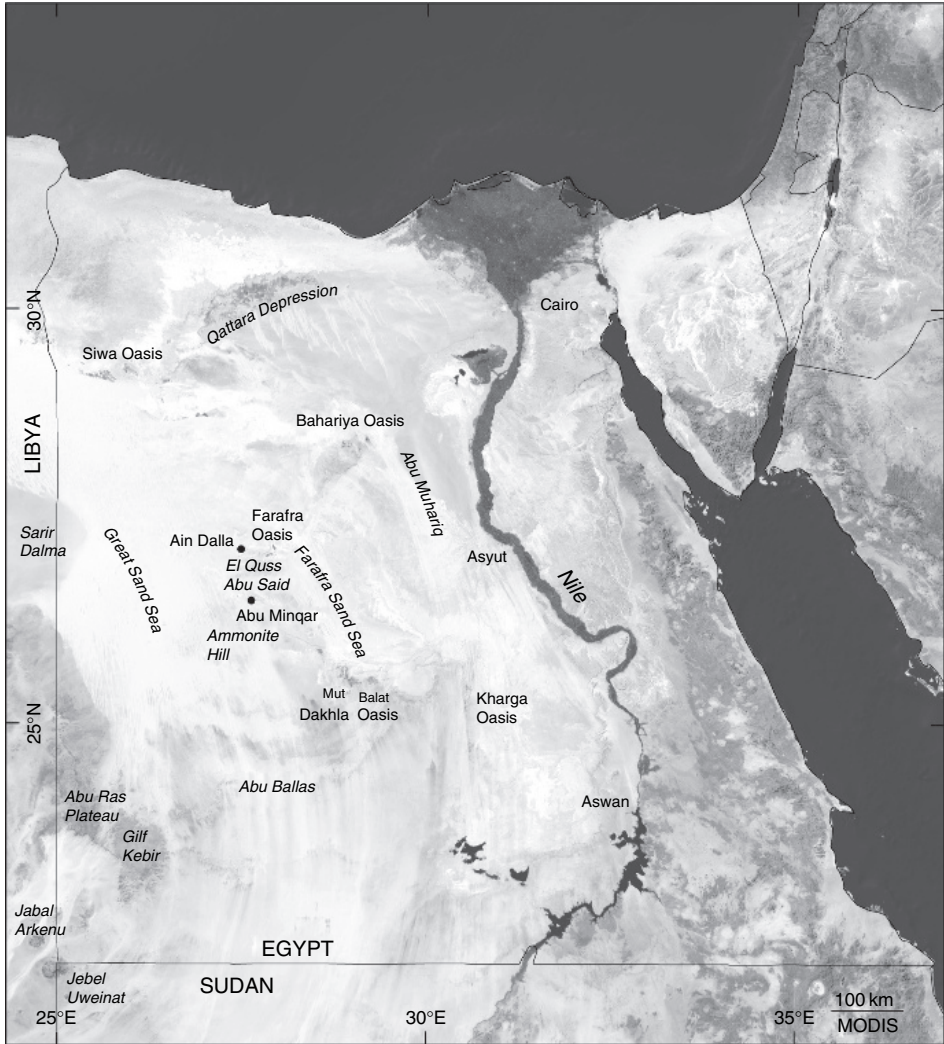


**Fig. 1** The Great Sand Sea in Egypt – an overview.

forced to Siwa in the east (Rohlf's, 1871). He then attempted to explore the “desert of all deserts”. Once more, however, his attempt to reach Al Khufrah failed, due to the impassable (mega)dune chains (Rohlf's, 1875). Instead, in the course of this expedition, he crossed the eastern Great Sand Sea from Dakhla to Siwa in 1874.

Early geographically important works about the sand sea exist from the English explorers Beadnell (1910) and Ball (1927), and especially from Bagnold (1931, 1935), but also from the Hungarian Kádár (1934), who was a member of the Almásy expedition in 1933. German studies in the Great Sand Sea were resumed within the long-term BOS Project (Besiedlungsgeschichte der Ost-Sahara = Settlement History of the Eastern Sahara) of the Universities of Cologne and Berlin (mainly

prehistoric studies: a.o. Kuper, 1989, 1995) and within the Collaborative Research Centre 69 (Geoscientific Problems in Arid and Semiarid Areas) of the two Universities of Berlin (a.o. Pachur et al., 1980, 1984, 1987; Pachur, 1999).

Despite its uniformity on satellite images, showing long sand ridges running approximately north–south, the Great Sand Sea turned out to consist of two large areas with different types of megadunes of different ages and of diverse formation dynamics. They cannot be distinguished on satellite images but only by field survey. Therefore, they were not known before, although early explorers mentioned some peculiarities in this direction that they did not understand (Bagnold, 1931; Uhden, 1932). This means that the area of the Great Sand Sea experienced different climatic conditions during the Late Pleistocene. The same holds true for the Holocene climatic optimum, during which a differentiated environment was provided for human occupation.

This page intentionally left blank

## METHODS OF INVESTIGATION

### Contents

2.1. The Main Objectives	5
2.2. Selection of Suitable Methods	6
2.3. Brief Description of the Procedures	8
2.3.1. Digital elevation models and watershed analysis on the basis of satellite and radar data (A. Bolten and O. Bubenzer)	8
2.3.2. The topographic surveys	19
2.3.3. Sedimentological analysis	24
2.3.4. Salinity measurements	27
2.3.5. Luminescence dating of sand deposits (A. Hilgers and A.J. van Loon)	27
2.3.6. Meteorological observations	30

This chapter briefly discusses the main objectives and the questions arising in connection with the exploration of the Great Sand Sea and its developmental history. All methods and techniques used here may be applied to any other sand sea and are promising with regard to the results. A wealth of information may be drawn from the sedimentary analysis which is particularly emphasized.

### 2.1. THE MAIN OBJECTIVES

Overall objectives are the documentation and – as far as possible – the explanation of all features found in the Great Sand Sea. These objectives comprise a catalogue of important questions – with numerous minor questions in their wake – that are briefly presented.

1. The distinction between dunes and megadunes is the most important prerequisite to understand the history of the Great Sand Sea. How can this distinction be achieved?
2. What are the formation processes of megadunes and dunes?
3. How old are megadunes and dunes, and how fast have they grown?
4. This necessarily involves the questions of sand transport, accumulation, deflation and re-activation, in summary: What are the sand dynamics behind the history?
5. Which are – and which have been – the effective winds during the formation of megadunes and modern dunes?
6. Where are the possible sand sources, and to which extent did they supply sands?

7. As the megadunes certainly are ancient features, have they experienced climatic changes and humid conditions after their formation?
8. Because of the size of the Great Sand Sea (114 400 km<sup>2</sup>), and particularly because of its large meridional extent (almost 600 km), a question has to be raised: Is there a spatial differentiation within the Great Sand Sea with regard to the aspects mentioned?



## 2.2. SELECTION OF SUITABLE METHODS

The numbers refer to the questions in Section 2.1.

1. On satellite images the distinction between dunes and megadunes is not possible because dunes are not visible, and aerial photographs of the Great Sand Sea are not available. Therefore, field observations and particularly cross-section measurements of megadunes during the topographic survey are a first approach (see Fig. 2). Valuable information is drawn from the grain-size frequency distributions (see granulometry) and salinity measurements.
2. In order to explain the formation of megadunes, their pattern on satellite images together with the ground check during the topographic survey, and once more the cross-section measurements, are most decisive. With regard to the question of dune formation and dynamics, the granulometry of dunes and megadunes, in combination with field observations, plays a major part.
3. The question of megadune ages and growth rates is answered by luminescence dating. Supplementary information is drawn from their granulometry and from scanning electron microscopy (SEM) of the quartz grains. The ages of dunes are inferred from luminescence dating combined with radiocarbon data existing already in the area.
4. With regard to the processes of sand transport, accumulation, deflation and reactivation, the grain-size parameters and the grain-size frequency distributions (see granulometry) provide important evidence. In addition, the processes in dunes, particularly the answer to the question of migration or stationary oscillation, can be inferred from the total heavy-mineral content.
5. The effective winds during the time of megadune formation are deduced from the combination of cross-section measurements (see topographic survey) and luminescence datings. In the absence of weather stations near the Great Sand Sea, the granulometry of dune sands can be used for the reconstruction of the modern wind field, particularly with regard to sand-transporting winds.
6. The sand sources are inferred from the combination of satellite-image interpretation with field observations (see topographic survey) and various analytical methods. The granulometry of megadunes and sandstones, the total heavy-mineral content and the heavy-mineral assemblages, as well as SEM are most important.
7. The climatic change is mainly reconstructed with the aid of the SEM. In addition, the heavy-mineral analysis and salinity measurements are indicative. Contributions also come from the cross-section measurements (see topographic survey) in combination with luminescence datings.

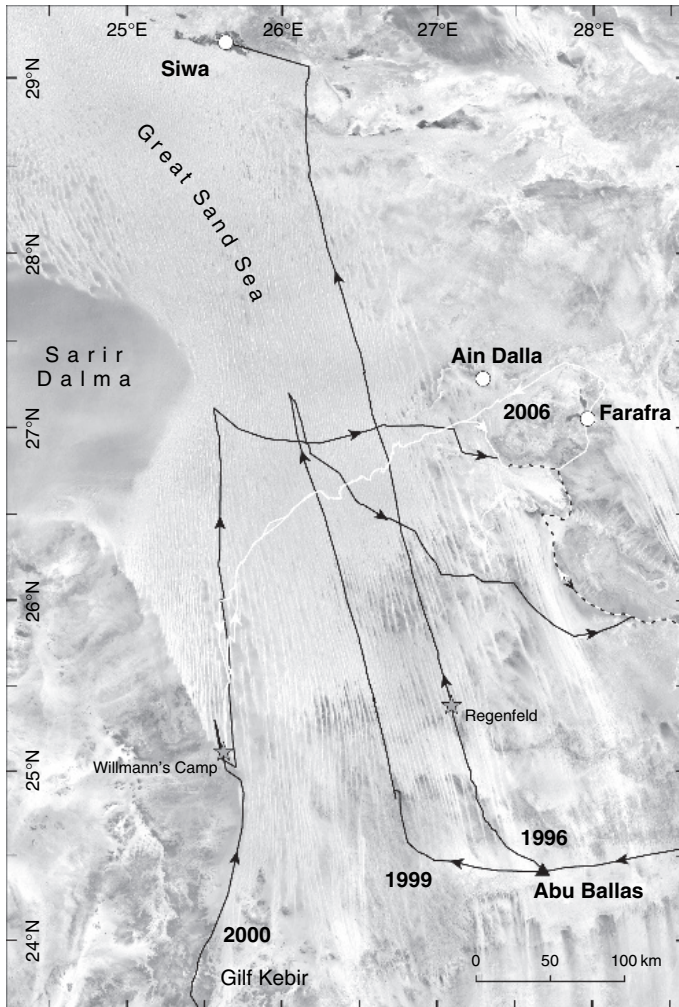


**Fig. 2** Routes of investigation in the Great Sand Sea. Stars indicate important archaeological sites.

To answer the respective questions, only the most important methods are mentioned in each paragraph. In fact, all methods applied deliver supplementary, complementary or supporting information to almost all questions. On the other hand, it should be mentioned that – apart from luminescence dating – none of the methods listed is – in a strict sense – adequate to answer any of the raised questions without supporting evidence from other methods. All isolated results have only an indicative value. The evidence of certain facts is finally deduced from various indications pointing into the same direction. This way of gathering “cumulative evidence” from different methods, in fact, represents a new method, i.e. a holistic approach (in the medical sense). Many cross-checks and cross-references are necessary, and the interpretation gets the touch of a detective’s work, putting together a puzzle.



It has to be pointed out that, unfortunately, the methods cannot include a stratigraphic analysis. Excavations in loose unconsolidated sands of megadunes are not possible without using a great quantity of water, which was not available. Even when heavy machinery (a bulldozer) and water sprinklers are provided, which was the case on the Toshka-Canal dune near Lake Nasser in southern Egypt (Besler, 1986), the cut dries so fast that the walls start to collapse immediately.



## 2.3. BRIEF DESCRIPTION OF THE PROCEDURES

### 2.3.1. Digital elevation models and watershed analysis on the basis of satellite and radar data<sup>\*,†</sup>

#### 2.3.1.1. Introduction

The Great Sand Sea of Egypt represents a large and remote area without any existing detailed topographical maps. Therefore, additional to the indispensable ground check and field measurements, elevation models are required to get area-wide relief data as a base for further investigations. It becomes increasingly obvious that remote sensing offers excellent opportunities to obtain such data. This is particularly true for arid regions, as they are often cloudless and void of vegetation in most parts and during most times of the year. Digital elevation data are applicable for various purposes. For example, it is possible to evaluate and quantify aeolian and/or fluvial processes such as accumulation and erosion on the basis of digital elevation data (Dikau, 1989; Wilson and Gallant, 2000; Bubenzer and Bolten, in press). In addition, elevation data are essential as a base for landscape modelling, e.g. for the calculation of watersheds and possible or potential drainage lines (Wilson and Gallant, 2000).

Most ergs of the world are situated in large topographic basins that received huge amounts of sediment, supplied by water currents, during wet periods (a.o. El-Baz, 1998). Therefore, the reconstruction of the palaeo-drainage system is also interesting in particular for sedimentological questions.

This section explores the cost-free digital elevation models derived by optical and radar satellite data that have been used. Against the background of reconstructing the bedrock relief and the palaeo-drainage system of the Great Sand Sea prior to the accumulation of dunes and dunes, the objective here is to describe the quality and accuracy of the data that are available for the Great Sand Sea, and to illuminate the techniques that were used. The results will be presented in Section 3.1.3.

#### 2.3.1.2. Digital elevation data

Digital elevation data are topographic data of the earth's surface with  $X$ ,  $Y$  and  $Z$  coordinates.  $X$  and  $Y$  represent the planar position and  $Z$  the elevation interpolated within the pixel area (a.o. Wilson and Gallant, 2000). In general, the quality of

\* A. Bolten, E-Mail: andreas.bolten@uni-koeln.de

† O. Bubenzer, E-Mail: olaf.bubenzer@geog.uni-heidelberg.de

terrain models depends on the amount of elevation data in a predefined area, i.e. the resolution, and on the accuracy of the  $X$ ,  $Y$  and  $Z$  data. In this context, accuracy means the error value of the elevation compared to reality, not to be mistaken for the precision of a data set. The quality also shows the usability of the data set for investigations in arid regions.

At the beginning of the twenty-first century, freely available high-resolution information about the earth's topography – especially in arid regions – was rare. Information about the heights of specific points in the Western Desert of Egypt came exclusively from the military working sheets of the 1940s (Survey of Egypt, 1941–1945), from the Geological Map of Egypt (List et al., 1990) and from conventional field data. These elevation data were derived from a few barometric information, and the maps give only an impression of the position and dimension of the sand accumulations. Later, elevation data from Global-Positioning Systems (GPS) became available; these were calculated from a combination of the runtime of the GPS-satellite signal and a compensation of a barometric altimeter in the GPS handheld. On a closer inspection, however, all these spatially limited data are only useful for local measurements or for comparison of several local recordings. They are imprecise for modelling larger regions because the area-wide amount of data is too small and often inhomogeneous. This holds also true for more recent field measurements with differential GPS (DGPS) units that have an accuracy of less than 1 m but demand a lot of time for the surveying of, for example, a few cross-sections of just one draa. Therefore, a homogeneous investigation of larger areas such as the Great Sand Sea is not possible up to now with this topographic information.

In particular, the determination of watersheds can only be achieved by using homogeneous relief data with a favourable relation between pixel size and investigation area. The use of digital elevation models taken from satellite data provides this coherent data set for modelling at both small and large scales. Against this background, efforts were made during the last years to get area-wide relief data having a higher resolution and coherence than older worldwide elevation models, e.g. the Global Topographic Data Model (GTOPO 30, a.o. Gesch and Larson, 1996), which has only a low resolution of 30 arc seconds ( $\sim 1000$  m). Unfortunately, the GTOPO 30 model has been calculated from eight different sources with different resolutions and accuracies. For example, the height error (or  $Z$ -error) is about  $\pm 30$  m in areas where the “Digital Terrain Elevation Data Level-1 (DTED)” of the US military was used, but up to  $\pm 160$  m where only the “Digital Chart of the World (DCW)” was available (Gesch and Larson, 1996). Therefore, this hybrid model is applicable only at a rough scale (Bubenzer and Wagner, 2002) of about 1:500 000 or smaller.

After some regional experiences with spatially limited strips of shuttle-imaging radar data (SIR) in the 1980s (a.o. McCauley et al., 1982), the new and freely available digital elevation data derived from the Advanced Spaceborne Thermal Emission and Reflection Radiometer (ASTER) sensor (see Section 2.3.1.2.1) and the Shuttle Radar Topography Mission (SRTM) mission (see Section 2.3.1.2.2), for the first time, allow the use of area-wide high-resolution elevation models, since about 5 years.

In the following, these two different free sources of elevation data are presented and evaluated, and the technique to derive drainage lines and watersheds from these data is introduced.

### 2.3.1.2.1. ASTER elevation data

The ASTER is a high-spatial-resolution, multispectral global imager on the NASA spacecraft TERRA. TERRA was launched in December 1999 and provides several passive sensors that are able to receive both the reflected sun energy, as for visible wavelengths, and the absorbed and re-emitted sun energy, as for thermal infrared wavelengths (a.o. Lillesand et al., 2004). Therefore, the sensor can only be used to detect energy when the naturally occurring sun energy is available. Reflected sun energy is only measurable during the day. Energy that is naturally emitted, e.g. thermal infrared, is detectable by day and at night, provided that the amount of energy is large enough to be recorded. Other prominent imagers with variable operations are present on the TERRA platform. A well-known instrument is Moderate-resolution Imaging Spectroradiometer (MODIS), which provides naturally coloured medium-scaled (up to 250 m pixel size) images with a high repeat rate. Most online “earth viewers” use MODIS images for an overview. The real purpose, however, is the monitoring of large-scale changes in the biosphere, which will yield new insights into the processes of the global carbon cycle. Besides the ASTER sensor, the other instruments (CERES, MISR and MOPITT) are designated as a means to investigate changes in the earth’s atmosphere, including the occurrence and composition of clouds.

The spectral and geometric capabilities of the ASTER sensor include 15 bands in different wavelengths (Fig. 3), three bands in the visible and near infrared (VNIR) region with a 15-m resolution, six bands in the short-wave infrared (SWIR) region with a 30-m resolution, five bands in the thermal infrared (TIR) region with a 90-m resolution and an along-track stereo-band with a 15-m resolution looking backward

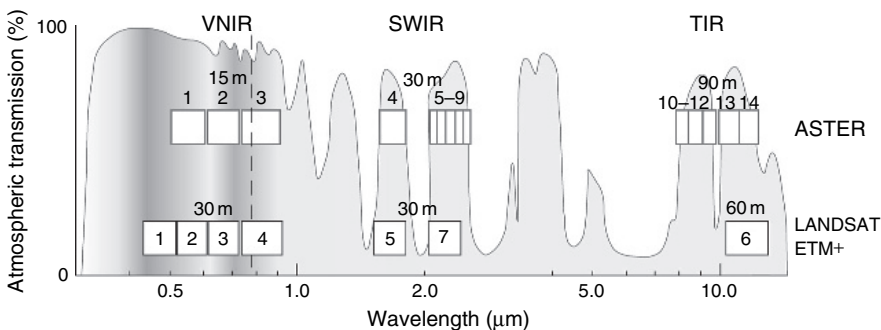


**Fig. 3** ASTER spectral bands compared to Landsat ETM + (modified after Käab et al., 2002). The rectangular boxes (top: ASTER, bottom: Landsat ETM +) indicate the multispectral sensor channels. The background curve represents the atmospheric transmission dependent on the wavelength. The vertical dashed line marks the approximate margin of visible light. Abbreviations for the sections of the light spectrum: VNIR = visible and near infrared; SWIR = short-wave infrared; TIR = thermal infrared.

with the same wavelength as band 3 (nadir) (Yamaguchi et al., 1998) (Table 1(a)). This means that the satellite camera takes a nadir image of  $60 \times 60$  km dimension, and only a few seconds later, while the satellite moves on, a second camera records the same region, but at a discrete angle (Abrams, 2000). For generating elevation models, the raw data including the mentioned two stereo bands (3b and 3n) are available free of charge for research institutes at the Earth Observation Data Gateway (EOS DG 2007).

**Table 1** (a) Specifications of ASTER and SRTM-3 models

	ASTER-DEM	SRTM-3
Resolution	30 m	3 arc seconds $\sim$ 90 m
Error	Corresponds to the quality of the two used visual data bands (clouds, pixel gap)	Pixel but also large connected regions with voids, especially in sand-covered regions (sand thickness, due to radar sensor).
Availability	Global coverage planned	$60^{\circ}\text{N}$ – $56^{\circ}\text{S}$
Scene size	$60 \times 60$ km	$1^{\circ} \times 1^{\circ}$
File type	GeoTIFF	HGT
Source	<a href="http://edcimswww.cr.usgs.gov/pub/imswelcome/">http://edcimswww.cr.usgs.gov/pub/imswelcome/</a>	<a href="ftp://e0dps01u.ecs.nasa.gov/srtm/">ftp://e0dps01u.ecs.nasa.gov/srtm/</a>

(b) Evaluation of the height accuracy (Z-error) of the ASTER and SRTM-3 models

	Description	Source
ASTER (Z-error)		
$\pm 11.6$ m	Comparison to USGS 7.5' DEM and SPOT DEM	Toutin and Cheng (2002)
$\pm 60$ m (high mountain terrain) $\pm 18$ m (smooth terrain)	Comparison to a photogrammetrically generated DEM	Kääb et al. (2002)
$\pm 7$ – $15$ m	Comparison to DGPS and USGS 7.5' DEMs	Hirano et al. (2003)
$\pm 13$ m (RMSE)	DGPS	Cuartero et al. (2005)
$\pm 5.9$ m	Comparison to DGM 50 (Surveying and Mapping Agency of North-Rhine Westphalia, Germany)	Bolten and Bubenzer (2006)
SRTM-3 (Z-error)		
$\pm 7$ m	Comparison to DGM 50 (Surveying and Mapping Agency of North-Rhine Westphalia, Germany)	Czegka and Braune (2005)
$\pm 16$ m	Comparison to 1:250 000 topographic map extracted DEM	Miliaresis and Paraschou (2005)
$\pm 6.9$ m	Comparison to DGM 50 (Surveying and Mapping Agency of North-Rhine Westphalia, Germany)	Bolten and Bubenzer (2006)

The extraction of the elevation data from the combination of the two stereo images is divided into several steps.

- First, the correct swapping and/or registration of the two stereo images by acquiring tie points in both images. In this step, it is important to identify the same structures in both images. In inhabited regions with anthropogenic structures (e.g. settlements or cross-roads), this is simple, and an automatic detection of tie points is possible. Regions without anthropogenic structures are more difficult to assess; hence, a manual determination of tie points is necessary. The accurate tie-point collection is fundamental. On one hand, the satellite geolocation of the images is not good enough (the position of the taken scene is estimated only from the position of the satellite and its velocity at  $\sim 700$  km above the earth). On the other hand, a mismatch of fewer pixels highly affects the quality of the result of the elevation model for the following processing steps.
- Second, the generating of epipolar images and measuring the parallax value of every pixel in both images. The epipolar images are comparable with the two images seen with the left and the right eye, which is fundamental to calculate distances of objects.
- Third, the automatic conversion of the parallax values to relative and – with orbital or ground information – to absolute elevation data.

These three steps are included in the PCI Orthoengine software package; they are similar to the working process of the ASTER science team. Cuartero et al. (2005) show that, compared to other extraction software, the use of PCI Orthoengine gives the best result for the derivation of regular grids, due to the integration of the satellite specification in this software package.

In very smooth terrain, as well as under problematic conditions, e.g. a diffuse cloud cover, the generation and the quality of Digital Elevation Models (DEMs) are imprecise. Another problem concerns the merging of several generated elevation models when the study area lies between two track rows, because data artefacts might arise from small absolute elevation differences in the models. As mentioned above, information with high accuracy of the absolute elevation in the investigated region is sparse. Thus, the use of ground-control points with exact elevation data cannot solve the problem. With regard to the additional availability of the SRTM-3 data (see Section 2.3.1.2.2), a scale-reflection and the complexity of merging, it is recommended to merge only  $3 \times 3$  ASTER-DEM scenes (Bolten and Bubenzer, 2006). Regarding the quality and accuracy of the ASTER data (see Section 2.3.1.2.3), it is possible to create digital elevation models up to around a scale of 1:50 000 with the ASTER data (Bubenzer and Bolten, 2006).

### 2.3.1.2.2. *Elevation data from the Shuttle Radar Topography Mission*

The SRTM mapped the topography of the earth's surface area-wide for latitudes between  $60^\circ\text{N}$  and  $56^\circ\text{S}$  (Schmullius et al., 2000; Rabus et al., 2003). The instrument consisted of (1) the main antenna, which was located in the payload bay of the Space Shuttle Endeavour, (2) the mast, which was connected to the main antenna

truss, and (3) the outboard antenna, which was connected to the end of the mast. In contrast to the ASTER sensor, the radar technique used is an active remote-sensing method. This means that the system emits microwaves with a wavelength in the cm-band, which are directed towards the target to be investigated and which measure the proportion and the running time of the reflected wave (Lillesand et al., 2004). Advantages of active sensors include the ability to obtain measurements any time, and the independency of atmospheric conditions (e.g. clouds or dust). In addition, active sensors can be used for examining wavelengths that are not sufficiently provided by the sun, such as microwaves.

The interferogram of the combination of the two radar images taken during the shuttle mission is in principle similar to the ASTER stereo images from which the elevation data are derived. As a result of mechanical problems – the vibration of the antenna truss – and of the processing of a huge amount of digital data, the derivation of the elevation model was complex and took a long time (Farr et al., 2007). For example, the data set for the African continent is available only since 2004, 4 years after the main mission.

The SRTM-3 elevation model has a resolution of 3 arc seconds ( $\sim 90$  m) (Table 1(a)), but was calculated from the detailed but unpublished military SRTM-1 model with a resolution of 1 arc second. Whereas the latter is only available for the USA, the SRTM-3 data are available free of charge worldwide (GLCF, 2007). Further improved versions are probably expected, because the present data are named as preliminary (see Section 2.3.1.2.3). At present, the NASA SRTM website (JPL, 2007) documents the following specifications and their problems:

- data may contain numerous voids (regions with no data) and anomalous values,
- coastlines of water bodies are typically not well delineated and may not appear “flat”,
- no-data evaluation for conformance with National Mapping Accuracy standards and
- significant differences exist between the SRTM and the traditional Digital Terrain Elevation Data (DTED) standards.

For the Great Sand Sea, the first point is important and will be exemplified below, because the SRTM data show large areas with no-data values for the Great Sand Sea. Therefore, a technique is necessary to fill these areas with other data (see Section 2.3.1.3). Regarding the quality and accuracy of the SRTM data (see Section 2.3.1.2.3), it is in general possible to create digital elevation models up to a scale of around 1:100 000 (Bolten and Bubenzer, 2006).

Generally, these data are used at scales smaller than 1:100 000 where no other elevation data are available. For example, Almeida-Filho et al. (2005) improved structural interpretations of a geologically complex terrain in Brazil. Karátson and Timár (2005) calculated volumetric data of a Carpathian volcanic chain, and Bubenzer and Bolten (2007) evaluated the elevation data sets SRTM-3 and ASTER in the southern Namib (Namibia) and the Great Sand Sea of Egypt with respect to their suitability for the differentiation between draa and dunes and the morphometric quantification.

### 2.3.1.2.3. Quality and accuracy of the digital elevation models used

The use of digital elevation models in geomorphological investigations depends on several characteristics of the data. The resolution has to be suitable for the investigation area. In this respect, it is possible to calculate a quotient between the model resolution and the investigated area. Thus, the use of different elevation models can be compared. The elevation error of the model should be considerably lower than the geomorphological unit that is examined, and the quality of the model concerning no-data areas or other voids (e.g. spikes and wells) must be considered. In the Great Sand Sea, the analysis of draa and dunes – with heights of 30–50 m and with a horizontal dimension of several hundreds of metres – is suitable for the resolution of SRTM and especially for the ASTER data. However, a small drainage channel of about 1 m width, for example, is not a suitable research object for such elevation models.

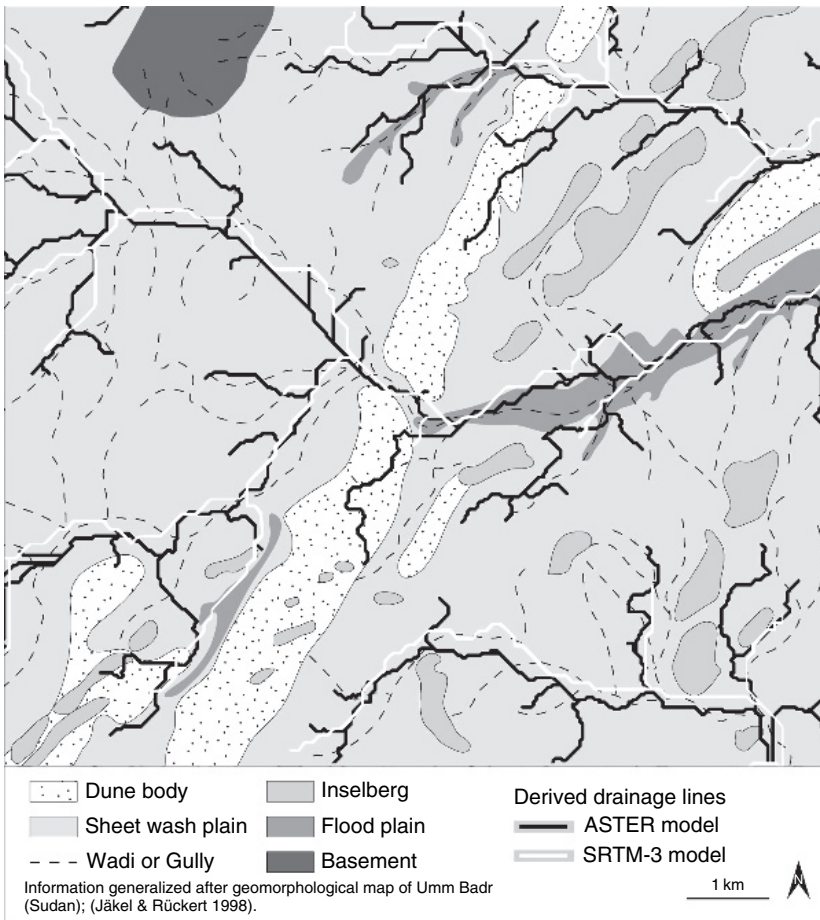


**Fig. 4** Comparison of ASTER and SRTM-3 elevation data using a drainage system derived from field work mapping.

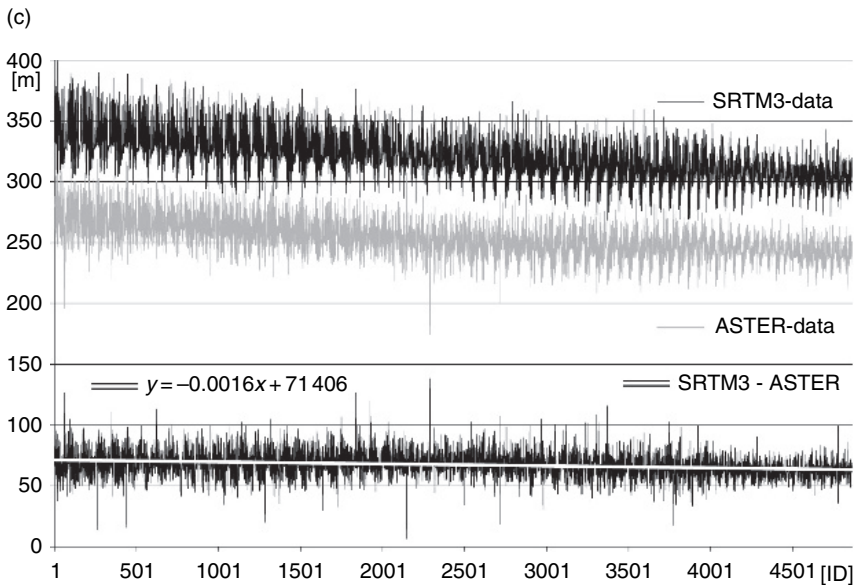
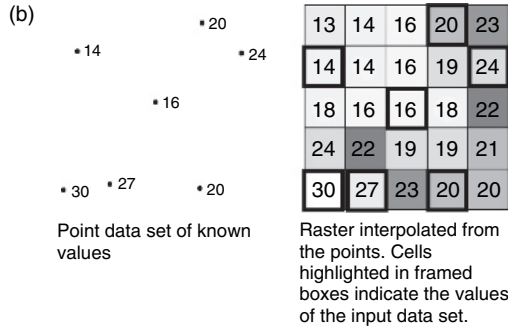
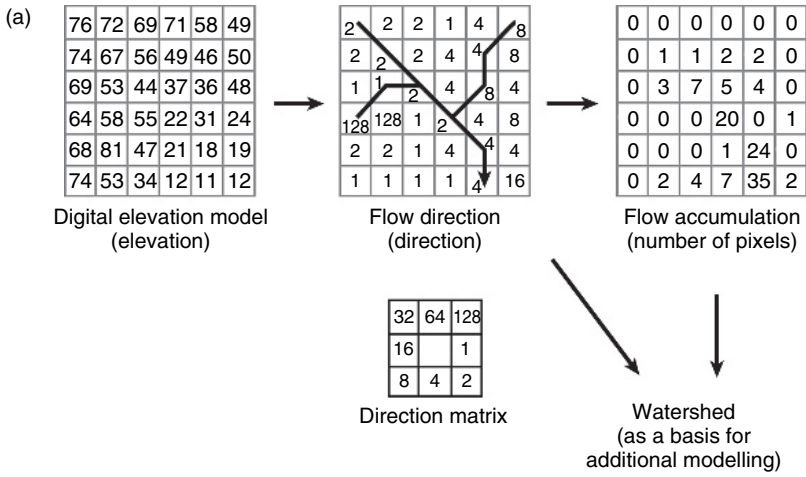
An evaluation of the accuracy of the ASTER and SRTM-3 data compared with that of other elevation models is given in Table 1(b). Investigations by Bolten and Bubenzer (2006) show the difference of the ASTER and the SRTM-3 models to the well-known German digital elevation model 1:50 000 (DGM 50) that was derived from airborne laser-scan measurements. First, the resolution of each model was calculated to an equal value of 90 m, using a bicubic resampling method. In general, the results are strongly consistent. Statistically, the average absolute deviation of the SRTM-3 model from the DGM 50 model is  $\pm 6.9$  m (standard deviation: 9.7 m). In comparison, the ASTER data differ with an average value of  $\pm 5.9$  m (standard deviation: 7.8 m).

Figure 4 shows another possibility to test the accuracy and quality of both elevation models. A field-work mapping of drainage lines in the Um Badr region of Sudan presented by Jäkel and Rückert (1998) is used for verification. As this region is also arid and shows landforms comparable to those of parts of the Western Desert of Egypt, it is particularly suitable for an evaluation. For both models, SRTM-3 and ASTER, a drainage-line system is derived by use of the Topographic Parameterization (TOPAZ: a.o. Garbrecht et al., 2004) module of the Watershed Modelling System (WMS). Using this module, the geomorphometric features are derived by calculating the flow accumulation and the flow direction of an elevation model. The flow direction describes the direction of potential water flow in eight direction classes. The flow accumulation cumulates for each pixel the number of pixels that have a flow-direction reference. Figure 5(a) shows the relation of the two primary geomorphometric parameters and the determination of a potential drainage line. Finally, a watershed basin can be derived based on the drainage system and the elevation data.

The derived systems (Fig. 4) are in good accordance with the field data. The principle system and the fluvial gaps in the dunes are reproduced. The ASTER drainage lines show more detail, because of their higher resolution. This means that the drainage-line algorithm for both elevation models uses the same number of flow-accumulation data at the calculation starting point. In conclusion, both models give a coherent view of the relief situation.

Due to the fact that no-data regions or regions with a low quality of elevation data still exist in the SRTM-3 data, a solution to get a uniform database for modelling has to be found. Figure 6(a) shows no-data regions of the SRTM-3 data located mostly in the sand-covered regions of the Great Sand Sea, and the position of available ASTER scenes. In fact, at a closer look we find further no-data pixels on the dune tops, in addition to the large regions with no-data pixels. This means that there are two different types of no-data problems, which have to be solved. The isolated pixels with no height value pose no problem. The gaps can be closed with an easy interpolation technique by using the height information of the direct eight neighbouring pixels or the pixels in the vicinity, dependent on the used mathematical technique. For this purpose, several techniques are in use, depending on the number of adjacent pixels and their weighting (Wackernagel, 2003). Normally, only the neighbouring pixels are used with an inverse-distance weighting method. This means that a closer pixel has more weight for the resulting elevation value than a pixel farther away.





The larger gaps can be closed only by using height information of other sources, preferably with similar resolution and quality (see Section 2.3.1.3). The mentioned improved versions of the SRTM-3 model meanwhile exist by the CIGAR Consortium for Spatial Information working group (CIGAR-CSI 2007). They processed a new SRTM data set by interpolating the no-data areas with neighbourhood data and with information from other data sets. Unfortunately, in the Great Sand Sea the large connected no-data regions are filled with low-resolution models (such as GTOPO 30, see Section 2.3.1.1) with very low quality, so that these large interconnected regions are still not suitable for modelling. A new approach tries to close the large no-data areas by a substitution of ASTER elevation data (cf. Blumberg, 2006; see also Section 2.3.1.3).

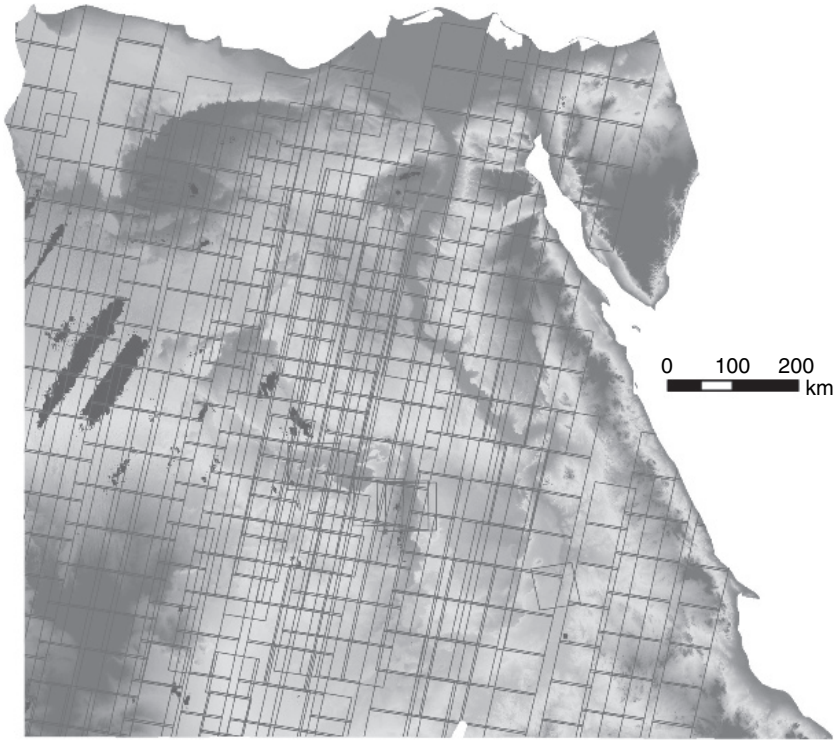
### 2.3.1.3. Generating a uniform elevation database for the Western Desert of Egypt

To model the main watersheds for the Western Desert of Egypt, a basis elevation model has to be processed. As mentioned above, the two elevation models used cannot accomplish the modelling of watersheds separately. In the following, a method is introduced (1) to generate a uniform elevation model without connected large no-data areas, and (2) to calculate a potential bedrock relief without draa and dune bodies to get a base for the undisturbed modelling of the palaeo-drainage system. The first method is a prerequisite for the second method; thus, the processing of an elevation data set composed of the ASTER and SRTM-3 data is presented first.

Figure 6(b) shows a detail of the central Western Desert of Egypt with the no-data regions of the SRTM-3 data and the position of the ASTER scenes. Primarily, the combination of ASTER and SRTM-3 data generates the problem that both data sets provide different absolute heights for similar pixels. To deal with this problem, an elevation adaptation of the ASTER data is done by random comparison of pixels to find out a linear combination for an ASTER scene with the SRTM-3 model (Bolten, in press.; Fig. 5(c)). For this reason, a point data set is generated in the overlapping area of the two models, and the  $Z$ -value of the two models is determined for each point. The difference between the points belonging together is calculated in a statistical environment, and a regression is derived. For instance, the regression for the ASTER scene 1074 to the SRTM-3 model is:  $y = -0.0016x + 71406$ . The equation shows that only a linear deviation of the ASTER data is present. The elevation-depending deviation with the factor 0.0016 is very low. Starting from this method, several conversions are necessary to combine



**Fig. 5** (a) Derivation of flow-direction and flow-accumulation using digital elevation data. The first step is to calculate for each raster cell the possible flow-direction to the nearby raster cell by using the direction matrix. The second step is to calculate a possible stream-line starting from an arbitrary raster cell and to cumulate the number of affected raster cells. (b) Two graphics showing the interpolation of a point dataset towards a regular raster dataset, using an inverse distance-weighted (IDW) algorithm (McCoy and Johnston, 2001). (c) Graphs showing the relation between the SRTM-3 and the ASTER dataset. The lower graph reflects the difference of the two datasets and shows the linear linking and the difference of about 71.5 m. Due to plotting the data W-E, the individual draa-and-dune bodies are displayed repeatedly.

(a)

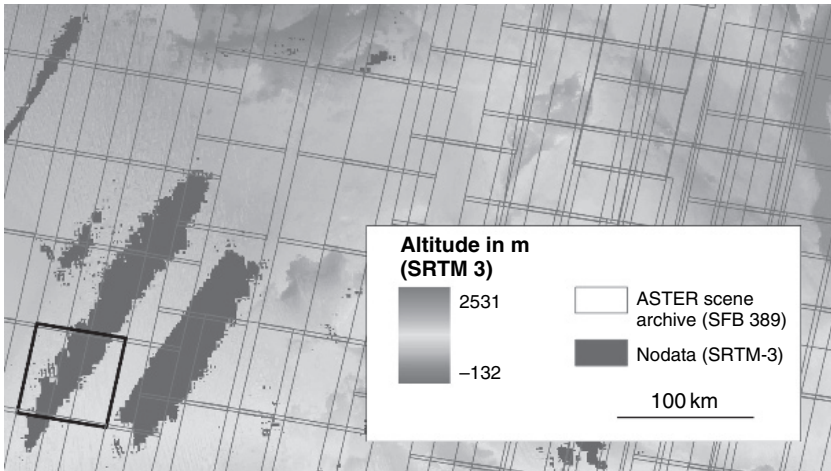


**Altitude in m  
(SRTM 3)**





-  ASTER scene archive (SFB 389)
-  Nodata (SRTM-3)

(b)



**Altitude in m  
(SRTM 3)**



-  ASTER scene archive (SFB 389)
-  Nodata (SRTM-3)

100 km

the two different models to get a uniform data set. A mask of the SRTM-3 no-data regions must be applied to get an exact puzzle piece of ASTER data fitting into the SRTM-3 model. Finally, both models have to be combined into one model with the same resolution and projection.

The second method tries to generate a basis elevation model for the Great Sand Sea void of draa and dunes to obtain a potential bedrock relief. For this purpose, only regions that are not covered by dunes or draa need to be identified. For this reason, a slope map of the elevation model is created to identify flat areas, which represent the interdune regions. It is assumed that the relief below the draa/dune areas is even, so that an interpolation of the edged interdune pixels is possible. Starting from this interdune data set, the remaining pixels are converted into points with elevation-attribute information, and a new elevation model is generated by interpolating (Fig. 5(b)) the now existing no-data (dune) regions. After these working steps, the watersheds for discrete outlet points may be derived and analysed.

Necessarily, the erasure of draa and dunes produces flat intermediate bedrock areas. With regard to the possible existence of further “radar rivers” in the Great Sand Sea (cf. McCauley, 1982), it is wise to consider the possibility that the sub-draa relief is probably not even. This point, the likelihood of the calculated drainage pattern, and the reliability of the derived partial catchment areas as possible sediment sources will be discussed in Section 3.1.3.

### 2.3.2. The topographic surveys

For various reasons, the investigation of large sand seas is always difficult and even hazardous. First of all, the accessibility for vehicles is restricted by dunes and particularly by the megadunes that are always present and are – in fact – the criterion for ancient sand seas or ergs. The exploration of unconsolidated ergs can only be achieved along transections following mainly the interdune or interdraa (see Section 3.2) corridors. Even here, however, restrictions are the rule. Due to the sand seas’ dimensions and their remoteness with regard to settlements or oases, the logistics (particularly supply of water, petrol and spare parts for vehicle repair) are extremely difficult and allow only a limited number of transections (Fig. 2). These have to be chosen very carefully. First experiences gained in the smaller Namib Erg in 1976 (Besler, 1977a, 1980, 1984a) proved to be very valuable.

Before the accomplishment of the first transection in the eastern Great Sand Sea in 1996, nobody knew what would be encountered along this route and whether it would be possible to reach the Siwa Oasis in the north. On LANDSAT images, the most promising dune-free corridor along the most continuous sand ridge was

**Fig. 6** (a) Situation of SRTM-3 and ASTER elevation models for Egypt. The position of ASTER scenes archived in the Collaborative Research Centre 389 and the large connected no-data SRTM-3 areas are displayed. (b) Situation of SRTM-3 and ASTER elevation models for a central region of the Western Desert of Egypt (enlargement of (a)). The position of ASTER scene 1074 mentioned in Fig. 5(c) is framed.

chosen, starting from the Abu-Ballas scarp in the south ( $24^{\circ}29'N$ ,  $27^{\circ}38'E$ ). On this first and longest transection, the survey procedures were developed and tested. For this reason, the survey was less systematic here than on the following transections. This was enhanced by the discovery of a very important prehistoric site at  $25^{\circ}25'N$ ,  $27^{\circ}05'E$  (Regenfeld 96/1-2; Riemer, 2003, 2004a, 2005) that needed much time for investigation. On the other hand, the northeastern part of the Great Sand Sea was found to consist of younger dunes only. They are a later addition to the ancient erg and less interesting for its history. Moreover, already north of  $27^{\circ}N$ , there are practically no corridors and therefore no prehistoric sites. On account of this, and because of the difficult logistics already mentioned, the middle transection and the western transection end around  $27^{\circ}N$ . From these endpoints, the sand sea was crossed towards the east on two different routes where observations, particularly on the shapes and wavelengths of the sand ridges, could be made.

The transections do not run parallel to each other (at least not in the west) because they necessarily follow the directions of the megadunes that diverge towards the south. As the satellite-image itinerary (Fig. 2) shows, we were forced to veer to the eastern or to the western corridor for several times because the leading megadunes ended or the sands in the corridors became impenetrable. At regular intervals of 10 km (5–6 GPS minutes), cross-sections were measured perpendicular to the sand ridges (height, width, slope gradient), and the crest sands of the highest secondary dunes on the megadunes were sampled. The cross-sections are plotted as sequences along the three transections and provide most important information for various questions (Figs 7–9).

North of  $25^{\circ}25'N$  on the first transection, however, these cross-sections are spaced at larger intervals of 30 km. In addition, the sampling was reduced to selected cross-sections because it was not sure whether we would be allowed to take the samples back to Germany for the analysis. The 11th cross-section at the prehistoric site Regenfeld was investigated with particular care in collaboration with the archaeologists. For this reason, the first coring for luminescence dating was carried out on the lower eastern slope of the sand ridge, in close vicinity to the prehistoric site. A second coring along this transection was conducted at  $27^{\circ}19'N$  on a western slope because meanwhile the character of the megadunes had changed drastically.

After the samples had proved to be suitable for luminescence dating, comparable dating sites along the following transections were chosen at similar latitudes. In the southern part, they are found between  $25^{\circ}25'N$  and  $25^{\circ}50'N$  on western and eastern flanks of the sand ridges wherever artefact assemblages were discovered. In the northern part, the coring was conducted only on western slopes between  $26^{\circ}50'N$  and  $27^{\circ}20'N$ . It should be mentioned that drilling and coring in unconsolidated dry aeolian sands is extremely difficult and not comparable to drilling into consolidated dunes as in the Sahel or in the Kalahari. Moreover, it has to be done by hand because heavy machinery cannot be brought to these remote places and cannot be moved across soft ground. Therefore, a special manual coring equipment had to be developed (Bubbenzer, 2001). Plastic liner tubes were inserted and drilling rods with bayonet connections and special sand augers were used to core below the tube. Each time the auger was lifted, the tube was pressed down. The sand samples

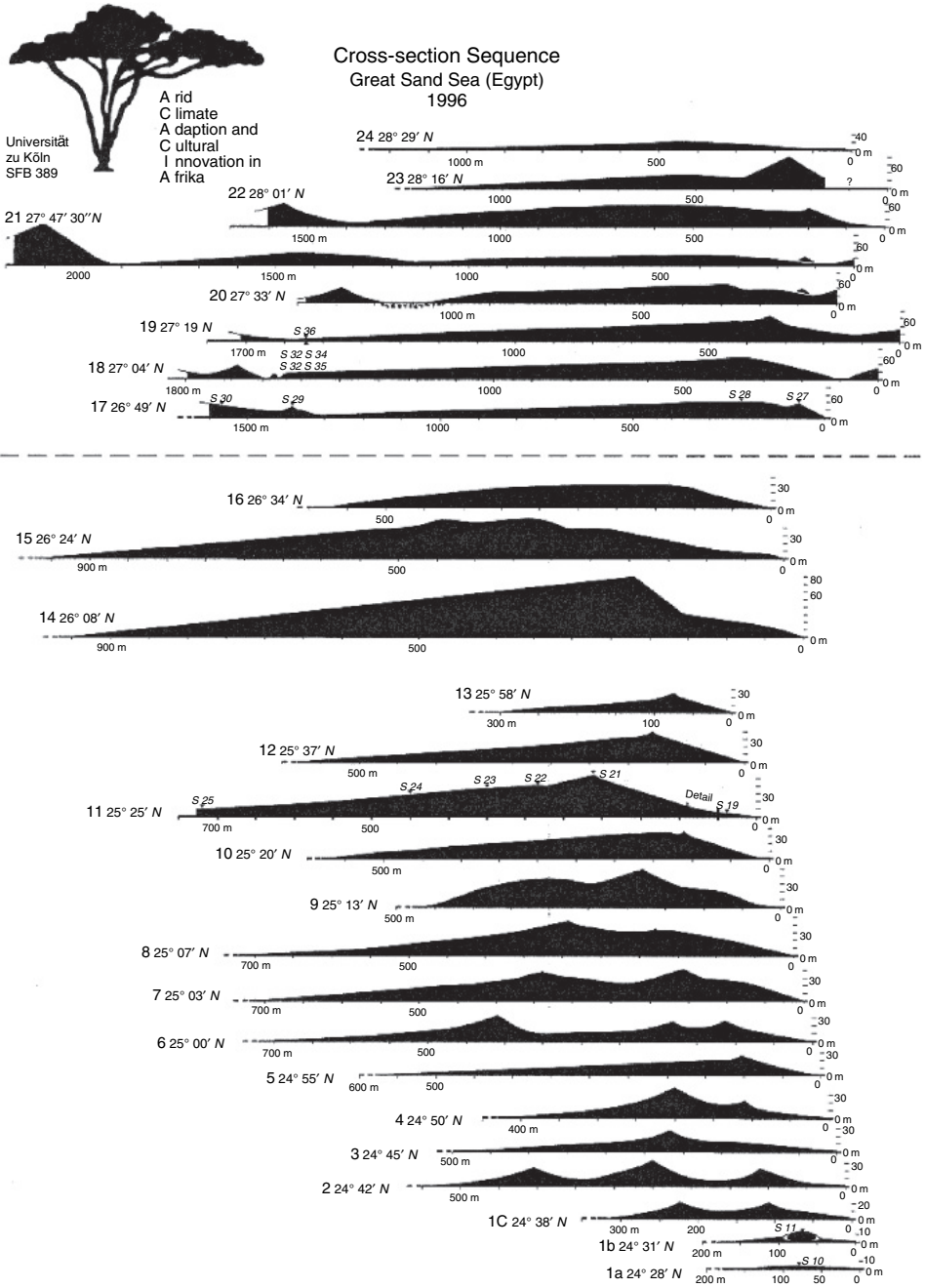


**Fig. 7** Cross-section sequence of draa with dunes at true angles and sampling sites with sample numbers along the eastern (1996) transection. Note the change in scale at the dashed line!

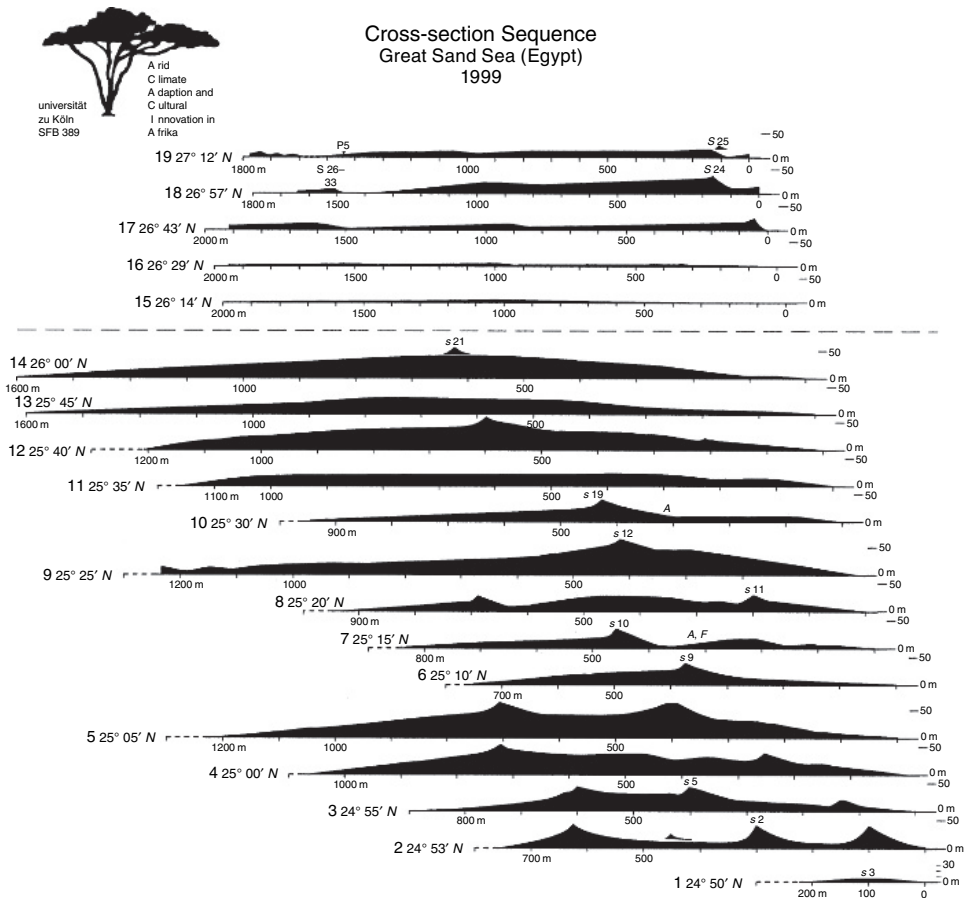


**Fig. 8** Cross-section sequence of draa with dunes at true angles and sampling sites with sample numbers along the middle (1999) transection. Note the change in scale at the dashed line!

collected during this procedure can only be used for sedimentary analysis. After the liner tubes had been driven down to a depth suitable for the collection of samples for dating, the sand auger was replaced by a stainless-steel tube with a core catcher, and the rod was hammered into the sediment. After hauling the steel tubes up, they were wrapped in black foil and disconnected from the rod. Samples for sedimentary analysis were collected at intervals of 0.5 m, and for luminescence dating at intervals of 1 m, down to a maximum depth of 5 m.

The access to the western transection proved to be particularly difficult because it was not possible to traverse the dunes piled-up just north of the Gilf Kebir Plateau. A route across the plateau, going up and down along very steep passages, had to be found. In the southern part of the western transection, another impressive prehistoric site already known (Haynes, 1982) and its vicinity were extensively investigated (Glass Area 81/62 = Willmann's Camp: 25°07'N,

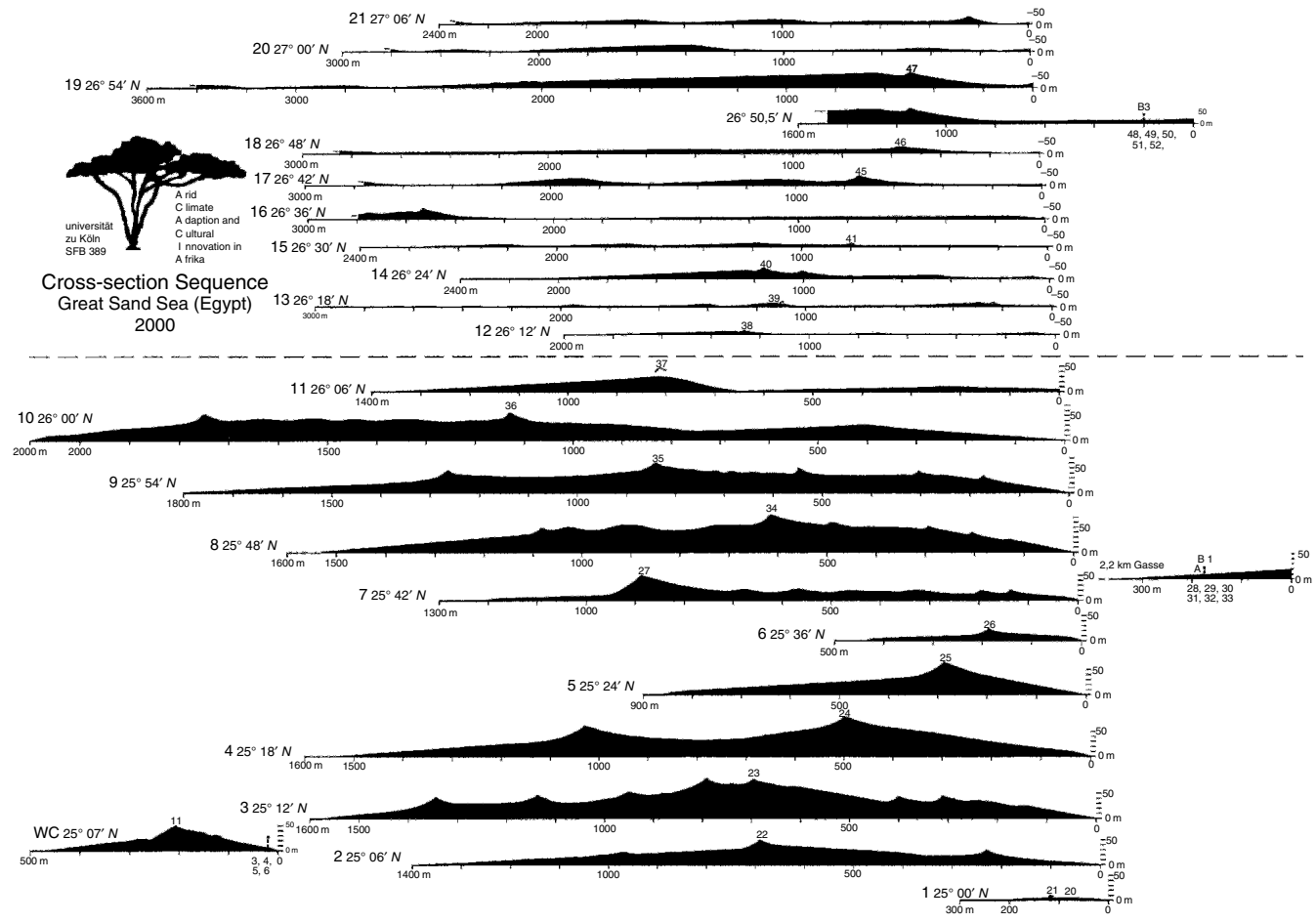


Fig. 9 Cross-section sequence of draa with dunes at true angles and sampling sites with sample numbers along the western (2000) transection. Note the change in scale at the dashed line!



25°37'E; Riemer, 2005). A final visit of the Great Sand Sea in 2006 included diagonal crossings from south of Ain Dalla in the east to Willmann's Camp in the southwest (and back). Meanwhile, this route had been explored, and GPS data were available.

Along all transections and crossings, the ground between the sand ridges was observed, and the bedrock was sampled where available from outcrops. All observations on dune shapes, draa surfaces and structures, sand colours, artefacts, fulgurites, etc. were entered into the field diaries and documented by photography.

### 2.3.3. Sedimentological analysis

The nature of a sand sea makes it an ideal subject of sedimentary studies. As much information as possible has to be drawn from the sand because this is the only material available everywhere. As the investigation of the Namib Erg (Besler, 1980, 1984a) has shown, the history of a sand sea can be reconstructed to a high degree by sedimentary analysis. In this respect, sedimentology has proved to be an exceedingly valuable discipline. Some methods of sedimentological analysis have been developed further by the present author and are adapted to the questions put forward in Section 2.1 (e.g. granulometry). A brief account of the developmental histories of these methods is given at the beginning of the respective chapters because the history is closely related to the interpretation. In this section, only the mechanical procedures are described.

The point has to be stressed, however, that in any case, not the properties of a sand sample are decisive, but the spatial (and temporal) distributions of these properties. This refers also to the methods that do not belong to the sedimentological analysis in a strict sense (e.g. salinity determination).

#### 2.3.3.1. Granulometry

For the granulometric analysis, all sand samples were fractionized using a  $\varphi$ -gauged sieving set, following  $\varphi = -\log_2$  grain diameter. Folk and Ward (1957) used  $\varphi/2$  intervals, Friedman (1962) and Harris (1958) used even  $\varphi/4$  intervals. There exist statements, however, that the results are comparable to those gained from  $\varphi$  intervals (a.o. Moiola and Weiser, 1968; Fenwick, 1991). Investigations on the  $\varphi$ - and  $\varphi/2$ -sieving's influence on the obtained results were also carried out for 47 Namib sands from various dune parts (Wiese, 1995). In all cases, the grain-size parameters did not change much or not at all.  $\varphi/2$ -sieving is more sensitive to slight alterations in the sand. In some cases, however, this may unnecessarily complicate the identification of a granulometric sand type (see Section 4.3) or may lead to too many types with inconspicuous and/or meaningless boundaries (Besler, 2005).

For the analysis, about 100 g sand per sample were collected from a sample partitioner of the RETSCH Type PT 21720 and treated in a sieving machine of RETSCH Type 3D for 20 minutes. The wet sieving, necessary for sandstones after crushing the samples in a mortar, was carried out in a Haver EML 20 digital for

15 minutes. A specific computer program was developed for the plotting on probability paper. The grain-size parameters were calculated after Folk and Ward (1957):

$$Mz = \frac{\varphi_{16} + \varphi_{50} + \varphi_{84}}{3}$$

$$So = \frac{\varphi_{84} - \varphi_{16}}{4} + \frac{\varphi_{95} - \varphi_5}{6.6}$$

$$Sk = \frac{\varphi_{16} + \varphi_{84}}{2(\varphi_{84} - \varphi_{16})} + \frac{\varphi_5 + \varphi_{95} - 2\varphi_{50}}{2(\varphi_{95} - \varphi_5)}$$

$$K = \frac{\varphi_{95} - \varphi_5}{2.44(\varphi_{75} - \varphi_{25})}$$

The grain-size frequency distributions were plotted after Walger (1964) as first differentials ( $dy/dx$ ) of the cumulative distributions, which means weight % divided by the fraction interval (in mm) on the Y-axis. Contrary to the traditional frequency distribution with only weight % on the vertical axis, this kind of curve was found to display the true characteristics of a sand type (see Section 4.3).

### 2.3.3.2. Morphoscopic analysis

No specific chapter is dedicated to the results of the morphoscopic analysis which studies quartz-grain shapes and surface textures under the microscope. This analysis was conducted mainly to select the most interesting samples for the SEM. A few particularly helpful results are mentioned in various subsections of the respective chapter. The advantage of the morphoscopy lies in the possibility to observe statistically more significant numbers of grains per sample. Moreover, very thin clay/iron-oxide coatings may be distinguished from thicker iron-oxide patches because the colours are visible.

The most important aeolian fractions (0.125–0.25 mm) of the samples, in some cases also additional fractions, were washed in concentrated hydrochloric acid to destroy the coatings of clay and iron oxides. This, however, was only necessary for samples from the southern part of the Great Sand Sea. At least 100 grains per fraction were studied with a stereo-microscope on a blackened plate under incident light at an angle of 45°. Based upon the work of Cailleux (1952, 1972), Tricart (1958) and Pachur (1966) and on own experiences in the Namib Erg (Besler, 1980) and in the Rub' al Khali (Besler, 1982), four grain classes were distinguished, their respective grains counted and their percentages calculated: angular-clear, angular-frosted, rounded-clear and rounded-frosted. The boundary between angular and rounded was determined between subangular and subrounded (according to Russel-Taylor-Pettijohn, e.g. in Müller, 1964). In addition, the percentage of quartz grains with a yellow or reddish patina was determined in the untreated fraction.

### 2.3.3.3. Heavy-mineral analysis

The – most important – aeolian main fraction, 0.125–0.25 mm according to Besler and Pfeiffer (1992), was used for the heavy-mineral analysis. It should be mentioned that the heavy-mineral content in different fractions of the same sample seems to follow a general rule. In an extended analysis of aeolian sands from Burkina Faso, it was found that the finer fraction always has a 10 times higher heavy-mineral content than the respective coarser fraction of the sample (Besler and Pfeiffer, 1992). This would allow a better comparison with values given in the literature. Unfortunately, however, the fraction is rarely mentioned.

About 17–20 g of the samples were boiled in hydrochloric acid (25%) to remove clay/iron-oxide coatings and then were washed in water three times. After desiccation, the total weight was measured as accurately as possible. For the separation of the heavy minerals with a density above  $2.86 \text{ g/cm}^3$  by the gravitative method, bromoform was used for the samples of 1996, and a solution of sodium polytungstate ( $\text{Na}_6(\text{H}_2\text{W}_{12}\text{O}_{40})^* \text{H}_2\text{O}$ ) in distilled water for the samples of 1999 and 2000. The heavy minerals were accumulated in the filters of the separating funnels after 30 minutes. They were weighed again after desiccation. In spite of the different separation liquids, the results are rather homogeneous throughout the sand sea.

For the qualitative analysis of the heavy-mineral assemblages, the grains of the samples from 1996 were mounted in LAKESIDE, which leads to an uncertainty of about 1% in the distinction between epidote and pyroxene. The samples of 1999 and 2000 were mounted in MOUNTEX with better distinction possibilities. From each sample, at least 100 grains were chosen at random and identified.

### 2.3.3.4. Scanning-electron microscopy

With the aid of the morphoscopic analysis, subsurface samples with the greatest differentiation were selected from each coring site. In addition, the surface sands of the megadunes and the dune-crest sands of the respective cross-sections at the sites were analysed.

The aeolian main fraction (0.125–0.25 mm) was used. Coatings were removed by washing the sands in concentrated hydrochloric acid. Untreated, coated grains of the same samples were additionally examined. In order to prepare the grains for the SEM analysis, they have to be sputtered with gold, because only this microlayer allows the complete reflection of the electron beam which in turn is a prerequisite for clear pictures of the highest magnification. A CAMSCAN CS44 ED was used since here a microprobe can be directed into the tiniest deposits on the grain surface. It delivers energy-dispersive X-ray spectra for the chemical analysis. The element-specific spectra can be printed out immediately and are a great help for the analysis (e.g. for the distinction between silica precipitations and silicate deposits).

During the work at the SEM, all interesting features of the grains were scanned and photographed in various magnifications. These paper photomicrographs represented the major objects of analysis and interpretation. Details of the analysis procedure, the results and their interpretation are discussed in Chapter 8.

### 2.3.4. Salinity measurements

The point has to be stressed that salinity in this context does not refer to the geochemistry. Not the presence of specific salts in the sands is of importance, but only the question whether a sand is saline or not. Moreover, salinity is not used in a hydrological or pedological sense. The salinity of the sediments is interesting only as an indicator of more humid conditions of the past. The specific definition and the effective classification of salinity used here were developed during the study of the Namib Erg in Namibia (Besler, 1979, 1980; Besler and Gut, 1997). It allows the distinction between dune sands (not saline:  $<10^2 \mu\text{S}/\text{cm}$ ), megadune sands (saline:  $>10^2 \mu\text{S}/\text{cm}$ ), aeolian sediments subjected to surface-water infiltration and evaporation during longer time-spans (strongly saline:  $>10^3 \mu\text{S}/\text{cm}$ ) and littoral sands influenced by sea water (extremely saline:  $>10^4 \mu\text{S}/\text{cm}$ ).

The relation between the salinity and the ion (salt) content of the sands in aqueous suspension was investigated in a theoretical and experimental study by Schlösser (1995), who also improved the measurement procedure. In fact, the salinity measured as electrical conductivity corresponds to the total (salt) ion content of the sands. Based on the International Mean (at  $25^\circ\text{C}$ ), a conductivity of  $1 \mu\text{S}/\text{cm}$  is equivalent to  $0.640 \text{ mg salts per litre}$ . Depending on a linear correlation, the used threshold value of salinity of  $10^2 \mu\text{S}/\text{cm}$  represents  $64 \text{ mg salts per litre}$  or  $64 \text{ ppm}$ .

All samples from the Great Sand Sea were subjected to measurements of salinity as electrical conductivity, using the conductometer WTW-LF 191, measuring  $\mu\text{S}/\text{cm}$ . About  $20 \text{ g}$  of each sample was suspended in  $50 \text{ ml}$  distilled water and shaken for 20 minutes. The first value was read after sedimentation, the second one after 1 hour, the third one before filtration and the last one 24 hours after filtration in the filtrate. According to Schlösser, the last reading in the filtrate is most reliable although the deviation from the third value is not substantial.

### 2.3.5. Luminescence dating of sand deposits<sup>‡,§</sup>

Luminescence-dating techniques are currently widely applied to date the deposition of sediments over a timescale of tens to tens of thousands of years. The event being dated is the last exposure of sand or silt grains to daylight.

Luminescence dating is based on the process of a time-dependent accumulation of electrical charge at – and its later release from – light-sensitive traps that are associated with imperfections in the crystal lattice of common minerals such as quartz and feldspars. These structural defects and charge transfer are induced by ionizing radiation resulting from naturally occurring radioactive processes; these include alpha ( $\alpha$ ) radiation (the nucleus of a helium atom), beta ( $\beta$ ) radiation (electrons or – much more uncommon – positrons) and gamma ( $\gamma$ ) radiation (electromagnetic waves). Natural (so-called “background”) radiation also includes a contribution from cosmic rays (mainly neutrons).

<sup>‡</sup> A. Hilgers, E-mail: a.hilgers@uni-koeln.de

<sup>§</sup> A.J. van Loon, Geological Institute, Adam Mickiewicz University, Poznan, Poland. E-mail: tom.van.loon@wxs.nl

When a quartz grain is buried, the ionizing radiation from within the sediment results in an increasing trapping of charge at structural defects. When the grain becomes exposed to sunlight again, the solar energy induces release of the electrical charge (heating has a comparable effect). The previously stored energy, usually assumed to be electrons, that is released from the light-sensitive traps, is emitted mainly in the form of heat. A small percentage of electrons recombines, however, at other defect structures in the lattice. This process takes place under the emission of energy as visible light, and this light emission is known as luminescence. It is called “optically stimulated luminescence” (OSL) if the electrons are released from the traps by light stimulation, or “thermoluminescence” (TL) if the stimulation was conducted by heating the crystal.

In the laboratory, the light emission (luminescence) from quartz or feldspar crystals can be measured and translated into dose values through calibration of the luminescence signals against those of known doses of radiation. This experimentally determined dose value is an equivalent of the radiation dose which the crystal received while buried in its natural environment (for a description of the equipment used to carry out these measurements, the reader is referred to Bøtter-Jensen et al., 2003). While this so-called palaeodose ( $P$ ) results from the absorption of the sum of  $\alpha$ ,  $\beta$ ,  $\gamma$  and cosmic radiation, the equivalent dose ( $D_e$ ) determined in the laboratory by luminescence measurements results from irradiation with mono-energetic  $\beta$  or  $\gamma$  sources. The unit of a radiation dose, and therefore also of the  $D_e$ , is the gray (Gy: 1 Gy = 1 J/kg). This unit belongs to the International System of Units, abbreviated SI (from the French “Système International”).

To use the light emission for dating purposes, a reference point is required. The so-called “zeroing event”, at which any previously trapped charge is released, serves as such a point. The zeroing event in nature (in the case of sediment dating) is the optical stimulation by exposure to sunlight (the so-called “bleaching”) during sediment transport and deposition. This implies that, in general, only the time passed after the last zeroing event (i.e. the release of electrical charge from the traps in defect crystals) is datable, thus the last exposure of the investigated sand grains to daylight (see Fig. 10).

Godfrey-Smith et al. (1988) have demonstrated that bleaching by bright sunlight for a few seconds (quartz) up to a few minutes (feldspars) is sufficient for re-setting the OSL signal down to 1% of the initial value. Aeolian environments thus provide ideal conditions for the application of luminescence dating. In aeolian materials, the degree of optical re-setting at deposition is rarely a problem (Duller, 2004), as during the transport processes of saltation, reptation and suspension the sediment most likely is exposed to sufficient light for bleaching prior to burial.

To derive the age information from the light-emission or  $D_e$  values, respectively, the factor of time has to be introduced by including the environmental dose rate ( $D_0$ ), which describes the amount of radioactivity in the environment of the investigated grains per time unit. The radioactivity of a sample and its surroundings is assessed by chemical or radiometric methods, and the contribution by cosmic radiation is estimated on the basis of the burial depth of the sediment sample and the geographical situation (particularly the latitude and the elevation above sea level) of

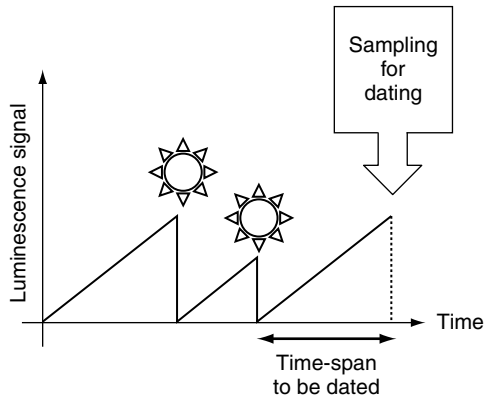


**Fig. 10** Basic principles of luminescence dating. The number of electrons trapped in crystal defects of quartz and feldspar grains increases at a rate that depends on the time-span that the sediment sample is exposed to ionizing radiation emitted by the decay of naturally occurring radionuclides within the surrounding deposit. In proportion, the luminescence signal intensity increases. By exposing the sample to sufficient energy (such as sunlight) during sediment transport, the stored energy is released, and by that the luminescence signal intensity is set to zero, often referred to as “bleaching”. When the grains are subsequently concealed from daylight, e.g. by burial, they again begin to accumulate a trapped-electron population until sampling. By measuring the luminescence intensity, the last zeroing event is datable.

the sampling site. Given a constant  $D_0$  throughout the time of burial of a sample, its luminescence age is calculated by the simple equation:

$$\text{age (ka)} = \text{equivalent dose } (D_e \text{ in Gy}) / \text{dose rate } (D_0 \text{ in Gy/ka})$$

Luminescence dating of 20 samples from the Great Sand Sea was carried out using either the OSL response of quartz or the infrared-stimulated luminescence (IRSL) emission of potassium-rich feldspars. For  $D_e$  measurements, multiple- and single-aliquot techniques were used (aliquots are subsamples) (Fig. 11). Dose rates were calculated from radionuclide concentrations in the bulk sediment samples, as determined by neutron activation analysis (NAA).

All relevant details regarding the different techniques applied in the present study will be discussed in Section 5.2; for more detailed information on luminescence dating and the protocols involved, the reader is referred to the literature. The most comprehensive account of luminescence dating has been given by Aitken in his books on TL (Aitken, 1985) and on OSL (Aitken, 1998). Recently, the state of the art regarding OSL dosimetry has been presented by Bøtter-Jensen et al. (2003), who include detailed descriptions of the OSL properties of quartz and feldspars used as natural dosimeters, and of the application of OSL for geological dating. Wintle (1997), Clarke et al. (1999), Murray and Olley (1999), Stokes (1999) and Duller (2004) discuss the various methods and protocols used in luminescence dating, and review recent advances in OSL dating of Quaternary sediments.

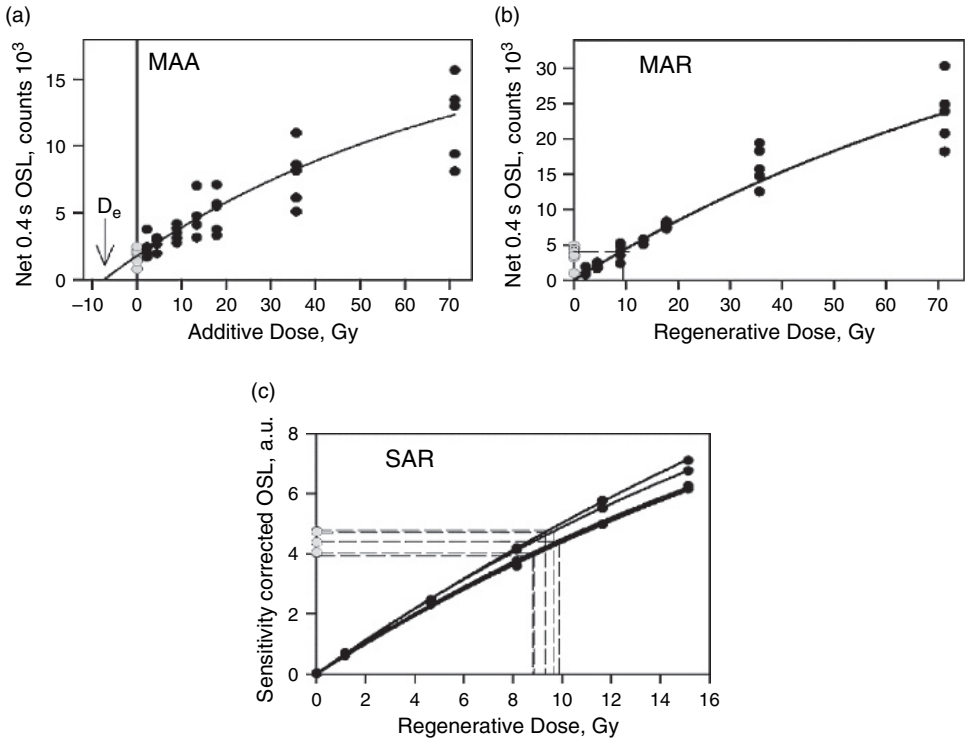


**Fig. 11** Methods of luminescence measurements for equivalent dose determination. OSL growth curves for quartz samples extracted from aeolian sand using the multiple-aliquot additive (a) multiple-aliquot regenerative (b) and single-aliquot regenerative (c) dose protocols (a and b from Hilgers et al., 2001). Each multiple-aliquot measurement results in one equivalent dose estimate only, with its error determined from the mathematical uncertainty with which the OSL growth curve is defined. In contrast, each single-aliquot measurement yields an equivalent dose value (here growth curves are shown from five different aliquots from the same sample). The  $D_e$  estimate is finally calculated from the mean of the results obtained from several sub-samples with the error derived from the deviation of the individual values about the mean. For the multiple-aliquot data, the results show a large degree of scatter about the fitted growth curves, despite the use of a normalization procedure. This scatter is due to differences in behaviour and problems of normalizing between the aliquots, and results in substantial errors of the  $D_e$  estimate. In contrast, the single-aliquot data show very little scatter away from the fitted growth curve, and correction is possible for differences in behaviour among the grains (such as changes in luminescence sensitivity). With only little scatter of the five individual equivalent dose values, a much higher precision of the derived equivalent dose is achievable.

### 2.3.6. Meteorological observations

During all field campaigns, climatic parameters were measured three times a day whenever possible. Depending on the daily programme, on difficulties with the vehicles and on the time of setting up camp in the evening, it was not always

possible to use the same hours for the readings. Efforts were made to use the time just before sunrise (6–7 am), lunchtime (1–2 pm) and 7 pm in the evening. Apart from the first transection in the eastern sand sea, where an anemometer was not yet available, wind velocity (wind path) and wind direction were measured at a height of 2 m (on the windward side of the camp). Dry and wet temperatures were measured with an Assmann aspiration psychrometer, allowing the calculation of the relative humidity. The degree of cloud cover and special events like sandstorm, rain drops, dewfall, hoar frost, etc. were observed and entered into the field diaries. To verify the minimum temperature before sunrise, a minimax thermometer was laid out.

The data from 1996 (eastern transection) and 1999 (middle transection), together with the measurements during a similar expedition in northern Sudan in 1997, and together with readings during field work along the Abu Muhariq in Egypt in 1999, were analysed and compared to the regional climate by Bergmann (2000). Bergmann, applying special climatological and mathematical-statistical methods and procedures, achieved a comparative study in spite of the spatial and temporal differences in the measurements. For these reasons, the meteorological observations are not discussed in a special section, but may be mentioned in the text.

A new meteorological station of the Collaborative Research Centre 389 ACA-CIA was installed in Balat in the Dakhla Oasis at the end of 2003. First results concerning the wind field are particularly interesting and are discussed in relation to the Holocene dunes in Section 3.3.4.



This page intentionally left blank

## TOPOGRAPHY OF THE GREAT SAND SEA

### Contents

3.1. Geological Setting and Bedrock Topography	33
3.1.1. Geological formations and their spatial pattern	33
3.1.2. Bedrock landforms	34
3.1.3. Reconstruction of palaeo-drainage systems by digital elevation data (O. Bubenzer and A. Bolten)	39
3.2. The Pleistocene Draa	46
3.2.1. The southern longitudinal draa of the trades	49
3.2.2. The northern transverse draa of the westerlies	52
3.3. The Holocene Dunes	58
3.3.1. Dunes on the transverse draa	59
3.3.2. Dunes on the longitudinal draa	60
3.3.3. The southward progradation and the northern extension of dunes	67
3.3.4. Comparison with modern winds	68
3.4. The Sand Budget	71

Regarding its geomorphology, the Great Sand Sea consists of three units or land-form generations in a vertical succession. The oldest generation is represented by the bedrock surface exposed in the corridors between the sand ridges. The ancient megadunes represent the second generation, and the smaller, modern dunes on top are the third generation. These generations influence each other; the influence of the respectively lower/older unit on the upper/younger one being greater than vice versa. The external boundaries of these units are not identical; the area of the youngest dune generation is much larger than the area of megadunes. In order to reduce the complexity, the generations are discussed separately. Their influences and interactions, however, are pointed out, as far as this can be done without considering the sedimentological analysis.

### 3.1. GEOLOGICAL SETTING AND BEDROCK TOPOGRAPHY

#### 3.1.1. Geological formations and their spatial pattern

According to the Geological Map of Egypt 1:500 000, sheets NH 35 SW Siwa, NG 35 NW Sakhret El-'Amud, NG 35 SW Wadi El-Qubba and NG 35 SE Dakhla

(Klitzsch et al., 1986–1987), the bedrock consists of a succession of Cretaceous to post-Miocene sedimentary units, that continually decrease in age towards the north. In the south, the succession starts with the Early Cretaceous Sabaya Formation leading via the Late Cretaceous formations (Maghrabi, Taref, Quseir, Duwi, Dakhla with Ammonite Hill Member) and the Early Tertiary formations (Tarawan, Naqb, Moghra) south of the Siwa Oasis Depression to the post-Miocene Minqar El-Talh Formation. In two places, the general succession is spatially inverted: the Dakhla Formation appears around  $25^{\circ}30'N$ , south of the older Ammonite Hill Member, and the post-Miocene Minqar El-Talh Formation appears around  $27^{\circ}40'N$ , south of the Miocene Moghra Formation that only forms the surface from  $28^{\circ}N$  to Siwa. According to their respective depositional environments, the sedimentary facies vary strongly. Almost all of them, however, contain sandstones which have been potential sand sources for the Great Sand Sea. Only the Palaeocene Tarawan Formation and the Eocene Naqb Formation entirely consist of limestones. Even the Dakhla Formation, mainly consisting of shales, contains sandy intercalations.

The complete succession is only met along the eastern transection, where small outcrops in the sandy corridors are found even in the north. Along the middle transection, the bedrock can only be traced up to the Ammonite Hill Member of the Dakhla Formation, because north of  $26^{\circ}20'N$  the sand cover is thick and continuous, also according to the geological maps. Along the western transection, the last outcrops are already found at  $25^{\circ}25'N$ . The succession can be deduced, however, from the close western margin of the sand sea. The Late Cretaceous Taref Formation is followed by the Saad Formation (replacing the Quseir Formation) and by the Ben Afen Beds replacing the Dakhla Formation and perhaps the Duwi Formation. Even along the western margin, however, the bedrock can only be traced up to  $26^{\circ}45'N$ , where a large gravel plain (Sarir Dalma) from the west extends eastwards. North of this gravel tongue, near the Libyan border, more than 120 m of sands were penetrated in a test well of the Continental Bahariya Oil Company and 200–300 m of sands are seismically indicated, suggesting a depression in the bedrock (Haynes, 1982).

A comparable thickness was found in sands underlying the Zallaf Sand Sea in Libya (300 m of aeolian sands: McKee and Tibbitts, 1964). This suggests that an even older erg may have existed, which could also have been the case below the Great Sand Sea in Egypt. A good example of a superposition of several ergs of different ages are the Wahibah Sands and their surroundings in Oman (Warren, 1988) where the oldest dune sands were dated at 110 000–117 000 BP (Juyal et al., 1998) and at about 100 000–120 000 BP (Preusser et al., 2002). The corridors' sand cover in the Great Sand Sea increases from east to west. Besides, in the southwest the corridor deposits are distinctly coarser than the megadune sands, which cannot be stated for the middle and the eastern transections. According to Embabi (1998), 74.6% of the area is covered by sands.

### 3.1.2. Bedrock landforms

Including the sand cover in corridors, the surface is slightly sloping towards the north. Only few elevation points are found on the geological maps. Measurements

(Thommen and Alpin altimeters) could only be made along the transections and do not provide exact data. Comparing all measurements between 25°N and 27°N, the elevation gradually decreases from around 500 m a.s.l. in the south to around 200 m a.s.l. in the north. These values go together with elevations presented by Embabi (1998, his Table 2). Along the eastern transection, however, a stronger decrease in elevation down to 250 m a.s.l. was already measured south of the 100 m high, south-facing Ammonite Hill Escarpment at 26°N (see Fig. 1 and Section 3.1.3.2). The surface above, however, is also more inclined towards the north. The elevation, therefore, goes down to 230 m a.s.l. already at 26°20'N, whereas the elevation at this latitude is still 250–280 m a.s.l. on the middle and on the western transection. Along the middle transection, the surface is generally slightly higher than in the east and in the west, particularly north of the Ammonite Hill Escarpment that is only weakly developed here and forms a low ridge around 26°–26°20'N.

The east–west differentiation of the geological formations seems to have influenced the topography of the bedrock. In the east, the petrographic properties vary considerably, and many intercalations like shales, limestones, ammonitic and nummulitic layers are present in the sandstones, leading to the formation of scarps. In the west, the formations are very homogeneous and seem to consist almost exclusively of sandstones, sometimes containing palaeosols. Weathering conditions supporting granular disintegration have led here to a more subdued relief than in the east. In addition, the sand cover thickens towards the great subsurface depression in the northwest, masking irregularities in the bedrock surface.

Along the eastern and the middle transections, the southern Sabaya Formation that, according to the geological map, consists of coarse- to medium-grained floodplain sandstones interbedded with channel deposits is eroded into a rugged terrain. Scarps with outliers are dissected into many small hills with their steeper slopes facing south, consistent with the northward dip. The channel sandstone of the Maghrabi Formation, for example, is dissected into many debris-covered hills that stand up to around 20 m above the corridor floor. In addition, it crops out in the megadune flanks. Subaqueous (delta) and aeolian cross-bedded units are exposed where sandblasting has destroyed the dark weathering crust of the surface. The prominent scarp remnants of both geological formations are starting points of lee or shadow dunes (Fig. 12). The same holds true for the fluvial and aeolian sandstones of the Taref Formation that frequently form red hills up to 10 m high. In the Quseir Formation, that is widely distributed along the middle transection and is rich in shales, the terrain is more subdued. Nevertheless, it has small back scarps looking north. The most resistant weathering remnants are spherical quartz geodes with cauliflower-like surfaces.

The glauconitic sandstones of the Duwi Formation are only found around the first coring site (Regenfeld 96/1–2; Fig. 2) and form small plateaus above a large palaeo-pan or playa depression (Riemer, 2003, 2004a, 2005) in the corridor. Below the dune-sand cover at the eastern and the western bases of the investigated megadune, a dark red loam (2.5 YR 4/4) with desiccation cracks filled with yellow blown sand is preserved (Fig. 13). The Dakhla Formation is mainly represented by carbonate-bound siltstones and sandstones of the Ammonite Hill Member, rich in ammonites. It produces the most conspicuous escarpment in the Great Sand Sea. Rising in steps of 10–20 m, it reaches a maximum height of almost 100 m in the east

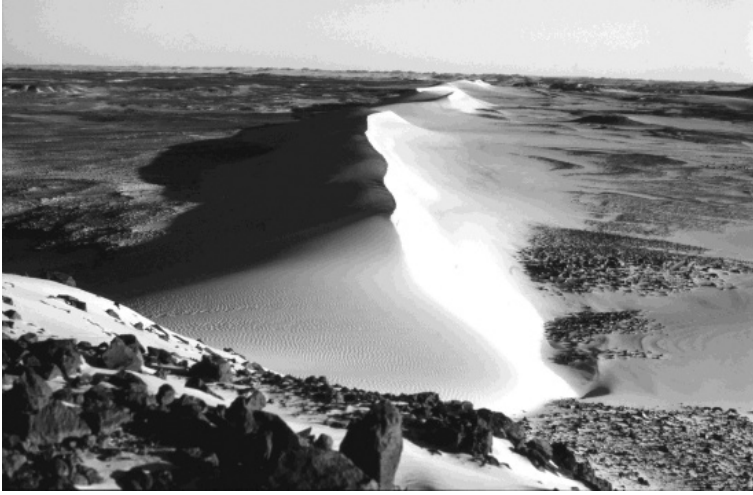


**Fig. 12** Looking SSE onto the starting point of a typical lee (shadow) dune behind a small sandstone hill south of the middle transection. The rather straight shape in the foreground changes into a sinuous pattern farther away from the hill. The depression between hill and dune is due to the steep hillslope causing vortices in the air flow (photo, 28 February 1999).

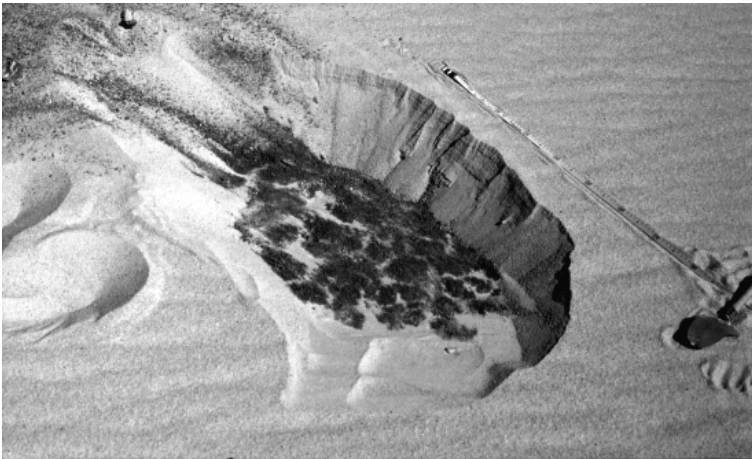


**Fig. 13** Excavation at the western base of the draa on the 11th cross-section at Regenfeld on the eastern transection: red playa sediment with desiccation cracks filled with yellow blown sands that form a 20–30 cm thick cover (scale is 2 m long; photo, 3 March 1996).

(compare Section 3.1.3.2). Obviously, the escarpment was an obstacle that interrupted the formation of megadunes, which was already noticed by Bagnold (1931). The northern dip slope is scoured by the wind. The height of the escarpment decreases towards the west and only reaches 10 m along the middle transection.

Moreover, it is dissected into sand-blasted conical hills, heavily mantled by debris. In some places, only the spherical case-hardened bases are the last remnants, strongly resembling man-made stone circles.

The younger formations of the north are not found at all on the middle transection. On the eastern transection, only tiny remnants arise from the flanks of megadunes. A 20 m high scarp cropping out at the base of a megadune at 27°04'N, 26°35'E appears as the Eocene Naqb Formation (nummulitic platform limestone) on the geological map and is of special interest. The scarp consists of sandstone capped by limestone which is characteristic for the post-Miocene Minqar El-Talh Formation, of which remnants overlie the Naqb Formation. Close to the sand sea, the Minqar El-Talh Formation starts farther north (see Section 8.6.3.4). North of 28°N, the bedrock consists of continental to marine clastic sequences of the Moghra Formation, exposed in great scarps, back scarps and large basins with numerous channels.

Apart from a few tiny outcrops (see below), the bedrock is not exposed along the western transection, not even in the very wide corridors. In the south, the surface consists of red (5 YR) alluvial material of various grain sizes and shapes (up to very well rounded pebbles) that, according to the granulometric analysis, is slightly deflated. The undulating surface of the quartzitic Taref Sandstone with weathering crusts is buried beneath some tens of centimetres of gravels. A Middle Pleistocene age was suggested for the corridor sands by Embabi (1998, 2004) because of Acheulean artefacts found by Pachur and Röper (1984). Acheulean artefacts were also found at Willmann's Camp (Glass Area 81/62, Riemer, 2005; see Fig. 2) on a playa floor and below younger alluvial sands at the contact between the megadune and the corridor. This site also yielded younger stone implements in the vicinity of a large palaeo-pan (Haynes, 1982). At least six successions of dune sands alternating with playa deposits are exposed (Fig. 14).

This seemed to be a very promising site with regard to luminescence dating. Therefore, a dredger – transported on a heavy lorry – was brought to Willmann's Camp during the final field campaign in 2006. A trench, 50 m long and several metres deep, was excavated in slightly sloping terrain. The stratigraphic record comprises 11 layers of calcareous playa material and intercalated aeolian sands. Twenty-four samples for sedimentary analysis and 12 samples for OSL dating were collected. The surrounding sediments are exceedingly red. Pieces of desert glass were found below the megadune sands, and exposed pieces were more sand-blasted than the Acheulean artefacts (Haynes, 1982). Pachur and Altmann (2006) mention playa deposits and intercalated dune sands also in the southern sand sea north of the Gilf Kebir Plateau.

The following western corridor is part of the true Desert Glass Area, where chunks of desert glass are abundant and were used as material for prehistoric implements. The clear, apple-green silica glass was first mentioned by Clayton and Spencer (1932). It is supposed to be the product of an ancient meteoritic impact 28.5 million years ago. Meanwhile, more than 190 contributions on this phenomenon have been published. A special congress was dedicated to this event in 1996. The controversial debate, however, about the origin of the desert glass is still going on (De Michele, 1997). The glass was used in situ to produce artefacts (Fig. 15). Later, apparently it was a precious gemstone, since a desert-glass scarab is set in the centre of a pectoral of Pharaoh Tut-anchamun. The archaeologists in our team documented and investigated



**Fig. 14** Test dig at Willmann's Camp in 2000: thick layers of calcareous playa deposits form small steps in the eastward sloping surface and protect the intercalated aeolian sands (photo, 12 March 2000).

the site and collected the pieces of desert glass to prevent the destruction of the place by tourists. In this corridor, the strongly weathered Taref Sandstone forms small ridges.

Along the transection, however, the only small scarp is found at  $25^{\circ}03'N$ , and a debris-covered ridge lies between  $25^{\circ}06'N$  and  $25^{\circ}12'N$ . Everywhere else the corridor is covered by alluvial material with a desert pavement protecting the subsoil

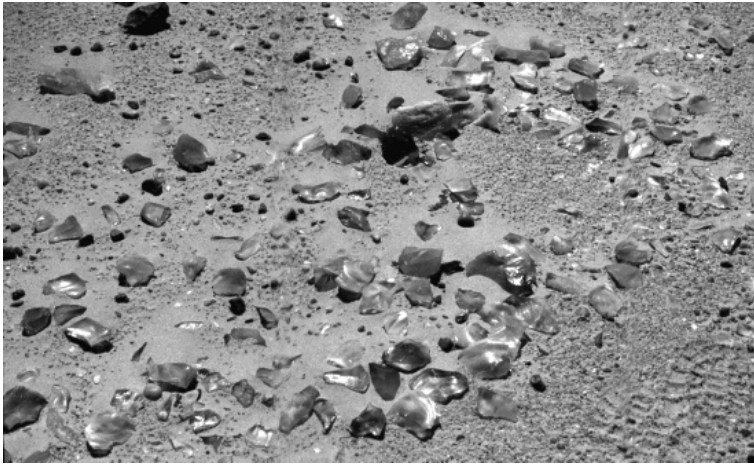


**Fig. 15** Prehistoric working site in the Desert Glass area: the light, glossy stones consist of desert glass. Most of them are sand-blasted, and some are worked artefacts (e.g. in the middle foreground; photo, 13 March 2000).

against deflation. At  $25^{\circ}25'36''\text{N}$ , an enigmatic ancient pottery was found (Riemer and Kuper, 2000; Riemer 2004b). A cut at this site down to a depth of 2 m did not reach the bedrock. Contrary to the surface, the subsurface material looks bleached and contains more gravels. According to Embabi (1998, 2004), fluvial and alluvial sands and gravels have been deposited by a Gifl Kebir river in the Oligo-Miocene. Kröpelin (1993) suggested a Middle to Late Tertiary age.

It may well be that the even surface in the western sand sea and the eastward increasing erosional features are the reason for the divergence of the megadunes that in the west run  $170^{\circ}$ – $180^{\circ}$  and in the east are aligned at  $165^{\circ}$ . The more pronounced relief would cause a frictional deviation of strong northerly winds (modelling the megadunes) towards the east (see Section 3.2.1).

### 3.1.3. Reconstruction of palaeo-drainage systems by digital elevation data<sup>\*,†</sup>

#### 3.1.3.1. Introduction

Like most ergs of the world, the Great Sand Sea of Egypt is situated in a topographic low (see Section 3.1.2). The reconstruction of ancient water courses that transported sediments into this depression provides a chance to differentiate between individual catchments and possible sand-source areas. In this context and based on satellite images and radar data, El-Baz (1998) suggested that sand was transported by palaeo-rivers from the Gifl Kebir Plateau northward into the

<sup>\*</sup>O. Bubenzer, E-Mail: olaf.bubenzer@geog.uni-heidelberg.de

<sup>†</sup>A. Boltzen, E-Mail: andreas.boltzen@uni-koeln.de



deepest part of the area during Pleistocene and Holocene humid intervals (Szabo et al., 1995). Pachur and Altmann (2006) assumed that the palaeo-drainage system was already generated during the Tertiary. Northerly winds prevailed during the Quaternary dry intervals accumulating the sand into (mega)dunes (see Sections 3.2 and 3.3).

Today, distinct wadis are visible particularly at the edges of the Gilf Kebir Plateau (Fig. 16) (Note the different spelling of wadi names according to the publications used). North of the plateau, the wadis (e.g. Wadi Hamra, Wadi El-Malik) disappear below the sands of the Great Sand Sea. In the east, the lower wadi courses (e.g. Wadi Maftuh, Wadi Bakht, Wadi Akhdar) are buried by the sands of the Selima Sand Sheet. The existence of a distinct palaeo-drainage system is proven in these two regions by radar data (McCauley et al., 1982; El-Baz et al., 2000). In addition, geoarchaeological investigations in the southern part of the Great Sand Sea have shown (Haynes, 1982; Bubenzer and Besler, 2005; Bubenzer and Riemer, 2007) that archaeological sites there – as well as in other parts of the Western Desert (Wendorf and Schild, 1980; Kindermann et al., 2006; Pachur and Altmann, 2006; Bubenzer et al., 2007) – are associated with remnants of Pleistocene and Holocene playa or lake deposits.

Unfortunately, completely sand-covered areas and sand thickness increase in the Great Sand Sea from south to north. A seismic exploration of the CONOCO oil

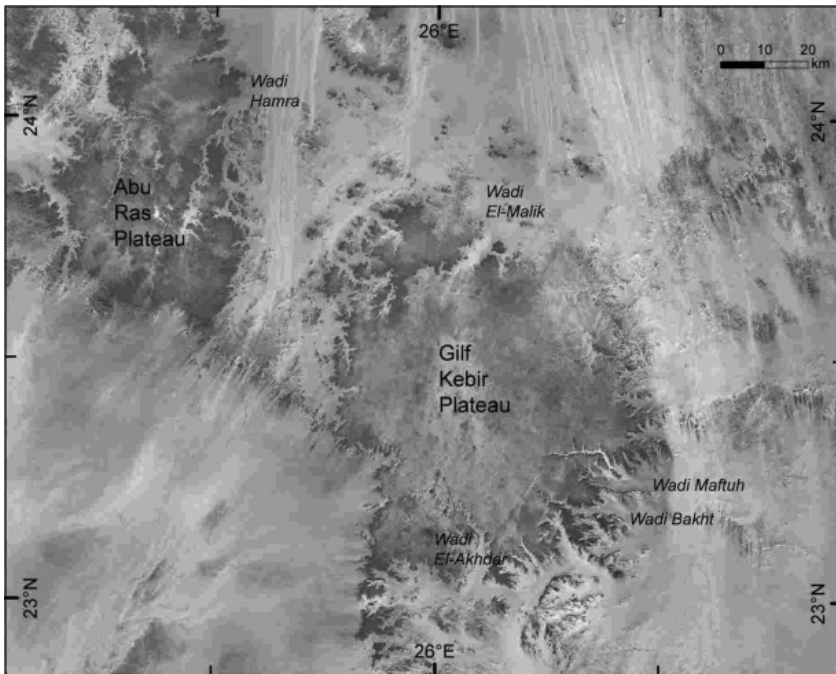


**Fig. 16** The Gilf Kebir and Abu Ras Plateaus. The wadis disappear below the sands of the Great Sand Sea (in the north) and the Selima Sand Sheet (in the east).

company, for example, recorded a sand thickness of 200–300 m in its northern part (Haynes, 1982). With regard to the fact that the radar data are able to penetrate only up to 5 m of sand, it is obvious that a detection of palaeo-drainage channels by radar data is not possible in most parts of the Great Sand Sea.

As described in Section 2.3.1, the ASTER and SRTM data allow the calculation of detailed elevation models. If the existence of palaeo-drainage systems beneath the (mega)dunes of the Great Sand Sea is assumed, it seems possible to gain information about ancient water courses by the calculation of an elevation model discarding the aeolian accumulations. Therefore, this section discusses how close such an elevation model can reflect the actual situation with regard to the drainage pattern, and to the catchments as possible source areas of sediments.

### 3.1.3.2. The potential bedrock relief and the hypothetical palaeo-drainage system

The reconstruction of the potential bedrock relief of the Great Sand Sea, void of (mega)dunes, needs an area-wide elevation model and therefore initially a virtual erasure of aeolian sand bodies. In Section 2.3.1.3, it is shown that it is possible to fill the SRTM-3 no-data regions by ASTER data because only a linear deviation between the two data sets exists (compare also Fig. 5(c)). Then the identification of areas in the Great Sand Sea that are not covered by (mega)dunes (i.e. corridors) was demonstrated by the calculation of a special slope map. The result is a new data set as a basis for a potential bedrock-relief map (Fig. 17) and for the calculation of a hypothetical palaeo-drainage system (Fig. 18). The outlet points used here indicate the endpoint of the drainage-line calculation and the starting point of the watershed estimation. Hence, the position of the outlet point does not affect the calculation of the drainage system. The specific position of the outlet points used in Fig. 18 results from the margins of the newly calculated elevation model. However, the outlet point of the Willmann's Camp region is exceptional (Fig. 18). For this archaeologically important region, a sub-watershed was derived from an ASTER elevation model. Table 2 contains additional information on the catchments, their size and their maximum and minimum elevation values.

Following these working steps, several preconditions and restrictions have to be born in mind. First, the amount of data decreases from south to north due to the increasing sand cover. Second, the topography beneath the (mega)dunes is not known and has to be interpolated from the corridor areas as a flat plain. Consequently, the calculated drainage lines are probably incorrect in some parts; nevertheless, they will show a general drainage direction. Third, the described procedures are suitable to erase the aeolian accumulation bodies but not the possibly existing sand sheets that most probably mask the old water courses completely. These constraints demonstrate that the calculated results have to be interpreted carefully and must be regarded as tentative.

A look at the hypothetical palaeo-drainage map (Fig. 18) shows, however, that the data set is able to reflect the correct location of the visible wadis in the southern Great Sand Sea, the radar rivers (cf. El-Baz, 2007) and, in addition, their possible

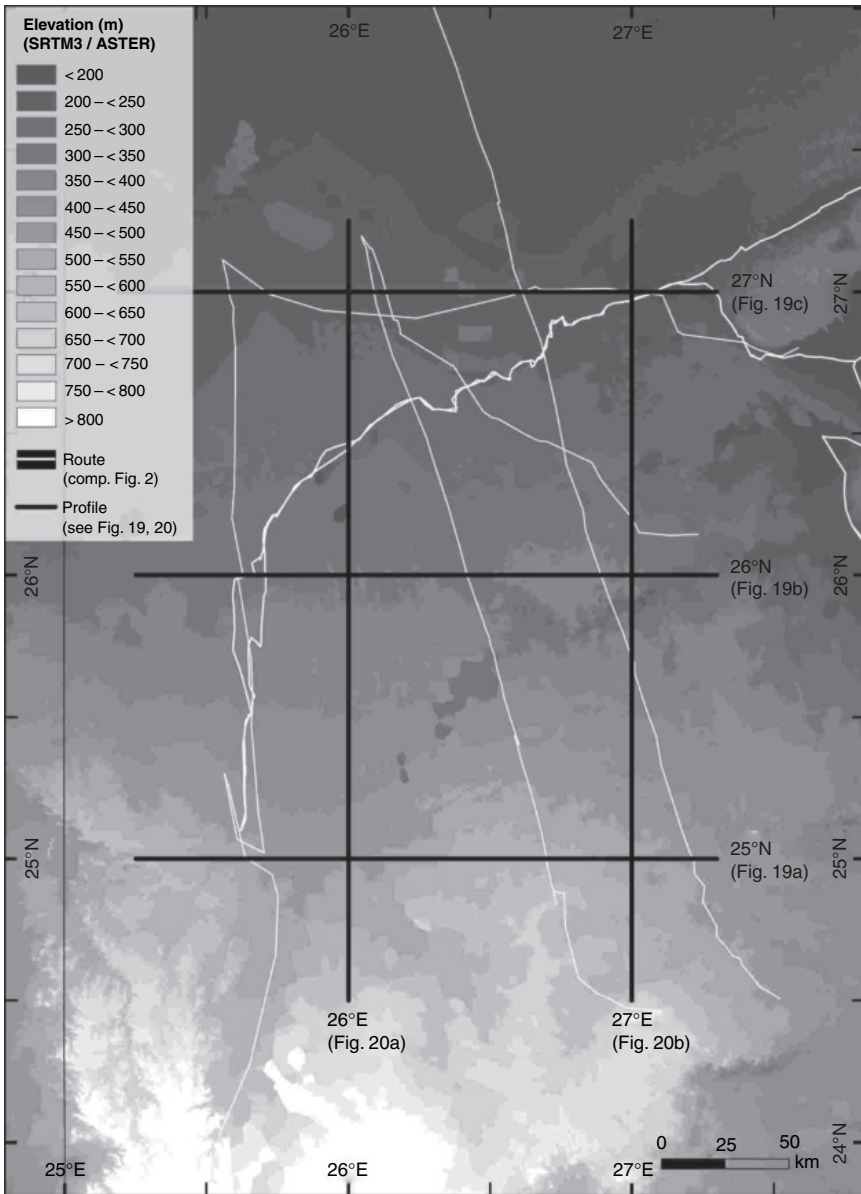


**Fig. 17** New elevation dataset of the potential bedrock relief of the Great Sand Sea. White lines represent the routes of investigation. The bold black lines mark the position of profiles presented in Figs 19 and 20. For further information, see Section 3.1.3.2.

northward continuation. In general, a downward gradient from south to north becomes obvious. Therefore, the Gilf Kebir Sandstone most probably is the main source for the sands in the Great Sand Sea. The catchment area of the archaeological site “Willmann’s Camp” in the southwestern part of the map was calculated

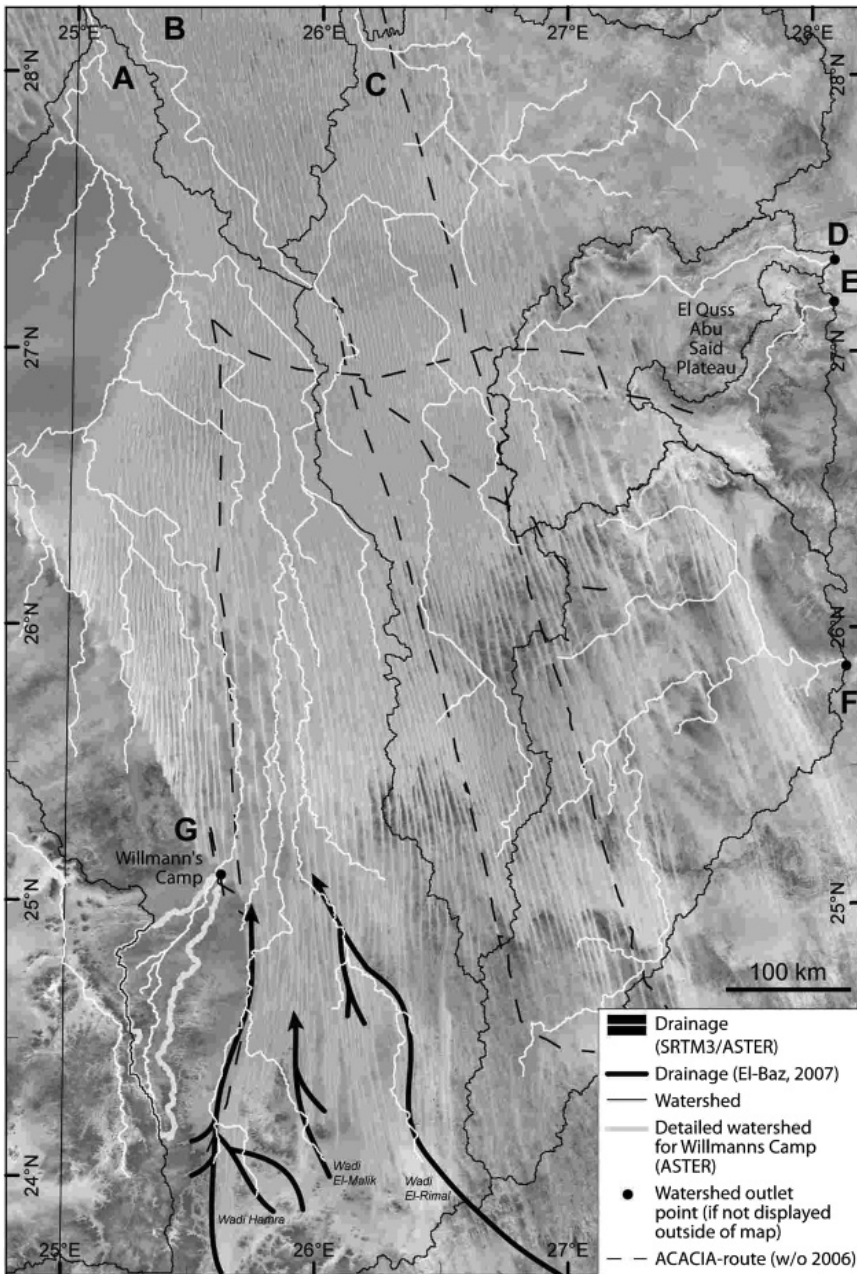


**Fig. 18** Drainage system of the Great Sand Sea as reconstructed on the basis of the newly generated bedrock-elevation model (see Fig. 17). The letters that mark the catchments (A–G) are explained in Table 2. Wadi names from El-Baz (2007).

**Table 2** Additional parameters of the catchments presented in Fig. 18, derived from the newly generated bedrock-elevation model: sizes and differences in elevation

Catchment (see Fig. 18)	Size (km <sup>2</sup> )	Maximum elevation (m)	Minimum elevation (m)
A	61 323	913	127
B	6 101	332	122
C	28 699	678	105
D	8 687	358	30
E	4 160	416	36
F	23 081	837	105
G	1 594	878	486

A: Western catchment from the Gilf Kebir and Abu Ras Plateaus.

B: Northern catchment.

C: Central catchment.

D: Catchment north of El Quss Abu Said towards the Farafra Depression.

E: Catchment south of El Quss Abu Said towards the Farafra Depression.

F: Eastern catchment directed towards New Valley.

G: Sub-catchment feeding the archaeological site Willmann's Camp.

separately with the ASTER data set. The limits of the western catchment are very similar in both the ASTER and the new combined data sets. Since the SRTM data are complete in this part of the Western Desert, the latter data set is composed only of SRTM data. Again, the conformity of the western catchment-area limits demonstrates that the two data sets are compatible in their position accuracy ( $X$ - and  $Y$ -values). The correction of their height deviation ( $Z$ -value) is described in Section 2.3.1.3.

In addition to the northward trend of the hypothetical water flow, a division of main catchment areas into a western and an eastern part is apparent. This division probably points at two different sand sources, one more from the eastern margin, the other one more from the western margin of the Great Sand Sea. Furthermore, a linear structure of pixels with lower altitudes runs from northeast to southwest (Fig. 17) around 75 km SW of the El Quss Abu Said Plateau (Fig. 18) (see Section 3.1.2). This structure most probably marks the extension of a major fault that is displayed on the geological map only east of the sand sea (Klitzsch et al., 1987, sheet NG 35 NE Farfara; Pachur and Altmann, 2006). This explains the dissected bedrock on the eastern and – to a lesser degree – on the middle transection. The prominent Ammonite Hill Escarpment obviously represents the northern side of the fault (see Section 3.1.2).

Along three latitudes (Fig. 19) and two longitudes (Fig. 20), profiles were generated for a better characterization of the topography below the Great Sand Sea. The profile at 25°N (Fig. 19(a)) clearly shows the northward influence of the Gilf Kebir Plateau from approximately 26°E to approximately 27°E as well as the position of the Wadi Hamra at about 25°45'E. The comparison of the profiles at 26°N and 27°N (Fig. 19(b, c)) seems to demonstrate that the surface roughness is higher at 26°N than at 27°N. The reason could be the decreasing amount of elevation information from south to north already mentioned, which would cause

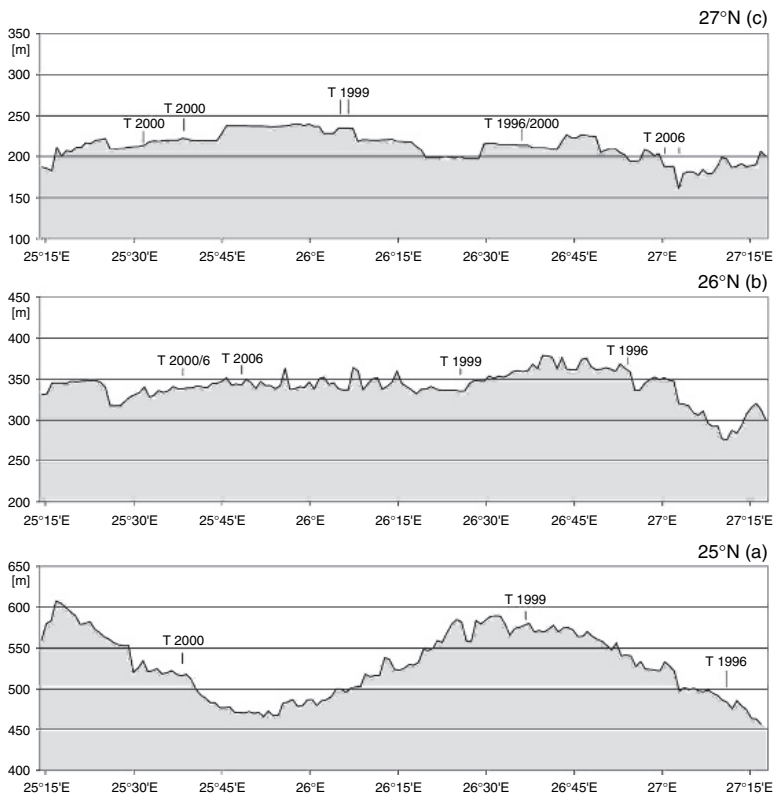


**Fig. 19** Profiles along 25°N (a), 26°N (b) and 27°N (c) of the newly generated potential bedrock-elevation model (see also Fig. 17). The labels refer to the various ACACIA-routes. For further information, see Section 3.1.3.2.

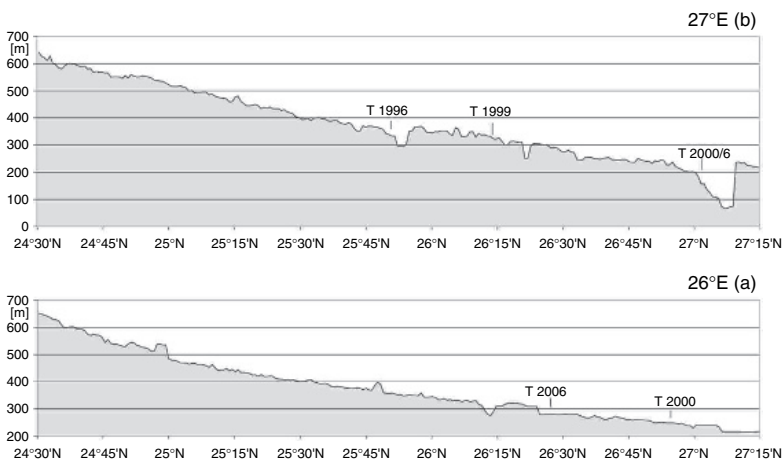


**Fig. 20** Profiles along 26°E (a), 27°E (b) of the newly generated potential bedrock-elevation model (see also Fig. 17). The labels refer to the various ACACIA-routes. For further information, see Section 3.1.3.2.

a smoother profile run. Clearly visible are the low elevation values between 27°E and 27°15'E in the 26°N profile (Fig. 19(b)) that are due to the fault, and are particularly conspicuous in the longitudinal profile (27°E, Fig. 20(b)) between 25°45'N and 26°N. Both longitudinal profiles (Fig. 20) show the general elevation gradient from south to north. The abrupt elevation increase north of 27°N in the 27°E profile (Fig. 20(b)) indicates the rise of the Nummulite Scarp by more than 100 m (mentioned by Pachur and Altmann, 2006).

### 3.1.3.3. Conclusions

New digital elevation data were used to derive a potential bedrock relief of the Great Sand Sea without (mega)dunes as a base for the reconstruction of a possible drainage system. With regard to the hypothetical catchment areas as possible sand sources and their drainage lines as routes of sand transport into the Great Sand Sea, we conclude that the main and general gradient is from south to north, as already suggested by McCauley et al. (1982) and El-Baz (1998). The currently known radar-discovered channels extend farther north below the (mega)dunes. Therefore, the sandstone of the Gilf Kebir probably is the main source of the sands that later were accumulated in (mega)dunes by aeolian processes. In addition, the extension of a tectonic fault from outside the Great Sand Sea could be traced below the (mega)dunes towards SW, which explains the greater surface roughness in the southeastern sand sea. Although a sand source in the west, mainly from the Sarir Dalma, is also likely (see Section 8.6.3.5), a drainage system directed to the east is not detectable with the elevation data. This is due to the sand cover that masks possible drainage channels in the bedrock. Especially in this region, for which no radar data exist up till now, rivers beneath the sand cover may be found by radar. Appropriate data and new topographic data, also badly needed for the whole Eastern Sahara, will be available in the near future from the German TerraSAR-X satellite, which started successfully on 15 June 2007 (<http://www.dlr.de/rd/fachprog/eo/terrasar-x>, DLR Raumfahrtagentur).



## 3.2. THE PLEISTOCENE DRAA

Before discussing the megadunes in the Great Sand Sea, it must be emphasized that megadunes or draa are distinguished from dunes by their dimensions and particularly by their wavelength (>1 km). While dunes are formed by surface winds only, the entire Planetary Boundary Layer of the atmosphere (the lower kilometre where the free air flow is influenced by the frictional effects of the earth's surface; see Fig. 21) is involved in the modelling of draa, which explains their greater dimensions. Because of the completely different aeolian dynamics, dunes and draa have to be considered separately.

Today, most draa are covered by smaller Holocene dunes. Any approach to understand the complex features as a unit leads, however, necessarily to misunderstandings and failures in the interpretations because of the different formation

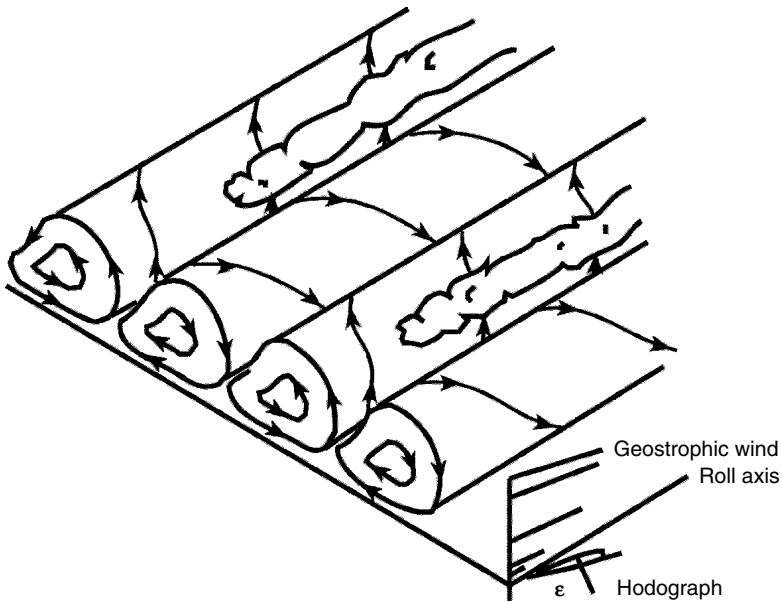


**Fig. 21** Typical secondary flow in the Planetary Boundary Layer. The turning of the wind from freestream (geostrophic) to the surface through angle  $\epsilon$  is shown (reproduced from Brown, 1983, with author's permission). Draa accumulation occurs below the cloud streets.

processes. Many examples of this can be found in the literature (see below). In the following, only the term “draa” will be used because the term “megadune” tempts to neglect the “mega” and to think of dunes, which should be prevented. To better understand the concept of draa formation and its importance, and because there is still confusion in recent literature, a brief account of the developmental history of the draa concept and also of its progressive use is necessary. The following citations originally do not mention the term draa, which here is only introduced for clarification.

In the Great Sand Sea, Bagnold (1931) already noticed the difference between dunes and draa that he called whaleback dunes or whalebacks, on the basis of their shape. Later, Kádár (1934) described the combination of whalebacks and barchan dunes on top as characteristic for “Libyan Dunes”. In southern Arabia, Bagnold (1951) cited Thesiger, who distinguished between four dune types: dune chains, downs, crescents and sand massifs. Dune chains were described as longitudinal dunes with a base width of up to 2 miles (3 km) and with or without crestlines on top. In the Algerian Sahara, Behrmann (1932) distinguished between stable dune ridges (Dünenwälle) and mobile crests on top. Aufrère (1932, 1934), also observing the difference between draa and dunes in Saharan ergs, supported the hypothesis of Madigan (1936), who assumed that the corridors were erosional features and the draa – as the remaining parts of a former uninterrupted sand body – were a by-product. In Inner Persia, Gabriel (1934) noticed that the dunes (draa!) did not change their position.



Brosset (1939) was the first author who mentioned Dzrâa, meaning only the vegetated draa in the southern Sahara, in contrast to the unvegetated Algerian ergs. In the Fezzan, Kanter (1943) observed the finer dune sands and coarser sands of the draa, the immobility of the latter and their inconsistency with regard to modern wind systems. Therefore, he tried to explain the corridors as ancient fluvial channels. In the Great Western Erg, Capot-Rey (1945) also suggested the corridors to be part of a fluvial system. In his book on the Sahara, Gautier (1950) explained the longitudinal draa and the corridors (*gassi*) as phenomena resulting from an underlying bedrock relief. From the “Ramla des Daouada” in the Fezzan, Bellair (1951) reported that calcretes formed terraces in the draa flanks 6–10 m above the corridor floor, a clear case of erosion. Bagnold (1953) was one of the first to postulate that longitudinal vortices in the atmospheric Boundary Layer might be the reason for these long parallel dunes. Smith (1968), who compared Nebraska dunes with those of North Africa, mentioned long (16 km) ancient dune ridges with a width of 1 km, now topped by soil layers and vegetation. These dimensions suggest that draa formation has taken place also in North America.

In 1969, two articles in meteorological journals connected helical vortices in the Planetary Boundary Layer to phenomena like streets of seaweed and of clouds as well as – for the first time – to longitudinal sand dunes. This observation was also based on experiments (Hanna, 1969; Wippermann, 1969, 1973). Hanna listed the important prerequisites for the formation of these counterrotating helical vortices and therefore for the modelling of draa (see Fig. 21): flat underlying terrain, little variation with height in the direction of the wind, above-normal wind velocities, strong curvature of the wind profile and unstable lapse rate of temperature near the surface. Capot-Rey (1970) was one of the first to use the term “draa” for dune chains in the northern Saharan ergs (Erg Igidi, Great Western Erg and Great Eastern Erg). He also mentioned distances of 2–3 km between the parallel longitudinal ridges, a pattern he found particularly well developed in the Aleb dunes of Mauritania. In a short but very important note on sand waves, Wilson (1972) statistically distinguished between ripples, dunes and draa(s) based on their wavelength and grain size. In addition, he noted that with regard to these parameters no transitions exist between dunes and draa(s), and therefore he concluded different formation mechanisms. Already in 1973, the term “draa” in combination with helical vortices, called “Taylor-Görtler Motion”, appeared in the text book by Cook and Warren, but for many years the literature on sand seas did not take notice of this concept.

The draa concept was applied to the Namib Erg (Besler, 1980, 1984a) and was found to be the only model that could explain all given phenomena without any contradiction. The dimensions as well as the erosional features, found elsewhere in the corridors, and a high age fit into this model. For the stronger winds needed, only a small equatorward shift of the present zone of high wind velocities around the mouth of the Orange River – which was highly probable during the Pleistocene – would have been necessary. In fact, in a region with a scarce sand supply south of the Namib Erg, where wind gusts frequently reach velocities of 80–100 km/h, Corbett (1993) observed several modern barchan streets with spacings of 1–2 km. Draa were found to be the legacy of cold Pleistocene epochs (the glacials) with stronger winds (because of the higher temperature and pressure gradients). Today, they are covered

by secondary dunes. Meanwhile, a Pleistocene age has been found for many draa, e.g. in Mali (Petit-Maire 1994, from proxy data), southern Africa (Stokes et al., 1997), Mauritania (Lancaster et al., 2002) and Oman (Preusser et al., 2002).

An earlier volume of this book series (Brookfield and Ahlbrandt, 1983) on aeolian sediments and processes contains important contributions to draa and the draa concept. Longitudinal draa are recognized in the Permian sands of North-East England (Steele, 1983; Chrintz and Clemmensen, 1993). The flow in the Planetary Boundary Layer and its role in the formation of draa are highlighted and informatively illustrated (Brown, 1983). On the other hand, Lancaster (1983) still tried to explain the Namib draa by modern winds, although he recognized later (Lancaster, 1989) that the controlling factors for dunes and draa seem to be different. Comparing the Namib Erg with the Wahibah Sands in Oman, he finally came to the conclusion that the draa are not in equilibrium with modern winds (Lancaster, 1998). Livingstone and Thomas (1993) stressed the point that the longitudinal Namib dunes are active today, which is in contradiction with Besler's (1980) findings. Here the importance to distinguish between draa and dunes becomes obvious, because only the draa are supposed to be inactive, and secondary dunes may alter the shapes of draa and advance ahead (supporting measurements were provided already by Besler, 1975). Some authors see the genetic difference between draa and dunes but, nevertheless, think of both features as present-day formations. In his remote-sensing study on the Libyan sand seas, Linsenbarth (1996) distinguishes the sand ridges formed by helical vortices (= draa) from the dunes. However, the present-day wind directions and their sand-drift potential are used to explain the sand-ridge pattern.

In summary, the difference between dunes and draa had been noticed by geoscientists a long time ago. The formation dynamics of draa, however, were only recognized with the aid of the atmospheric sciences. Draa are found in all sand seas of the world and are of Pleistocene origin. They are distinguished from dunes by their larger dimensions (especially length and spacing), the threshold wavelength lying around 1 km. The conspicuous pattern of sand seas seen on satellite images is a legacy of the Pleistocene. In the case of the Great Sand Sea, however, the uniformity suggested on satellite images (Fig. 2) is rejected by the field survey. This sand sea has been found to consist of two different types of draa. This emphasizes the importance of a field check.

### 3.2.1. The southern longitudinal draa of the trades

Draa patterns in deserts near the tropics are usually connected with trade winds because the alignments of the draa more or less match the prevailing wind direction. Regarding the Great Sand Sea, the trade winds evolve at this latitude and increase southward in strength. According to the model (Wippermann, 1973; Brown, 1983), the counterrotating helical vortices of the Taylor-Görtler Motion in the Planetary Boundary Layer made sands accumulate beneath their opposite ascending branches and induced sand erosion below their opposite descending parts. On the northern hemisphere, the vortex axis deviates about  $15^{\circ}$ – $20^{\circ}$  to the left from the geostrophic wind (Fig. 21). The draa in the sand sea run  $170^{\circ}$ – $180^{\circ}$  in the west and

165° in the east, which was already noted by Bagnold (1931). Kádár (1934) mentioned directions of 165°–175°. This would imply a geostrophic wind around 345°–360°. This is, however, a very rough estimate because the divergence of the draa already shows that the frictional effects of the land surface induce a strong influence. Speculations about the origin of the palaeo-tradewinds and the position of the palaeo-anticyclone are not realistic.

In this context, an article on aeolian erosional lineations by Brookes (2001) is of interest. He found long, 1–5 km wide, wind-scoured “streets” in the Dakhla region. Oriented at 160°–180°, they cross plateaus and bear no evidence of modern sand transport. Because several younger small-scale aeolian erosion cycles could be detected, he assigned the large-scale features to the pre-Holocene. Steffan (1983), who in his remote-sensing study on aeolian accumulations in the eastern Sahara clearly distinguished between draa and dunes, nevertheless compared the draa to the calculated sand-transport resultant of the summer seasons and found a consistent alignment. He seems to see the draa as well as the dunes as modern products of the atmospheric circulation. This is another example of the confusion resulting from insufficient knowledge about the formation dynamics.

According to Brown (1983), the wavelength of the draa generally represents twice the Boundary Layer depth, but it also depends on the friction. In the Great Sand Sea, the wavelength is 3 km in the east and 2.5 km in the middle and in the west. The exception is a conspicuous disruption of this pattern north of several channels (e.g. Wadi Hamra) from the Gifl Kebir Plateau, where the interdraa corridors are extremely wide and the draa shorter. Kröpelin (1993) even mentioned 1–10 km wide corridors; the latter value, however, is an exception over a short distance. The western transection runs along the western margin of this irregularity which could have been provoked by ancient alluvial fans of the Gifl Kebir rivers providing relief and/or abundant coarser material (see Section 3.1). Therefore, it is assumed that this has been the centre of the fan. In addition, even after the beginning of draa formation, ephemeral heavy flood events could have created channels and dissected younger draa (see Section 5.4). Because heated air is rising above the draa and fixes the position of the vortices, the draa grow in a feedback mechanism, and a system once installed is not easy to change (Brown, 1983).

Usually, the coarser material of fans is deposited in their proximal parts. It is therefore surprising that, immediately north of the Gifl Kebir, the wavelength of the draa is homogeneous and again reduced to 2.5 km. Obviously, fine-grained material was amply supplied. This can be explained by a lateral inversion of gradation (which means coarsest materials in the distal part). This phenomenon is frequently observed in arid sedimentary basins where the aridization after a humid phase leads to a reduction of the transport capacity of endorheic rivers and therefore to a vertical gradation in the proximal parts of fans (a.o. Briem, 1977; Besler, 1992). With regard to this aspect, the draa pattern in the southwest of the Great Sand Sea allows the conclusion that the discharge from the Gifl Kebir did not cease abruptly but was very slowly petering out. Wilson (1973) mentioned wavelengths of 0.5–5 km from Algerian ergs. According to Brown (1983), longer wavelength circulation can be forced when the secondary flow in the Planetary Boundary Layer is confined, for example, by a capping inversion (temperature increase with height). Most probably,

this was not the case in the Great Sand Sea because the area of wider corridors is surrounded by the normal wavelength pattern.

The necessary atmospheric circulation given, width and height of the draa depend on its continuity and on the sand supply. Width and height have, however, been changed by post-Pleistocene processes (e.g. lowering, broadening, dune formation) in the sand sea. In spite of this, it is possible to make some statements about the Pleistocene conditions with the aid of the geological maps and the three cross-section sequences along the transections (Figs 7–9). Without the dunes on top, the draa in the eastern and the middle parts are 20–30 m high. Where their width is extreme, the central part is frequently shaped like a plateau. In the west, the heights are 40–50 m. Kádár (1934) mentioned general heights of 30–40 m. Draa heights of 10–400 m were offered for the Algerian ergs (Wilson, 1973). According to investigations of the present author with measurements in the Namib Erg (Besler, 1980), in various parts of the Sahara and in China (near Dunhuang, where the dunes are towering above the town), all sand bodies higher than 150 m seem to rest upon elevated bedrock parts, and frequently spill their sands over scarps, river banks or terraces. Besides, without elevation measurements, dune – and particularly draa – heights are easily overestimated. The sand ridges in the Great Sand Sea only represent the basal parts or plinths of ancient draa that surely have been higher, but probably also narrower (see Section 3.3.2).

According to Embabi (1998), the draa length increases from 50 km to 120 km in the south; the longest draa lie between 24°N and 26°N. In downwind direction, the draa in the eastern part end around 25°N. This can be deduced from the changing cross-sections where the flanks are now more concave than convex, and several dune chains without a shared base are dominant. It is possible that smaller draa – because of a shortage of sands – now are overrun by the modern dunes. In this case, draa and dune sands may be distinguished by their granulometry (see Section 4.3.1) and their salinity (see Section 6.1.2). An example is presented from the middle transection: according to the granulometric sand type and the salinity, the southern end of a small sand ridge at 24°50'N represents the ancient draa. Along the western transection that starts with the first cross-section at 25°N, the draa are also found farther south, at least until 24°45'N. According to satellite images and the geological maps, they are also present in the extension of the sand sea north of the Gilf Kebir which could not be investigated (see wavelength discussion above). This means that the southern margin of the sand sea is receding northwards from west to east, most probably because of a decreasing sand supply. Only in the alluvial sands from the Gilf Kebir, the conditions for draa formation seem to have been favourable in the south.

The varying sand supply is also reflected in the cross-section sequences which are all drawn at the same scale but look very different. The draa along the eastern transection with their widths of 500–700 m (in some cases 900 m, statistical mean 700 m) are small compared with the western draa with an average width of 1.5 km. Along the middle transection, the draa reach >1 km in width (statistical mean 1.25 km). Particularly here, the width gradually decreases towards the south, and a positive statistical correlation between the width and the geographical latitude exists ( $r_s = +0.75$ , probability 99%). Therefore, a main sand source has to be assumed in the north (see Section 4.2). No correlations were found in the west and in the east,



**Fig. 22** Looking south across a lower outlier of the Ammonite Hill Escarpment on the eastern transection: several rows of dunes cross the foreland of the scarp in varying directions due to a locally modified wind field. The ordinary draa (below dunes) starts in the left background. The undisturbed neighbouring draa (with dunes) forms the skyline in the west (photo, 3 March 1996).

although the heights of the draa on the eastern transection are comparable to the middle transection. Only in the west, huge sand bodies have accumulated in the draa.

In some parts, the cross-sections suggest dunes without underlying draa because of their smaller dimensions, e.g. the 6th cross-section on the western and the 13th cross-section on the eastern transection. Cross-section 6/2000 passes through a break in the draa where ending and starting draa likewise are smaller. Such a break also exists at 13/1996 on the eastern transection just below the Ammonite Hill Escarpment. The draa already end north of the scarp and start again some kilometres south of it. These gaps cannot be discovered on satellite images because they are bridged by dunes (Fig. 22). A disturbance in wavelength and direction, however, can be recognized. Bagnold (1931) already noticed these gaps in rough terrain that are quite consistent with the draa-formation model where a flat surface is one of the prerequisites (see Section 3.2). Obviously, the lower scarps (some tens of metres) in the Great Sand Sea did not influence the atmospheric vortices. Therefore, the critical scarp height can be assumed to lie between 50 and 100 m. In spite of comparable dimensions, the draa with dune (6/2000) can be distinguished from the dune (13/1996) due to the whaleback plinth of the former (compare the cross-section sequences, Figs 7 and 9).

### 3.2.2. The northern transverse draa of the westerlies

On the eastern transection, a drastic change in the draa pattern occurs around  $26^{\circ}45'N$ , which is particularly well-documented on a LANDSAT TM scene (Fig. 23). The number of draa in the area is doubled and the wavelength – in consequence – is

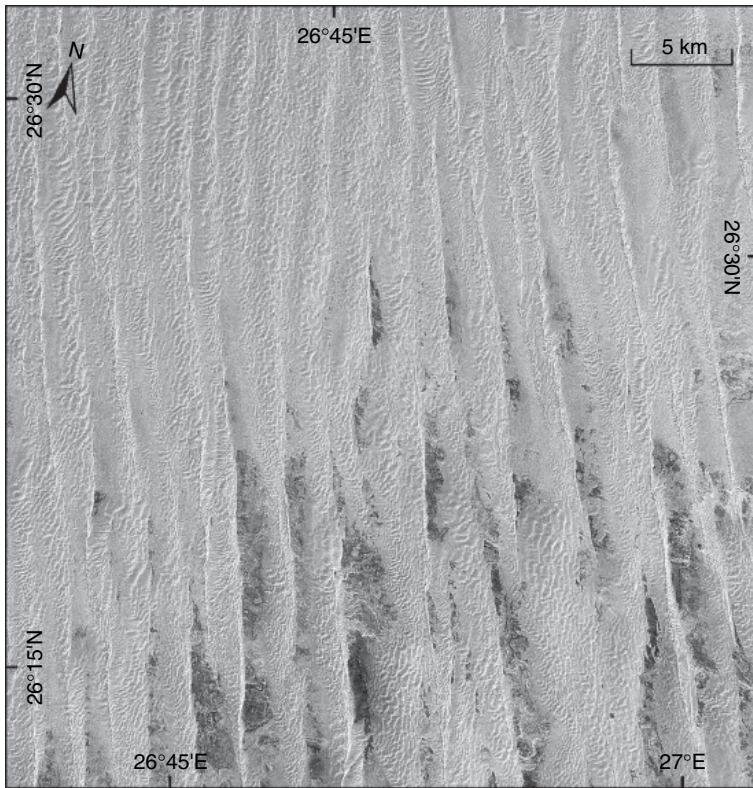


**Fig. 23** Section of LANDSAT TM scene 179-42 around the eastern transection, showing the change in wavelength of the draa around  $26^{\circ}30'N$ . The interdraa corridors of the south are replaced by additional transverse draa in the north. The undulating surfaces of their large upwind slopes may be mistaken for sandy corridors. Along the investigated draa, this change occurs farther north at  $26^{\circ}45'N$ .

reduced to about 1.4 km. This means that the interdraa corridors disappear and are replaced by the respective second draa. In addition, the cross-sections become extremely asymmetrical with a very long ( $>1$  km) and only slightly inclined west flank and a very short and steep ( $>20^{\circ}$ ) east flank. At the eastern base, the next west flank starts immediately, leaving only a narrow groove instead of a corridor. Bagnold (1931) again was the first to notice that the lowest surface lies immediately east of the highest sand crests. Uhden (1932) even recommended investigations to explain the strange east–west cross-sections of these ridges. On most satellite images, the differences between northern and southern draa cannot be detected, and only the north–south trends are visible.

This pattern is explained as transverse draa (Besler, 1997a, 2000a), based on the discussion of instability waves by Brown (1983). He stated that no equilibrium theory existed for these lateral waves. According to his Fig. 13, however, the difference with lateral waves seems to lie in a vertical speed shear within the Boundary Layer (called Kelvin-Helmholtz Instability), which can occur in thin

atmospheric layers with correspondingly shorter wavelengths. In contrast, in the case of the longitudinal features, the important vertical change lies in the direction of the flow. Hanna (1969) already cited Brunt (1937, 1951), who observed that the roll vortices in laboratory experiments were transverse to the air flow when the shear was small. In fact, the bedrock topography in this part of the sand sea is much more subdued than in the south.

In any case, the observed pattern in the sand sea cannot represent longitudinal draa because according to the model, wide corridors are necessarily formed between more or less symmetrical draa. If we look for a wind system to generate these transverse ridges, this must be the dry extratropical westerlies. Usually, the latter are known to bring cyclonic precipitation, but in this case they must have been extremely dry. Strong support for this assumption comes from two directions: the geomorphology outside the sand sea and the hydrology.

Donner and Embabi (2000) investigated yardangs (stream-lined, wind-sculptured hills developed in any bedrock that is at least weakly consolidated) and other ventifacted rock outcrops in the Western Desert of Egypt. Whereas these features in most places are aligned more or less north–south (see Brookes, 2001), they found yardangs in a west–east direction south of the oases of Bahariya (~28°N) and Farafra (~27°N) but not farther south. At Bahariya, the west–wind ventifacts were older than the north–wind ventifacts, and only western directions were found near Siwa (~29°N). For various reasons, a pre–Holocene age was suggested for the west–wind features near Bahariya and Farafra. In a later LANDSAT–interpretation study, Brookes (2003) found aeolian palaeo–features aligned NNW–SSE (170°) and WNW–ESE (110°) in the sand–sea area as far south as 25°N. Because the west–east trending yardangs near Farafra – developed in playa sediments – were <sup>14</sup>C–dated at 9000–6000 BP, he assumed an Early Holocene age for all palaeo–westerlies. It should be mentioned, however, that the cited radiocarbon ages stem from ostrich eggshells sampled on the playa surface between the yardangs (Donner and Embabi, 2000) that may well be much younger than the yardangs.

According to groundwater studies in Egypt by Sonntag et al. (1980) and by Thorweihe (1990a, b), an arid phase without groundwater recharge prevailed between 20 000 and 14 000 BP, after a period with precipitation brought by the westerlies (deduced from heavy isotopes decreasing towards the east). If Brinkmann and Heintz (1986) are right in assuming that the geological conditions in this region result in a low infiltration rate so that a refill of the aquifer would already have been possible under semi–arid conditions, this must have been a hyper–arid phase.

Nicholson and Flohn (1980) already assumed very strong extratropical westerlies to extend southward over the northern Sahara between 20 and 12 ka ago. According to Leroux (1991), the core of the west jet was located at 30°N during the Last Glacial Maximum (18 000–15 000 BP), i.e. roughly at the latitude of Anti–Atlas, Ghadamis and Siwa. The stronger winds caused an acceleration of the oceanic circulation and an increased upwelling along the coast of northwest Africa. Estimates for the decrease in temperature of the cold Canary Current vary from 3.5 to 10°C (Van Zinderen–Bakker, 1982). Rognon (1989) claimed that the westerlies were dryer due to 6–8°C lower surface temperatures of the Atlantic Ocean off the coast. The lee effect of the Atlas Mountains would also have to be considered. In addition,

the western Mediterranean Sea was also 5–9°C colder (Van Zinderen-Bakker, 1982) so that the westerlies could not pick up moisture here. To sum up, there is much evidence that, indeed, the extratropical westerlies could have been strong and dry during some time in the Late Pleistocene.

In this context it is of interest that Kanter (1943) was the first to notice the difference between the Idhan Awbary with draa aligned partly west–east (around 27°N) and the Idhan Murzuq farther south (around 24°N–26°N) with draa running north–south. Bellair (1951) also mentioned the Awbari draa as trending WSW–ENE. The longitudinal draa of the Idhan Awbari could have been formed by the same dry westerlies as the transverse draa in the Great Sand Sea. Transverse draa seem to be rare. Meanwhile, however, they have been identified in other sand seas, e.g. in the Wahibah Sands in Oman (Warren, 1988), where longitudinal and transverse megadunes are distinguished from mesodunes and modern dunes.

The following transections in 1999 and 2000 confirm the change in the draa pattern around 26°45'N. Nowhere, however, it is so abrupt and conspicuous as in the eastern transection where the southern sand-free corridors enhance the difference. The disappearance of the corridors associated with half the wavelength was chosen as the main criterion allowing to find the boundary between the longitudinal draa of the trades and the transverse draa of the westerlies. Along the middle transection, the last clearly symmetrical draa is found at 26°N (14th cross-section in Fig. 8). At 26°14'N, an undulating sand surface with only 10 m vertical difference makes the decision difficult; the interdraa corridor, however, still exists. At 26°29'N, the undulations are higher and clearly asymmetrical. The wavelength is only 500–700 m, and the corridors are also still present. This is considered as the boundary between the two draa systems because the next cross-section (17th at 26°43'N) shows asymmetrical draa of 30 m height and 1.5 km wavelength. Generally, the heights of the transverse draa increase towards the north.

Along the western transection with a thicker sand cover, the transition is even more gradual. The asymmetry already starts at 26°06'N. The distinct interdraa corridors, however, disappear around 26°45'N. Around 27°N, a uniform sandy plateau begins east of the gravel tongue from the west (Sarir Dalma, see Section 3.1). Only slight traces of the draa-and-groove pattern are visible. With regard to the westerlies, this sandy plain is situated at the windward side of the erg and may represent the field of initial formation of the lateral flow pattern in the Planetary Boundary Layer. For the longitudinal pattern, the critical horizontal formation distance is about 20 km (Brown, 1983). Perhaps, the surface looked like this everywhere at the beginning of draa formation in the Pleistocene. According to the model, the pattern at the upwind side of an erg is always blurred, and on the downwind side it is always distinct with a sharp boundary. This can be observed in many sand seas (e.g. Namib Erg, Wahibah Sands), and apparently it also is the case in the Great Sand Sea.

The return route from the western transection towards the east was chosen perpendicular to the draa. Further observations on draa wavelengths and shapes were made. The transverse draa pattern with narrow grooves is found everywhere between the western and the eastern transection around 27°N. Between the middle



and the eastern transection, however, it is more regular and more pronounced with more dunes (see Section 3.3.1). Some grooves disappear where two draa coalesce. This was also noticed by Embabi (2000, his Fig. 3(B)) on satellite images. He interpreted this as Y-junctions because he thought of longitudinal features. Along the return route from the middle transection, running more towards the southeast, the impressive interdraa corridors between the longitudinal draa are found again south of  $26^{\circ}30'N$ .

Within the transition zone between longitudinal and transverse draa, some regularities are observed on the western and on the middle transection. At first, the longitudinal draa become broader (carrying fewer dunes); the corridors, however, are still present. Second, several asymmetrical undulations are shaped by westerlies (corridors still present). At last, the corridors disappear, and the now extremely asymmetrical draa with dunes sitting on their utmost eastern edges (see Section 3.3.1) close up to narrow grooves. This transition is particularly well developed along the middle transection, whereas, the wavelength decreases very gradually in the west. In this context, it is interesting that in the Calanscio Sand Sea west of the Great Sand Sea, a change in the draa pattern is also noticeable on satellite images. The rather straight draa aligned NE–SW in the south show a more wavy and irregular pattern around  $27^{\circ}N$ . They slowly change their direction towards north–south around  $28^{\circ}N$ . This change in the dune (draa!) alignment was already mentioned by Hecht et al. (1964). Nothing can be said, however, on the draa types without the necessary field check.

Consistent with the wavelength, the draa widths are about 1.4 km in the east, 1.5 km in the middle and 1.3 km in the west, if only the clear pattern without the transitional features is considered. The heights vary considerably and amount to 40 m in the west and the east, whereas only 30 m is the average in the middle part. The deviation from this mean was found to be smallest in the east with the most pronounced pattern which is displayed in the cross-section sequences. If the smaller scale of the northern parts in the drawn sequences (Figs 7–9) is taken into account, a comparison of draa heights shows that the transverse draa are higher than the longitudinal draa in the east and vice versa in the west, whereas comparable heights of both types are reached in the middle. These characteristics additionally underline the different formation processes. Moreover, the TM scene (Fig. 23) shows that the transverse draa, in contrast to the rather straight longitudinal draa (consistent with the model), have slightly sinuous shapes and more undulations on their long upwind flanks. Whether the latter are modern or palaeo-features may be decided with the aid of the granulometric analysis (see Section 4). On satellite images, these undulating surfaces can be easily interpreted as sandy corridors that form a prolongation of the southern sand-free streets. Therefore, the genetic boundary between the draa types in the sand sea was not recognized earlier.

In summary, a genetic boundary between two different draa types runs across the Great Sand Sea around  $26^{\circ}40'–26^{\circ}45'N$ . This boundary is very distinct in the east and is blurred in the west because here the longitudinal draa with corridors are asymmetrical as far south as  $26^{\circ}05'N$ . This can be explained as later reworking of the longitudinal draa of the trade winds by westerly winds. Therefore, the transverse draa should be younger than the longitudinal draa (see Section 5.3.1).

The boundary, that does not run parallel to the latitude but is slightly curved towards the east–northeast, can also explain the strange – and at first inexplicable – phenomenon that the transverse draa – like the longitudinal draa – are aligned at about  $165^\circ$  in the east and at  $170^\circ$ – $180^\circ$  in the west. According to the formation model, the geostrophic wind should have been from  $260^\circ$ – $270^\circ$  in the west and from  $255^\circ$  in the east. In fact, a slight curvature of the westerly palaeo-jet is found in some drawings (a.o. Nicholson and Flohn, 1980). This directional change, however, could also be due to a different surface roughness. In any case, the dynamics resulted in a continuous transition from the transverse draa in the north to the longitudinal draa of the south without a break or a change in their direction. This makes a distinction without a field check impossible.

A complete ground check of this transition zone was achieved during the last visit to the Great Sand Sea, in 2006. Meanwhile, a route had been explored that crosses the sand sea diagonally from south of Ain Dalla in the east to Willmann's Camp in the southwest (Fig. 2). The GPS points were found to follow almost precisely the southern limit of the palaeo-westerlies influence on the draa morphology. This position of the borderline was already suggested in 2002 (Fig. 5 in Besler, 2002a). In fact, the route crosses the three south–north transections in the most favourable places.

The eastern transection is passed at the 17th cross-section ( $26^\circ 49'N$ , Fig. 7) that represents the southernmost transverse draa. Towards the north, the transverse draa are higher; towards the south, the wide corridors between the longitudinal draa are deeply covered by recently blown sands. It has to be mentioned that the steep eastern flanks ( $>20^\circ$ ) of the transverse draa are compacted and possess firm surfaces that – in places where they are not carrying dunes – allow the ascent of vehicles (still a hazardous endeavour). The route passes the middle transection between the 16th and the 17th cross-sections (see Fig. 8). Along the 16th cross-section, the transverse draa are particularly low, but a sandy corridor still exists. Along the 17th cross-section, the draa are a little higher, and the corridors are reduced to narrow grooves. Before reaching the western transection (Fig. 9), the route enters the wide gravelly corridors of the alluvial fan where driving is no problem. Between the western and the eastern transection, the surface topography along the route is rather subdued, forming mainly rolling sands. Thus, the 2006 route in Fig. 2 depicts in addition the southern margin of the morphological effectiveness of the palaeo-westerlies.

The northern boundary of the transverse draa is not so easy to define. At the northern end of the western transection, the pattern looks more like a sandy plain with small singular dunes. At the northern end of the middle transection, however, the draa-and-groove pattern is clearly visible. Along the eastern transection, the last distinctly asymmetrical draa occurs at  $28^\circ 15'N$  (23th cross-section); it is, however, associated with a wider corridor. The last cross-section (24) at  $28^\circ 29'N$  represents a sand shield. Here, the draa/dune pattern becomes completely irregular. Dominant draa-sized features are low elongate sand shields stretching west–east. The majority of sand bodies, however, are smaller dunes running in various directions due to a rugged bedrock topography (see Sections 3.1 and 3.3.1). It should be mentioned that the transection here runs close to the

eastern margin of the sand sea. Also according to LANDSAT images, the northernmost sand sea seems to be dominated by shorter dunes with changing directions. On the whole, the northern boundary of the Pleistocene draa seems to lie around or shortly north of 28°30'N.

### 3.3. THE HOLOCENE DUNES

Due to a humid period with draa consolidation and a later reactivation during aridization (see Section 5.3.3), there is a clear discontinuity in slope inclination between draa and dunes in the Great Sand Sea. This is an important difference with various other sand seas, e.g. the Namib Erg (air photo 3 in Besler, 1980), where the distinction between draa and dunes is much more difficult. Haynes (1982) already mentioned that the transition between plinth or whaleback and dunes is marked by a break in slope from gentle to steep, by a textural change of the sands (see Section 4) and by a subtle colour change (see Section 6.2). According to Steffan (1983), only 7% of the Great Sand Sea is covered by dunes.

Everywhere in the sand sea, the longitudinal dune type of silk is dominant (Fig. 25; Besler 1992). The term “silk” was first used by Brosset (1939) and was introduced by Mainguet (1976) in her proposal for a new classification of dunes, based on satellite-image interpretation of Saharan ergs. The silk is a second-order dune and consists of a longitudinal row of sif (also sief, seif) dunes as first-order elements. Both terms are of Arabic origin. According to the glossary by Capot-Rey et al. (1963), sif (plural sioûf) literally means sabre, and this term is applied because of the slightly curved shape of this active dune. Silk (plural sloûk) means a string of active dunes. To facilitate the application of this terminology, the plural forms are usually neglected. In English literature, this type is often called “linear dune”. Because of its characteristic sinuosity, however, the Arabic term is preferred in continental literature. Sif are rather rare, and many dunes mentioned as sif in literature are actually silk (a.o. Becker, 1979).

Silk are formed in a mainly bimodal wind system where slip faces change their exposure accordingly. Because of this oscillation, both slopes are steepening and, apart from the uppermost crestal part with active avalanches, they have gradients of about 20°. The vector resultant of both winds determines the general direction of these longitudinal dunes. However, they do not migrate but only extend or prograde in this direction. A wealth of literature exists on linear dunes and longitudinal dunes, and the debate about their genesis is still going on (a.o. Pye and Tsoar, 1990; Wang et al., 2002; Munyikwa, 2005). In many cases, however, the investigated “dunes” may represent draa or secondary dunes covering older draa, which enhances the confusion (a.o. Breed et al., 1979; Stokes et al., 1997). It would lead beyond the scope of this book to enter the discussion about this topic.

Dependent on the draa type underneath, the spatial pattern of dunes in the sand sea is different. Therefore, the boundary between transverse and longitudinal draa is also perceptible in the dunes, and both patterns are discussed separately. Besides, the area of Holocene dunes is larger than the area of Pleistocene draa, especially at the southern and the northern margins, which both are additionally discussed.

### 3.3.1. Dunes on the transverse draa

Generally, longitudinal draa carry more dunes than transverse draa. This is also displayed in the cross-section sequences. On the transverse draa, only one dune rests on the highest eastern edge and sometimes even east of it, clinging to the steep draa slope next to the groove (Fig. 24). In the latter case, these dunes cannot be seen from a distance if they are low. They only appear now and then like small islands in a sand sea (literally). Therefore, the transverse draa frequently seem to be dune-free, which means that they seem not to have been reactivated. On LANDSAT images, these silk cannot be detected because of their coincidence with the highest edge of the draa. Moreover, the number of dunes decreases towards the west. This area is therefore indicated as “rolling sands” on the geological map. In his remote-sensing study, Steffan (1983) goes so far as to call the Great Sand Sea a giant sand shield with only few dunes. On the return route from the endpoint of the western transection along 27°N, the draa-and-groove pattern was often observed without any dune; farther east, however, dunes were seen regularly.

Frequently, a silk starts on the highest part of the draa and progrades obliquely across the slope above the groove while a little farther south another silk again starts on the draa top. The active tips of the dunes always point to southerly directions. After formation on the highest edge of the draa with full access of winds from all directions, the dunes prograding towards (S)SE indicate a northerly and a westerly component of the bimodal wind system. This is consistent with wind-sculptured bedrock outside the sand sea (Donner and Embabi, 2000; Brookes, 2001) and with wind data from the meteorological stations of Siwa in the north with most frequent westerly winds, and of Farafra in the east with prevailing northerly winds (El Baz and Wolfe, 1982). No conclusion can be drawn, however, about the winds that are



**Fig. 24** Looking north towards a silk prograding onto the steep east slope of a transverse draa on the western transection. From the distance only the highest dune part in the background is visible. The area in front is perceived as rolling sands (photo, 15 March 2000).

effective for sand transport in the sand sea (see Sections 3.3.4 and 4.2.2). According to Cooke and Warren (1973), the bimodality may also be caused by winds of unequal proportions, i.e. a major direction and a supplementary one. When the silk move down the eastern flank of the draa, they seem to arrive in a different (bimodal) wind field where the westerly component is weaker and the northerly is stronger because of air-flow channeling in the grooves. In addition, the sudden reduction of surface friction east of the draa top may cause a deviation of westerlies to the right. This can actually be observed in the Ghard Abu Muhariq farther east (Bubenzer, 2000). After all, a silk crossing the groove was never observed. All dunes keep at the eastern flanks of the draa where their progradation seems to slow down. Only one case was observed near the eastern transection where three parallel silk advanced towards the southeast on the same eastern draa slope. There exist indications, however, that dune formation takes place on the long stoss-side slopes of the transverse draa as well (see Section 4.3.2).

The highest silk are met along the eastern transection, where dunes of 80 m to even 100 m height are frequently found on the edge of draa of about 30 m height. In this case, the eastern slopes of the draa are completely buried below the huge slip faces of the dunes. According to the monthly stream-flow charts of the year 2004 (see Section 3.3.4), the wind velocity above the area of transverse draa slightly increases towards the east. This is noticeable only, however, in February (Fig. 30), June and November, and the observations cover only one year. On the other hand, comparatively low silk of 10–20 m occur as well. The statistical mean is a height of 45 m. The dune heights along the middle and the western transections are more homogeneous and comparatively low: 10–15 m in the middle and 20 m in the west. The silk are higher than the draa in the east and lower than the draa in the west. This could be due to different grain-size parameters of the sands (see Section 4.2). The general dune length was found to be 10–20 km, because at almost every cross-section site silk start or end, either on the investigated draa or on its neighbours.

### 3.3.2. Dunes on the longitudinal draa

Dunes are more numerous on the longitudinal draa than on the transverse draa; however, sections without any dunes occur as well. A statistical comparison of all cross-sections may not be very indicative because some of them do not include dunes at all. It provides, however, an idea about the degree of reactivation of the draa. Apart from the western transection with three silk per very broad draa section, the ratio is just one dune per section. The spatial distribution of the dunes is also different. They always rest on the draa top and – apart from a few exceptions mentioned below – never on the flanks or in the wide interdraa corridors. It has frequently been observed that the dunes pull across the draa diagonally NW–SE and end near the east flank (Fig. 25). Kröpelin (1993) mentioned dunes under a bimodal wind system consisting of northerly trade winds and occasional east winds. As already pointed out above, however (see Section 3.3.1), the dune directions indicate northerly and westerly winds. The closest meteorological station, at

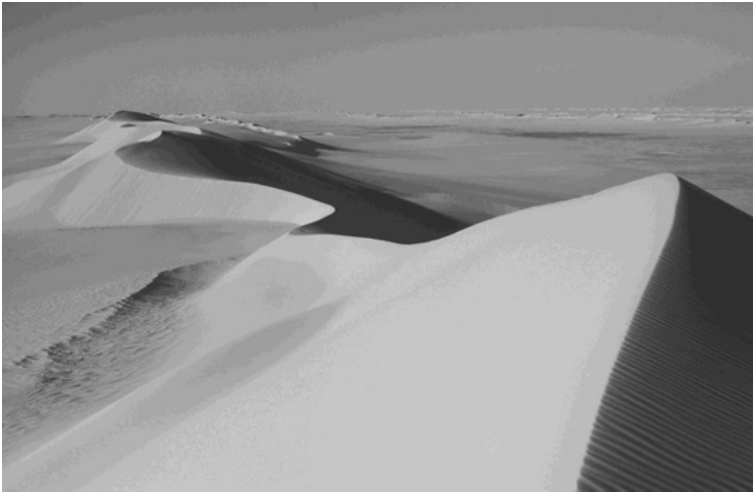


**Fig. 25** Looking north along the sinuous crestline of a small silk, running NW–SE across the draa (a second silk in the background). The unconformity between the Pleistocene draa and the Holocene dune is displayed by the whaleback shape of the draa and by the erosional feature (wind scour) on the left side, due to a slight consolidation. The neighbouring eastern draa with dunes follows the horizon (photo, 1 March 1999).

Dakhla, shows highest frequencies from NNW followed by N and NW, but no east winds at all (El-Baz and Wolfe, 1982). This does not indicate, however, whether their velocity is high enough for sand transport (see Section 4.3.2). Silk from the western part sometimes end on the top of the draa or on the east flank, while another silk begins farther west. Occasionally, a connection between both silk is created, i.e. when the eastern one turns towards the west.

It should be emphasized here that the diagonal pattern aligned NE–SW across the draa seen on satellite images is not due to dunes but to large undulations. They were also identified as such by Embabi (1998, 2004). Because of their huge dimensions and only slight differences in elevation, they frequently could not be recognized during field check. In his remote-sensing study of sand accumulations in the eastern Sahara, Steffan (1983) measured undulation spacings between 120 m and 180 m in the Great Sand Sea. On the other hand, Steffan stated that a distinction between undulations and dunes is not even possible on a grey-scaled image. According to field experience of the present author, however, distinctly larger spacings do exist. Certain differences are observed between the individual transections. Therefore, they are discussed separately, including observations on the neighbouring draa.

On the eastern transection, a gap in the silk frequently occurs above a smaller scarp that, however, did not affect the draa formation (see Section 3.2.1). This gap may be due to locally stronger winds with increasing sand transport. Between 25°20'N and the Ammonite Hill Escarpment, singular dunes prograde from the northwest to the eastern margin of the symmetrical draa. Bagnold (1931), however, mentioned “two chains of crests” on the same whaleback (draa) near Ammonite

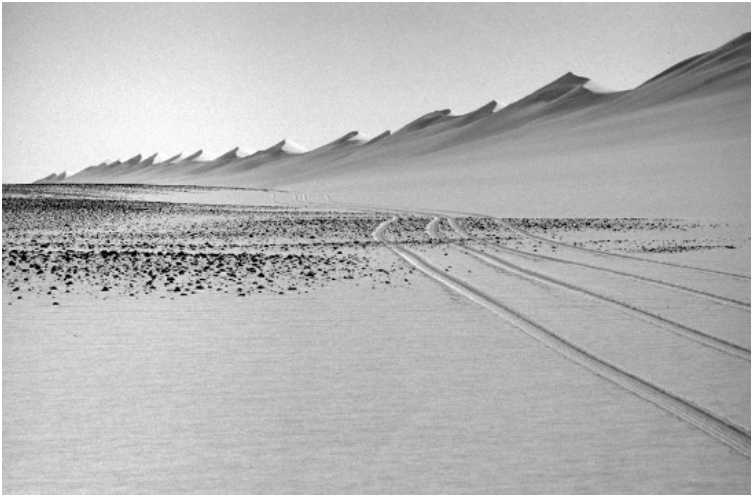


**Fig. 26** Looking south along the eastern transection north of the 12th cross-section. The silk follows the eastern side of the draa top and displays a cock's-comb skyline (for explanation see Section 3.3.2) with slip faces pointing east. The debris-covered sandstone floor of the inderdraa corridor becomes sandier towards the north (photo, 03 March 1996).

Hill. The silk close to the eastern margin show not only the usual lateral sinuosity but also a strong vertical waviness of their crests. The side-view of these dunes offers a cock's-comb skyline (Fig. 26). With their steep summits, these sand bodies resemble small star dunes. The generating force may be occasional trimodal or even polymodal winds (including southerly directions) that are supposed to be the cause of star dunes. This was even confirmed by computer-simulation modelling (Nishimori et al., 1998).

Steffan (1983), who also noticed this pattern in his remote-sensing study, calls these shapes "hooked dunes" and "tear-drop dunes". According to observations by the present author, the shapes of "hooked dunes" and "tear drop dunes" include additional characteristics which will be discussed below. At the disruption of the draa around 26°N, caused by the Ammonite Hill Escarpment, the modern silk close the gap and connect the draa above with the draa below the escarpment. Because the draa wavelength is also disturbed, the corridors here are sandier, and some dunes extend onto these sands. These silk also possess the cock's-comb appearance. North of the escarpment, the silk are again oblique to the draa (NW-SE), and their number decreases towards the north.

Not only upwind slopes and slip faces change their position according to the prevailing winds, but the entire silk shape is subjected to strong aeolian dynamics. This was particularly observed in 1999 during a second visit to the coring site to collect some equipment left behind in 1996. While all slip faces in spring 1996 had been exposed towards the east, they pointed westward in spring 1999. In addition, the cock's-comb crestline was disrupted at the 11th cross-section, and a large deflation gap with cross-ripples (W-E and NW-SE) had developed. The top of the dune – rounded in 1999 – was located west of the old (1996) position.

Along the middle transection, the dune/draa ratio is slightly higher than in the east, with a statistical mean of 1.3. This is due to the fact that up to three silk are found on the same draa in the south. Also here, however, dune-free sections increase towards the north. Many silk do not reach the eastern margin of the draa but end in the middle, while some hundred metres farther west a new silk starts. As another exceptional feature, the respective eastern silk in this case is sometimes a ridge without a distinct crestline. After the third cross-section around 25°N, the already mentioned cock's-comb structure was found in the eastern silk, and farther north it also occurred in the western silk of the same draa. This conspicuous pattern includes a south to southwest exposure of the slip faces instead of their normal position, facing west (in spring 1999). In these cases, almost barchan-like shapes are generated within the silk. These are the hooked dunes of Steffan (1983), who classified them as transitional between barchans and silk (compare Section 4.3.2).

At the 10th cross-section, a large deflation gap was observed in the cock's-comb crest, comparable to the one on the eastern transection at about the same latitude. In some places, small silk with exceptional barchan shapes are found at the eastern base of the draa. Reversing of small slip faces could be observed during south winds. From the fourth cross-section towards the north, large NE-SW undulations shape the draa. All dunes, however, run NW-SE. Near the Ammonite Hill Escarpment, that is very low here (see Section 3.1), the 13th cross-section is dune-free. The western draa carries a silk on its eastern flank, and the eastern draa carries a silk on its western flank, as well as additional dunes in the east. In the transitional zone between longitudinal and transverse draa, the former have no dunes.

The dune pattern in the west is much more complex. Beside silk, also transverse dunes and large barchans occur in various positions (Fig. 27). This was already noticed by Haynes (1982). Barchan dunes are observed on relatively firm draa surfaces as well as on soft sand, here associated with distinct lee depressions (Besler, 2002). The northernmost transverse dunes are found on the eighth cross-section (25°48'N). In the south, the silk are aligned N-S and also include barchan-like shapes, with their slip faces pointing south. Farther north, the silk direction gradually turns towards NW-SE, and the dunes reach the eastern corridor floor, where stripes of blown sands – in clear contrast to the gravelly corridor – lie ahead. These features are usually easier to detect on satellite images. Brookes (2003) mapped sand drifts from LANDSAT-MSS images and found this direction well documented in the southern sand sea. NE-SW undulations are found on the third and the eighth cross-sections. Subdued cock's-comb patterns were observed on the third and the fifth cross-sections. In addition, the lateral sinuosity is also exceptionally large. Some draa sections, particularly their eastern halves (e.g. on the third cross-section), possess undulations, silk (eight in this case!), transverse dunes and giant barchans as well as depressions and deep hollows to such an extent that they look like sand massifs or sand mountains, comparable to the gourd of the Great Eastern Erg (see Section 9.2). This complexity decreases in general towards the north.

Special attention has to be drawn to the occurrence of longitudinal silk indicating a bimodal wind system, together with transverse dunes indicating unidirectional





**Fig. 27** Looking north along the draa top at Willmann's Camp in the southwestern sand sea. The longitudinal silk is only recognizable by the highest crestline with westward pointing slip faces. In addition, transverse dunes developed on the eastern draa flank in the background. In front of them, barchan shapes with slip faces pointing south can be seen. The association of longitudinal and transverse dunes is possible only in abundant fine-grained sands. This is rare in sand seas, and also is an exception in the Great Sand Sea (photo, 11 March 2000).

winds on the same draa. Recently, computer simulations of dune formation dependent on wind regime and sand supply were carried out where the sand supply was gradually increased in a bimodal wind system. After sif formation in the direction of the vector resultant, transverse dunes perpendicular to this resultant were formed (Nishimori et al., 1998). This corroborates the earlier assumption of Mainguet and Chemin (1983) that transverse dunes always indicate a positive sand budget and longitudinal dunes a negative sand budget. Therefore, the association of longitudinal and transverse dunes seems to be rare in nature, and it is not mentioned in the literature on sand seas. However, in the central Taklamakan (China) near the Keriya river flood-out, where a bimodal wind regime is attested, sif are found in the interdrea corridors with a thin sand cover, and transverse dunes perpendicular to the sif rest on the draa (Besler, 2000b). In the southwestern Great Sand Sea, longitudinal and transverse dunes occur on the same draa, which is a different situation and not easy to explain. Farther east, the lack of transverse dunes is most probably due to the shortage of fine-grained sands. Only in the area of the alluvial fans from the Gilf Kebir, the broad draa throughout contain finer and better sorted sands (see Sections 4.2 and 4.3). There seems to be an unlimited supply for dune formation after reactivation. Transverse dunes seem to be the natural consequence there as are the silk farther east. But why are silk also present here? A clue is offered by their comparatively low height.

It is difficult to measure the heights of silk on the draa because the elevational difference between draa and dune is larger on the respective slip-face side than on

the actual windward side, where the gradient changes gradually from draa to dune (not so abrupt as in the eastern sand sea, see Section 3.3). In the cross-sections, transverse dunes and barchans only appear as undulations perpendicular to their direction of progradation. The following numbers present minimum heights.

The silk on the middle and the eastern transections are about 15 m high with one exception of 50 m height above the Ammonite Hill Escarpment (14th cross-section). The sands may be piled up here because the velocity and the sand-transport capacity of northerly winds are reduced by the increasing friction on the southward rising surface (compare Section 3.1.2). On the western transection, the numerous silk have heights between 5 m and 30 m. Because the majority is small, however, the statistical mean is 13 m. Maximum heights around 30 m are found between 25°18'N and 25°42'N, where the sands are exceptionally fine-grained (see Section 4.2). Generally, the heights of silk on draa decrease while their numbers increase. Apart from the middle transection without much difference, the silk on the longitudinal draa are lower than the silk on the transverse draa. This may be related to weaker modern winds in the south or to different sand characteristics (see Sections 3.3.4, 4.2 and 4.3). In the southwest, however, where in spite of fine-grained draa most silk are lower, a difference in the dune age (within the area of longitudinal draa) may play a part. Perhaps the larger transverse dunes are older than the smaller silk which may exist due to a local environmental change in wind or sand supply. According to Mainguet and Chemin (1983), this could indicate an increasingly negative sand budget when most fine-grained sands selected from the draa (that now have coarse-grained deflated surfaces, see Section 4.3.1) had already gone into the transverse dunes.

Unfortunately, no investigation was possible in the extension of the Great Sand Sea between about 25°N and the Gifl Kebir Plateau. South of the western-transection draa, another low isolated draa that carries a silk prograding SSE down from the draa body is situated between 24°47'N and 24°54'N. The dunes in this area do not, however, represent a general progradation towards the south (see Section 3.3.3) but are mainly formed in situ, either on or between the draa (see Section 3.2.1). The western margin of this sand-sea extension consists of a typical, 30 m high marginal dune with a rounded top running N–S that was investigated around 24°16'N, 25°39'E. Longitudinal dunes aligned NE–SW that are found nowhere else in the sand sea are conspicuous there (even on LANDSAT images, Fig. 28). They are parallel silk with sandy corridors that house small barchan-like transverse dunes with their slip faces pointing southwest. Where the silk meet the whale-back-shaped marginal ridge, barchan-like transverse dunes are superimposed, giving the long and narrow sand body the structure and appearance of pewter-grass (*Equisetopsida*). In a bird's-eye view, these shapes look precisely like a row of tear drops. Most probably, these are the teardrop dunes mentioned by Steffan (1983) in his remote-sensing study.

Looking east from the highest part of this dune, many silk starting as shadow or lee dunes behind small outcrops in the NE can be seen. Indeed, the LANDSAT image also shows that these NE–SW aligned dunes are found only to the west of a rough bedrock topography, whereas meridional features dominate the east. This additional dune direction is therefore topographically-induced. This means that on the windward



**Fig. 28** LANDSAT 7 subset of the southern draa immediately north of the Gilf Kebir Plateau. Superimposed silk dunes cross the western draa NE–SW, frequently starting as lee dunes behind small bedrock outcrops.

side of the obstacles northeasterly winds should already exist, which do not seem to be present in the sand sea in a morphologically effective way. The Gilf Kebir itself could provide the reason because the generally meridional air-flow direction deviates around it. Similar ideas were communicated by Embabi (2000, 2004) (see also Section 3.3.4). In this part of the sand sea, the association of longitudinal dunes with transverse dunes is easy to explain. The silk are formed under a bimodal wind system generated by the bedrock obstacles dividing the air flow. In the narrow corridors between them, the flow is channelled and becomes unidirectional. On LANDSAT images, the diagonal dunes (NE–SW) seem to be superimposed on the meridional features, and therefore

they are younger (see also Embabi, 1998, 2004). Unfortunately, this could not be investigated in the field because the access with vehicles was too difficult and time-consuming. Anyway, the uniform wavelength of 2.5 km in the meridional pattern is characteristic for draa and not posing a chronological problem (see Section 3.2.1).

### 3.3.3. The southward progradation and the northern extension of dunes

A true progradation of dunes beyond the draa towards the south is observed only along the eastern transection where the first to sixth cross-sections represent dunes without underlying draa (Besler, 1997a, 2000a). The dunes have advanced some 60 km towards the south. Applying the extension rate of 5 m/year that was measured in silk of the Toshka Depression in southern Egypt (Besler, 1986), 12 000 years would have been needed for this advance, which is not realistic. On the other hand, the southern end contained a barchan dune (Fig. 29), and barchan-breeding silk have been observed in the Toshka Depression in 1982. This was also observed by Mainguet and Callot (1978) in the Fachi-Bilma Erg. Therefore, it is assumed that the southward progradation included temporary barchan migration. According to Ball (1927), the advance of smaller dune chains in the Libyan Desert is 15 m/year. The same rate is mentioned by Beadnell (1910) for barchan migration in the Kharga Depression. Müller (1981), who measured barchan migration in relation to barchan height in the Kharga Depression, found that 5–10 m high specimens moved about 20 m/year. In the shape of barchans, the dunes could have travelled up to 20 m/year, and 3000 years would have been sufficiently long for a propagation of 60 km.



**Fig. 29** Looking towards a 13 m high barchan dune at the southern end of the eastern transection. The uppermost metre of the brink is reversed by southerly winds. A longitudinal dune was found in this place in 1999 (photo, 29 March 1996).

As barchan migration cannot be assumed to have taken place during all the time, and periods of silk existence have to be taken into account as well, a few thousand years should be added. The time then is consistent with the results of luminescence datings (see Section 5.3.3). Bagnold (1931) and Kádár (1934) already noticed barchan dunes at the southern margin of the sand sea. Rejoining of barchans to silk was observed during the second visit to the eastern transection in 1999, when no barchans were found, but in their place a longitudinal dune ridge with barchan-like structures. The southward progradation may have been supported by an additional mechanism: bedrock erosion has led to numerous small scarps that provide excellent conditions for trapping blown sand and for the formation of longitudinal lee or shadow dunes. These dunes could have coalesced to form the dune ridges existing today (see Section 6.2).

Remarkably, the dunes follow the same direction as the draa, in spite of their different formation dynamics. The two main components of the Holocene wind system more or less seem to have a vector resultant in the direction of the Pleistocene vortex axis. This also holds true for isolated lee dunes farther south. The higher, south-facing Abu-Ballas Escarpment, however, causes an air-stream deviation towards the west, most probably due to reduced surface friction (see Bubenzer, 2000). In addition, the general veer of the trade winds over southern Egypt from north to northeast has to be considered (see Section 3.3.4).

On the middle transection, the draa was already met at the first cross-section, which means that no dune progradation has taken place. Only isolated lee dunes up to 15 m high are observed farther south behind hills. Here and on the western transection, the draa end without dunes on top. This may indicate a stronger northerly component in the wind system of the east, whereas a stronger westerly component in the west seems to be indicated by dunes reaching the eastern corridors (see Sections 3.3.2 and 3.3.4).

As already mentioned above (Section 3.2.2), the draa pattern underlying the dunes ends around 28°30'N. This means that the northernmost part of the Great Sand Sea between this latitude and the Siwa Oasis (29°N) is a Holocene extension of dunes only. These dunes are aligned in various directions, and many of them start as lee or shadow dunes behind elevated bedrock outcrops. Near the eastern transection, the types of silk and sif (the first-order element) seem to be dominant. The sands are very soft and make access by vehicles impossible. The sedimentological analysis indicates the input of sands from a younger source, not yet available for draa formation (see Section 7.2). Embabi (2000, 2004), interpreting air photographs of this area, describes a network pattern of dunes. According to El-Baz and Wolfe (1982), the modern winds at Siwa show a higher directional variation than at all other stations around the sand sea. Together with the rugged bedrock topography, this may explain the almost chaotic dune pattern.

### 3.3.4. Comparison with modern winds

Sand seas generally pose the problem that meteorological stations with wind records are very remote. As investigations at the northern fringe of the Great Eastern Erg in southern Tunisia have shown, even the data from marginal stations are not

applicable (Besler, 1989). A first attempt to evaluate the wind pattern in the Western Desert of Egypt used data from the local World Meteorological Organization (WMO) stations covering 7–13 years (El-Baz and Wolfe, 1982). The annual resultant of wind vectors at the stations indicates northwesterly winds, and the calculated resultant sand-drift potential – getting weaker towards the south – shows southeasterly directions. The authors stressed the point that a full understanding of the wind regime is hampered by the lack of meteorological stations in the open desert and by the location of the existent stations in depressions. They also stated that the sand-drift potentials do not provide the same directions as the dunes. The used satellite images, however, show only the draa pattern that, of course, is not related to the modern wind regime. With regard to the Holocene dunes, this analysis gives reasonable results.

An evaluation of the first year of records from the new weather station installed by ACACIA at Balat in the Dakhla Oasis shows that the wind regime is even different within the same oasis if compared to the older WMO station at Mut. This is due to a strong influence of the local topography (Ritter, 2005). Ritter presented a set of aerodynamic stream-flow charts for the Egyptian part of the Libyan Desert which were plotted from the data provided by the European Center for Medium-Range Weather Forecast (ECMWF). All available records from meteorological stations, weather buoys, weather ships, aircraft, satellites and balloon ascents were assimilated and calculated for 61 different barometric levels from 0.1 hPa down to the land surface. The land surface, however, was modelled with a grid of  $0.25^\circ \times 0.25^\circ$  and did not meet reality with its small-scale differentiation. In Egypt for example, the Gilf Kebir stands out very prominently, and the Farafra Depression can be recognized; the area of the Great Sand Sea, however, is a rather uniform plain, rising slowly towards the south. Draa and dunes and small scarps are completely neglected. Nevertheless, the stream-flow charts for the 10 m level deserve a discussion.

The charts were plotted for every month of the year 2004, in analogy to the records from the new station. Because of the high aerodynamic roughness of the sand sea, a strong frictional deviation of the stream lines towards the left has to be considered. February and October are the most interesting months because of the highest wind velocities and an additional difference in the direction of the stream flow above the Great Sand Sea (Fig. 30). In February 2004, the stream lines followed a NW–SE direction as far south as  $27^\circ\text{N}$ , changed then towards NNW–SSE up to  $26^\circ\text{N}$  and veered to almost N–S north of  $25^\circ\text{N}$ . Around  $25^\circ\text{N}$  they reached a NNE–SSW direction. A mean value above the threshold velocity for sand transport (5.5 m/s) was, however, reached only north of  $27^\circ\text{N}$ . If the surface friction is taken into account, the respective directions would have been around WNW, NW, NNW and, at last, N. In October 2004, the average wind velocity above the sand sea was higher than 7.5 m/s everywhere. The stream lines show a very homogeneous pattern of NNE–SSW directions. This would mean strong N winds.

If the charts of all months are evaluated in this way, trends towards an overall pattern can be recognized, although it has to be kept in mind that this is only valid for the year 2004. In almost all months (nine), a major change in wind direction is

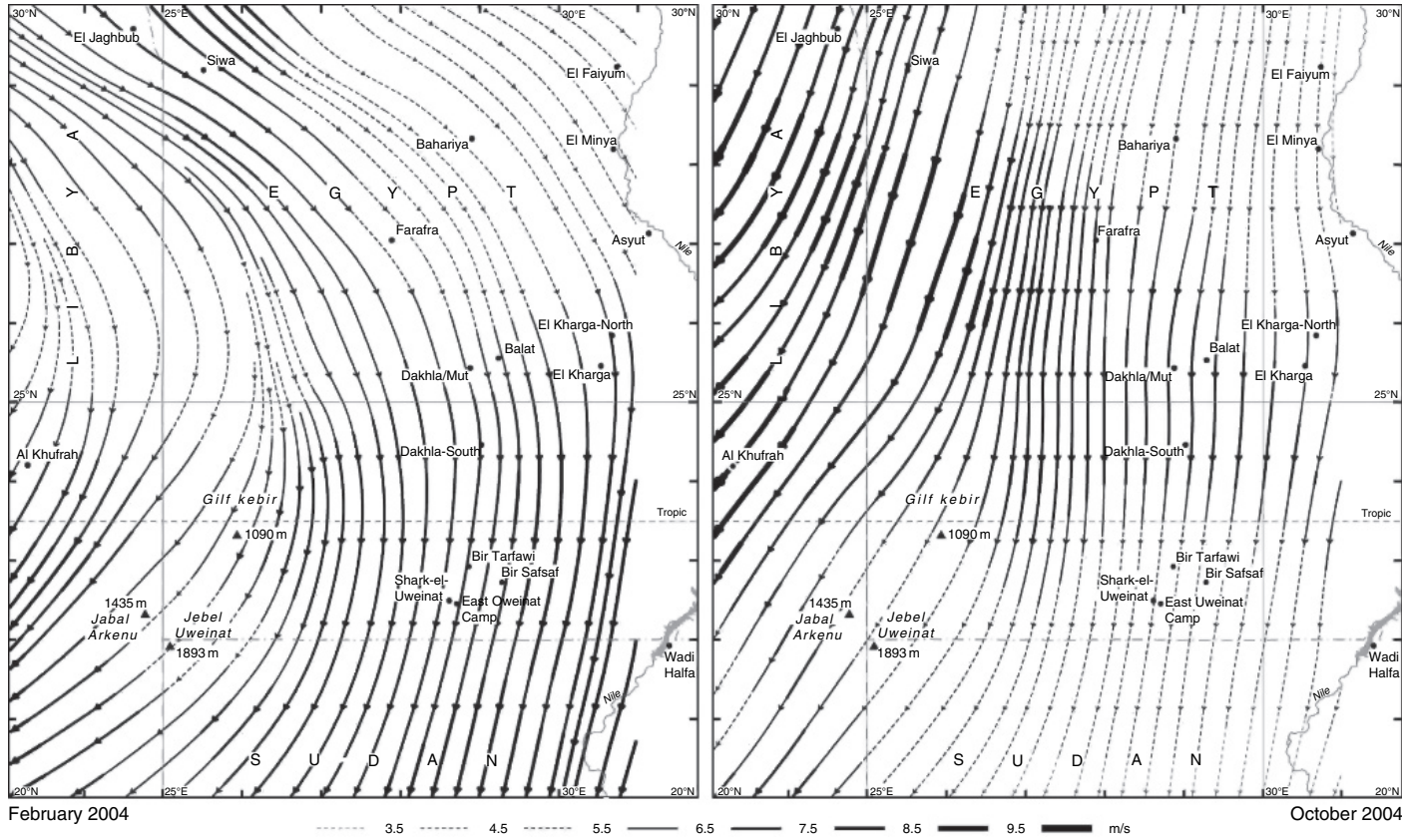


**Fig. 30** Aerodynamic stream-flow charts for the 10 m level above western Egypt for February and October 2004, based on data provided by the European Center for Medium-Range Weather Forecast (ECMWF). An additional frictional deviation towards the left has to be taken into account because the land surface is only poorly modelled by the  $25^\circ \times 25^\circ$  grid.

most conspicuous around 25°N. Strong NNE winds occur only south of this latitude. Regarding the charts, it becomes clear that this is mainly caused by the stream-flow deviation around the mountainous complex of Gilf Kebir, Jabal Arkenu and Jebel Uweinat farther south. This goes well together with the exceptional dune pattern superimposed on the longitudinal draa immediately north of the Gilf Kebir (see Section 3.3.2).

Generally, the wind velocities are higher in the north and decrease between 26°N and 27°N. This could explain why the dunes on the transverse draa are higher than on the longitudinal draa (see Sections 3.3.1 and 3.3.2). North of 25°N, the directions vary from WSW (only in January) to NNE (only in December). In the remaining months the range is much smaller and covers only NW to N. This would account for the general dune alignment in a southeastern direction where – according to Cook and Warren (1973) – NW would be the major component. A locally more unidirectional or more bimodal wind system deduced from the granulometric changes (see Section 4.3.2) cannot be recognized in the stream-flow pattern. As already mentioned, however, just 1 year of processed data is not enough. For example, the heavy south winds frequently recorded during field work do not appear at all in the charts.



### 3.4. THE SAND BUDGET

According to Mainguet and Chemin (1983), transverse dunes indicate a positive sand budget and longitudinal dunes a negative one. In this sense, the whole sand sea, with the exception of the southwestern part, has a negative sand budget. What is correct for dunes, however, need not necessarily be so for draa (that Mainguet and Chemin did not distinguish from dunes).

Independent of the topography of the Great Sand Sea, the largest sand mass lies in the bedrock depression below the northwestern sand sea (see Section 3.1). These sands are neglected in the sand budget that is discussed only for the draa. The question where the sands in the Great Sand Sea came from is of greatest interest. They may have been supplied by local sandstone weathering or by alluvial deposits from mountainous areas in the vicinity (like the Gilf Kebir, the Abu-Ballas Escarpment or the dissected terrain between Ain Dalla and Siwa), or even by streams from more distant sources. In any case, it has to be assumed that the sands were particularly abundant in the centres of alluvial deposition. The model of draa formation does not need long-distance aeolian sand transport but only implies short diagonal motion in the vortices. This was corroborated in the Namib Erg, where ancient alluvial fans could be reconstructed due to different sand characteristics in the draa (Besler, 1980). In the Great Sand Sea, the major bulk of sands should also be found in the draa close to former alluvial fans.

A rough calculation of the sand volume stored in the draa may provide a clue to where these ancient centres of deposition have been. For this reason, the volume of sand prisms along the transections was roughly calculated. Transverse and longitudinal draa were considered separately, using the heights, the widths and the distances between the cross-sections for the calculation. This is, of course, only a



**Table 3** Sand budget of the draa calculated from sand prisms along the transections based on cross-section measurements

	W	Middle	E	
Transverse draa	1.2	1.0	1.4	$\times 10^9 \text{ m}^3$
	Without underlying sand body			
Longitudinal draa	1.5	0.8	0.5	$\times 10^9 \text{ m}^3$

poor approximation to the actual conditions. Not the absolute values are therefore important, but the comparison between the sand prisms in transverse and longitudinal draa on the three transections. Because only short cross-section sequences are available for the transverse draa (see Section 2.3.2), all prisms had to be reduced to the minimum length of 44 km (Table 3). As Table 3 shows, no general direction of volume increase or decrease exists, but a centre of abundant sands is indicated in the southwest and another one in the northeast. Here, major sand sources can be assumed.

In the southwestern sand sea, the connection to fluvial systems draining the Gifl Kebir and the adjacent Abu Ras Plateau west of it had already been recognized during the field survey (see Sections 3.1 and 3.2.1). Further support for this connection is provided by the granulometry (see Section 4.2). According to RADAR-image (SIR-C, L-band) interpretation by El-Baz et al. (2000), buried palaeo-channels can be traced from the western Gifl Kebir to almost  $25^\circ\text{N}$ , i.e. the southern margin of the sand sea west of its southern extension (compare Section 3.1.3). East of the Gifl Kebir, palaeo-channels extend from the tropic near  $27^\circ\text{E}$  towards the northwest up to  $24^\circ30'\text{N}$ ,  $26^\circ20'\text{E}$  (Fig. 3 in El-Baz et al., 2000). This buried drainage channel seems to end in the eastern part of the southern sand-sea extension (compare Fig. 18). Another palaeo-channel can be traced from the tropic near  $28^\circ\text{E}$  up to  $24^\circ\text{N}$ ; it does not, however, seem to have reached the sand sea.

The high northeastern sand budget refers to the area of transverse draa around  $27^\circ\text{N}$ . With regard to the entire sand sea, it is therefore more correct to call this part an eastern centre of abundant sands. No fluvial traces can be found there because of the sand cover in the interdraa corridors. However, strong evidence of an alluvial centre is again provided by the granulometry (see Section 4.2). Moreover, the heavy-mineral assemblage of the eastern draa sands is similar to that of the Minqar El-Talh sandstone that, east of the sand sea, is mostly eroded (see Section 7.2; Besler, 1998).

The conspicuous shortage of sands in the southeastern part of the sand sea can already be recognized in the cross-sections of the eastern transection and excludes a sand source in this direction. Another depositional centre of alluvium could have been the area of the gravel plain (Sarir Dalma) in the west because this feature resembles a deflated fan, and the sand volume in its vicinity is also exceptionally large. No investigations were, however, possible in the Libyan part of the sand sea.

The sand volume in the draa can provide valuable information on possible sand sources. It was used here as a first hint that was followed and tested by applying various other criteria. In a wider frame and in more detail, the sand sources will be discussed conclusively in Section 8.6.3.

## THE GRANULOMETRIC ANALYSIS

### Contents

4.1. Historical Developments	73
4.2. Grain-Size Parameters	75
4.2.1. Mean grain size ( $M_z$ )	76
4.2.2. Sorting ( $S_o$ )	79
4.2.3. Skewness ( $S_k$ )	80
4.2.4. Kurtosis ( $K$ )	81
4.3. The System of Granulometric Sand Types	82
4.3.1. Granulometric sand types of the draa	85
4.3.2. Granulometric sand types of the dunes	88
4.3.3. Granulometric types of the sandstones	94
4.4. The Response Diagram	95

### 4.1. HISTORICAL DEVELOPMENTS

After a few early forerunners in the 1930s (a.o. Trask, 1932; Krumbein, 1934, 1936; Krumbein and Pettijohn, 1938; Otto, 1939), numerous contributions dealing with grain-size parameters were published in the 1950s and 1960s of the twentieth century. One of the earliest publications, the study on Brazos River Bar by Folk and Ward (1957), turned out to be most important for several reasons: Folk and Ward used  $\varphi$ -gauged sieving sets and probability paper for plotting the cumulative grain-size distributions. They developed formulas (based on Inman, 1952) in which the significant marginal parts of a grain-size distribution (the coarsest and the finest fractions) are used for determining the grain-size characteristics. Furthermore, with the aid of a four-variate graph, they discussed the geological meaning of parameter values for the history of sediments. The formulas of Folk and Ward turned out to be most appropriate for statistical sand analysis, by geologists and geographers, and are used worldwide now. For the investigations of the present author, they provided valuable information on sand sources and on sand-transport directions (Besler, 1980, 1987c, 1989) as well as on the aeolian age of sands (Besler, 1991b, 1995). Grain-size parameters and their spatial distributions are discussed in Section 4.2.

Numerous publications dealt with the possibility to distinguish between sands from different environments by comparing their grain-size parameters (a.o. Mason and Folk, 1958) or by plotting various combinations of parameters

(a.o. Friedman, 1961, 1967; Moiola and Weiser, 1968). These combinations were also used for sands from the Namib Erg (Besler, 1980). With only one exception, however, they did not turn out to be very helpful. Most probably for this reason, grain-size characteristics play only a minor role in later geoscientific publications. The exception is a plot of mean (grain size) and standard deviation (sorting) for dune and river sands by Friedman (1961, his Fig. 5). When this was applied to Namib sands (Besler, 1980), active dune-crest sands and fluvial sands could be distinguished. In addition, the undefined section of overlap in the Friedman plot could be identified as the section of aeolian sands that are no longer mobile.

Numerous analyses of sand samples from various deserts of the world led to an improvement of the graph, which now allows the distinction between fluvial deposits, mobile aeolian sands, stable aeolian sands and aeolian residuals. Because this plot demonstrates the actual response of sandy deposits to present-day winds, it was named the “response diagram” (Besler, 1983). The application of this diagram by other authors gave supporting results, for example, for the ancient Qoz dunes in northern Sudan (Gläser, 1984). Critical comments came from Vincent (1985, 1988), Thomas (1986) and Livingstone (1987, 1989). They could, however, partly be explained as misunderstandings (Besler, 1996a). On the other hand, these comments were very inspiring to understand the unique character of the barchan dune as a soliton (Besler, 1997b, 2002b; Schwämmle and Herrmann, 2003; Herrmann, 2005). The response diagram is still valid and will be applied in Section 4.4.

A more significant method to gain information on the aeolian mobility and stability of sands as well as on the history of sands has been found by applying special grain-size frequency distributions. Bellair (1940), who worked for the Geological Map of Algeria, was one of the first authors who used a kind of grain-size frequency distribution to characterize and differentiate between sediments in the Sahara. Unfortunately, he used an exceptional sieving set. As a consequence, the fractions are not comparable to the general  $\varphi$ -sievings, but they can nevertheless be approximated. Interestingly, the frequency distributions were drawn as compass cards normally used at weather stations for directions and frequencies of winds: the polar coordinates represent the different sieves. Alimen (1957) also contributed to the Geological Map of Algeria. Apart from using grain-size parameters (median, quartiles) and cumulative distributions, she already plotted weight percentages against grain diameters in frequency distributions at a logarithmic scale, which comes close to later standards. These graphs allowed the distinction between deposits in ergs and sebkhas (salt pans). Different sand types within one dune could be distinguished by the position of the modes (the largest fractions) and by their numbers within one sample.

Bagnold, in his benchmark book (1941), also developed a type of frequency distribution. This was, however, a more complex method; he applied this method at double logarithmic scales for components of the sand moved in his wind-tunnel experiments. This has rarely been applied later (a.o. Kuhlman, 1959). In their samples from various ergs of the Sahara, Capot-Rey and Grémion (1964) distinguished between four sand classes according to their frequency distributions as histograms. Their criteria were the number and the widths of the modes. All grain-size frequency distributions mentioned so far represent sediments from the

Algerian Sahara and show weight percentages on the ordinate. A comparison between different deserts did not exist.

An important paper on the mathematical background of grain-size distributions was published at the time by Walger (1964), who defined the grain-size frequency distribution as the first differential of the cumulative distribution which changed the ordinate ( $dy/dx$ ) to weight percentage divided by the fraction interval in millimetres. The great advantage of this graph is that the importance of aeolian single-grain processes is stressed and that the few coarse grains (over-represented in the former graphs) only appear in smaller modes appropriate to their significance for aeolian processes.

This type of grain-size frequency distribution has been tested against the traditional one (weight percentage on the ordinate) and also against the other extreme with grain numbers on the ordinate (at logarithmic scale) for the same samples (Besler, 1984b). The first-differential graph proved to be most sensitive to aeolian processes and, applied to a large stock of samples from various deserts, allowed the distinction and characterization of granulometric types of aeolian sands (Besler, 1996a). Meanwhile, the analysis has been extended to more than 1000 samples, which always yielded the same few (about a dozen) granulometric types. Moreover, the same – and only these – granulometric types (though not all of them) were also discovered in Pleistocene inland dunes of Middle Europe (Möckel, 2004) and in aeolian sandstones (Besler and Pfeiffer, 1995; Besler, 1996b). Their existence was also mathematically-statistically confirmed by cluster analysis (Bolten, 2001). There only seem to exist a limited number of granulometric sand types in all deserts, past and present. Moreover, all types can be seen as parts of a system of the granulometric evolution of aeolian sands (Besler, 2005). This system provides a clue to the history of sandy deserts with regard to processes of dune and palaeo-dune dynamics, to sand budgets and even to the wind regimes. This concept of granulometric sand types is applied to the samples from the Great Sand Sea in Section 4.3.



## 4.2. GRAIN-SIZE PARAMETERS

Grain-size parameters of individual samples are not very significant as can be deduced from the wide range of their values (see Appendix 1). In order to find the spatially and dynamically characteristic pattern of the sands, the grain-size parameters have to be grouped according to localities or sediment types. Therefore, the samples of each transection were divided into a group of dune sands and a group of draa sands, and the latter were again divided into sands of transverse draa and sands of longitudinal draa with respective subgroups of interior draa sands and surficial draa sands. The dune sands were not grouped according to the underlying draa because all sands come from the silk type, and because only few samples exist from dunes on transverse draa.

Only the parameter of mean grain size is suitable for statistical means because it is not divided into categories in the concept of Folk and Ward (1957). All other parameters have to be considered according to their different categories that would

be lost in the mean values. For example, a certain number of platykurtic sands with kurtosis values  $<0.9$  together with leptokurtic sands with kurtosis values  $>1.11$  may result in a mean value representing mesokurtic sands (0.9–1.11). The characteristic differences between platykurtic and leptokurtic sands that are diagnostic for the sand sources (see Section 4.2.4) would disappear. Table 4, showing comparative grain-size parameters, was found to be very indicative.

#### 4.2.1. Mean grain size ( $Mz$ )

Everywhere, the mean grain size of the dune sands is distinctly smaller than  $Mz$  of the draa sands. This was already observed by Capot-Rey (1947) in the Idhan Murzuq in Libya. Although he did not distinguish between draa and dunes, he described a sudden increase of the gradient towards the top with finer sands. According to Thomas (1986) citing Sahu (1964), the mean grain size represents the average kinetic energy of the depositing agent. This already shows the greater strength of the Pleistocene winds. While the dune sands are relatively coarse in the east and in the middle, they are distinctly finer in the west. This corroborates the great supply of fine-grained sands in the southwest (see Section 3.2.1) and helps to explain the occurrence of transverse dunes on the longitudinal draa. It should be mentioned, however, that for the statistical mean only few values are available along the eastern transection. Though Table 4 does not differentiate between dunes on transverse draa and dunes on longitudinal draa, this has to be discussed. There are significant differences within the dune sands of one transection. The dune sands on transverse draa in the east are finer than on the longitudinal draa which goes well together with the greater dune height of the former.

The differentiation is particularly well marked along the middle transection where dune sands on transverse draa are coarser by 0.1 mm. This also correlates with the dune height that is only 12 m here (see Section 3.3.1). The generally smaller mean grain size of dune sands on longitudinal draa also shows great differences. If all individual values (see Appendix 1) along the longitudinal draa are compared from south to north, a sudden decrease in  $Mz$  occurs at  $25^{\circ}25'N$ . This cannot be related to the sand transport because the winds blow from northerly directions. Therefore, the assumption that the sand transport in ergs is always in the direction of finer and better sorted sands (Cooke and Warren, 1973) has to be challenged. There exists no correlation with dune height. The granulometric sand types, however, were found to be different (see Section 4.3.2).

On the western transection, the dune sands on transverse draa are also coarser than on longitudinal draa, but the difference is not so great. Conspicuously, the dunes in the transition zone between both draa types are even coarser grained than in the north, which, on the other hand, causes a sudden decrease in mean grain size towards the south at  $26^{\circ}06'N$ . Another exceptional reduction in  $Mz$  is found on three cross-sections of the longitudinal draa between  $25^{\circ}24'N$  and  $25^{\circ}42'N$ , where the highest dunes (30 m) occur (see Fig. 9).

Apart from a few exceptions, a negative correlation exists between dune height and mean grain size. This, by the way, was also noticed by McKee (1983), who

**Table 4** Comparative grain-size parameters (D = dune sands; M = megadune (draa) sands; LM = longitudinal draa; TM = transverse draa; SM = surface of draa; IM = interior of draa)

	West (mm)			Middle (mm)			East (mm)		
<i>M<sub>z</sub></i>									
D		0.2170			0.2468			0.2421	
M		0.2803			0.3454			0.3410	
LM		0.2597			0.3568			0.3308	
TM		0.3147			0.3369			0.3513	
SM		0.3080			0.3511			0.3574	
IM		0.2622			0.3432			0.3165	
<i>S<sub>o</sub></i>	Good <0.5	Moderate <1.0	Poor >1.0	Good <0.5	Moderate <1.0	Poor >1.0	Good <0.5	Moderate <1.0	Poor >1.0
D (%)	95	5		80	20		50	50	
M (%)	15	77	8		64	36		50	50
LM (%)	21	79			33	67		60	40
TM (%)		71	29		88	12		40	60
SM (%)		71	29		25	75		17	83
IM (%)		79	21		80	20		100	
<i>S<sub>k</sub></i>	+ >+0.1	±	- <-0.1	+ >+0.1	±	- <-0.1	+ >+0.1	±	- <-0.1
D (%)	26	74		80	20		67	33	
M (%)	15	46	39	71	29		70	20	10
LM (%)	11	37	52	67	33		80		20
TM (%)	29	71		75	25		60	40	
SM (%)	43	14	43	75	25		67	17	16
IM (%)	5	58	37	70	30		75	25	

(Continued)

**Table 4** (Continued)

<i>K</i>	West (mm)			Middle (mm)			East (mm)		
	Platy <0.9	Meso	Lepto >1.11	Platy <0.9	Meso	Lepto >1.11	Platy <0.9	Meso	Lepto >1.11
D (%)		68	32	7	53	40		83	17
M (%)	23	62	15	64	36		70	30	
LM (%)	21	63	16	50	50		60	40	
TM (%)	29	57	14	75	25		80	20	
SM (%)	57	43		25	75		100		
IM (%)	11	73	16	80	20		25	75	

D = dune sands; M = megadune (draa) sands; LM = longitudinal draa; TM = transverse draa; SM = surface of draa; IM = interior of draa.

stated that in the Great Sand Dunes of Colorado, the highest dunes ( $>30$  m) were finer grained and better sorted than the lower dunes. Because the grain size differentiation is not induced by the draa (see below), this seems to be a consequence of small-grain selection by the wind. However, the correlation between silk height and mean grain size is not statistically significant. This may be due to the sudden changes in  $Mz$  and to the difficulties in discerning the correct dune heights (see Section 3.3).

A comparison of all draa sands gives the same relations as with dunes: the mean grain size is comparable on the eastern and middle transections, and smaller on the western transection. This might suggest a correlation between draa and dune sands. However, a separate consideration of sands from transverse and longitudinal draa contradicts this suggestion. The former show an increasing mean grain size towards the east, where their dunes are highest and finest grained. Because this was also the palaeo-wind direction, the coarsest sands in the east can only be explained by a sand source near this part (see Section 3.4). In the longitudinal draa, the sands in the west are 0.1 mm finer than the rest. Indeed, this corroborates the inheritance of particularly fine sands in the dunes (see Section 4.2.4). The dune sands are more comparable to the draa sands here than in the middle and in the east, where a difference of 0.1 mm exists. The Holocene winds seem to have selected more or less the same grain sizes everywhere; only in the west, however, the supply seems to have been almost unlimited (see Sections 3.2.1 and 3.4). On all transections, the mean grain size is large if only the surface sands of the draa are considered. This is due to modern deflation and is well documented in comparison with the interior draa sands.

On the whole, the mean grain size gives support to a southwestern and a northeastern sand source and to a grain selection from the draa by weaker winds. The sudden changes along the longitudinal draa put forward some questions that ask for additional evidence (see Section 4.3.2).

#### 4.2.2. Sorting ( $S_o$ )

The sorting of sands varies greatly from very good ( $<0.35$ ) to poor ( $>1.0$ , see Appendix 1). According to Thomas (1986) citing Sahu (1964), the sorting represents the fluctuations in the kinetic-energy conditions (about the mean) of the depositing agent. This would mean that the fluctuations in the Pleistocene winds were relatively large and decreased towards the east (Table 4, interior draa), whereas the fluctuations in the modern winds get stronger in this direction (Table 4, dunes). However, the Great Sand Sea shows well that different sand sources cannot be neglected in this respect. The few very well sorted samples are integrated into the category of good sorting in Table 4. In the west, however, 63% of the dune sands are very well sorted. This correlates with the well-sorted draa sands that also occur only in the west.

Vossmerbäumer (1974), who compared German inland dunes to modern desert dunes, stated that the latter generally are very well sorted. This has to be challenged because apparently it depends on the sand sources and on the stage of aeolian sand evolution (Besler, 2005). A comparison of sands ( $>1000$ ) in the data bank of the



present author yielded 41% of very well sorted sands in “dome sands” of desert dunes, which is the maximum compared to other granulometric sand types (see Section 4.3). According to Friedman (1961), inland dunes generally have a sorting of  $<0.5$ , which means that they are at least well sorted. Later, Friedman (1962) suggested that inland dunes were moderately well sorted ( $<0.8$ ). According to McKee (1983), who compared aeolian sand bodies around the world, most dune sands are moderately sorted. This at least holds true for several granulometric sand types in the database but not for the types in the Great Sand Sea (see Section 4.3.2). According to Folk and Ward (1957), the sorting reaches a maximum during transport and thereafter decreases again if the transport goes on. Indeed, some support for this assumption is found in the Great Sand Sea (see Section 4.3.2).

Generally, the sorting increases towards the west, in combination with decreasing mean grain sizes. This correlation is not statistically significant because, for example, the rather coarse dune sands in the transition zone between both draa types are very well sorted. The poorest sorting is found in the draa-surface sands due to the modern deflation (see Section 4.2.1). Among all longitudinal draa, samples from the middle transection have the highest percentage of poor sorting going together with the largest mean grain size. This suggests a sand input from additional sources (see Section 4.2.4).

Taking all together, the sorting supports the conclusions drawn from the mean grain size and supplies some evidence for additional sand sources in the southern middle part of the Great Sand Sea.

### 4.2.3. Skewness ( $Sk$ )

The skewness indicates the deviation from the (normal) symmetrical grain-size distribution. Positive values of  $Sk$  indicate a tail of fines in the sample, negative values indicate a tail of coarser grains (Folk and Ward, 1957). According to the literature, dune sands and river sands are positively skewed, and beach sands are negatively skewed (a.o. Friedman, 1961, 1962; Vossmerbäumer, 1974; Binda, 1983). Brezina (1980), however, emphasized that water-transported sands show a negative skewness after  $\varphi$ -sieving. In the longitudinal dunes (draa) of the Simpson Desert in Australia, Folk (1971) found 92% positive skewness.

In the Great Sand Sea, the majority of dune and draa sands are positively skewed. In the west, however, the large proportion of symmetrical skewness, especially in the dunes, is conspicuous. On the other hand, the sands of the longitudinal draa as the source material, in their majority, are negatively skewed here, due to a tail of coarser grains. This may still be the heritage of their water transport before draa formation (according to Brezina, 1980). In this respect, the symmetrical skewness of the dune sands could mean that they are undergoing a process of adjustment to the modern aeolian environment, a stage which the draa sands had not reached in the Pleistocene.

Negative skewness is hardly found in the sands of the transverse draa, and not at all along the middle transection, in spite of very coarse sands. Binda (1983), investigating the skewness of aeolian sands from Saudi Arabia, came to the

conclusion that the tail of fines augmented with increasing mean grain size, and that the skewness therefore became more positive. This is corroborated by the evaluation of grain-size parameters in the own sand database grouped according to granulometric sand types (see Section 4.3). The skewness turned out to have the best indicative character because it almost linearly increases along a series of seven granulometric sand types with increasing  $Mz$ , based on the “aeolian age” of the dunes. Starting with “young dune sands” with only 9% positive skewness and ending at “deflated sands” with 100% positive skewness, the average increase in positive skewness from one granulometric sand type to another in the series is 13.5%. No other grain-size parameters show such a strictly unidirectional change. Therefore, the skewness seems to be characteristic and indicative for the “aeolian age” of a sand (see Section 4.3). Again, however, the influence of the sand sources has to be taken into account.

If this concept is cautiously applied to the Great Sand Sea, the dune sands along the middle transection should have the highest aeolian age. With regard to the western transection, this concept also seems applicable to draa sands. In this case, the transverse draa in the middle and the longitudinal draa in the east would have the highest aeolian age, with a positive skewness of 75 and 80%. In this context, the western draa seem to have been subjected to the formation processes during a shorter time interval (see Section 8.6.3.3). The aeolian age, however, is not only a function of time but also a function of wind velocities and underlying topography exposing the sand or channeling the air flow (Besler, 1996a).

#### 4.2.4. Kurtosis ( $K$ )

More than sorting and skewness, the kurtosis is very indicative for the aeolian history of sands. According to Folk and Ward (1957), the kurtosis measures the ratio of the sorting in the extremes of the grain-size distribution compared to the sorting in the central part. A leptokurtic curve (value  $>1.11$ ) is excessively peaked and a platykurtic one (value  $<0.9$ ) deficiently peaked. Extreme high or low values of  $K$  imply that part of the sediment achieved its sorting elsewhere in a high-energy environment and that the new environment is one of less effective sorting energy. They emphasized that a mixed sediment is strongly bimodal. In fact, investigations of the present author, restricted to aeolian sands, only found this in platykurtic sands which seem to be a mixture that is not yet adjusted to the actual aeolian environment. Leptokurtosis, on the other hand, is not always associated with bimodality and seems to indicate that the bulk of the sand (not only part of it) had been pre-sorted in an earlier aeolian environment. In his note on kurtosis and peakedness, Baker (1968) demonstrated that graphic kurtosis is in no way related to moment kurtosis, and that the shape connotation should be abandoned. This debate referred to the normal Gaussian frequency distribution. It has to be stressed that the first-differential graph in any case does not display the kurtosis or the peakedness.

According to the literature (a.o. Folk, 1971; Vossmerbäumer, 1974), dune sands are generally mesokurtic. This has to be challenged because the evaluation of all kurtosis values in the own database, grouped according to granulometric sand types,

shows that this is only true for “inactive crest sands” with a mesokurtosis of 92%. The average dune sand, however, belongs to the type of “active crest sands” with a mesokurtosis of only 66% (see Section 4.3).

In the Great Sand Sea, a certain proportion of dune sands on all transections is leptokurtic. This is quite natural because they represent reactivated draa sands which necessarily had been pre-sorted in an earlier aeolian environment. But along the western transection – and only there – leptokurtosis is also found in draa sands. This is outstanding and has not been observed in draa before, neither in – for instance – Mali (Besler, 1987c) nor in Burkina Faso (Besler and Pfeiffer, 1992). In the Namib draa, however, leptokurtosis is found to a lesser degree as well (Bubenzer et al., 2007a). In the southwest of the Great Sand Sea, aeolian pre-sorting apparently indicates the heritage of the aeolianite in the Gilf Kebir Sandstone (see Section 4.3.3). A sample of this yielded a value of  $S_o = 0.51$ , which is an extremely good sorting for a sandstone. It is strange, however, that the transverse draa in the west also show this proportion of leptokurtic sands. The question is how far northwards the Gilf Kebir river sands had been transported (see Sections 4.3.2 and 8.6.3.3).

On the draa surfaces, the effect of pre-sorting is destroyed by modern deflation, which leads to the disappearance of leptokurtosis and even to strong platykurtosis. The latter is particularly pronounced in the interior of the longitudinal draa on the middle transection. This means that the sands there have not been adjusted to the aeolian environment during accumulation of the draa. Sands from different sources were incorporated and only insufficiently mixed. With regard to the modern platykurtic surface sands, however, this could also mean stronger deflation during the draa-formation processes. To answer this question, the granulometric sand types and the SEM analysis may offer a clue (see Sections 4.3.1 and 8.6.3.6). Even the modern dune sands seem to have partly inherited this poor mixing because – contrary to the other transections – a small proportion (7%) of them is platykurtic.

In summary, the kurtosis gives strong support to the Gilf Kebir Sandstone as a southwestern sand source and some support to sands coming from various sources in the southern middle part of the Great Sand Sea.



### 4.3. THE SYSTEM OF GRANULOMETRIC SAND TYPES

The granulometric sand types belong to the system of granulometric evolution of aeolian sands which seems to be valid for all deserts, past and present (Besler, 2005; Fig. 31). Criteria for the distinction of sand types (Fig. 32) are the occurrences and the heights of modes in the different fractions as displayed in the first-differential grain-size frequency distributions. Besides coastal sands and decaying sandstones, alluvial sands deposited by endorheic rivers are supposed to be the main material for aeolian activities in deserts (a.o. McClure, 1978; Besler, 1992).

The most important branch of the system is the meso-scale dune evolution. The sequence starts with “aeolian terrace sands” (1), found on river terraces, with a characteristic peak in the finest sand fraction (0.063–0.125 mm) and a lower shoulder up to 0.5 mm. Clay- and silt-sized grains are blown off as dust while the

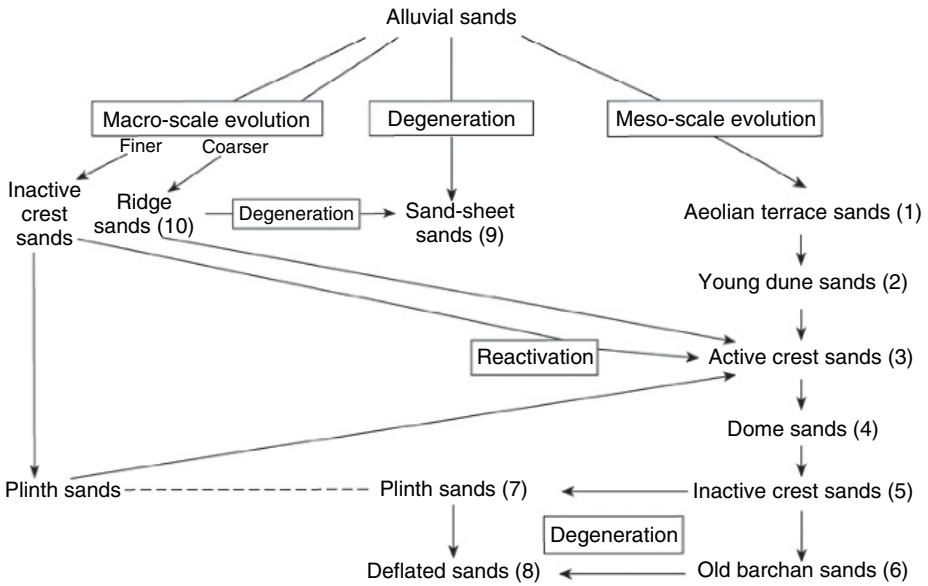


Fig. 31 Granulometric sequences of aeolian sand evolution.

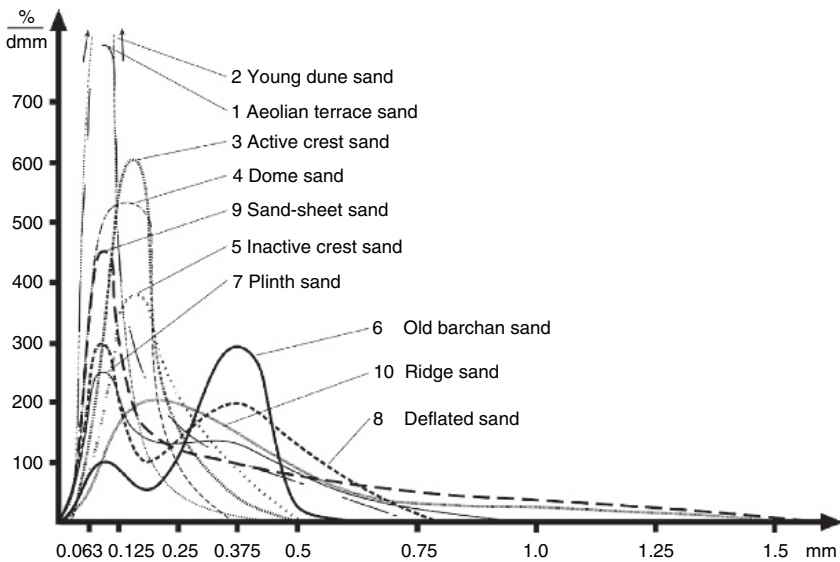


Fig. 32 Characteristic grain-size frequency distributions of granulometric sand types.

sands are shifting, but no dune formation takes place yet. From these sands, the fine-grained part is selected to form “young dune sands” (2) with an excessively high peak at 0.063–0.125 mm, where the coarse-grained shoulder is left behind. This type is found in small longitudinal and transverse dunes and in young barchans as well. The smallest grains sooner or later are gone with the wind, and the bulk of sands now falls into the next fraction (0.125–0.25 mm), represented by the type of “active crest sands” (3). They are found in primary longitudinal and transverse dunes and in barchans as well as in secondary dunes on draa after their reactivation.

As the next step, “dome sands” (4) represent a retardation in the evolution which only occurs if an abundance of finest sands for aeolian input is provided by repeated nearby runoff. This type has a characteristic broad mode covering 0.063–0.25 mm and was first observed in dunes on dome-shaped draa (hence its name). “Dome sands” are relatively rare and therefore do not seem to represent the usual transition from “young dune sands” (2) to “active crest sands” (3). Without this retardation, the “active crest sands” gradually lose grains from the main fraction (0.125–0.250 mm), which means an increase in the coarser fraction (0.25–0.5 mm). This type of “inactive crest sands” (5) is mainly found in lower parts of longitudinal and transverse dunes, but also in the brinks of barchan dunes. The threshold between active and inactive crest sands was found to lie – according to cluster analysis (Bolten, 2001) – in the main fraction at 500%/dmm on the ordinate ( $dy/dx = \text{weight percentage divided by the fraction interval of } 0.125 \text{ mm}$ ).

For quasi-stationary longitudinal and transverse dunes where only the upper parts of crests are oscillating, the sequence ends here. Only in the migrating barchan dune where the entire sand body is shifting, the evolution gradually continues by further reduction of the former main fraction and an increase in the coarser fraction. The final “old barchan sand” (6) is unimodal in the fraction 0.25–0.5 mm. This seems to be the last stage of the granulometric dune evolution in modern wind systems. No coarser main fractions or modes have been found in dunes (but in megarripples). In this context, it should be mentioned that Bellair (1940) already noticed the differences in the grain-size distributions of barchan sands. Alimen (1957) emphasized that particularly the grain-size distributions of barchan sands can give very different curves. In addition, Capot-Rey and Grémion (1964) observed that barchan dunes are found in fine and coarse sands and even in gravels. Indeed, initial barchan shapes have been found in gravel heaps in the southern Namib. However, the heaps, consisting of waste material, were made there by people in search of diamonds. They are not the result of migration. Apparently, the unique character of barchan dunes, changing their grain-size distributions, has been recognized long ago.

Regarding their different formation processes, it is clear that draa do not belong to the dune sequence but to the macro-scale evolution (see Section 3.2). Characteristics are a rather low single mode in the fraction 0.125–0.25 mm accompanied by relatively high amounts in the neighbouring fractions of 0.063–0.125 mm and/or 0.25–0.5 mm, together with a long tail in the even coarser part. This type is found as surface sand and by coring as interior sand of draa. With regard to the long sand ridges, it was named “ridge sand” (10). The stronger winds explain the coarse-grained tail and the reduced proportions in finer grains. If there are only

fine-grained source materials, however, no coarse tail can develop, and the draa consist of “inactive crest sands”. This short sequence ends here, because a reactivation by weaker winds leads to the selection of “active crest sands” (3).

The degenerative branch includes the following three different ways of degeneration. First, “sand-sheet sands” (9) are characterized by their long tail of coarse grains which – as a desert pavement – protects the finest sand grains (0.063–0.125 mm) in the small mode. They represent residuals that were left behind after dune formation and that in many deserts cover vast areas. If “ridge sands” (10) in draa are reactivated by modern winds that select “active crest sands” (3), the residuals may also be “sand-sheet sands” (9). According to Bellair (1940), in the Sahara these sands are bimodal with a second smaller mode in the coarser part. Investigations by the present author show that sand sheets with ripples in the Teñéré (Niger), northern Mali and the Taklamakan (China) either have a bimodal grain-size frequency distribution or a unimodal one. Sand sheets without ripples in the same areas, however, always have a unimodal distribution (Besler, 1992, 1996a). It must be mentioned, however, that coarser modes are suppressed in the first-differential curve.

Second, when giant old barchan dunes are slowed down or smaller barchans coalesce, the balance between sand entrainment and sand input is severely disturbed (Besler, 2002b). They may become quasi-stationary dunes where the fine-grained input is not removed because the sand body is no longer turned over. In this case, the strongly bimodal granulometric type of “deflated sands” (8) develops. It is characterized by a higher mode in the finest sand fraction, a lower second mode in the 0.25–0.5 mm fraction and a strong reduction in the aeolian main fraction. Almost 40% of the “deflated sands” in the database were sampled from huge, complex barchan dunes. In addition, sand shields as a result of “failed” barchan formation (Besler, 1997b, 2000a) are covered by deflated sands.

Third, “plinth sands” (7) are characterized by a plateau from  $>0.063$  to  $<0.5$  mm and may have a little peak in the finest sand fraction. Their history is most complicated and less well understood. A gradual transition from “inactive crest sands” (5) along the lower flanks of modern dunes to “plinth sands” (7) at the bottom was observed in Algeria and Egypt. It is not clear, however, whether “plinth sands” found in draa also represent their plinth or basal part. This could well be, because only the lower parts of draa have survived since the Pleistocene. On the other hand, plinth sands with a frequency distribution between “inactive crest sands” (5) and “ridge sands” (10) may reflect the intermediate grain sizes supplied by the alluvial source (see Section 4.3.1).

The concept of granulometric sand types provides exceedingly valuable information on the aeolian history of draa and dunes. Therefore, it is applied to the Great Sand Sea.

#### 4.3.1. Granulometric sand types of the draa

According to Haynes (1982) citing Bagnold (1941), whaleback dunes (draa) in the Great Sand Sea have a bimodal grain-size distribution and are covered by a surface armour of fine pebbles or coarse sands. This was repeated by Kröpelin (1993) and

Embabi (1998), and it is a nice example how a misunderstanding is propagated through literature. On the quoted pages, Bagnold referred to sand sheets (p. 157) and to bottom zones of dunes covered by grit and small pebbles from the surrounding desert floor (p. 229). The grain-size frequency distributions show that the majority of draa sands belong to the granulometric type of ridge sands (53%, Table 5) where the maximum is found in fine and middle-sized sands, and only the tail is composed of coarser sands. Gravels are not found, not even on the surfaces. Only 8% of draa sands represent sand-sheet sands, which means that they are deflated. Indeed, all of them were sampled from draa surfaces. Also here, however, gravels are not integrated. Three quarters of these sand-sheet sands come from the transverse draa. This may indicate a higher velocity of the modern westerlies compared with the trade winds. In fact, according to the stream-flow charts (see Section 3.3.4), the velocities of westerlies as well as of trade winds are higher above the northern sand sea.

A separate discussion of granulometric sand types along the three transections is of interest (Table 5). In the east, two thirds of the draa sands are ridge sands, and 22% are sand-sheet sands from the surfaces of transverse draa. Only one interior sand (at Regenfeld) is a plinth sand, and this is a younger cover sand (see Section 5.3.3).

Along the middle transection, 86% of draa sands (14) represent the type of ridge sands. Only at the drilling site on the east flank of the longitudinal draa, the surface sand belongs to the type of plinth sands, whereas the draa interior again yielded ridge sands. All interior sands are ridge sands and not deflated. The high degree of platykurtosis mentioned in Section 4.2.4 is therefore not caused by deflation during accumulation of the draa, but seems to reflect a poor mixing of different sands.

Once more, the western transection is different. There exists not only a greater variety of sand types, but also a stronger differentiation between longitudinal and transverse draa. With 71% ridge sands and one sand-sheet sand, the transverse draa are comparable to the other transections. In addition, they contain one old barchan sand at a depth of 2 m. This does not necessarily mean that barchans developed during draa formation. It indicates, however, that the sands have been shifting and have lost more fines during their accumulation (see Section 5.3.2). In the longitudinal draa, however, the majority of sands (19) represent the granulometric type of inactive crest sands (47%), clearly indicating a fine-grained sand source. The second place is even held by active crest sands (32%) that are the main type in modern dunes and that have not been found in draa before. This explains the surprisingly good sorting (see Section 4.2.2) and the leptokurtosis (see Section 4.2.4). The type of ridge sands covers just 16% and is only found on draa surfaces, where the concentration of coarser grains can be interpreted as the result of modern ongoing deflation, eventually leading to a desert pavement. Unfortunately, the ridge sands on the draa surfaces conceal the interior transition from inactive and active crest sands in the south to ridge sands in the north. This boundary most probably comes close to the northern margin of the ancient Gilf Kebir alluvial sands which must have been somewhere between the drillings at 25°42'N and 26°51'N. One old barchan sand was met at a depth of 1 m in the drilling on the west flank. Although it should not be overestimated, this type only occurs in western flanks (see Section 5.3).

**Table 5** Granulometric types in draa sands

		Ridge sands	Inactive crest sands	Active crest sands	Sand-sheet sands	Old barchan sands	Plinth sands
Transverse draa							
W transection	(n = 7)	5			1	1	
Middle transection	(n = 8)	8					
E transection	(n = 5)	3			2		
Longitudinal draa							
W transection: W slope	(n = 7)	1	4	1		1	
E slope	(n = 12)	2	5	5			
Middle transection: W slope	(n = 3)	3					
E slope	(n = 3)	1			1		1
E transection: W slope	(n = 0)						
E slope	(n = 4)	3					1
Σ	(n = 49)	26	9	6	4	2	2
		53%	18%	12%	8%	4%	4%



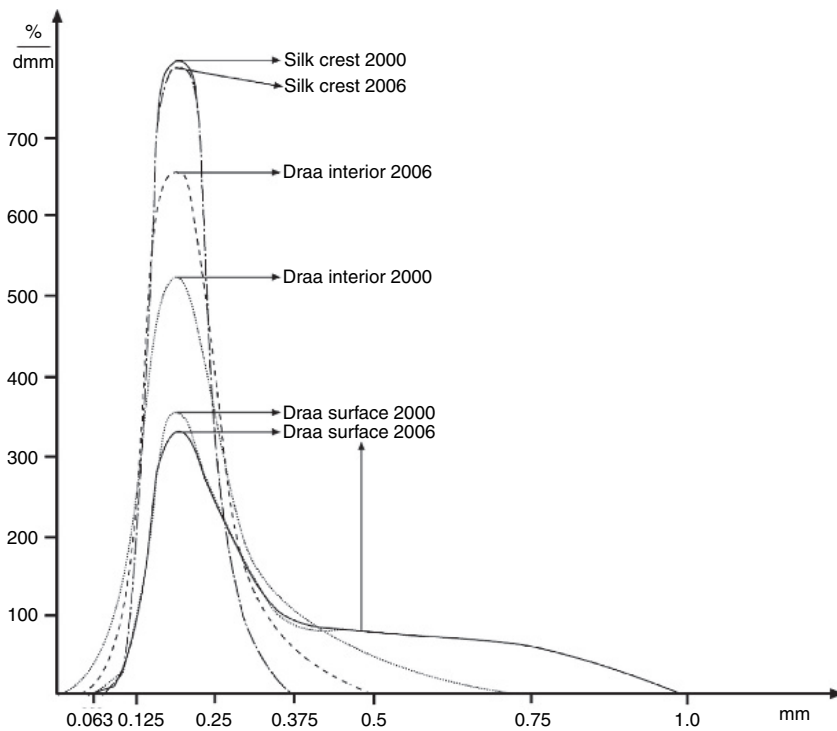


**Fig. 33** Comparison of grain-size frequency distributions in draa and dune sands sampled at Willmann's Camp in 2000 and 2006.

In summary, the granulometric sand types of the draa give strong support to relatively coarse-grained source sands with the exception of the southwestern sand sea, which has a source of distinctly finer sands. They also answer the question about the origin of the platykurtosis in the southern middle part. In addition, the surfaces of transverse draa in the north show a tendency to develop residual cover sands on their windward slopes.

During the field work at Willmann's Camp in 2006, draa and dunes were sampled again at comparable sites 800 m farther south than in 2000. The samples of 2006 represent the same granulometric sand types as the sands from 2000. Some of the grain-size frequency distributions even display identical curves in both years (Fig. 33). This underlines once more that the granulometric distribution in an aeolian deposit is not a random or an ephemeral property but represents a proper characteristic of the adjustment to the depositional environment.

#### 4.3.2. Granulometric sand types of the dunes

The granulometric sand types of the dunes are more homogeneous than the sand types of the draa. The majority of sands belong to two types: active crest sands and old barchan sands with inactive crest sands as a type with a transitional grain-size

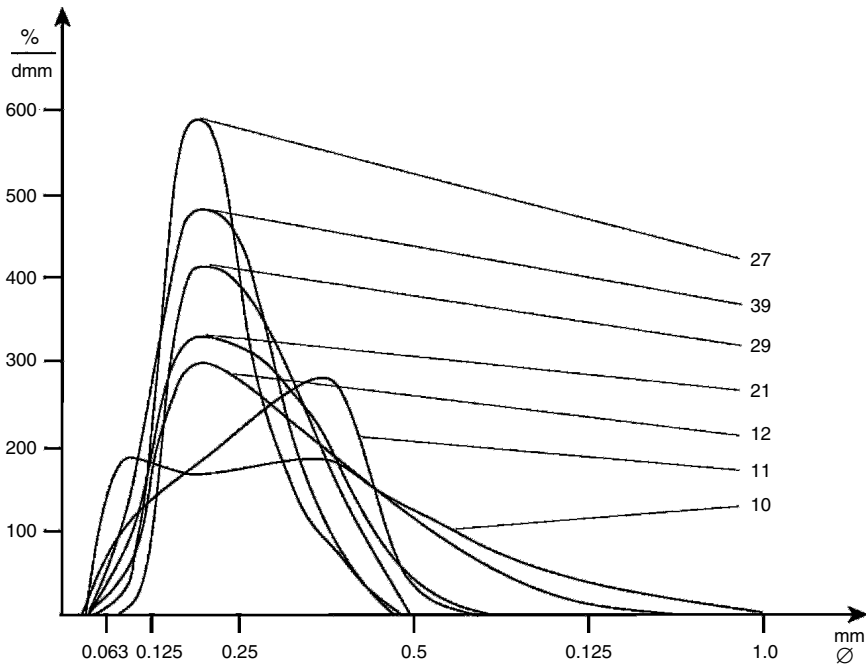


**Fig. 34** Grain-size frequency distributions of dune sands in the east.

distribution between them. Active crest sands were expected because all samples had been collected from (active) crestral parts of silk with the exception of no. 11/96 at the southern end of the eastern transection, where the only barchan dune was sampled (see Fig. 7, cross-section 1b).

Unfortunately, the samples from the eastern transection are sparse and statistically not sufficient. Therefore, they are discussed individually (Fig. 34). The barchan (brink) shows the grain-size frequency distribution of an old barchan sand with the characteristic peak in the 0.25–0.5 mm fraction, but still with moderate amounts in the finer fractions. This means that it migrated ahead of the draa and the southern silk over some distance but has not yet reached the final stage of the granulometric evolution (see Section 4.3). No. 12/96, sampled from the flank of a silk (not on a cross-section), shows the normal distribution of inactive crest sands with a reduced peak in the 0.125–0.25 mm fraction. This is also true for the crest sand of a *sif* in the northern extension of dunes (no. 39/96). With a mode height of almost 500%/dmm, it comes close to an active crest sand. At the southernmost end of this transection, a sand shield (no. 10/96) was sampled that yields the type of a typical plinth sand. According to the system of granulometric evolution (4.3), this may be the transition towards the type of deflated sands that develops if the barchan formation is hampered by – for example – a lack of strong winds. The only example of a silk sand on the longitudinal draa (no. 21/96) shows the distribution of an inactive crest sand. Indeed, this reflects the actual situation because at the time of

sampling, the silk top on the cross-section was rounded and did not have a distinct crestline. Both silk on the transverse draa belong to the same cross-section (17). Their different positions are reflected by the granulometric sand types. No. 27/96 shows the normal active crest sand. In contrast, no. 29/96, from a silk that progressed down from the draa on its eastern flank towards the groove – where it slows down and ends – (see Section 3.3.1 and Fig. 24), is represented by an inactive crest sand.

On the western and the middle transections, a distinct change in the granulometric sand types of dunes occurs around 26°N. This is the beginning of the transition zone from the southern longitudinal draa to the northern transverse draa (see Section 3.2.2). The silk on the untransformed longitudinal draa are represented by active crest sands (the majority), whereas the silk on the asymmetrical draa in majority have distributions of old barchan sands.

This is particularly conspicuous along the western transection, where all southern silk (with only one exception at the southern end: no. 21/00) show much higher peaks in the aeolian main fraction than the threshold value to inactive crest sands (500%/dmm; Fig. 35). All northern silk (with only one exception: no. 45/00) are represented by the granulometric type of (old) barchan sands (Fig. 36). Although

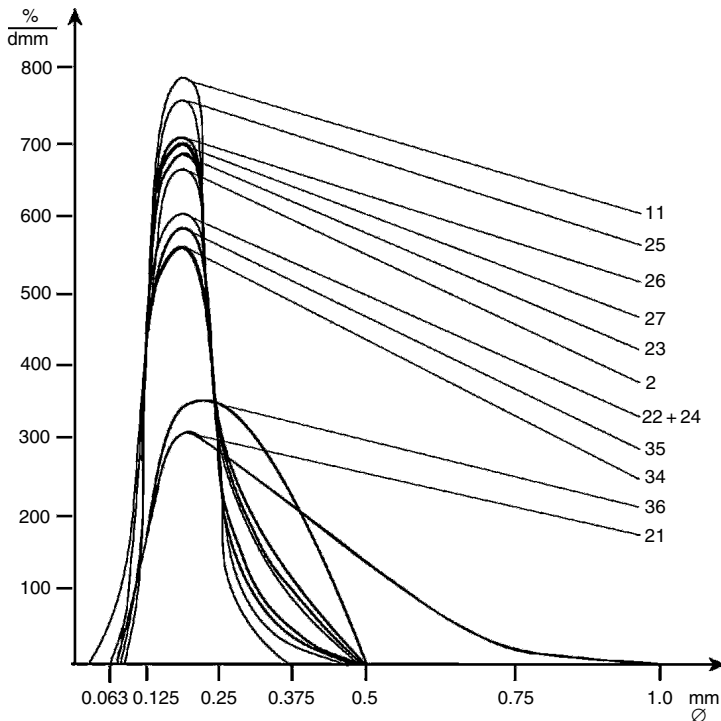


**Fig. 35** Grain-size frequency distributions of dune sands in the west (cross-sections 1–10). Dominance and homogeneity of the granulometric type of active crest sands are apparent (for explanation of exceptions see Section 4.3.2).

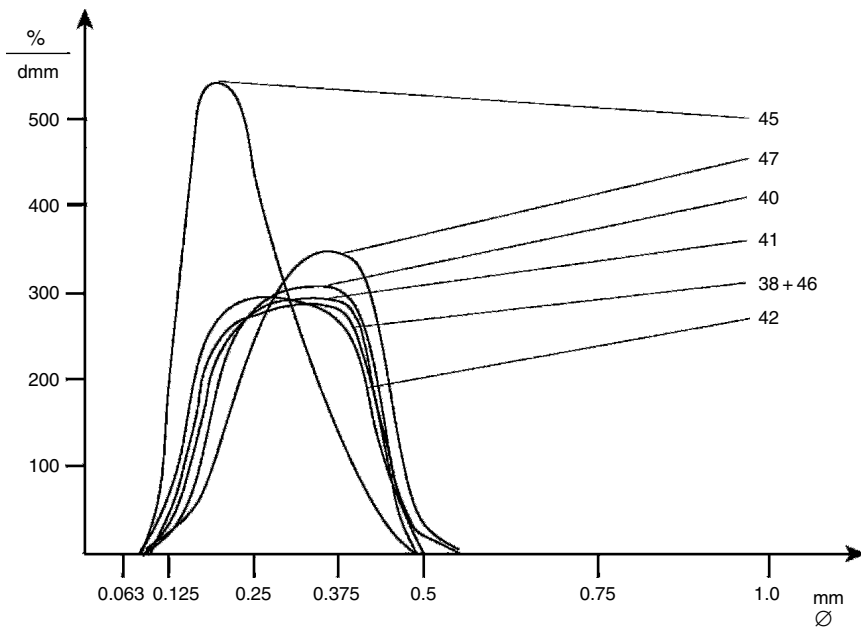


**Fig. 36** Grain-size frequency distributions of dune sands in the west (cross-sections 11–19). Dominance and homogeneity of the granulometric type of barchan sands are apparent (for explanation of the exception see Section 4.3.2).

these sands show the highest part of their broad mode in the 0.25–0.5 mm fraction – characteristic for old barchan sands – most of them still have a high amount of sand in the 0.125–0.25 mm fraction. Thus, they represent the granular transition from inactive crest sands to old barchan sands and are still far from reaching the final barchan stage. The decrease in the aeolian main fraction and the shift of the maximum to the coarser fraction are only possible if the whole sand body is turned over (Besler, 2002b). Therefore, these sands must have migrated in the shape of barchans or barchan-like transverse dunes for some time, even though at the moment of sampling they were silk. From this granulometric sand type, depending on a unimodal wind system, the conclusion may be drawn that north of 26°N western winds are at least temporarily responsible for sand transport. The granulometric type does not reflect the grain sizes provided by the draa which are coarser in the transverse pattern. In this case, the change in the granulometric types should occur farther north and not at the southern end of the transition zone (no. 36/00 in Fig. 35). On the other hand, the difference in the granulometric types can explain the sudden southward decrease in mean grain size around 26°N mentioned above (see Section 4.2.1).

For various reasons, the situation is a little more complex along the middle transection. In the first place, less samples are available for analysis because two cross-sections did not have dunes on the transverse draa. Only no. 24/99 is a typical old barchan sand (Fig. 37). No. 25/99 represents the type of plinth sands and

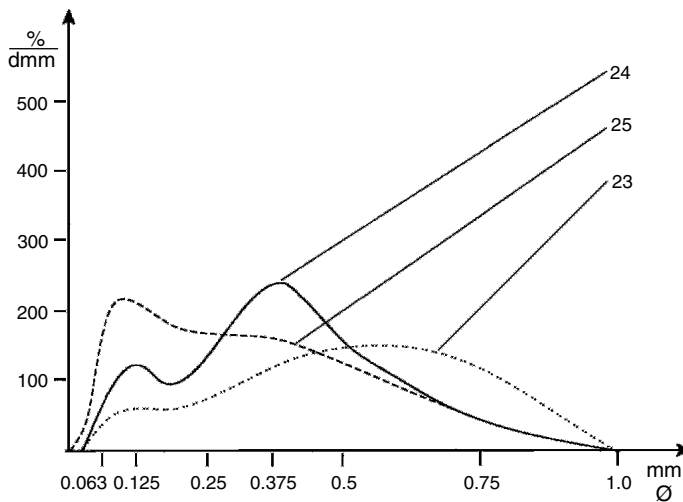


**Fig. 37** Grain-size frequency distributions of dune sands on transverse draa in the middle.

was sampled from the rounded top of a silk without a distinct crestline. As silk can be eroded during strong winds (see Section 3.3.2), this may have been a true dune plinth. The silk on the 17th cross-section had a poorly developed crest, and the sample (no. 23/99) has a grain-size distribution resembling those of megaripple sands from various deserts (Fig. 18 in Besler, 1992). No conspicuous ripples are mentioned in the field diary. The subdued topography, however, may even have represented a giant ripple in the place of a silk. In this case, it would also indicate strong westerlies because ripples are always transverse to the wind direction.

In the second place, the series of active crest sands in silk dunes south of  $26^{\circ}\text{N}$  (Fig. 38) already ends around  $25^{\circ}20'\text{N}$  (no. 11/99 on the 8th cross-section), where almost the same grain-size distributions as in the northern silk of the western transection are found (old barchan sands and their transition from inactive crest sands). This seems to suggest that only in the middle part, between  $25^{\circ}20'\text{N}$  and  $26^{\circ}\text{N}$ , the bimodal wind system for silk formation is dominant, and that in the south the northerly component of winds is responsible for barchan formation. The change in the granulometric sand types around  $25^{\circ}20'\text{N}$ , however, explains the sudden northward decrease in mean grain size at this latitude as mentioned above (see Section 4.2.1).

A comparison of the middle transection with the western transection is difficult as far as this aspect is concerned because silk with active crest sands and transverse dunes are co-existent in the western transection. Unfortunately, the transverse dunes were not sampled. It is of interest, however, that at this latitude ( $25^{\circ}25'\text{N}$  between the 4th and the 5th cross-sections) an increase of mean grain size towards the south is measured (see Section 4.2.1), although this is not correlated with a change in the granulometric sand type. The excessively fine-grained draa sands may be the reason for the hardly recognizable granulometric change that will take much more time here.

The transformation of silk to barchan-like structures has been observed and documented within the Abu-Muhariq dune belt north of the Kharga Oasis in

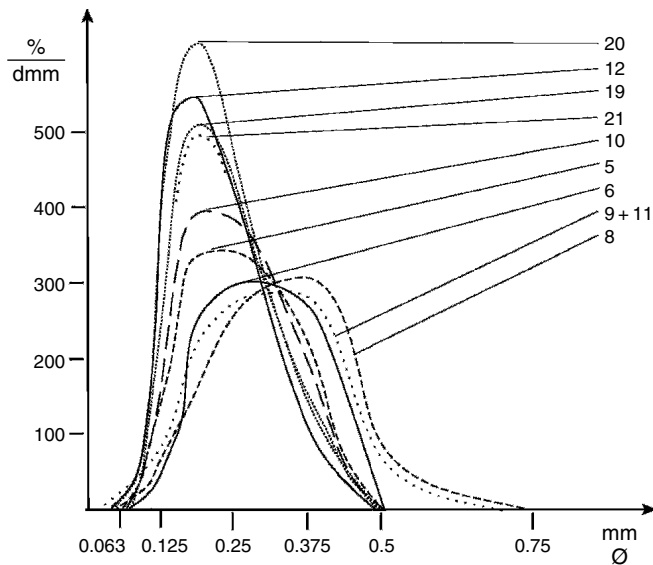


**Fig. 38** Grain-size frequency distributions of dune sands on longitudinal draa in the middle. The change from active crest sands in the north to old barchan sands in the south via inactive crest sands is displayed.

autumn 1999. At that time, the strong winds had exactly the same direction as the NNW–SSE trending silk (photo 2 in Besler, 2000b). The resulting shapes precisely resemble the “hooked dunes” that Steffan (1983) described in his remote-sensing study as transitional between barchans and silk.

In addition, the regularly sampled dune sands allow some conclusions on the northward extent of the Gilf Kebir alluvial fans, which was not possible on the basis of the few interior draa sands. Where the granulometric type of old barchan sands with a maximum in the 0.25–0.5 mm fraction is present, the source sands from the draa have to be coarser. As this is the case north of 26°N, coarser material must have been provided, most probably from a western sand source (see Sections 3.1 and 3.4). In this context, two samples collected from the desert floor of the interdrea corridor down to a depth of 1.4 m at 26°25'3"N (see Section 3.1) are of great interest. They are not included in the statistical evaluation because they are neither draa nor dune sands. Their grain-size frequency distributions, however, clearly identify them as the granulometric type of ridge sands. This similarity to the sands in the northern transverse draa allows the conclusion that the boundary between the southwestern and another western sand source may be expected between 26°N and 26°25'N.

The concept of the granulometric evolution of aeolian sands is very useful to understand the history, the dynamics and the spatial pattern of dunes in the Great Sand Sea. Moreover, in the absence of close meteorological stations – a problem in many sand seas – the granulometric sand types seem to be suitable to give information on the long-time morphologically effective winds at a local scale. In this context, only the part between 25°20'N and 26°N in the Great Sand Sea seems

to lie in a continually balanced bimodal wind field effective for sand transport. North of  $26^{\circ}\text{N}$ , temporarily unimodal westerly winds help to explain why many dunes on the transverse draa cling to their steep eastern downwind slope. South of  $25^{\circ}20'\text{N}$ , the evidence of temporarily unimodal northerly winds is not so apparent but nevertheless it exists. In addition, the granulometric sand types provide information about the extent of the southwestern alluvial fan.

#### 4.3.3. Granulometric types of the sandstones

The granulometric sand types are classified according to their actual aeolian dynamics (for draa also according to the palaeo-dynamics). Therefore, this concept cannot be applied to sandstones – not even to aeolianites – without some restrictions, because sedimentary rocks always contain diagenetic material, mostly fines. In any case, the grain-size frequency distributions will be different. In the Great Sand Sea, the major objective was to find out whether the sampled sandstones contain the aeolian main fraction (0.125–0.250 mm) and whether they possibly provide suitable sand sources. Surprisingly, the grain-size frequency distributions display the same granulometric sand types as discussed above (see Section 4.3). It should be mentioned that the more or less abundant clay/silt fraction has to be neglected to some extent in the interpretation because it contains diagenetic material (Fig. 39).

On the eastern transection, the terrestrial to lacustrine sandstone of the Minqar el-Talh Formation, that east of the sand sea is mostly eroded, was sampled in the

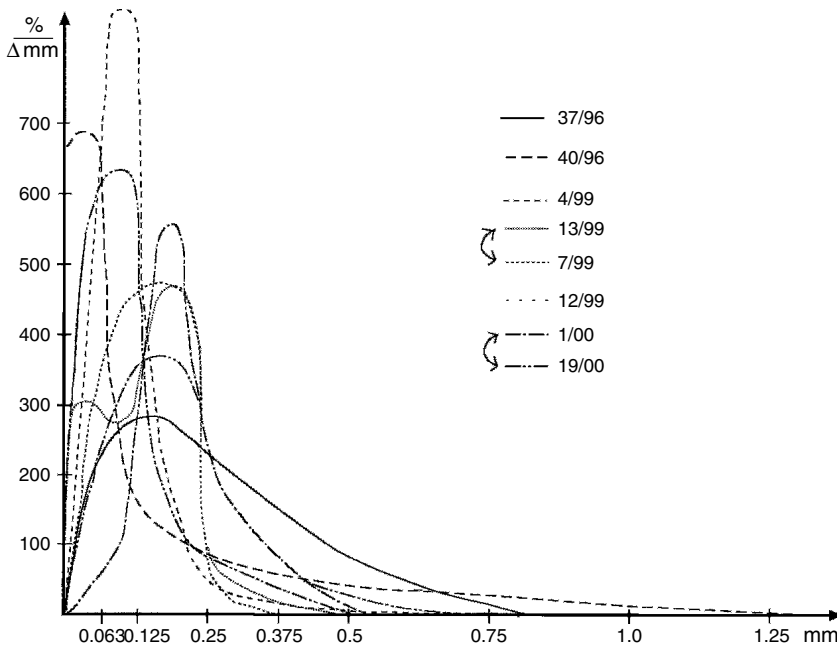


**Fig. 39** Grain-size frequency distributions of sandstones (double arrows indicate partly identical curves, for explanation see Section 4.3.3).

area of the transverse draa (no. 37/96). The grain-size distribution very much resembles the granulometric type of ridge sands with a somewhat reduced tail in the coarse fractions. This sandstone, therefore, could theoretically have supplied all draa sands in the eastern sand sea. In contrast, the continental to shallow-marine sandstone of the Moghra Formation sampled in the Siwa Oasis (no. 40/96) was apparently taken from the marine facies with a large maximum in the clay/silt fraction. This does not exclude that the continental facies may have delivered sands for the sand sea. In fact, some evidence is provided by the heavy-mineral analysis (Besler, 1998, see Section 7.2). Even the sampled facies of the sediment may have been involved because all the fines could have been blown away as dust.

Along the middle transection, four sedimentary rocks were sampled which all turned out to be potential sand sources. In the south, this is the marginal-marine and channel sandstone with deltaic cross-bedding of the Maghrabi Formation (no. 4/99). The grain-size distribution identifies a typical “young dune sand”. According to some authors, this distribution is still possible if dune sands are reworked in the marginal area of an ocean. Almost the same distribution – but with a higher clay/silt content – is found in the submarine siltstones and sandstones of the Dakhla Formation, Ammonite Hill Member (no. 22/99). Apparently, both formations contain facies that are favourable for aeolian accumulation. This is also true for the fluvial and local aeolian sandstone of the Taref Formation (no. 7/99), which represents the granulometric type of “dome sands”. Even the flaggy sandstone of the Quseir Formation (no. 13/99) would supply an inactive crest sand if the rather high proportions of clay and silt were blown off as dust. Perhaps, several local sandstones have delivered source materials for draa formation and therefore caused the platykurtosis of sands on the middle transection (see Section 4.2.4).

On the western transection, only the Taref Sandstone could be sampled (no. 19/00), which is comparable to the Taref Sandstone on the middle transection, belonging to the granulometric type of “dome sands”, but with a reduced mode and additional coarser grains. In a valley tributary to the Wadi Hamra from the Gifl Kebir Plateau, the strongly red sandstone of the Gifl Kebir Formation was sampled (no. 1/00). This grain-size distribution shows a typical active crest sand and is almost identical to the distribution of interior draa sands sampled at Willmann’s Camp, which explains their leptokurtosis.

According to the granulometric sand types, almost all geological formations underlying and surrounding the Great Sand Sea (as far as sampled) contain sandstones favouring aeolian accumulation and draa formation. Without any change in the granulometric composition, particularly the Minqar el-Talh Sandstone is most suitable for the development of ridge sands in the draa, as are the aeolianites in the Gifl Kebir Sandstone for the evolution of (in)active crest sands of the draa in the southwest.



## 4.4. THE RESPONSE DIAGRAM

To understand the history of a sand, the response diagram is not quite as valuable as the system of granulometric sand types. Nonetheless it allows the display of all samples in a single comparative overview (Fig. 40). All sands are situated in an



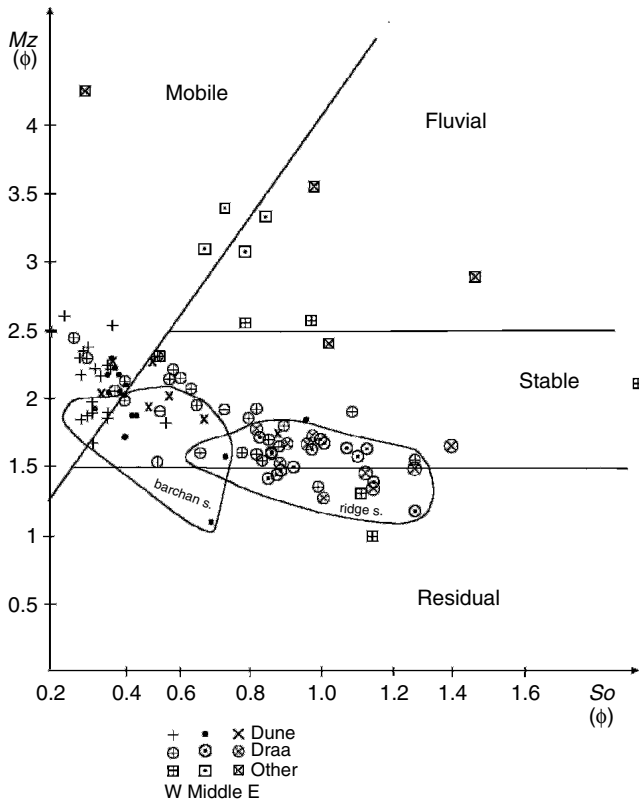


**Fig. 40** The response diagram: distinction between fluvial deposits, mobile and stable aeolian sands and residuals.

elongate cluster, reaching from the section of aeolian mobility via the section of aeolian stability into the section of residuals. Regarding the respective grain-size parameters (mean grain size and sorting), this shows how the centre is shifting from the coarsest and least sorted sands of the eastern transection via the sands of the middle transection to the finest and best sorted sands of the western transection.

The leading parameter decisive for the axis of the cluster is the sorting in draa sands, more so than in dune sands. If both sand categories are considered separately, it becomes obvious that their difference is greatest on the middle transection. This is not so much true for the dune sands which are relatively closely grouped, but rather for the draa sands due to their varyingly poor sorting. In the west, the difference between the dune sands and their source sands (draa) is not so great. On the other hand, the range between individual samples is larger and covers the whole cluster, extending from the absolutely best sorted extreme (no. 11/00: active crest sand of silk at Willmann's Camp) to the almost least sorted extreme (no. 49/00: ridge sand from surface at drilling in transverse draa), and from the absolutely finest extreme (no. 25/00: active crest sand of silk) to the almost coarsest extreme (no. 20/00: almost a megaripple sand from the southern tip of longitudinal draa).

Within this cluster, the granulometric sand types are grouped in three sub-clusters. Of course, the active crest sands of dunes and of the western draa are found in the section of aeolian mobility. Most of the draa sands, however, are concentrated in a sub-cluster along the threshold-line between stable aeolian sands and residuals. These are the ridge sands with their stable majority not being residuals yet. The third sub-cluster is composed of (old) barchan sands and extends from the section of aeolian mobility across the section of aeolian stability (with its centre) into the section of residuals. This is quite consistent with the “aging” and decreasing mobility of barchan sands already emphasized in 1996. As a matter of fact, the distribution of these sands shows almost the same pattern as in Fig. 9 in Besler (1996a) (unfortunately, the  $Mz$ -axis of the diagram was not correctly scaled and the numbers should be increased by 1  $\varphi$  everywhere.). This is of some importance because only sands from the brinks of true barchan dunes had been included in 1996 whereas in the Great Sand Sea only the granulometric types without an existing barchan shape (one exception) are considered. This emphasizes the conclusions in Section 4.3.2 with regard to bimodal and unimodal wind systems.

The majority of sampled sandstones are found in the fluvial section because of the poor sorting in consequence of the diagenetic materials. The outstanding role of the Gilf Kebir Sandstone is displayed by its position on the threshold between mobile and stable aeolian sands. But the Maghrabi (“young dune sand”) and the Taref (“dome sand”) Sandstones of the middle transection are also found in the section of aeolian mobility, which in this case includes additional dust transport. Contrary to these, the Minqar el-Talh Sandstone is positioned in the section of aeolian stability indicating that the present-day winds would not move these sands but would only select some small grains, as they do on the draa made up of ridge sands.

The diagram also includes some other sediments not mentioned in the granulometric sand types. On the western transection, these are the sediments from the corridor sampled at 26°25'36"N, which, according to their granulometric type, are found within or close to the sub-cluster of ridge sands (see Section 4.3.2). In the southern part, two more corridor sediments were sampled. The first one is a deflated deposit (no. 16/00; see Appendix 1 for sample parameters) immediately above the buried Taref Sandstone that is found in the section of aeolian stability to the extreme right. The second one was collected 40–45 cm below the surface of a red yardang-like (see explanation in Section 3.2.2) erosion remnant with cross-bedding in the corridor with the desert glass (no. 17/00). In the diagram, it is situated to the left of the Taref Sandstone in the fluvial section close to the threshold-line to the section of aeolian stability. This deposit was only little consolidated in comparison to the Taref Sandstone and looked much younger. According to the grain-size distribution, it represents an inactive crest sand if the clay/silt content is neglected. The latter may be due to pedogenic processes because a grey horizon and root traces were found. Most probably, this is a reworked and redeposited sandstone. Pachur and Röper (1984) mention yardang shapes in indurated dune sands, covered by Neolithic artefacts in the southern sand sea (see also plate IV, Fig. 3 in Pachur et al., 1987). Without a granulometric analysis, however, cemented dune sands cannot be distinguished from reworked sandstone.

The finest-grained sediment in the section of aeolian mobility represents a sample of the intensely red loam with desiccation cracks near the playa site at Regenfeld on the eastern transection (no. 25/96). With its silt-sized mean grain size and its very good sorting, this deposit is comparable to loess and is easily blown away as dust. At the sampling site it was preserved beneath dune sand (see Section 3.1, Fig. 13). Comparable playa deposits in unprotected places may have been more frequent in the interdrea corridors but have disappeared long ago (see Section 6.2).

Besides giving a comparative overview, the response diagram supports the interpretations so far, and particularly the history of that part of silk which temporarily had been transformed into barchan shapes. It also demonstrates the loess-like character of playa deposits. In addition, the diagram visually corroborates the statistical observation (see Section 4.2.1) that the present-day winds always select the same grain sizes, independent of the different coarseness of the draa sands.

## LUMINESCENCE DATING

### Contents

5.1. The Sampling Sites	99
5.2. Laboratory Procedures and Results (A. Hilgers)	105
5.2.1. Equivalent-dose determination	106
5.2.2. Dose-rate determination	112
5.3. Interpretation of Dating Results	118
5.3.1. OSL ages of the draa	118
5.3.2. Growth rates of the draa	119
5.3.3. Younger aeolian reworking of draa	121
5.4. Comparative Discussion of Regional Datings: Time Slices in the Great Sand Sea	123

### 5.1. THE SAMPLING SITES

For various reasons, a detailed description of the sampling sites (Fig. 41) is necessary. First, it helps to better understand the dating results. Second, drilling and coring provided insights that are useful for the interpretation of the developmental history. All luminescence ages from the Great Sand Sea are displayed in Table 6 according to their spatial distribution.

On the eastern transection, the first sampling site (Fig. 42) was induced by the discovery of a rich prehistoric site on red playa deposits at Regenfeld 96/1 (25°25'N, 27°05'E; Riemer, 2003, 2004a, 2005). In order to investigate the connection between the prehistoric finds and the draa, a drilling profile was placed upslope from the draa base (Fig. 43) (Besler, 1997a, 2000a). At the start of the profile (P0), a grinding stone was found below 40 cm of blown sand. Below the yellow (10 YR 6/5) cover sands, the reddish (7.5 YR 5/8) draa body is rising upslope with a somewhat lesser gradient than the modern surface. At a distance of 40 m from P0 as well as 3 m higher (4.2 m above the corridor level), P8 was chosen to drill cores from the draa. Samples were collected for sedimentological analysis, and three cores were obtained for luminescence dating. One core was sampled from the reddish sediment at a depth of 175–215 cm (2.0 m in Table 6). From a parallel drilling immediately beside P8, a core was drawn from the yellow cover sands at a depth of 100–140 cm. It was divided into two samples for dating (1.0 m and 1.4 m in Table 6). A third core was drawn from the transition zone between yellow and reddish sands at a depth of 140–180 cm, which was also divided (1.5 m and 1.8 m in

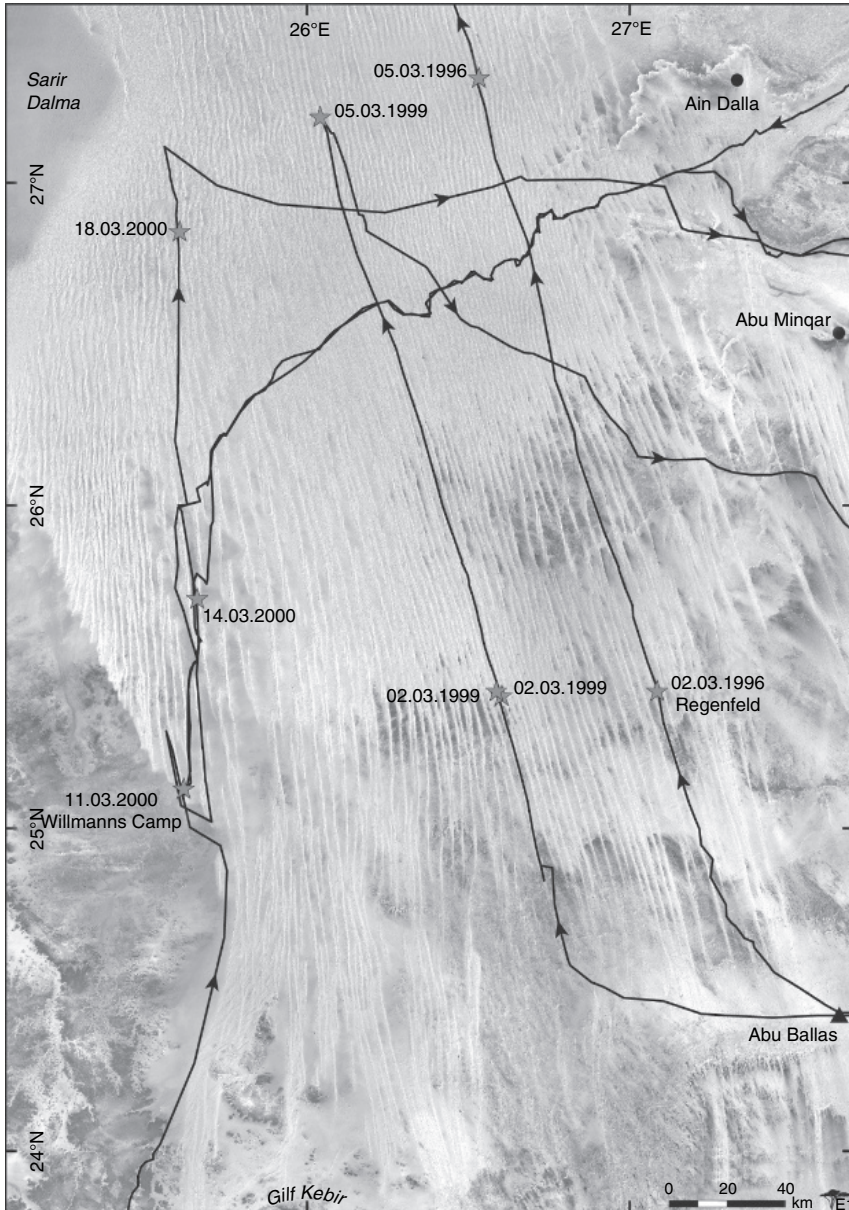


**Fig. 41** Routes of investigation in the Great Sand Sea with drilling sites for dating (marked with asterisks).

Table 6). The partition of cores was possible because the sediment was stabilized by pouring a little water into the drilling hole.

The 11th cross-section measured at this site (compare Fig. 7) shows a longitudinal draa with a width of 700 m and a height of 40 m with a 15 m high silk on

**Table 6** Spatial distribution of OSL data along the transections (numbers in brackets refer to the respective sample numbers in Table 7)

	<i>West</i>			<i>Middle</i>			<i>East</i>		
	<i>Position</i>	<i>Depth (m)</i>	<i>Age (ka)</i>	<i>Position</i>	<i>Depth (m)</i>	<i>Age (ka)</i>	<i>Position</i>	<i>Depth (m)</i>	<i>Age (ka)</i>
Transverse draa	N 26°51' E 25°36'	(7) 2	17.1 ± 2.7	N 27°12' E 26°02'	(3) 2	11.1 ± 1.8	N 27°19' E 26°32'		
		(8) 3	18.1 ± 1.6		(4) 3	12.7 ± 1.8			
		(9) 4	20.4 ± 3.1		(5) 4	15.9 ± 2.1		(6) 4	12.5 ± 3.0
Longitudinal draa (western flank)	N 25°42' E 25°40'	(3) 2	20.4 ± 3.8	N 25°24' E 26°36'	(2) 2	21.3 ± 3.0			
		(4) 3	21.3 ± 2.9						
		(5) 4	21.9 ± 4.5						
		(6) 5	22.8 ± 3.8						
Longitudinal draa (eastern flank)	N 25°07' E 25°37'	(1) 2	11.8 ± 3.0	N 25°25' E 26°36'			N 25°25' E 27°05'	(1) 1.0	0.24 ± 0.05
		(2) 3	11.5 ± 2.1		(1) 3.5	9.8 ± 1.6		(2) 1.4	0.28 ± 0.06
								(3) 1.5	0.25 ± 0.07
								(4) 1.8	0.24 ± 0.06
								(5) 2.0	5.0 ± 1.05



**Fig. 42** Looking east from the upper part of the drilling profile (compare Fig. 43) at Regenfeld across the shallow deflated playa depression towards the eastern draa at the horizon. Note the traces of drilling points along the lower profile. A small scarp is visible in the right background (photo, 2 March 1996).

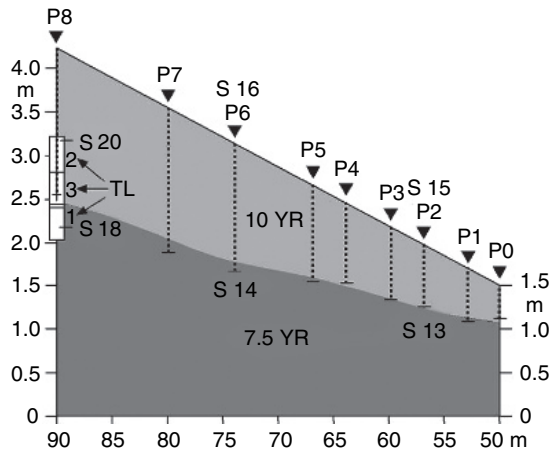


**Fig. 43** Detail of the 11th cross-section in the eastern transection with drilling succession on the eastern draa slope (P: drilling point; S: sediment sample; TL: cores for dating).

the eastern top. Red sediments were also found below yellow cover sands at the western draa base (see Section 4.4). Therefore, a first conclusion was that an ancient reddened Pleistocene draa had been covered by yellow sands after reactivation.

For the purpose of comparing longitudinal and transverse draa, a second coring site was selected on the 19th cross-section at  $27^{\circ}19'N$ ,  $26^{\circ}32'E$  (Figs 7 and 41). In order to avoid drilling through thick younger cover sands, the lower windward slope a few metres above the deepest part of the groove was chosen (see Section 3.2.2). At a depth

of 4 m, the drilling had to be stopped because of a heavy sandstorm with exceptionally strong gusts from the SSE (Besler, 1997a, 2000a). The core was drawn from a depth of 400–435 cm. If the cores were not partitioned, the respective lower parts were used for dating. Before the coring, samples for sedimentological analysis were collected from the surface and at depths of 1 m intervals (nos. 32–36/96). Reddened sands were not discovered. The cross-section measurement yielded a transverse draa with a width of 1500 m and a height of 50 m where the long windward slope (1200 m) was about 6° inclined and had shallow depressions. On the eastern edge, a 15 m high silk was spilling its slip-face avalanches across the eastern lee slope of the draa. The groove level in front of the next windward slope was 15 m higher than the western one.

At the time of the middle transection (1999), the experience with sampling on the eastern transection could be applied for a smoother sampling procedure. As the data from the east show that the sands on the draa flanks are actually shifting down to a depth of 1.8 m, cores for dating were only sampled from 2 m downwards. The drilling was made easier by repeatedly pouring small amounts of water into the tube, on the whole about 1 litre per drilling. For reasons of comparability to the eastern transection, a similar latitude and a draa shape with a long eastern flank were preferred. This was found on the 9th cross-section at 25°25'N, 26°36'E (Figs 8 and 41), but without any prehistoric implements or playa deposits. The drilling profile was placed along 250° from the corridor onto the eastern flank. In a drilling 3.2 m above the corridor level, the bedrock (sandstone) was already met at a depth of 3 m. Farther upslope, the bedrock was reached at a depth of 3.4 m and still 5 m farther upslope at 4.25 m. Reddened sediments were not found, and therefore only one core was sampled, from a depth of 335–365 cm. The sample collected for sedimentological analysis at a depth of 3.4 m (no. 14/99), however, turned out to be a surprise. After drying the sample, a weak reddish hue (7.5 YR 6/6) that had not been detected in the moist state could be discerned in comparison to the yellow cover sands (no. 18/99: 10 YR 7/4). The cross-section measurement shows a particularly broad draa (1500 m) with 400 m of N–S undulations in the western part, perhaps belonging to the western corridor. The draa has a 45 m high plateau with a superimposed 20 m high silk of the cock's-comb type (see Section 3.3.2).

A small prehistoric site was discovered on the western flank of the eastern neighbouring draa. In order to possibly explain this situation, which apparently was more favourable compared to that on the eastern flank, a coring site was chosen at about 5 m above the corridor level. In fact, the archaeological investigation yielded two different sites of human occupation. At a distance of only 20 m from the drilling point, an age of 7800–6700 cal BC (9800–8700 BP cal) was inferred from the artefacts. At a distance of 250 m, another site with a mixed inventory of artefacts did not allow a conclusion about the age (Kindermann, pers. comm., 7 October 2003). A test dig revealed weak pedogenic features with consolidation and obliteration of the layered structure below 5 cm of stratified sands. A sample for sedimentological analysis was collected at a depth of 2 m. At a depth of 2.5 m, a greenish (2.5 Y 5/4), partly aggregated sand was met immediately above the bedrock. In a parallel drilling, a core was sampled from a depth of 216–247 cm (2 m in Table 6). Also here, the bedrock was reached at 2.5 m, consisting mainly of water-laid sediments of the Quseir Formation.

Within the area of transverse draa, a situation comparable to that in the east could not be realized because the middle transection ends at 27°12'N (see Section 2.3.2).



Therefore, the coring had to take place on the 19th cross-section, seven minutes farther south ( $27^{\circ}12'N$ ,  $26^{\circ}02'E$ ). A few metres above the groove, small isolated shrubs with their roots exposed by deflation were found on the windward slope. Samples for sedimentological analysis were collected from the surface and at intervals of 0.5 m down to a depth of 4 m (nos. 26–33/99). Since an age of already 12.5 ka had been found on the eastern transection at a depth of 4 m, the site on the middle transection was used to verify this and to provide a more reliable series of data. Therefore, cores for dating were taken at depths of 2 m (199–235 cm), 3 m (295–330 cm) and 4 m (387–420 cm).

The procedure proved to be exceedingly difficult with regard to the drilling as well as to the recovery of the tubes. A comparison of the grain-size distributions with those from the eastern transection shows that the sands contain less coarse grains here ( $>1$  mm) and more small grains ( $<0.125$  mm, see Section 4.2.1). As already experienced in the artefact-stabilized dunes in Sudan (Besler, 2002c), it is particularly difficult to drill in fine-grained, well-sorted sands. All sands are light yellow (10 YR 7/4). The cross-section shows a 1475 m broad and 30 m high, strongly asymmetrical transverse draa that almost exclusively consists of the windward slope with a large shallow depression at a distance of 600 m from the western base. The section here does not carry dunes, and the sampled silk (no. 25/99) lies farther north.

On the western transection – as in the east – the first coring spot was induced by the rich prehistoric site of Willmann's Camp (Glass Area 81/61) at  $25^{\circ}07'N$ ,  $25^{\circ}37'E$  (Riemer, 2005). A drilling profile was placed from the site onto the about  $4^{\circ}$  inclined eastern flank of the draa. The first drilling occurred 5 m west of the site and about 6 m above the corridor level. Samples for sedimentological analysis were collected at intervals of 0.5 m down to a depth of 3.5 m (nos. 4–10/00). At depths of 1 and 1.5 m, a slightly more brownish hue in the overall reddish sands (7.5 YR 6/6) was observed which, however, could not be related to a different value or chroma in the soil colour chart. At a depth of 2 m, the sands were normal again. A weak pedogenic horizon seems to exist, which is also shown in earlier drawings of archaeologists. Cores for dating were drilled from depths of 219–247 cm (2 m in Table 6) and 310–348 cm (3 m in Table 6). A second drilling 5 m farther upslope gave almost identical results. The slightly brownish layer was discovered not sooner than at a depth of 1.5 m. This means that the horizon is more or less level and not following the inclined draa surface, as do the reddish sands on the eastern transection. The conclusion may be drawn that the younger cover sands had not been deposited yet at the time when pedogenic processes were active here. The measurements along the cross-section (WC, without no.) show a 475 m broad and 25 m high draa, carrying a complex of silk and barchan-like transverse dunes. The slip face of the highest silk (25 m) was pointing westwards, whereas the slip faces of the transverse dunes were exposed to the south (Fig. 27).

A situation comparable to the western flank on the middle transection was first found farther north between the seventh and the eighth cross-sections at  $25^{\circ}42'N$ ,  $25^{\circ}40'E$  (compare Fig. 9). Also here, stone implements were scattered over the lower draa flank, and the drilling was carried out immediately upslope. Samples for sedimentological analysis were collected from the surface and at intervals of 1 m down to a depth of 5 m (nos. 28–33/00). Their colour was yellowish everywhere

(10 YR 7/4). Since drilling was comparatively easy, cores for dating were drawn from depths of 2 m (196–236 cm), 3 m (303–347 cm), 4 m (392–436 cm) and 5 m (486–528 cm). Even the retrieval of the tubes was easy. The granulometric analysis yielded the granulometric types of (in)active crest sands and old barchan sands that had been difficult to drill in Sudan (Besler, 2002c). The grain-size distributions, however, show that not only large grains ( $>1\text{mm}$ ) are lacking but that also fine grains ( $<0.125\text{mm}$ ) are almost completely absent. Apparently the finest fractions are decisive for the difficulties in drilling.

In the area of transverse draa, the latitude of the middle transection was not reached because the topography is subdued north of  $27^{\circ}06'\text{N}$ . To find a situation comparable to the middle transection, a southward return was necessary. For logistic (shortage of petrol) reasons and lack of time, only two of the five vehicles could be moved to the drilling site. This had to be chosen as close to the old route as possible. Therefore, it is not situated on the draa along the transection but immediately east of it on the lower windward slope of the neighbouring draa between the 18th and the 19th cross-sections at  $26^{\circ}51'\text{N}$ ,  $25^{\circ}36'\text{E}$ . The groove between the draa is wider than usual and contains patches of gravels above a very white (bleached) sand. The sampling site lies 200 m east of the slope margin and about 8 m above the groove level. Drilling was extremely difficult between a depth of 2 and 2.5 m, but normalized thereafter. Samples for sedimentological analysis were collected from the surface and at intervals of 1 m down to a depth of 4 m (nos. 48–52/00). There is neither a differentiation in colour nor in granulometry to explain the difficulties in drilling. The sands contain little fines, but at a depth of 2 m they contain more salts (see Section 6.1), which perhaps lead to a kind of cementation. This could not be proven because – as already mentioned – a little water was added during the drilling procedure. The cores for dating were drawn from depths of 2 m (191–231 cm), 3 m (294–324 cm) and 4 m (396–430 cm).



## 5.2. LABORATORY PROCEDURES AND RESULTS\*

The luminescence dates discussed in this section were collected throughout the last decade. During this period, the field of luminescence dating has seen major technical developments, in particular a substantial improvement of the precision of OSL ages, due to the introduction of single-aliquot measurement protocols (for a review, see a.o. Lian and Roberts, 2006). The heterogeneity of the data set presented here for the Great Sand Sea can be traced back to these developments.

As described in Section 2.3.5, two parameters have to be determined in the laboratory for calculation of luminescence ages, the equivalent dose ( $D_e$ ) and the dose rate ( $D_0$ ). In the following section, the different approaches which were used for palaeodose estimation will be explained and advantages and disadvantages will be evaluated. With regard to the  $D_0$  determination, a focus is placed on the various assumptions which are incorporated in the calculation process and which thus may represent sources of error.

\* A. Hilgers, E-mail: a.hilgers@uni-koeln.de

## 5.2.1. Equivalent-dose determination

### 5.2.1.1. Sampling, sample preparation and measurement facilities

All samples were collected with steel tubes from augered cores in the dune flanks using the hand-augering system for loose sand deposits as described by Bubenzer (2001). In order to prevent any signal loss, the sample preparation for luminescence dating was carried out in the laboratory under low-intensity red light. Material from the outer ends of the steel tubes was rejected as it might have been exposed to some daylight during sampling. The material from the inner core of the tubes was then dried at temperatures not exceeding 50°C in order to prevent any luminescence signal loss due to thermal eviction. Afterwards, the fine-sand fraction was extracted from the bulk samples by dry sieving. This fraction was chosen because it is within the grain-size range which is most easily transported by aeolian processes and therefore supposed to be best bleached by sunlight during the aeolian transport. The samples were then subjected to hydrochloric acid, hydrogen peroxide and sodium oxalate to remove carbonates, organic material and clay, respectively, to prevent any interference of luminescence signals from these substances with the signal from quartz or feldspars used for dating. The quartz and potassium (K)-rich feldspar fractions were isolated from the bulk samples by density separation using heavy liquids (sodium polytungstate, 2.68, 2.62 and 2.58 g/cm<sup>3</sup>). Finally, the quartz samples were etched in hydrofluoric acid (HF) (40%) for 40 minutes to remove the outer volume influenced by  $\alpha$  particles and to remove any feldspar contamination, in particular of Na–Ca-rich feldspars with densities in the range of 2.62–2.76 g/cm<sup>3</sup>. After washing in HCl to dissolve fluorides, the purified quartz grains were re-sieved. To prepare the subsamples (aliquots) for the luminescence measurements, the quartz and feldspar grains were mounted on stainless steel or aluminium discs (diameter about 1 cm) in a mono-grain-layer using silicone oil for adherence.

All luminescence measurements were carried out on an automated Risø TL/OSL reader type TL-DA-12 equipped with infrared (880 ± 80 nm, IRSL in Table 7) light-emitting diodes (LED) for illumination of K-rich feldspars (a.o. Bøtter-Jensen, 1997). Optical stimulation of quartz was by blue LED (470 ± 30 nm, BLSL in Table 7) (Bøtter-Jensen et al., 1999) or by broad-band blue-green light (420–550 nm, GLSL in Table 7) filtered from a white halogen bulb (Bøtter-Jensen and Duller, 1992). For luminescence detection, the reader was equipped with a photomultiplier (PM) tube (e.g. type EMI 9235). Narrow-band filters discriminate between the stimulation light and the emission light of the samples and prevent scattered excitation light from entering the PM tube. Detection of the luminescence emission of quartz samples was in the UV and, for the K-rich feldspars, in the blue-violet wavelength range. Artificial irradiation was carried out using either a <sup>60</sup>Co  $\gamma$  source [for all multiple-aliquot additive-dose (MAA) and multiple-aliquot regenerative-dose (MAR) measurements in Table 7] or a <sup>90</sup>Sr/<sup>90</sup>Y  $\beta$  source [for the single-aliquot regenerative-dose (SAR) measurement in Table 7]. A detailed description of the measurement equipment can also be found in Bøtter-Jensen et al. (2003).

### 5.2.1.2. Measurement procedures for $D_e$ estimation

The  $D_e$  value is the laboratory radiation dose that produces the same population of trapped electrons in the crystal lattice of mineral grains as did the environmental

**Table 7** Luminescence-dating results obtained for sand-sized K-rich feldspar (K-F) or quartz (Q) samples from the Great Sand Sea (Egypt). Summary of the results of neutron activation analysis, dose-rate calculation, equivalent-dose determination and OSL-age calculation. Dose rates ( $D_0$ ) and ages are calculated assuming a water-content uncertainty of 0.5% to 5% (by weight) of water. The contribution of cosmic rays was calculated according to the actual sampling depth following Prescott and Hutton (1994). An internal potassium content of the K-feldspars of  $12 \pm 0.5\%$  (Huntley and Baril, 1997) was included in the dose-rate calculation with the alpha efficiency assumed to be  $0.07 \pm 0.02$  (Preusser et al., 2005).

Site	Sample	Mineral	Depth (m)	U (ppm)	Th (ppm)	K (%)	Dose rate (Gy/ka)*	Luminescence technique	Equivalent dose (Gy)	Luminescence age (ka)*
25°25'N 27°05'E	East-1	K-F	1.0	$0.10 \pm 0.03$	$1.50 \pm 0.08$	$0.25 \pm 0.03$	$1.06 \pm 0.23$	MAA IRSL	$0.25 \pm 0.01$	$0.24 \pm 0.05$
	East-2	K-F	1.4	$0.10 \pm 0.03$	$1.10 \pm 0.06$	$0.26 \pm 0.03$	$1.04 \pm 0.23$	MAA IRSL	$0.29 \pm 0.01$	$0.28 \pm 0.06$
	East-3	K-F	1.5	$0.40 \pm 0.04$	$1.10 \pm 0.06$	$0.25 \pm 0.03$	$1.10 \pm 0.22$	MAA IRSL	$0.28 \pm 0.05$	$0.25 \pm 0.07$
	East-4	K-F	1.8	$0.10 \pm 0.03$	$1.30 \pm 0.07$	$0.33 \pm 0.03$	$1.11 \pm 0.22$	MAA IRSL	$0.27 \pm 0.03$	$0.24 \pm 0.06$
	East-5	K-F	2.0	$0.50 \pm 0.06$	$2.00 \pm 0.10$	$0.31 \pm 0.02$	$1.24 \pm 0.22$	MAA IRSL	$6.20 \pm 0.73$	$4.99 \pm 1.05$
27°19'N 26°32'E	East-6	K-F	4.0	$0.10 \pm 0.03$	$1.10 \pm 0.06$	$0.33 \pm 0.03$	$1.05 \pm 0.23$	MAA IRSL	$13.15 \pm 1.44$	$12.49 \pm 3.01$
25°25'N 26°36'E	Middle-1	Q	3.5	$0.97 \pm 0.05$	$1.91 \pm 0.10$	$0.37 \pm 0.02$	$0.83 \pm 0.04$	MAR GLSL	$8.11 \pm 1.28$	$9.81 \pm 1.61$
25°24'N 26°36'E	Middle-2	Q	2.0	$0.33 \pm 0.05$	$1.25 \pm 0.06$	$0.23 \pm 0.01$	$0.53 \pm 0.02$	MAR GLSL	$11.29 \pm 1.51$	$21.28 \pm 3.00$
27°12'N 26°02'E	Middle-3	Q	2.0	$0.68 \pm 0.05$	$1.31 \pm 0.07$	$0.26 \pm 0.01$	$0.64 \pm 0.02$	MAR GLSL	$7.11 \pm 1.09$	$11.11 \pm 1.76$
	Middle-4	Q	3.0	$0.24 \pm 0.06$	$1.47 \pm 0.07$	$0.31 \pm 0.02$	$0.58 \pm 0.03$	MAR GLSL	$7.36 \pm 0.95$	$12.70 \pm 1.81$
	Middle-5	Q	4.0	$0.43 \pm 0.05$	$1.31 \pm 0.07$	$0.21 \pm 0.01$	$0.51 \pm 0.02$	MAR GLSL	$8.04 \pm 0.96$	$15.92 \pm 2.05$
25°07'N 25°37'E	West-1	Q	2.0	$0.34 \pm 0.09$	$1.47 \pm 0.07$	$0.12 \pm 0.03$	$0.44 \pm 0.05$	MAR GLSL	$5.24 \pm 1.18$	$11.79 \pm 2.97$
	West-2	Q	3.0	$0.60 \pm 0.09$	$1.46 \pm 0.07$	$0.09 \pm 0.02$	$0.46 \pm 0.04$	MAR GLSL	$5.31 \pm 0.84$	$11.53 \pm 2.09$
	West-3	Q	2.0	$0.28 \pm 0.07$	$1.33 \pm 0.07$	$0.28 \pm 0.03$	$0.57 \pm 0.05$	MAR GLSL	$11.71 \pm 1.97$	$20.42 \pm 3.82$
25°42'N 25°40'E	West-4	Q	3.0	$0.22 \pm 0.06$	$1.15 \pm 0.06$	$0.30 \pm 0.02$	$0.55 \pm 0.03$	MAR GLSL	$11.63 \pm 1.38$	$21.26 \pm 2.86$
	West-5	Q	4.0	$0.44 \pm 0.11$	$1.28 \pm 0.06$	$0.26 \pm 0.03$	$0.55 \pm 0.05$	MAR GLSL	$11.99 \pm 2.18$	$21.90 \pm 4.54$
	West-6	Q	5.0	$0.21 \pm 0.05$	$1.12 \pm 0.06$	$0.25 \pm 0.03$	$0.47 \pm 0.04$	MAR GLSL	$10.62 \pm 1.44$	$22.84 \pm 3.77$
26°51'N 25°36'E	West-7	Q	2.0	$0.39 \pm 0.10$	$1.21 \pm 0.06$	$0.27 \pm 0.03$	$0.58 \pm 0.05$	MAR GLSL	$9.86 \pm 1.26$	$17.09 \pm 2.68$
	West-8	Q	3.0	$0.28 \pm 0.07$	$1.26 \pm 0.06$	$0.31 \pm 0.02$	$0.57 \pm 0.04$	SAR BLSL	$10.30 \pm 0.65$	$18.05 \pm 1.63$
	West-9	Q	4.0	$0.43 \pm 0.11$	$1.22 \pm 0.06$	$0.21 \pm 0.02$	$0.49 \pm 0.05$	MAR GLSL	$10.00 \pm 1.18$	$20.35 \pm 3.05$

\* Dose rates and ages have been re-calculated using the updated dose-conversion factors according to Adamiec and Aitken (1998), and the same water-content variation of 0.5% to 5% for all samples. Therefore the results slightly deviate from those presented in Besler (2002).

dose during the time-span of burial. To obtain this  $D_e$  value, the natural luminescence signal of a sample is compared with that induced by laboratory irradiation. Commonly this comparison is made by using dose-response or growth curves. These are constructed by plotting different given laboratory irradiation doses versus the resulting luminescence signal intensities. The methods used to determine the  $D_e$  can be divided into the additive and regenerative dose method. Furthermore, dependent on the number of subsamples (aliquots) used for the  $D_e$  determination, multiple-aliquot protocols are distinguished from single-aliquot protocols. In this study, the MAA, the MAR and the SAR protocols were used. Illustrations of growth curves obtained with these different methods for quartz samples are shown in Fig. 44. More detailed explanations on the different measurement protocols used in luminescence studies can be found, for example, in Aitken (1985, 1998), Wintle (1997) and Lian and Roberts (2006).

Measurements of the Great Sand Sea samples following the multiple-aliquot approach were made on up to 72 subsamples with each disc consisting of about 1000 grains (cf. Duller, 2004). The aliquots prepared from the same sample are, however, not identical; each aliquot may contain grains with different luminescence brightness, and most of the measured luminescence arises from a small fraction of grains only. This is due to differences in luminescence characteristics between the grains with a high percentage showing no luminescence signal at all (Adamiec, 2000; Duller et al., 2000; Duller, 2004). Consequently, the total luminescence output from different subsamples, which were exposed to the same irradiation dose, is not necessarily the same. This inter-aliquot scatter is illustrated, as an example, in Fig. 44. It is obvious that fitting of the dose-response curve through such scattered data points is problematic and a substantial source of error in  $D_e$  determination. A method that is in common use for alleviating this problem is to make a brief OSL measurement of each aliquot prior to irradiation in the laboratory. This “short shine” luminescence signal of each individual aliquot is finally used to normalize the data. “Short-shine normalization” was applied in this study as well in order to minimize the inter-aliquot scatter and, thus, to increase the precision of the  $D_e$  determination.

After the normalization measurements, a set of 45 aliquots was divided into groups of five discs, with each group being irradiated with different radiation doses. For the regeneration method, the aliquots were bleached for several hours by sunlight exposure prior to irradiation. All aliquots used for the multiple-aliquot measurements were irradiated with a  $^{60}\text{Co}$   $\gamma$  source. Prior to the luminescence measurements, all discs were subjected to preheating in order to remove thermally-unstable luminescence signals which are not suitable for dating purposes. These signals are induced by the laboratory irradiation, but due to their thermal instability they are not present in the natural samples, which were irradiated by the environmental dose only. Between 10 and 22 discs were used for measuring the intensity of the “natural” luminescence signal resulting from the radioactivity in the sample’s environment accumulated during the burial period. These subsamples also have been normalized and preheated in the same manner as the artificially irradiated aliquots (e.g. thermal pre-treatment of 220°C for 300 seconds in case of the quartz samples).

The luminescence response to optical stimulation is measured for each aliquot, and the normalized signal intensity is plotted against the strength of the laboratory

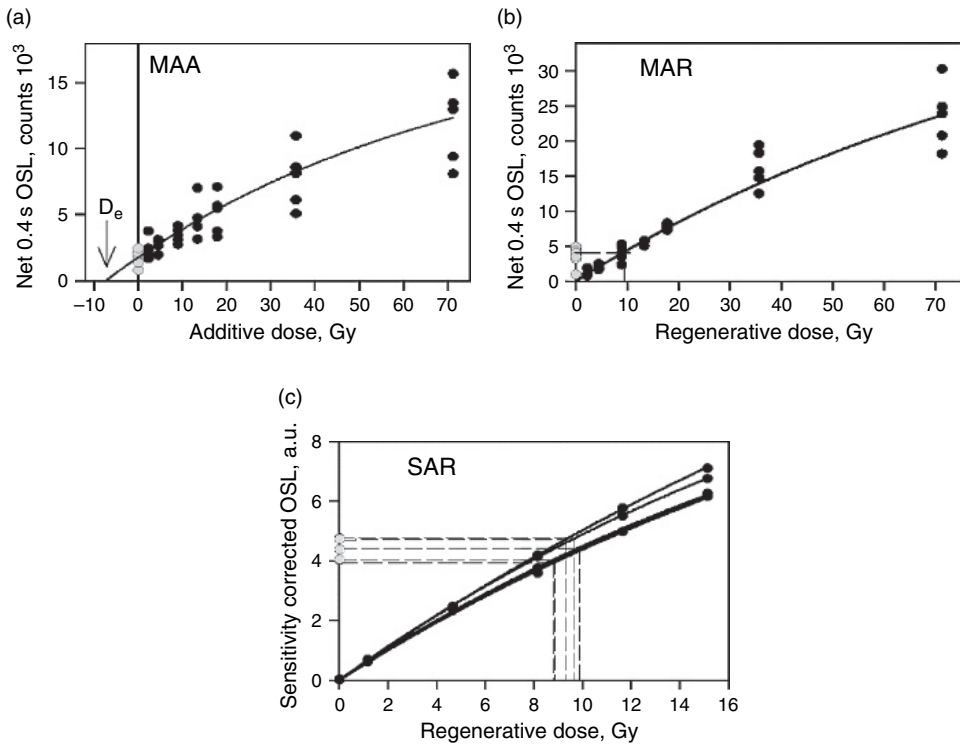


**Fig. 44** Methods of luminescence measurements for equivalent-dose determination. OSL growth curves for quartz samples extracted from aeolian sand using the multiple-aliquot additive- (a), multiple-aliquot regenerative- (b) and single-aliquot regenerative- (c) dose protocols (a and b from Hilgers et al., 2001b). Each multiple-aliquot measurement results in one equivalent-dose estimate only, with its error determined from the mathematical uncertainty with which the OSL growth curve is defined. In contrast, each single-aliquot measurement yields an equivalent-dose value (here growth curves from five different aliquots from the same sample are shown). The  $D_e$  estimate is finally calculated from the mean of the results obtained from several subsamples, with the error derived from the deviation of the individual values about the mean. For the multiple-aliquot data, the results show a large degree of scatter around the fitted growth curves, despite the use of a normalization procedure. This scatter is due to differences in behaviour and to problems of normalizing between the aliquots, and results in substantial errors of the  $D_e$  estimate. In contrast, the single-aliquot data show very little scatter away from the fitted growth curve, and differences in behaviour among the grains – such as changes in luminescence sensitivity – can be corrected for. With only little scatter of the five individual equivalent-dose values, a much higher precision of the derived equivalent dose is achievable. (Note that for sample West-8, which was measured using the SAR approach, in total twelve aliquots were used.)

irradiation dose in order to construct the dose–response curve as shown in Fig. 44 (a, b). A line is then fitted to the average luminescence intensities of each dose step. In case of the additive method, the  $D_e$  value is obtained by extrapolation of the line to zero intensity, and the dose intercept taken to be the  $D_e$ . The problem related to the additive dose protocol, especially when larger doses are involved (as with older samples), is the complication of sublinearity – the rate of increase of growth falls off

as the applied dose increases. This complicates the extrapolation of the growth curve onto the dose axis, and increases the uncertainty in the  $D_e$  estimation.

In case of the regenerative-dose method, the natural OSL is directly compared with the OSL resulting from laboratory irradiation. The  $D_e$  value is then determined by interpolation. The advantage of interpolation instead of extrapolation is that uncertainties due to a non-linear, e.g. exponential, shape of the dose-response curve are reduced, if not eliminated. The critical disadvantage of the regenerative approach is the possibility of sensitivity changes. Luminescence sensitivity is the measure of the amount of luminescence emitted by a sample for a given radiation dose. This efficiency is sample-dependent, as it is related to the ability of the material to store energy from the radiation it is exposed to. Many of the processes involved in luminescence measurements, such as thermal treatment, repeated optical stimulation and artificial irradiation with generally strong doses over time-spans that are short compared to the natural irradiation conditions, cause changes in the luminescence sensitivity. It is hardly possible to avoid these changes and, as the amount of change varies from sample to sample and from measurement cycle to measurement cycle, no constant factor can be used for correction. Such sensitivity changes may prevent accurate estimates of the  $D_e$ , which finally may result in an over- or under-estimation of the luminescence age.

With the introduction of single-aliquot regeneration protocols, both monitoring of changes in sensitivity throughout the luminescence measurement and internal correction were enabled. In the SAR protocol after Murray and Wintle (2000) for quartz, the OSL signal from a fixed test dose administered subsequent to the measurement of the natural and regenerated OSL is used as a surrogate for sensitivity changes in the natural and regenerated OSL signals. By dividing the natural and regenerated OSL signals by their subsequent test-dose signals, sensitivity correction is achieved.

### 5.2.1.3. $D_e$ determination for the Great Sand Sea samples

At the beginning of the study, luminescence dating was carried out on K-rich feldspars. For well-bleached sediments, feldspar samples usually show less inter-aliquot scatter than the quartz fraction. Hence,  $D_e$  estimates often yielded a higher precision when compared with the quartz fraction of the same sample and thus more precise ages were obtained (a.o. Hilgers et al., 2001a; Radtke et al., 2001). An increasing number of comparative studies on independently dated sediments showed the tendency of feldspar ages, however, to underestimate the expected ages (a.o. Radtke et al., 2001; Wallinga et al., 2001). One likely explanation for this observation is an instability of the luminescence signal, a phenomenon known as “anomalous fading”. This loss of trapped charge affects many, though not all, feldspars but is not known to affect quartz samples. To avoid any problems with “anomalous fading”, all subsequent  $D_e$  measurements were carried out on the quartz fraction.

The results derived from the MAA measurements of K-rich feldspars and MAR measurements of quartz are summarized in Table 7. Due to the smaller inter-aliquot scatter, the feldspar  $D_e$  values are more precise than the quartz results, with a relative error of about  $10 \pm 5\%$  compared to  $15 \pm 3\%$ . Because of the large effort involved in making the multiple-aliquot measurements, it is generally not feasible to make multiple measurements of one sample, and finally only one  $D_e$  estimate per sample is available for age calculation.

For sample West-8,  $D_e$  determination was impossible by using the MAR technique, because no dose–response curve could be fitted through the scattered data points at all. Therefore, after the SAR protocol for dating sand-sized quartz grains had been proposed by Murray and Wintle (2000) and when the measurement equipment was upgraded to enable irradiation of the aliquots by a  $^{90}\text{Sr}/^{90}\text{Y}$   $\beta$  source integrated into the luminescence reader, measurements on sample West-8 were repeated. The SAR technique avoids inter-aliquot normalization, as for each aliquot an individual dose–response curve and thus an individual  $D_e$  value are measured (see Fig. 44(c)).

First, the sample's natural luminescence intensity is measured. Then the same aliquot, with its luminescence signal completely removed during stimulation in the first cycle, is exposed to increasing laboratory irradiation of well-defined  $\beta$  doses with each irradiation procedure followed by an optical stimulation to read out the artificially induced luminescence. By plotting these luminescence intensities against the corresponding laboratory dose, the SAR dose–response curve is constructed (see Fig. 44(c)). Finally, the  $D_e$  is determined by interpolation in the same way as for MAR measurements. In contrast to the multiple-aliquot procedure, however, the SAR protocol internally corrects for the effects of sensitivity changes. Furthermore, the reproducibility of the sensitivity-corrected signal – and hence the reliability of the correction procedure – can easily be checked by measurement steps integrated into the measurement procedure (Murray and Wintle, 2000).

Several SAR measurements on different aliquots of the same sample finally provide the basis for estimating the  $D_e$  by population statistics (see Fig. 44(c)). Measurement of a range of aliquots allows a more detailed investigation of the dose distribution within the sediment. This is one of the major advantages of the SAR technique, especially for sediments which are suspected to have their accumulated dose not completely removed during transport and deposition. The same is valid for samples taken from sediments which indicate strong bioturbation processes which could result in mixing of material of different depositional ages, thus inducing a broad data spread in the  $D_e$  estimation.

In case of sample West-8, an  $D_e$  estimate could be derived from SAR measurements carried out on 12 aliquots. The uncertainty in the  $D_e$  is calculated from the reproducibility of the measurements. With a relative error of only 6% for sample West-8, the higher precision of SAR measurements if compared to MAR measurements regarding well-bleached sediments is already indicated.

The SAR age of sample West-8 is in good agreement and chronostratigraphic order with the ages of the over- and under-lying samples (Table 7). As the SAR protocol allows for correction of sensitivity changes, it is considered to yield the more reliable ages compared to the MAR technique (a.o. Hilgers et al., 2001b). But the good agreement of the ages obtained with different measurement protocols (sample set West-7 to West-9) supports the reliability of the multiple-aliquot ages. If changes in luminescence sensitivity occurred and remained uncorrected in the multiple-aliquot data sets, they obviously had only a minor effect on the  $D_e$  estimate and hence on the OSL ages. However, despite the “short-shine” normalization procedure applied to all aliquots used for  $D_e$  measurements, the inter-aliquot scatter was still large and resulted in a lack of precision of the  $D_e$  values. This is the major source of error in the luminescence-age calculations. Therefore, the application of single-aliquot protocols is recommended for future studies.



### 5.2.2. Dose-rate determination

For calculation of luminescence ages, the  $D_e$  of a sample is divided by the radiation dose per unit time (Gy/ka or  $\mu\text{Gy/a}$ ), the  $D_0$ . The strength of the radiation field to which the mineral grains were exposed during burial is dependent on the concentration of radioactive elements within the grain and its surrounds. Hence, internal and external  $D_0$  have to be assessed independently. In addition to this terrestrial natural radioactivity, the radiation dose resulting from cosmic rays contributes to the environmental  $D_0$ , which varies according to the sampling depth and geographical position of the sampling site (Prescott and Hutton, 1994).

The external  $D_0$  summarizes the radiation dose in the sediment matrix. The major part of ionizing radiation in sediments results from the disintegration of the naturally occurring radioisotopes uranium (U)-238 and U-235, thorium (Th)-232, potassium (K)-40, and the members of their respective decay chains. Due to their variable abundance in rocks and their specific geochemical behaviour during geological and pedogenic processes, the concentration of U, Th and K varies in sediments. Therefore, the radionuclide contents have to be determined for each sediment sample used for luminescence dating. In this study, the concentrations of the relevant radionuclides were determined by NAA. The results are summarized in Table 7. These concentrations were finally converted into  $\alpha$ ,  $\beta$  and  $\gamma$  radiation dose rates by using the conversion factors reported by Adamiec and Aitken (1998).

An internal-radiation dose results from radionuclides incorporated in the crystal lattice or in inclusions of the mineral grains finally used for luminescence measurements. Compared to U and Th, K is a common element in nature, and because of its comparatively small ionic radius it is easily incorporated into the crystal lattice, especially in feldspars. Hence, for all K-rich feldspar samples, an internal dose contribution from the decay of K-40 was taken into account assuming a K concentration of  $12.5 \pm 0.5\%$  (cf. Huntley and Baril, 1997). In contrast to K-feldspars, the internal  $D_0$  of quartz is commonly assumed to be negligible.

Because of their appreciable mass and heavily ionizing nature,  $\alpha$  particles have only a very localized effect. They are absorbed in air already after a few centimetres (Siehl, 1996), and in matter, e.g. in sediments with a density of  $2.5 \text{ g/cm}^3$ , already within approximately  $20 \mu\text{m}$  distance from the decaying radionuclide (Grün, 1989). Thus, the outer rim of sand grains receives a substantial external  $\alpha$  dose, while the inner part of the grains is hardly affected by  $\alpha$  radiation. With respect to quartz samples, the outer  $\alpha$ -particle-irradiated shell is removed during sample preparation by etching in concentrated HF. Therefore, the  $\alpha$ -dose contribution is negligible for the quartz samples. In contrast to the relatively isotropic etching in the case of quartz crystals, etching in feldspar samples occurs mostly along dislocation lines in the crystal lattice. Therefore, the external  $\alpha$ -dose component is included in the  $D_0$  calculation rather than HF etching of the feldspar crystals.

Alpha particles travel in straight lines. Along its track into material, an  $\alpha$  particle ionizes neighbouring atoms and hence loses its energy rapidly, but it leaves a trail known as "fission track". Hence,  $\alpha$  particles are less efficient in their ionization of surrounding matter than  $\beta$  and  $\gamma$  rays, which are scattered after being released from the decaying nucleus. The ratio of  $\alpha$  effectiveness in induction of luminescence compared to that of the same dose of  $\beta$  or  $\gamma$  radiation is expressed by the  $\alpha$ -efficiency

factor, which is highly dependent on the density of the absorbing matter. In luminescence-dating studies, this factor can be determined by the comparison of the luminescence intensities derived from artificial  $\alpha$  and  $\gamma$  irradiation, respectively. For the feldspar samples from the Great Sand Sea, the  $\alpha$ -radiation dose was multiplied by an  $\alpha$ -efficiency factor of  $0.07 \pm 0.02$  following Preusser et al. (2005).

The interstices of sediment can be filled with either water or air, which have different radiation-attenuation characteristics. As water present in pore voids attenuates the radiation dose to the individual grains more effectively than air, the overall  $D_0$  is reduced with rising moisture content in the sediments. Therefore, the water content in the interstices of the sediment to be dated has to be taken into account for  $D_0$  calculation. The “as collected” water content of a sample can be measured and its influence on the radiation attenuation calculated by applying the appropriate attenuation factors for  $\alpha$ ,  $\beta$  and  $\gamma$  radiation, respectively (Zimmerman, 1971). For the samples from the Great Sand Sea no “as collected” water contents could be determined, because for sampling of the fine sands the drill holes had to be watered prior to augering. Hence,  $D_0$  calculation had to be based on an assumed variation range of water contents from 0.5 to 5%. This assumption was based on what is known about the past and present-day climatic conditions and the water storage capacity in dune sands resulting from the grain-size distribution.

If the concentrations of K, U and Th in the sediments have been determined by means of  $\gamma$ -spectrometry measurements or other methods of element analysis (e.g. NAA) and converted into  $\alpha$ -,  $\beta$ - and  $\gamma$ -dose rates, the total annual  $D_0$  (in  $\mu\text{Gy/a}$  or  $\text{Gy/ka}$ ) for a specific sampling position can be calculated. Combining the various details described above,  $D_0$  values for sand-sized K-rich feldspar samples are finally calculated from (see a.o. Aitken, 1985, 1998):

$$D_0 = \left( \frac{kD_{\alpha,\text{dry}}}{1 + HWF} \right) + \left( \frac{bD_{\beta,\text{dry}}}{1 + HWF} \right) + (D_{\beta,\text{intern}}) + \left[ \frac{(D_{\gamma,\text{dry}} + D_{\text{cosmic}})}{1 + HWF} \right]$$

where  $k$  is the relative measure of the poorer effectiveness of  $\alpha$  particles compared to  $\beta$  and  $\gamma$  radiation [a value of 0.07 was included here for K-rich feldspar samples following Preusser et al. (2005); for etched quartz grains the  $\alpha$ -dose contribution is neglected];  $b$  takes into account the attenuation of the  $\beta$  contribution dependent on the grain size used for dating [values  $\pm 0.90$  were taken into account here following Mejdahl (1979)]; the factors  $H$ ,  $W$  and  $F$  correct for the effect of water in the sediment, with  $H$  being the attenuation factor for  $\alpha$ ,  $\beta$  and  $\gamma$  radiation with 1.5, 1.25 and 1.14 (Zimmerman, 1971), respectively,  $W$  describing the saturation water content and  $F$  the average water content during burial divided by  $W$ .

For etched sand-sized quartz samples, the equation is simplified to:

$$D_0 = \left( \frac{bD_{\beta,\text{dry}}}{1 + HWF} \right) + \left[ \frac{(D_{\gamma,\text{dry}} + D_{\text{cosmic}})}{1 + HWF} \right]$$

In  $D_0$  determination, it is usually assumed that the  $D_0$  does not change over the period of burial. This implies that the U- and Th-decay series are in state of equilibrium and that the moisture content and the burial depth did not vary substantially. These assumptions may, however, introduce a considerable source of error to OSL ages. These uncertainties have to be kept in mind when luminescence ages are discussed in terms of “absolute ages”. Their impact on the luminescence ages of the samples from the Great Sand Sea will be outlined and discussed in the following.

#### 5.2.2.1. Uncertainty about the state of equilibrium of the radioactive-decay chains

A decay chain is in equilibrium if the disintegration rate of each member equals that of the immediately preceding one. Thus, the specific decay rates or activities are the same for each radioisotope of the chain, although the half-lives may vary considerably. Disequilibrium results from geochemical sorting according to different geochemical properties of the radioisotopes, whereby some processes – such as solution, precipitation or gaseous diffusion – can move a parent or daughter either into or out of a system. Hence, an excess or deficit of the affected radionuclide can result. For a more general discussion of radioactive disequilibria, the reader is referred to, for instance, Ivanovich and Harmon (1992).

If the activities of individual chain members differ significantly, disequilibrium is indicated and the assumption of a constant  $D_0$  throughout the burial time is erroneous. Therefore, sediment samples used for luminescence dating ought to be checked for the presence of disequilibrium in the decay chains.

The radionuclide contents of the samples from the Great Sand Sea were determined by NAA. For the  $^{238}\text{U}$ - and  $^{232}\text{Th}$ -decay chains, NAA gives the concentration of the parent nuclides only. Thus, NAA is not useful in terms of the identification of radioactive disequilibria. However, disequilibrium in the  $^{232}\text{Th}$ -decay chain is unlikely to be important in sediments (a.o. Olley et al., 1996). Serious disequilibria are, however, known to occur in the  $^{238}\text{U}$ -decay chain, due to removal or addition of a particular member by post-sedimentary geochemical processes involving percolating water, or carbonate precipitation or dissolution. With respect to the depositional context, disequilibria most likely are to be expected at sampling sites showing wet conditions (e.g. due to present-day groundwater flow) or which probably have been wet for a significant time in their past. Disequilibria related to the precipitation of secondary carbonates in arid environments also have been reported. However, there is little or no evidence for disequilibrium in dune-sand deposits (a.o. Krbetschek et al., 1994; Prescott and Hutton, 1995; Olley et al., 1996). Because the samples from the Great Sand Sea were taken from dry dune sites without influence of groundwater fluctuation or marked calcrete horizons, the uncertainty about the state of equilibrium of the decay chains is considered to be of minor significance for the interpretation of the OSL ages. Notwithstanding, the reader is referred to a study of Olley et al. (1997) for an impression of the impact of an undetected disequilibrium on the resulting error in age calculation. They determined an age overestimation of less than 10%, if they used the parent nuclide concentrations only (e.g. determined by NAA, as also done in the present study) to assess the  $D_0$  for sediments showing disequilibrium, compared to the age values based on  $D_0$  which were modelled to allow for disequilibria.

### 5.2.2.2. Impact of varying overburden thickness on the cosmic-dose contribution

When the cosmic-dose contribution to the overall  $D_0$  of a sediment sample is determined, the relevant parameters controlling its intensity are the thickness and density of the overburden material. The “soft” component (electrons, positrons and photons) is already absorbed in the top half-metre of sediment with a density of approximately  $2 \text{ g/cm}^3$ , and is of minor influence on the cosmic-dose contribution. The “hard” component (protons, muons, neutrons and neutrinos) penetrates deeper and is attenuated with increasing depth, due to ionizing reactions with the surrounding material. The contribution of cosmic rays to the total  $D_0$  is usually calculated according to the sampling depth and geographical position of the sampling site (Prescott and Hutton, 1994). The dynamic character of sedimentary systems with repeated events of erosion and accumulation results, however, in variations of the thickness of the overburden experienced by a buried sediment sample. Therefore, the contribution of cosmic rays to the total  $D_0$  of such a sample is not constant over the entire period of burial time, but may vary significantly. Such fluctuations in the overburden thickness are less significant in sedimentary environments where the cosmic-dose component is generally low ( $< \sim 10\%$  of the total annual  $D_0$ ). In aeolian dune sand systems with sediments predominantly consisting of more or less source-free quartz grains with only low feldspar and heavy-mineral content; however, the terrestrial  $D_0$  resulting from disintegration of radioisotopes tends to be low. In these environments, the cosmic radiation can be a major component to the total  $D_0$ . In such cases, a substantial error in the total  $D_0$  calculation – and finally in luminescence ages – can be introduced if the cosmic-dose contribution is determined in correspondence to the present sampling depth.

The sediments from the Great Sand Sea receive on average 14% (K-rich feldspar samples) or 24% (quartz samples) of the total (dry) annual dose via cosmic radiation. To check the influence of uncertainties in estimates of the variation of the burial depth, the OSL ages were calculated for the sample set Middle-1 to Middle-5 for burial depths of 0.30 and 1.50 m, and compared to the OSL ages which were calculated including a cosmic component according to the actual sampling depth in the range from 2 to 5 m (see Table 7). As shown in Fig. 45, the ages calculated with the cosmic dose determined for the actual sampling depth still agree within the 1-sigma error range with those ages that were calculated assuming that the sample was buried by only 30 cm of sediments since deposition and initial burial. This demonstrates that, even if a certain sample was close to the surface (e.g. depth of 30 cm) for most of the time since deposition and has been buried by more than a metre of sediment just recently, the OSL ages would not be affected significantly. Hence, it is concluded for the samples from the Great Sand Sea that uncertainties related to the reconstruction of changes in the thickness of the overburden sediment over the history of the deposit are of minor importance for the final interpretation of the luminescence-dating results.

### 5.2.2.3. Influence of uncertainty in water-content variations

In terms of  $D_0$  assessment for dating, the variation in wetness over the whole time-span of burial has to be considered (see factor  $F$  in the equation above). This is the only parameter in the dose-rate moisture-correction procedure which cannot be

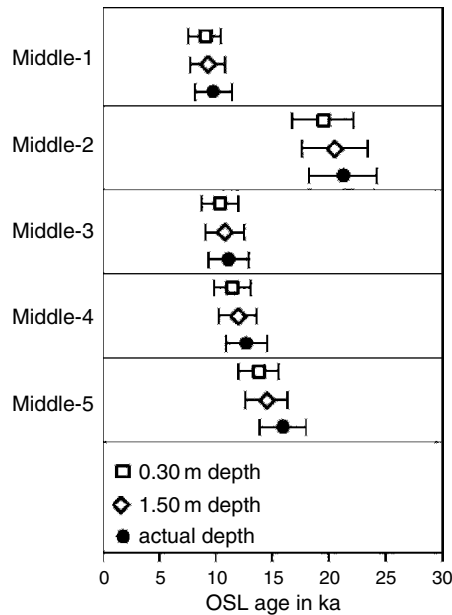


**Fig. 45** Impact of varying overburden thickness on the cosmic-dose contribution, and the resulting luminescence ages. As an example, OSL ages were calculated for the sample set “Middle-1 to Middle-5” for different sampling depths, thus implying different contributions of the cosmic radiation to the overall environmental dose. The actual positions of the samples range from 2 to 5 m below surface. It is demonstrated that, even if a certain sample was close (e.g. 30 cm) to the surface for most of the time since deposition, and even if it had become buried by more than a metre of sediment just recently, the OSL ages would not be affected significantly. The ages calculated with the cosmic dose determined for the actual sampling depth still agree within the 1-sigma errors with those ages which were calculated assuming that the sample was buried by only 30 cm of sediments since deposition and initial burial.

measured or calculated directly. The estimation of the average wetness of the sediment since deposition is loaded with problems. The water content of a sediment changes in response to the natural variations in precipitation. Furthermore, it may change significantly if the sediment layers are influenced temporarily by groundwater. Also variations of the climate conditions induced by climate change in the geological past have to be regarded. Furthermore, variations in the water content throughout the period of burial can result from changes in porosity due to significant post-sedimentary compaction of sediment layers by increased loading. This brief summary underlines some of the uncertainties related to the water-content estimation in luminescence-dating studies. The uncertainty related to this parameter represents a fundamental limitation in improving the luminescence-age error limits to below the level of about 5% (Aitken, 1998). Quantification of the range of variations in moisture is almost impossible. Qualification or identification of all the processes involved is all that can be achieved and allowed for. Taking all this into account, sediments from arid areas which are known to be arid since the deposition of the target sediment should be amongst the easiest samples to handle.

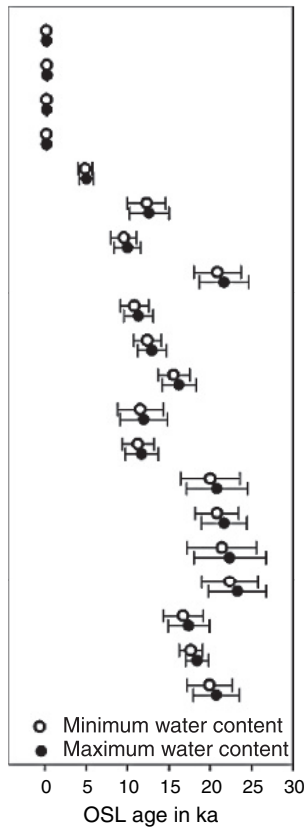


**Fig. 46** Impact of the water-content variation on the resulting luminescence ages. For each sample, the luminescence ages are shown which have been calculated using either a minimum moisture content of 0.5% water by weight or a maximum value of 5%. Due to the more effective radiation attenuation by water than by air, the overall dose rate is reduced with rising moisture content in the sediment. Hence, the luminescence ages based on dose rates calculated for 5% water content are slightly, but not significantly, older.

With respect to the samples from the Great Sand Sea, an additional problem in the water-content estimation was caused by the sampling procedure. The actual water content, usually measured as weight loss after drying, could not be determined, because for coring in the sand dunes the auger holes had to be watered. Lacking these data, the dose attenuation was finally calculated assuming a variation in moisture content of 0.5–5% by weight to allow for substantial changes in sediment wetness.

For comparably dry sediments with water contents of less than 10%, the additional error introduced in the ages by the uncertainty related to the water content-estimation is relatively small. This is illustrated in Fig. 46 for all samples from the Great Sand Sea. OSL ages, which were calculated for a water content of 0.5%, are compared here with those values based on a water-content estimate of 5%. The differences in

the mean age values is only about 4% on average, and the dating results still agree within the 1-sigma error range. It is concluded that the difficulties in estimation of the water content of the sediment samples from the Great Sand Sea have only minor influence on the interpretation of the OSL ages.



### 5.3. INTERPRETATION OF DATING RESULTS

#### 5.3.1. OSL ages of the draa

The dating results (Table 6) of the transverse draa are most homogeneous because all OSL ages cover the range from 20 ka to 11 ka ago. These ages go perfectly well together with groundwater data. Before 20 ka ago, groundwater recharge occurred from precipitation reaching the area from the west (Sonntag et al., 1980). A very arid phase reigned between 20 and 14 ka ago, and humid and dry periods alternated after 12 ka ago (Brinkmann and Heinel, 1986), with a dating error of  $\pm 1$  ka according to Thorweihe (1988).

The vertical dating records suggest, however, that the sands of the eastern transection at depths of 2 and 3 m, which have not been dated, may be younger than 11 ka. A comparison of ages at depths of 4 m shows that the windward slopes of the draa get younger towards the east. Remarkably, the age at a depth of 3 m (middle transection) is comparable to the age at a depth of 4 m 50 km farther east. This suggests either draa formation progressing from west to east or later windward draa deflation decreasing from west to east. The grain-size distributions of all surface sands at the drilling sites and elsewhere are very similar, showing deflation in the west as well as in the east, and therefore they do not support the latter possibility (see Section 4.3.1). If the position of the western site close to the palaeo-upwind margin of the sand sea is considered – the instability waves in the Planetary Boundary Layer developed there before reaching maturity towards the east – this pattern in the OSL ages seems to be reasonable. This would imply, however, that the upper draa sands in the east are much younger than 12.5 ka. Unfortunately, little is known about these lateral waves (see Section 3.2.2). The ages of the transverse draa will be discussed further in connection with their growth rates in Section 5.3.2.

The dating results of the longitudinal draa pose some problems because all OSL ages on the western flanks are over 20 ka. Therefore, they cover the time-span of groundwater recharge from westerly cyclones. On the other hand, the vertical record of OSL ages is convincing and cannot be discarded. In the draa-formation model, the sand accumulation progresses from the interior core towards the eastern and the western margins in both flanks. Because ages are only available for the western margin, the interior draa body has to be considerably older. Embabi (1998) supposed that the plinths of a still older generation of draa could exist below the present-day ones, particularly in the south. No evidence for this was, however, found along the transections. During the formation of longitudinal draa, westerly cyclones should not have been active, at least not south of the northern margin of the longitudinal draa around 26°45'N. This is inconsistent with groundwater-recharge data because,

according to Sonntag et al. (1980), isotopic groundwater properties provide evidence of a westerly origin of the precipitation north of 20°N before 20 ka ago. The Nubian aquifer system in Egypt, however, is not closed towards the west (Thorweihe, 1990a). Therefore, it may have been possible that groundwater reached Egypt from the west, whereas the cyclonic activity of the westerlies decreased towards the east.

At the end of the Pleistocene, however, dry westerlies must have pushed farther south, causing the asymmetry of the longitudinal draa as far south as 26°05'N, at least in the western sand sea (see Section 3.2.1). It seems that strong extratropical westerlies have shifted even farther towards the south at the end of the Pleistocene (see Section 5.3.3). Age problems of the longitudinal draa will be further discussed in Section 5.4.

### 5.3.2. Growth rates of the draa

With regard to longer time-spans in the formation of draa, the processes of deposition and deflation were necessarily active at the same time. This is corroborated by the grain-size distributions of the interior draa sands which all show an absence of clay- and silt-sized fractions, and a reduction in the 0.063–0.125 mm fraction, which certainly have been abundant in the original alluvium. On the other hand, bimodal grain-size distributions typical for deflation after the finished accumulation are found only in the modern surface sands (see Section 4.3.1). Therefore, the sands sampled from the interior represent the net accumulation, corresponding to the growth of the draa. Knowing well about the problems connected with calculating accumulation or growth rates, and with much reservation because of the few data, a discussion of net-accumulation rates is attempted. For this calculation, the exact numbers of years of the OSL ages have to be used (Table 8). After all, the results seem to be quite reasonable because – apart from one exception – the same

**Table 8** Net-accumulation rates in the draa (in cm per 1000 years), calculated from the exact OSL ages

	<i>W</i>		<i>Middle</i>	
	<i>Depth</i>	<i>Rate (cm/ka)</i>	<i>Depth</i>	<i>Rate (cm/ka)</i>
Transverse draa	2 m	100	2 m	60
	→		→	
	3 m	40	3 m	30
	→		→	
4 m		4 m		
		<i>W</i>		
Longitudinal draa	2 m	120		
	→			
	3 m	160		
	→			
	4 m	110		
→				
	5 m			



accumulation rates were obtained from the data published by Besler (2002a) and from the slightly different OSL ages calculated by A. Hilgers, using a homogenized water-content variation and updated software (see Table 7). Obviously, this kind of growth-rate calculation is rather resilient against minor changes in the ages of the accumulated sands.

Only one (but the longest) vertical record of OSL ages is available for the longitudinal draa on a west flank in the western transection. The differences from bottom to top are 940 years, 640 years and 840 years, which means net-accumulation rates of 1.1, 1.6 and 1.2 mm/year, respectively. Applied to a time-span of 1000 years – which duration is generally considered for geomorphological processes – this series yields rather homogeneous net-accumulation rates of 110–160 cm/1000 years (with a mean of 130 cm/1000 years). In this context, Munyikwa (2005) has to be mentioned, who emphasized that periods of dune stabilization and pedogenesis may be completely missed in the vertical dating record if the respective horizons have been eroded or reworked. In this case, a long time-span of aeolian accumulation under dry conditions may be inferred, whereas actually wetter intervals alternated with (shorter) dry spells. He underlined the importance of additional information on the stratigraphy. Homogeneous accumulation rates in the vertical records of OSL ages support a continual deposition without significant breaks.

Two shorter records with very different rates are available for the transverse draa. In the west, the age differences from bottom to top are 2300 and 960 years, and in the middle transection the differences are 3220 and 1590 years. These values are equivalent to net-accumulation rates of 40 cm/1000 years (bottom) and 100 cm/1000 years (top) in the west, and of 30 cm/1000 years (bottom) and 60 cm/1000 years (top) in the middle transection. In spite of the greater range in values, certain tendencies are present: first, in both records the rates are doubling towards the modern surface; second, at both depths the growth rates decrease from west to the centre of the sand sea. Causes could be either winds weakening towards the east or sands becoming coarser into this direction. The former assumption is contradicted by the heights of draa, which increase towards the east (see Section 3.2.2); the latter is corroborated by the mean grain size, which increases in this direction (see Section 4.2.1). The vertical increase in accumulation rate towards the top could also be due to diminished grain sizes. This cannot be tested with the values of Table 6, but may be investigated by analysis of the individual samples.

The comparison between transverse and longitudinal draa shows that the net-accumulation rates in the longitudinal draa are distinctly higher than in the transverse draa, independent of the more outspoken differentiation in the latter. Apparently, the draa modelled by the trade winds have grown faster. This may have been caused by stronger winds as well as by the different instability waves (see Sections 3.2.1 and 3.2.2), which may imply more deflation during deposition of aeolian sands in the transverse draa. This, of course, cannot be examined. On the other hand, differing grain sizes could play a part which may be tested. Indeed, the mean grain size along the western transection was found to be smaller, and even all individual samples drilled from the longitudinal draa are finer than the samples from the transverse draa. As a matter of fact, a statistically negative correlation was found between the net-accumulation rates and the mean grain size:  $r_s = -0.75$  (significant at 95%). For this purpose, the arithmetic means of the respective top and bottom

values of mean grain size were calculated and compared to the accumulation rates. Although the significance level is not so high, due to scarce data (seven cases), the correlation seems fairly convincing. Where the supply of fine-grained sands is larger, more sand grains can be moved by the average wind.

The growth of the draa seems to depend on the grain size of the sands supplied by the various sources. Nothing can be said on possibly different palaeo-wind velocities so far. More insight is to be expected from the heavy-mineral analysis (see Section 7.1).

The growth rates of the transverse draa are in no way related to their ages. They decrease with increasingly younger draa age towards the east; they increase, however, in the younger upper draa sands. Theoretically, the possibility exists that, at the end of the draa-formation interval, the extratropical westerlies became stronger and acted more as a deflating force in the west and more as a depositing agent in the east (where the draa are higher). This could have happened independently of the correlation between growth rates and mean grain size, and could explain the eastwards decreasing age of draa sands at comparable depths. Although this seems to be rather speculative due to the unknown secondary flow causing transverse draa (see Section 3.2.2), exceedingly strong westerlies are indicated at the transition of the Pleistocene to the Holocene (see Section 5.3.3).

### 5.3.3. Younger aeolian reworking of draa

On all sampled east flanks of the longitudinal draa, the sands have been shifting more than the usual upper 2 m after draa formation. The fact that the sands at depths of 2 and 3 m in the western transection at Willmann's Camp yielded the same OSL age of 11–12 ka had already been expected from their grain-size distributions. At depths of 0.5 and 3.5 m, the granulometric type of active crest sands comparable to modern dune crests and slip faces was sampled (see Section 4.3.1). From this sand type, a huge slip face was inferred where, of course, the upper and the lower part are of the same age. Dry end-Pleistocene westerlies did not only cause the asymmetry of the longitudinal draa down to 26°05'N, apparently they reached as far south as 25°07'N (Willmann's Camp). They did, however, not succeed there in changing the symmetrical draa shape.

As shown by the accumulation on the eastern draa flank of the middle transection, Willmann's Camp is not an exception. The age (10 ka) is comparable; however, the granulometric type there is a ridge sand. Most probably, the exceptionally narrow shape of the draa at Willmann's Camp was more favourable for slip faces reaching the base. The granulometric type of an old barchan sand, found at a depth of 1 m on a west flank of the longitudinal draa, goes well together with this reworking, although it was not observed in the same cross-section (see Section 4.3.1).

In addition to this interpretation as younger aeolian reworking, another possibility has to be considered. It may be that the layers deposited on the eastern flanks of the draa during the original draa formation have been preserved, whereas they have been eroded on the western sides long ago. This would mean an uninterrupted formation of longitudinal draa by the trade winds simultaneously with the modelling of the northern transverse draa until 12–10 ka ago. The eroded sand, however, must have been deposited somewhere. It cannot have been removed from the sand sea as blown sand, because of its

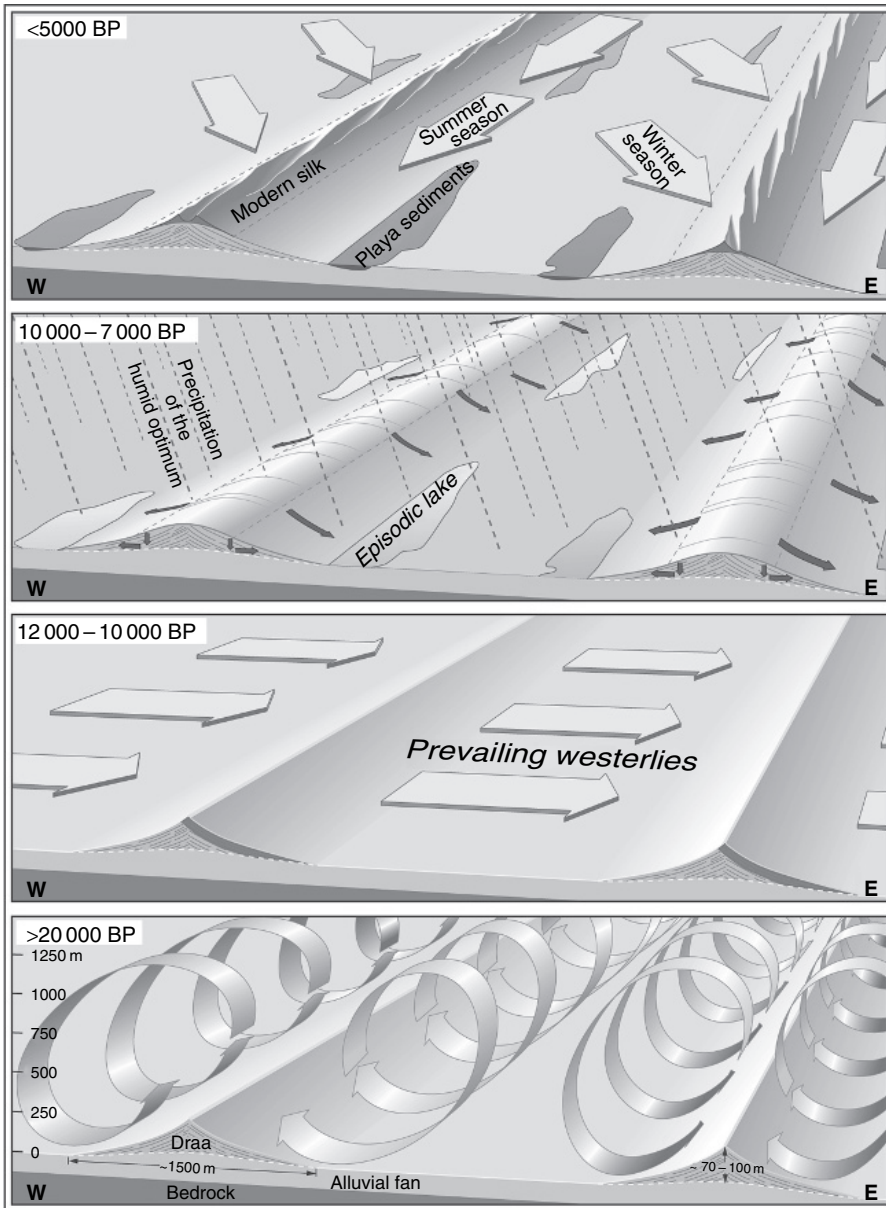


**Fig. 47** Proposed history of longitudinal draa (strongly idealized; modified after Bubbenzer and Boltén, in press). >20 ka: formation of draa below the ascending branches of vortices in the Planetary Boundary Layer, 12–10 ka: reworking of draa by strong, dry extratropical westerlies, 10–7 ka: wetting, flattening and consolidation of draa, and playa formation in interdrea corridors, <5 ka: reactivation of draa sands and formation of dunes.

coarseness (particularly in the middle transection). Today, the sands reactivated during the Holocene are found in dunes with their finer fractions, and in a few metres of cover sands with their coarser components protecting the finest fraction. These amounts of sand are much smaller than the huge bulk of sands which had to be removed from the western flanks if the upper parts had been deposited around 10 ka ago. An earlier reworking of the longitudinal draa by stronger westerlies around 12–10 ka ago seems to be much more realistic. Whether the flow of these westerlies was curved like the flow causing the asymmetry of the longitudinal draa (see Section 3.2.2) or not cannot be deduced, because the Holocene deposition (around 5 ka ago) may have buried the traces of the older reworking (around 10 ka ago) in the eastern transection.

At Reginfeld in the eastern transection, a reddened draa core was drilled from a depth of 2 m, which at first was thought to be a Pleistocene deposit with an Early Holocene rubification (Besler, 1997a, 2000a). The luminescence dating, however, gave an OSL age of 5 ka, which means that the Pleistocene body of the draa had not been reached by drilling. Apparently, the aeolian reworking took place in reddened sands that can be traced from the Reginfeld site far towards the south (Besler, 1997a, 2000a) (see Section 6.2). Contrary to the other east flanks, reactivation after consolidation with rubification and perhaps pedogenesis may have occurred. The question remains why this younger reactivation was not found on the other east flanks. It might have been met at a depth of 1 m, but dating was not carried out for this level, due to both the experience from the eastern transection (very young cover sands) and the high costs involved. On the other hand, the undisturbed, slightly brownish horizon at Willmann's Camp indicates that no reactivation occurred after its formation. This is further discussed in Section 6.2.

Anyway, after the deposition of the reddened sands around 5 ka ago, another humid interval of consolidation has to be assumed, because a sharp boundary between the reddish (7.5 YR 5/8) draa sands and the yellowish (10 YR 6/5) cover sands is present in all drillings (see Fig. 43). Without consolidation, the yellow and the red sands would have been mixed. The proposed history of the longitudinal draa is presented in Fig. 47.

## 5.4. COMPARATIVE DISCUSSION OF REGIONAL DATINGS: TIME SLICES IN THE GREAT SAND SEA

Only datings in and around the Great Sand Sea are considered here. Prior to the luminescence datings established at the Collaborative Research Centre 389 ACACIA (University of Cologne), radiocarbon ages regarding the Great Sand Sea and proxy data from classified artefacts indicated only the more humid conditions. The earliest  $^{14}\text{C}$  datings stem from the BOS project (Universities of Cologne and Berlin) and from the Collaborative Research Centre 69 (Geoscientific Problems in Arid and Semiarid Areas, Universities of Berlin). The majority of these data concern, however, the Holocene.

Hand axes and other Acheulean artefacts (~200 000 BP) under playa deposits and at the contact between draa and desert floor at Willmann's Camp (Glass Area

81/61) were mentioned by Haynes (1982). The accumulation of draa (whaleback dunes) was supposed to have taken place thereafter according to Pachur and Röper (1984), who also mentioned Aterian artefacts (~40 000 BP) scattered over the Gilf Kebir Plateau, but absent on the younger terraces. Apparently, the conditions in this elevated area south of the Great Sand Sea were then favourable for human occupation. Pachur and Braun (1980) mentioned fresh-water diatomites from 28°N, 27°E, dated at 26 100 BP. This is in the region between the oases of Farafra and Bahariya, east of the sand sea, where different conditions existed due to near-surface artesian groundwater. There also exist data, however, that indicate humid conditions within the Great Sand Sea.

The oldest date from the southern sand sea is 32 730 (+1380; -1170) BP; it was derived from a monocyclic calcareous crust associated with groundwater or lakes (phreatogenic crust: Pachur et al., 1987). Later on (Pachur, 1993), this crust was termed a “carbonaceous lake chalk”. The position is given with 25° 33.8'N, 26°00'E, which would be around the eastern margin of the Gilf Kebir alluvial fan, that is marked by the disturbance in the draa pattern with exceptionally broad corridors (see Section 3.2.1 and Fig. 41). The site is described as a shallow deflation basin with sands and gravels at the bottom. The <sup>14</sup>C age at the upper limit of radiocarbon dating as well as the crust material does not seem to be reliable. Calcareous crusts generally tend to yield too young ages because carbonates are easily dissolved and re-precipitated by water charged with carbon dioxide (CO<sub>2</sub>). Thus, any subsequent precipitation event (or groundwater input) may add <sup>14</sup>C from atmospheric CO<sub>2</sub> and re-set the radiocarbon clock. Therefore, the lake deposits could even be older than the fine-grained alluvium that theoretically could have covered the calcareous deposit. Later, this may have been exhumed during draa formation.

In the stratigraphic record of these lake sediments (Fig. 13 in Pachur et al., 1987), two more radiocarbon ages are presented: 20 960 ± 280 BP and 18 940 ± 540 BP at 25°36.4'N, 26°0.2'E. Unfortunately, they are not discussed in the text. The same figure is presented in the work of Pachur and Braun (1986, their Fig. 3), but with differing coordinates: 25°50'85"N, 26°07'84"E. This locality lies NNE of the one mentioned above and – if this position is more correct – would be at the easternmost margin of the alluvial fan. A charcoal-bearing substance in the lake sands was used for radiocarbon dating. These ages are comparable to the luminescence ages of draa at depths of 2 and 3 m at nearly the same latitude but farther west in the western transection (25°42'N, 25°40'E). Pachur and Braun suggested a singular occurrence “as the high permeability of the dune sands could mean that the erg amplified quasi-fluvial events”. This means that the draa were supposed to have already existed. Ephemeral flood events from the Gilf Kebir could have coincided with draa formation and do not contradict the luminescence ages.

An additional date in this time interval was mentioned by Pachur (1993) as derived from organic carbon: 21 370 ± 805 BP. The parent material seems also to have been carbonaceous lake sediments. Latitudes between 25°30'N and 26°30'N are mentioned as the location. Unfortunately, it is not made clear whether these are the same localities as the ones mentioned in 1986 and 1987, or additional sites. The same holds true for another three ages between 25 000 BP and 30 000 BP that

appear under the heading “Great Sand Sea” in Pachur’s (1993) Fig. 4. The caption of this figure reads: “. . .  $^{14}\text{C}$ -dates along ca  $23^\circ$  from west to east. . .”. In this case, they would not belong to the Great Sand Sea at all. On the other hand, the age mentioned above at  $25^\circ30'\text{N}$  is also found in this figure. According to Pachur et al. (1987), monocyclic calcareous crusts are found in the Great Sand Sea south of  $27^\circ\text{N}$  and indicate groundwater recharge between 40 000 and 20 000 BP.

Fortunately, these partly controversial data and localities in various papers by Pachur (et al.) are now summarized in an instructive overview of the Great Sand Sea in a book by Pachur and Altmann (2006; their Fig. 2.6.8.1) about the eastern Sahara in the Late Quaternary. The Late Pleistocene lacustrine deposits that are radiocarbon-dated cluster at two localities: in one area between  $25^\circ30'\text{N}$ ,  $26^\circ\text{E}$  and  $25^\circ53'\text{N}$ ,  $26^\circ08'\text{E}$  (33 000–19 000 BP) and in another area between  $26^\circ21'\text{N}$ ,  $26^\circ16'\text{E}$  and  $26^\circ45'\text{N}$ ,  $26^\circ32'\text{E}$  (36 000–20 000 BP). Interestingly, the authors who would have preferred a Holocene age suggest a possible contamination by calcareous dust blown out of Tertiary sediments, which increased the age. They admit, however, that a rejuvenation of the deposits by adding atmospheric  $\text{CO}_2$  via younger rhizomes cannot be excluded. The latter alternative seems to be more likely because the dated localities are situated in the distal parts of reconstructed alluvial fans (see Sections 8.6.3.3 and 8.6.3.4).

It should be mentioned in this context that, during the last diagonal crossing of the Great Sand Sea in 2006, calcified swamp sediments with reed moulds were found in one of the wide, gravelly interdrea corridors at  $26^\circ04'\text{N}$ ,  $25^\circ41'\text{E}$ . Unfortunately, an extended investigation was not possible, due to lack of time and the shortage of drinking water. The material, however, resembles very much an encrusted lake chalk with macro-pores from reed growth found at  $26^\circ32'\text{N}$ ,  $26^\circ19'\text{E}$  by Pachur and Altmann (2006; their Fig. 2.6.8.6), who assume a formation by groundwater discharge. It has to be pointed out that the radiocarbon data given as BP ages are uncalibrated, which means that the respective true ages have to be considered as being 500–1000 years higher (Lang, 1994). In comparison with luminescence ages, this difference is not taken into account, since this error is small with regard to the Late Pleistocene.

In summary, it may well be that the  $^{14}\text{C}$  ages of these lacustrine deposits are too young, and that much older lake beds were excavated in the corridors during the draa formation. This will be discussed in more detail in the sections on major sand sources of the Great Sand Sea. No problems arise with regard to the formation of transverse draa because there is agreement that no groundwater recharge occurred during this time interval (a.o. Thorweihe et al., 1984; Thorweihe, 1990b).

A human re-occupation of the Great Sand Sea occurred during the Holocene wet phase. The earliest documentation – which may be its onset – is represented by the “Regenfeld A unit” around 9400 BP (Fig. 1 in Riemer, 2005; Kuper and Kröpelin, 2006). Contrary to the Pleistocene, the difference between calibrated and uncalibrated  $^{14}\text{C}$  data is of great importance in the Holocene and has to be taken into account, particularly if a comparison with luminescence data is attempted. Calibration of the A-unit data at Regenfeld yields an age of around 10 600 cal BP. Both this age and the ages between the brackets below are graphically deduced by the present

author from the calibration curve provided by Riemer (2005; his Fig. 3: calibration by 2-D Dispersion Calibration Program Cologne 2001, B. Weninger, Radiocarbon Laboratory, University of Cologne) and are only approximate values. In a general evaluation of summarized data from various sources (lacustrine, marine and pollen records, palaeo-hydrological proxy data, etc.), Hoelzmann et al. (2004) state that the onset of the Holocene wet phase occurred in northeast Africa within “a very short time period of a few decades at ca. 10.9–10.5 ka cal BP”. Thus, the Regenfeld A unit provides a good example of this timing.

Riemer (2005) divided the archaeological finds of the Holocene wet phase into four units, according to the characteristics of their stone tools.  $^{14}\text{C}$  dates were obtained from charcoal and ostrich eggshells. In addition, the vegetation could be reconstructed from the charcoals (Neumann, 1989a, b) and the fauna from the bones (Van Neer and Uerpmann, 1989). Unit B, dated around 8600 BP (around 9600 cal BP), already shows more plant and animal species (mainly *Tamarix* sp. and *Gazella dorcas/leptoceros*). The longer time slice of unit C covers 8300–7900 BP (~9450–8700 cal BP), now with the presence of *Acacia* sp., *Addax nasomaculatus/Gazella dama* and *Struthio camelus* (ostrich), which all need more favourable conditions. This goes well together with the climax of monsoonal precipitation at 9.4 ka BP, according to Hoelzmann et al. (2004).

According to dated charcoal (~8000 BP = ~9000 cal BP), the evidence of human occupation at Willmann’s Camp starts at about the same time. The oldest date from another archaeological site in an eastern extension of the sand sea, Lobo (Abu Minqar 81/55) with 7700 BP (~8500 cal BP), is only a little younger (Kuper, 1989). A comparable age (7600 BP) of charcoal from a hearth north of Ammonite Hill in the eastern sand sea is provided by Pachur et al. (1987).

The data from Lobo already stop around 7000 BP (~7700 cal BP) (Kuper, 1989), and the data from Regenfeld at 6400 BP (~7300 cal BP) (Riemer, 2005). During this final time, unit D (7200–6400 BP = ~8050–7300 cal BP) covers the maximum of radiocarbon data and the greatest diversity in implements, including pottery and grinding stones. With regard to vegetation and fauna, the analysis is still going on (Riemer, 2005). The data from Willmann’s Camp go on, according to Haynes (1982), till 4780 BP (~5600 cal BP; lag concentration of ostrich eggshells), and till 4300 BP (~5000 cal BP; charcoal) according to Kuper (1989). At a site shortly north of the Gilf Kebir, a younger age of 5905 BP (~6800 cal BP) from a hearth is mentioned by Pachur et al. (1987). The same authors mention 5600 BP (~6450 cal BP) from a hearth north of Ammonite Hill. Their most recent age is given from Ammonite Hill with 2760 BP (not on the calibration curve); this, however, comes from a rhizome at the base of a dune beside an archaeological site and therefore may not be related to human activities.

The fact that most sites lie in the eastern sand sea is most probably a matter of modern accessibility, but may also be a consequence of the less sandy corridors between the draa in this part. Of course, the picture of the Early Holocene human occupation of the Great Sand Sea cannot be complete, because it entirely depends on what has been discovered so far along the few investigation routes. However, a statistical approach combining the data from the Great Sand Sea with those from the Abu Ballas Scarp in the south and from Abu Minqar (see Fig. 41) in the east is of

interest (Riemer, 2005). The probability distribution of 135  $^{14}\text{C}$  dates in years BP as well as in calibrated years BC shows a sudden drop in data around 6300 BP (~7300 cal BP) and an increase to the same level around 6100 BP (~7000 cal BP), before the final decrease to almost zero <6000 BP (~6800 cal BP). Riemer deduces therefore that the onset of aridization took place around 6300 BP (~7300 cal BP) and that a short revival of humid conditions occurred around 6100 BP (~7000 cal BP). In this context, the OSL age of 5 ka (which is a minimum age) of the reddish draa deposit at Regenfeld (Besler, 1998), which was consolidated and truncated later on (see Section 5.3.3), could be the sedimentary equivalent to the drop in radiocarbon data (aeolian activity) and their subsequent short recovery (returned humidity) before the final end of the Holocene climatic optimum.

Only at Willmann's Camp – a particularly favourable place (see Section 6.2) – evidence is found of later human occupation. A reduction of occupational activities can also be recognized there after 6000 BP (~6800 cal BP), however. Therefore, the reactivation of draa with the formation of dunes may have started around 5000 years ago (see Section 3.3.3). Pachur and Altmann (2006) summarize their radiocarbon data obtained from charcoal found at playas as covering the time interval between 11 and 5 ka BP. They state that all these playas are only peripheral to the Great Sand Sea and contain non-carbonaceous, pelitic sediments.

Since luminescence dating is not so well established yet as radiocarbon dating, every situation with the possibility to test the correlations and the compatibility or the fit of both data sets and their complementary character (see Bubenzer et al., 2007b) is of interest. From the combination of OSL ages and radiocarbon data, a chronology of time slices with changing environments in the Great Sand Sea can be reconstructed. Only the archaeological sites of Regenfeld and Willmann's Camp seem to have been occupied during longer time slices. All other localities mentioned may have been sporadic hunting camps. Compared to Willmann's Camp, Regenfeld is better documented, and the youngest OSL age is derived from this place. Therefore, the data from Regenfeld are used for the chronology. It has to be born in mind however, that the time resolution of OSL data is up to 10 times lower than that of the  $^{14}\text{C}$  data (Bubenzer et al., 2007b). Nevertheless, an attempt is made to deduce a chronology of time slices, using OSL ages and radiocarbon ages converted to cal BP (from oldest to youngest):

- |  |                    |
|--|--------------------|
| 1. formation of longitudinal draa by trade winds     | >20.4 ka           |
| 2. formation of transverse draa by westerlies        | 20.4–11.1 ka       |
| 3. westerlies pushing south                          | 11.8–9.8 ka        |
| 4. human occupation at Regenfeld                     | 10.6–7.3 ka BP cal |
| 5. last draa stabilization before final reactivation | <5 ka              |

The overlap between the formation of transverse draa and the southward shift of the westerlies seems quite explainable since the westerlies did not necessarily cease in the northern part during that time. They may even have been stronger, as suggested in Sections 5.3.2 and 5.3.3. Considering the low time resolution and the low number of OSL data compared to the numerous radiocarbon ages, the time-span of human occupation at Regenfeld fits surprisingly well into the OSL chronology



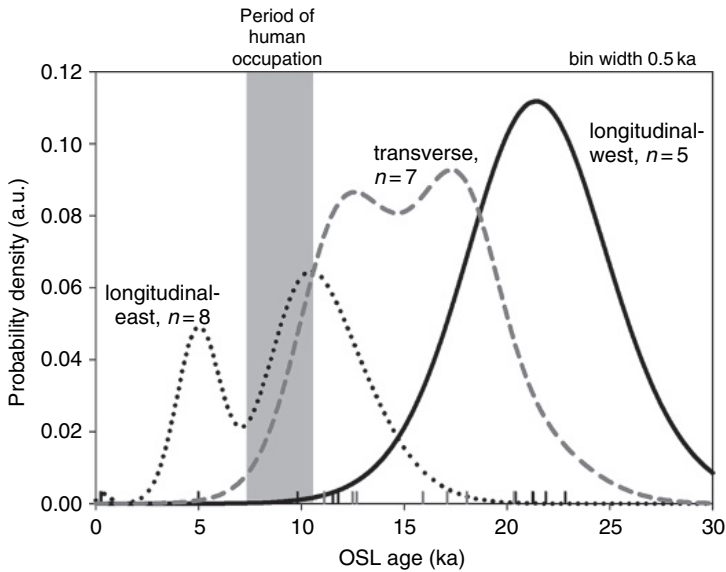


**Fig. 48** Compilation of all OSL dates grouped according to dune type and dune side sampled for dating. The graph was constructed following the probability density approach as described, for example, by Singhvi et al. (2001). This approach permits the construction of a histogram such that the errors (1-sigma) in ages are also included. The time span which is considered here, 30 ka, was subdivided into class intervals of 0.5 ka. For each OSL age, a Gaussian distribution is calculated with its mean representing its age value. The width of the distribution is determined by the individual error of the OSL age. The histogram value for each class interval is then calculated by summing the individual values of each age included in the compilation and dividing the sum by the total number of dates.

(see Fig. 48). A future improvement may be expected from an increase in data as well as from the application of more refined OSL-dating techniques with a better time resolution (see Section 5.2). The time slices of this chronology (Figs 47 and 48) are compared to that of other sand seas in the final chapter.

## QUARTZ SAND AS AN INDICATOR OF HUMID PERIODS

### Contents

6.1. The Salinity of Sands	129
6.1.1. Water in dunes	129
6.1.2. Interpretation and discussion of the salinity	130
6.2. The Rubification of Sands	135
6.2.1. Introductory discussion of red dune sands	135
6.2.2. Reddened sands in the Great Sand Sea	138

All methods of sedimentary analysis applied so far only provide information about aeolian processes and the arid history of the Great Sand Sea. But even without the more laborious methods of heavy-mineral analysis and microscopy or SEM, there are some very simple ways of gaining information about humid periods in a sand sea. Important indicators are the salinity and the rubification of quartz sands.

### 6.1. THE SALINITY OF SANDS

#### 6.1.1. Water in dunes

Bagnold (1938) already noticed the importance of different types of stratification in dunes for the infiltration and percolation of precipitation water and the resulting moisture content. Whereas accretion on the windward side compacts the dune surface and favours a quick evaporation, encroachment layers parallel to the slip face may lead water to greater depths before evaporation. This was also observed by Jäkel (2002) after some rainy days in the Badain Jaran Desert in China in 1995. Therefore, even in complex dunes, encroachment places – usually the “soft spots” dangerous for vehicles – are indicated by vegetation. This has been corroborated by Bagnold (1938) and own observations in the Namib Erg in 1976, but was of no help in the Great Sand Sea because even encroachment sites do not show any vegetation due to the hyper-aridity (see Section 6.1.2).

There is disagreement in the literature concerning the depth from which water through capillary action can be drawn to the surface and evaporate in loose sand. According to Knetsch's (1950) observations in the Libyan Sahara, the evaporation in dune sands may reach down to a depth of 2 m. On the other hand, he observed in the Namib Desert that a moisture horizon was preserved at a depth of 1.2 m.

According to Bagnold (1954), a moisture horizon may survive for several years even at a depth of 20–30 cm. This is not possible, however, if the sands are shifting. According to Wipplinger (1958), the evaporation ceases at a depth of about 1 m. Experiments on the evaporation of water from sand were carried out in Namibia by Hellwig (1974), who used various tanks filled with three types of river sand consisting of grains between 0.05 and 2.0 mm. During a test period of 71 weeks, the water tables were kept constant at depths of 30 and 60 cm below the surface. Using the pore volume, Hellwig calculated the upward water velocity during evaporation at 9.93 mm/day in fine sand, at 7.83 mm/day in medium-grained sand and at 5.4 mm/day in coarse sand in the tanks with water tables at 30 cm below the surface. Due to capillary action, salts removed from the solution accumulated in a thin sand layer near the surface. In the tanks with water tables at 60 cm below the surface, water was not transported to the surface in liquid form. The upper sand layers were always dry. However, precipitated salts were found in the sand 5–15 cm above the water table.

According to Wipplinger (1958), the finest sand has a permeability for water of approximately 3 m/day, fine-grained sand ( $\sim 0.3$  mm diameter) of approximately 20 m/day and middle-sized sand of approximately 60 m/day. This means that precipitation water may quickly reach depths from where the evaporation is no more effective. Most authors agree that water storage in dunes is possible because of rapid infiltration, low capillary rise and rapid fall-off in evaporation rates below the surface after its drying. According to Wilkinson (1977, his Fig. 11), a perched aquifer exists in the megadunes around the Al Liwa Oases in southern Abu Dhabi (eastern Rub' al Khali) with a mean annual precipitation (estimated) of 30–100 mm, which via seepage allows the cultivation of date palms in dune depressions. Date palms are known to demand high quantities of water (and to tolerate a certain salinity).

Dissolved salts are introduced into dunes by fog or rain. In addition, aeolian salt deposits (as dust) near the surface may be carried to greater depths during infiltration. These salts are not drawn to the surface during desiccation because the upward capillary motion is slower than the evaporation from the uppermost layers. In these dry subsurface parts, the evaporation is controlled by diffusion of water vapour (Ruck et al., 1987; Alaily, 1996). These statements refer to aridic soils; they are even more valid, however, for dune sands without pedogenesis. Even slight soil formation on the draa in more humid periods would not alter the processes. Therefore, the salinity of dune and draa sands indicates former precipitation events. Of course, a rising groundwater table can also add water and salts to dunes. This case will be neglected here because, at least for the longitudinal draa with their wide corridors, this situation does not seem applicable.

### 6.1.2. Interpretation and discussion of the salinity

The salinity of draa sands is considered as a legacy of humid periods. During draa formation with aeolian transport, no salts could have been incorporated into the sand bodies. The salts were added in solution by precipitation (or a rising groundwater table). Salinity measurements of the samples from the eastern transection have shown that all

draa sands (surface and interior) were saline ( $>100 \mu\text{S}/\text{cm}$ ), while almost all dune sands were not saline (Besler, 1997a). It should be remembered, however, that – compared to the other transections – only few samples were available for analysis from the eastern transection, particularly of the draa interior. Dune (crest) sands are usually not saline because salts are abraded and blown away as dust particles during the saltation transport. This had already been observed in the Namib Erg (Besler, 1979, 1980).

On the eastern transection, however, there were two exceptional dune sands which are saline. One sample (no. 12/96) was collected from an eastern dune flank south of the third cross-section ( $24^{\circ}45'\text{N}$ ). Some 20 cm of distinctly stratified and slightly consolidated sands were excavated below the dry cover sand. These features show the presence of water at some time, and also that the sands had not been shifting thereafter. As this locality is not too far from the “Regenfeld” place, where Rohlf’s (1875), during his expedition from Dakhla towards Al Khufrah in 1874, encountered a heavy rainstorm lasting 4 days, this may well be a modern phenomenon. On the other hand, it cannot be excluded that an ancient initial draa body is hidden below the modern dunes although, according to shape and size, the draa seem to start only at the seventh cross-section ( $25^{\circ}03'\text{N}$ , see Sections 3.2.1 and 3.3.3). The granulometry, in this case, is not decisive, because the sample belongs to the granulometric type of inactive crest sands which is found in dune flanks as well as in fine-grained draa (see Section 4.3).

The second sample (no. 39/96), with a salinity close to its threshold value ( $100 \mu\text{S}/\text{cm}$ ), was collected in the northern chaotic dune field without draa, immediately south of the Siwa Oasis Depression ( $29^{\circ}00'\text{N}$ ). The ground consists there in many places of “fesh-fesh”. According to the glossary of Saharan terms by Capot-Rey et al. (1963), this is an Arabic word (fechfâch) for a powdery, cohesionless soil rich in gypsum and difficult to traverse. In the handbook of soil science (Alaily, 1996), it is defined as a powdery upper soil horizon with high contents of chlorides, gypsum and carbonates, which may be up to 10 cm thick. Most probably this means a continuous input of dust to the dunes.

Three samples (nos. 17, 19, 25/96) are even strongly saline ( $>10^3 \mu\text{S}/\text{cm}$ ). It is not surprising that all three sediments are clay- and silt-rich playa deposits (see Sections 3.1 and 4.4).

Unfortunately, the salinity measurements along the middle and the western transections show a less convincing pattern (Fig. 49). Along the middle transection, only one crest sand (no. 21/99) is saline and close to the threshold value. This sample was taken from a low silk at its starting point. It may well be that the dune still carried the heritage of its draa source. On the other hand, 40% of the draa sands (6 out of 15) are not saline. Two sands were sampled from the draa surface and could be younger cover sands. Some of the interior sands at depths of 1 and 2 m, however, definitely belong to the “non-saline” group. Whereas a sand at a depth of 1 m may still be a modern cover sand (see Sections 5.3.1 and 5.3.3), this is not reasonable for a depth of 2 m. Particularly the vertical salinity profile in the transverse draa shows that saline and non-saline horizons are alternating (Fig. 49). The conclusion may thus be drawn that the moisture was not evenly distributed before desiccation and that the saline horizons correspond to discrete precipitation events. This assumption is supported by recent investigations in the Badain Jaran

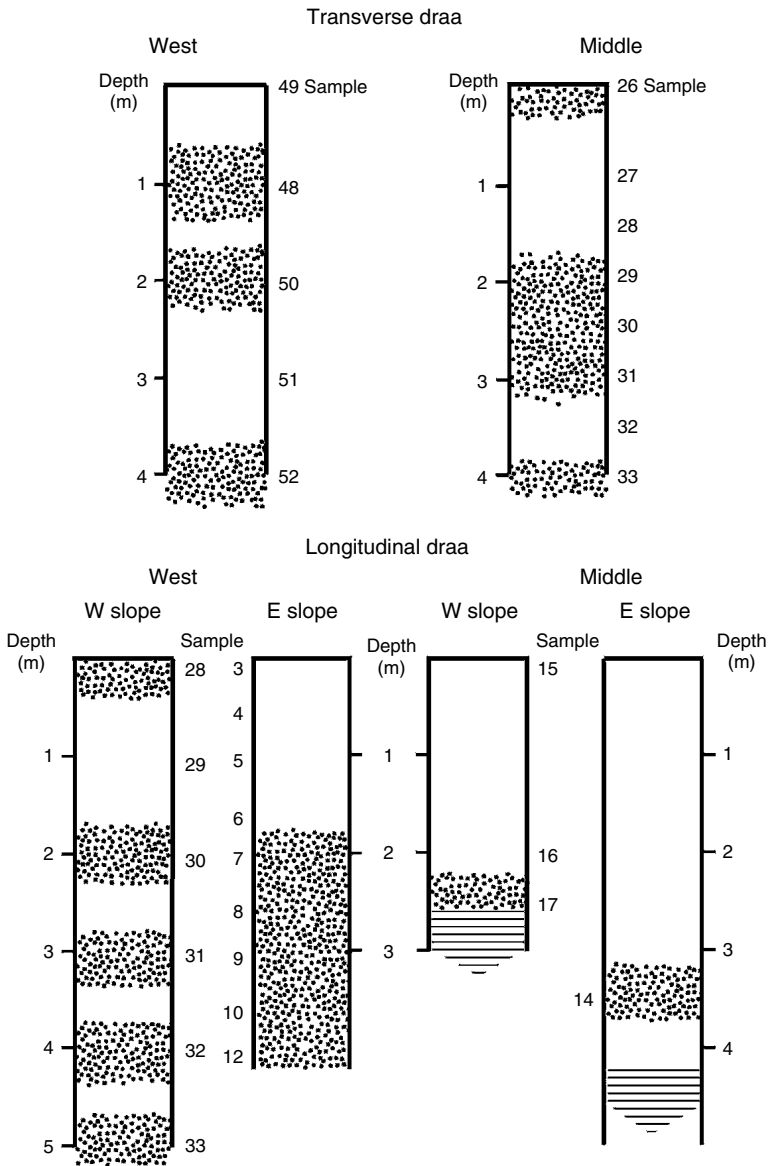


**Fig. 49** Saline horizons in the drilling profiles along the western and middle transections (for location see Fig. 41).

Desert in China, where Jäkel (2002) observed a moist surface-sand layer, varying in thickness according to the bedding type of the dune (compare Bagnold, 1938), 1 day after a rainfall event of 7.8 mm. Below this layer, several tens of centimetres of dry sand and another – rather thick – wet horizon followed that resulted from a precipitation event half a month earlier.

In this context, a comparative study in the southern Namib Erg (Bubenzer et al., 2007) yielded remarkable results. A wet horizon in dune sands was observed in September 2004. About 1 m of wet sands was excavated below 10 cm of dry surface sands. This would correspond to a winter rainfall of 100 mm. According to the National Atlas of Namibia (Mendelsohn et al., 2002), the Koichab Depression south of the investigated transection receives an average annual precipitation of >50 mm and the eastern erg around 100 mm (with a high variability). At the coring sites for luminescence dating, saline horizons of 1–1.5 m thick alternate with non-saline horizons in the western and the eastern flanks of the draa.

Unfortunately, little is known about the moisture budget in aeolian sands. The saline horizons found in the drillings could correspond to a precipitation of 100 mm or even less. According to measurements in the northern Namib Erg (Gut, 1988; Besler and Gut, 1997), the thickness of the moist horizons increases during the downward movement of the water. Necessarily, the moisture content decreases during this process. A precipitation of 14 mm, for example, had reached a depth of 56 cm after 30 days, which was four times the initial penetration depth. The moisture content of the sand had decreased, however, from 8.7% on the rainfall day to 1.0–1.8% (at a depth of 15–56 cm). Comparable results were obtained during infiltration experiments in the Wahibah Sands in Oman (Agnew, 1988). They were conducted in an interdune depression. Unfortunately, the amount of infiltrated water is not mentioned, but according to Agnew's Fig. 4 the moisture contents were determined by a neutron probe following saturation during the infiltration test. The moisture decreased from 19% at 20 cm depth to around 4% within 7 days. At a depth of 40–90 cm, however, a 4–5% moisture content was still measured after 16 days (when the field study ended). The salts most probably had been precipitated before these low values were attained. If, in a first approach, an earlier salt precipitation is neglected, a moisture penetration depth of 4 m could be achieved with a precipitation of 100 mm. Another mechanism may, however, also play a part: according to experiments in the Selima Sand Sheet in southern Egypt, a second rainfall event of the same intensity and amount will reach a deeper moisture front, even if applied after several months of drying (Ruck et al., 1987). On the other hand, experiments with artificial rainstorms on aridic soils have shown that the depth of the salt translocation only corresponds to about two-thirds of the downward water movement (Blume et al., 1985). In this case, the original moist horizon must even have reached deeper.

After desiccation of the surface, the water loss by gas diffusion is extremely slow and may be in the range of 0.01 mm/day (Ruck et al., 1987). If this value is applied to the Namib horizons of around 1 m thickness from 100 mm precipitation, the drying process would take about 28 years. Ruck et al. (1987) assume, however, that the drying time for deeper layers may be hundreds of years. It should be mentioned that the literature cited here deals with aridic soils and not with loose dune sands. In any case, the saline horizons in the Namib draa may well be the product of modern rainfall events and do not have to be palaeo-features.

The conditions in the Great Sand Sea are, however, quite different: the average annual precipitation amounts to only <5 mm. Blume et al. (1985) mention rainstorms with a maximum of 7.5 mm in 1 day during the last century. According to Smettan

and Blume (1987), a maximum precipitation of 8 mm occurred at Kharga/Dakhla in 1943. Under these circumstances, salt accumulations are relict phenomena of more humid periods of the past (Blume et al., 1985). For salt accumulations at a depth of more than 1 m found in the Fezzan, particularly heavy rainstorms of more than 50 mm are assumed. From the solubility succession of accumulated salts in sandy desert soils of Egypt (from bottom to top: nitrates and chlorides, sulphates, carbonates), Smettan and Blume (1987) conclude that, for this distribution by downward leaching, a precipitation of 50–100 mm/year was necessary. The wetter Neolithic period or episodic rainstorms during the last 5000 years are suggested to have provided these conditions. Pachur and Hoelzmann (1998) estimate the precipitation at Kharga as decreasing from <100 mm before to <50 mm after a maximum around 8000 BP (~9000 cal BP) (Pachur, 1999). Thus, the saline horizons in the Great Sand Sea are the heritage of more humid conditions, and an average precipitation of most probably 50–100 mm/year can be assumed. This assumption is supported by the literature cited as well as by the actual conditions in the southern Namib Erg. Independently of these conclusions, archaeo-botanical and archaeo-zoological investigations in the Regengfeld area mention an estimated precipitation of <50 mm in the Early Holocene and up to 100 mm in the mid-Holocene (Neumann, 1989a, b; Gehlen et al., 2002).

The sand sample (no. 14/99) from a depth of 3.4 m on the eastern flank of the draa, not too far from the bedrock, shows an exceptionally high salinity (strongly saline  $>10^3 \mu\text{S}/\text{cm}$ ). In this respect it is comparable to the playa deposits at Regengfeld in the eastern transection (compare Sections 6.2.2.2 and 8.6.1). In the transverse draa, the surface sand (no. 26/99) was saline. As salts are not accumulated near the surface in shifting dune/draa sands, an ancient moisture horizon must have been truncated by aeolian erosion on the windward draa side.

In the western transection, the same salinity phenomena were found: alternating saline and non-saline horizons and a saline one truncated at a western flank of – in this case – the longitudinal draa (Fig. 49). Following the discovery of these saline horizons in longitudinal and transverse draa on the middle and the western transections, the estimation of a 50–100 mm annual precipitation may be extended over the entire sand sea.

On the whole, 33% of interior draa sands (10 of 30) were non-saline, and even 50% of draa-surface sands (6 of 12) were non-saline. The high percentage of non-saline surface sands may be due to younger cover sands, particularly on eastern sides. All dune-crest sands on the middle and the western transection were not saline.

Even if not all draa sands are saline, the probability that a saline sand belongs to a draa and not to a dune is rather high. Together with other indicators, this fact allows the identification of draa sands in questionable positions. At the southern end of the middle transection, a sand shield had been interpreted in the field as being modern. The grain-size frequency distribution, however, yielded the granulometric type of ridge sands which according to their granulometric characteristics belong to draa sands (see Section 4.3). This sample (no. 3/99) is saline, in contrast to the sand from a true modern sand shield at the southern end of the eastern transection (no. 10/96). Another problematic sand is no. 25/99 from a low silk body (on draa) without a distinct crest line. This sand belongs to the granulometric type of plinth sands which is found in fine-grained draa as well as in basal dunes. Here, the salinity indicates that this sand body most probably is part of the draa.

The simple procedure of measuring the salinity of sands can provide evidence of more humid periods in the past and may even allow some conclusions on the former rainfall pattern and amount. In addition, it helps to distinguish between draa and dunes in doubtful cases. The vicinity to topographic depressions (today with oases) where salts are accumulated and to large ancient playas – as at Regenfeld – where salty loess-like sediments are found (see Section 4.4), may, however, also play a part. This could also explain why all draa-sand samples along the eastern transection are saline.



## 6.2. THE RUBIFICATION OF SANDS

The Concise Oxford Dictionary of Geography (Mayhew and Penny, 1992) defines the term “rubification” as the change of soil colour to yellow or red during intense weathering, liberating iron which then attaches to clay minerals. According to Kubiena (1957), the term rubification is restricted to the alteration of hydrates of iron oxide to crystalline goethite and haematite. A more recent definition combining these short statements is given by Zech and Hintermaier-Erhard (2002): rubification is a pedogenic process in warm climates with alternately dry and humid seasons. During the weathering of iron-bearing minerals (e.g. micas), hydrates of iron oxide and goethite are formed in a first step. These processes – leading to brown colours – are also active in humid climates of higher latitudes. During the dry seasons of warm climates, the iron oxides are dehydrated and their crystal structure is improved, resulting in the formation of the haematite that is responsible for the red colours.

### 6.2.1. Introductory discussion of red dune sands

Capot-Rey and Grémion (1964) were among the first who compared Saharan ergs and dunes with regard to their colour. They noticed that the sands in marginal parts of the ergs were lighter, which they ascribed to their higher aeolian mobility. Turner (1980), in the chapter on desert red beds in his book on continental red beds, mentions “considerable evidence” for the assumption that dunes get redder with increasing age. As examples he cites the Namib Sand Sea and the Great Eastern Erg. The first quotation is based on a long-lived misunderstanding with regard to the sand sources. The sand was believed to originate at the coast (where the dunes are lighter) and to travel inland to the eastern border of the sand sea, where draa and dunes are red. Meanwhile, investigations have shown that the colours are due to different sand sources, i.e. the red Tsondeb Sandstone in the east (Besler, 1980). One important piece of evidence (among others) is provided by the quartz-grain shapes, which to a high percentage are rounded near the coast but subangular in the east. With regard to the Great Eastern Erg, investigations have shown that the dominant colour is reddish yellow (around 7.5 YR 6/6: Besler, 1987c) and that the lighter sands in the northernmost part (very pale brown or pink: 10 YR



to 7.5 YR), where the hue correlates with the salinity, have their sources in gypsum-bearing local sediments (Besler, 1989). Of course, these small dunes are younger. But they have a different source which is decisive for their colour. The statement of dunes getting redder with age is only valid if periods of pedogenesis or diagenesis have interrupted their aeolian history. A good example are the fixed red Sahelian draa, which in many parts are not at all older than the yellowish draa in the Great Sand Sea. Also in the Great Sand Sea, however, reddening of quartz grains with increasing transport distance has been suggested (El-Baz, 1982).

The Namib Erg represents an extreme case with hues ranging from 10 YR near the coast via 7.5 YR in the middle to 5 YR in the east (Besler, 1980). Most ergs, however, are more homogeneous in colour. The Great Sand Sea rather uniformly consists of very pale brownish sands (mainly 10 YR 7/4). The same is true for the Fachi-Bilma Erg in the Ténéré in Niger (Besler, 1989). In the Taklamakan Sand Sea in the Tarim Basin (China), yellowish brown sand colours (around 10 YR 5/4) are dominant (Besler, 1991b). In the United Arab Emirates, the light yellowish brown sands (around 10 YR 6/4) of the eastern Rub' al Khali can be distinguished from the red dune sands (7.5 YR to 5 YR) along the western footslopes of the Oman Mountains (Besler, 1982).

In the rather uniformly coloured Great Sand Sea, some localities showing reddish (7.5 YR) and even red (5 YR) hues are particularly conspicuous and ask for an explanation (Fig. 50). The reddish colours of quartz sands are caused by iron oxides associated with clay coatings. A thin-section analysis (no. 19/96 from Regenfeld) revealed multiple layers of clay stained with iron oxides (Besler, 1998). An analysis of coatings on sand grains from southwestern Egypt was carried out by El-Baz and Prestel (1982). The red sands came from a dune in the Wadi El-Bakht in the eastern Gilf Kebir Plateau. The 0.5–4.5  $\mu\text{m}$  thick coatings were scraped off the grain surfaces and subjected to X-ray powder diffraction, which yielded crystallized kaolinite and little hematite that were also observed under the SEM. Unfortunately, nothing is said on the processes that are responsible for the formation of these minerals. Generally, two origins of red colours in dune sands are possible: in situ formation or inheritance from red deposits after a short transport.

The in situ rubification may be caused by pedogenesis under warm and humid conditions. However, with regard to the conditions, there is considerable disagreement in the literature. Price (1962), investigating the stages of oxidation colouration in dune and barrier sands on the east coast of North America, found a first stage of slightly yellow to yellowish brown colours in sands deposited before 1912, a second stage of reddish brown colours in deposits from before 1689 and a third stage of dark reddish brown colours in deposits older than 25 000 years. These results are, however, not transferable to desert conditions because all sands were heavily vegetated in a humid environment. For Capot-Rey and Grémion (1964), the rubification is evidence of long-term tropical climates, and alternating dry and rainy seasons are necessary (see latest definition). On the other hand, Capot-Rey (1970) states that dune sands in warm environments are bleached as soon as the annual precipitation exceeds 150 mm. A recent investigation on “dune whitening” in northeast Brazil (Levin et al., 2007) exemplifies this process in various dunefields, using spectral measurements and satellite-borne remote sensing. The study region is

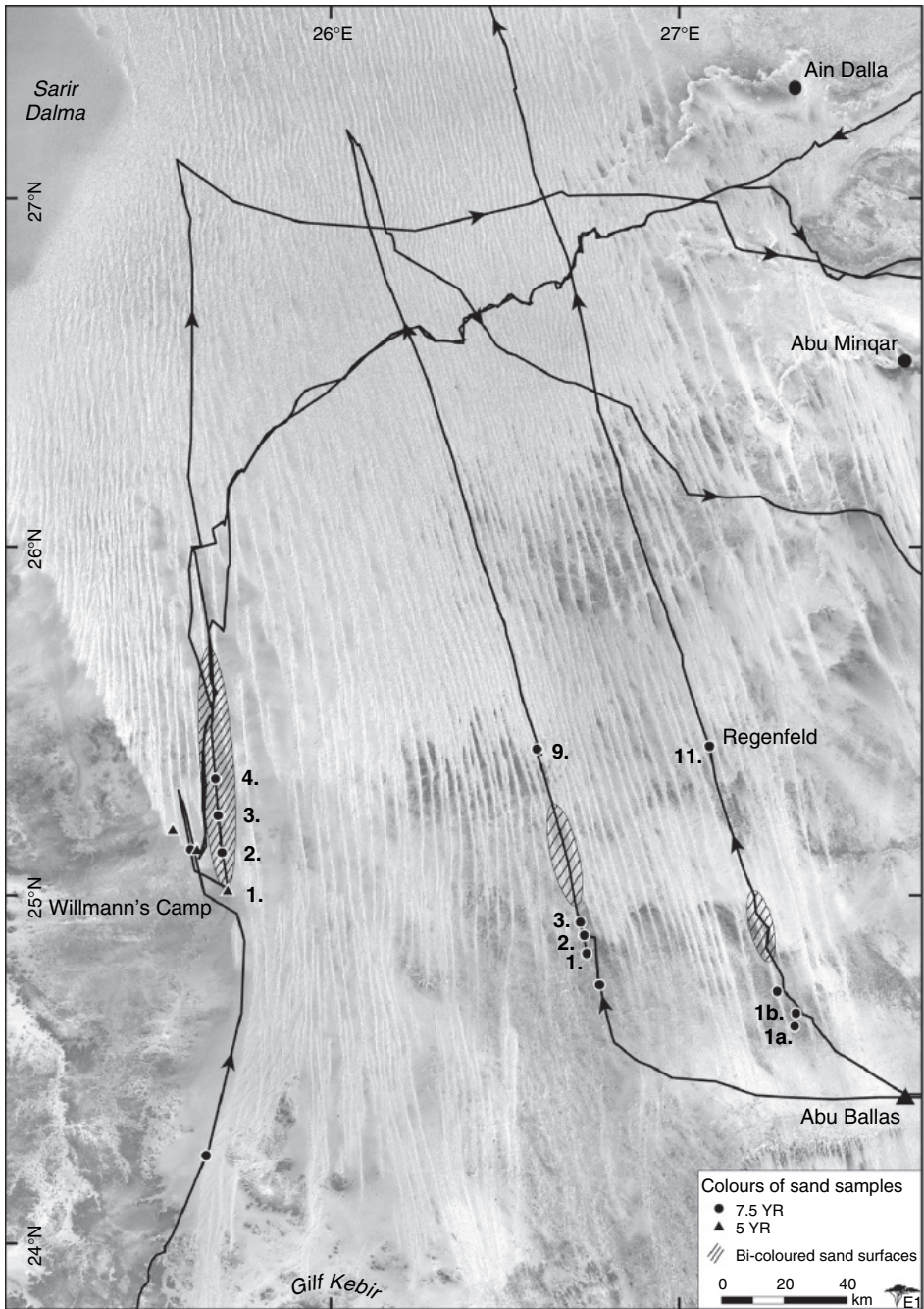


**Fig. 50** Colours of sampled sands differing from 10 YR, and stretches of bi-coloured sand surfaces along the transections. Numbers indicate the cross-sections.

only semi-arid and receives an annual average precipitation of 1600–2000 mm, separated by distinctly dry seasons. Red sands are supplied either by red source sediments or by rubification of light coastal sands that are blown inland, forming dunes partly fixed by vegetation. Where seasonal interdune fresh-water ponds are abundant in the dunefield (41% of the area), only gradually drying during the dry season, the dunes are water-saturated to a height of up to 2–3 m. Here and in the ponds, the rubification processes are reversed and the sands are bleached.

Experiments on the reddening in dune sands were carried out by Williams and Yaalon (1977). After 1 month of hot-water percolation (80–90°C) through a light sand (10 YR 5/6), a thin red upper horizon (2.5 YR 5/8) and a very weak bleached lower horizon (10 YR 6/4) had developed. This was achieved only in sand containing heavy minerals – which showed solution features – and not in pure quartz sands. Organic matter was not necessary for these processes.

The stages of diagenesis described by Turner (1980) cannot be transferred to the Great Sand Sea because the presence of groundwater seems to be a prerequisite. Turner himself states that the rubification of dunes is even more complicated than that of other desert sediments. Walker (1967), in his paper on red-bed formation in deserts, describes the stages of haematite formation, which may take millions of years. However, it also seems to need a high groundwater table. If Egyptian soils are considered, the reddening is suggested to have developed 5000–6000 years BP (Blume et al., 1984). Brownish soil horizons – like salt accumulations – are considered as phenomena of wetter climatic conditions in the past (Blume et al., 1985). On the other hand, the same authors mention rubification as being mainly inherited from a red source (Blume et al., 1987). They seem to differentiate between reddening and rubification, where the latter term refers to a stronger reddening.

The second possibility is rubification before the deposition of sands. Red sandstones may have been the source material, as in the Namib Erg (Besler, 1980); an alternative are tropical soils (laterites) as in the detritus model for the Simpson Desert in Australia (Turner, 1980). During aeolian saltation transport, the grain coatings are slowly destroyed and abraded. Therefore, longer times of transport or stronger winds lead to lighter sands. This was already noticed by Capot-Rey and Grémion (1964) in the Sahara. In the Namib Erg, some tens of kilometres of fluvial transport led to partial abrasion of coatings, but red remnants were preserved in the older solution depressions of the quartz grains, which reduced the original red colour from 5 YR to 7.5 YR. Rubification of quartz sand before the deposition on a dune may also occur in the oxidizing zone of playas. This was assumed at Regenfled in the eastern transection (Besler and Kuper, 2001) and – in a certain way – would correspond to the influence of groundwater mentioned by Walker (1967) and Turner (1980).

### 6.2.2. Reddened sands in the Great Sand Sea

Figure 50 shows the distribution of sand colours in the Great Sand Sea. Only aeolian sands and only hues deviating from the dominant colour (10 YR 7/4) are considered. It becomes very clear that, indeed, the Great Sand Sea is dominated by yellowish sands. The very homogeneous colouring of the sands, including the samples drilled

from the saline horizons, indicates that the precipitation during the Holocene climatic optimum was never high enough to cause bleaching processes as described by Levin et al. (2007) (see Section 6.2.1). Along all transections, reddish sands occur only in the southern part. They are found on the southern end of the sand ridges, but at 25°25'N they are also found below yellow cover sands in the corings in the middle and eastern transections. The various possibilities for the origin of this rubification are discussed for each locality separately.

#### 6.2.2.1. The western transection

The reddish surface sands (7.5 YR) on the western transection reach farthest north (up to 25°18'N). Most probably their colour has been inherited from the red Gilf Kebir Sandstone (partly 2.5 YR). This relationship had already been inferred from the granulometry (see Sections 4.2 and 4.3.3) and the morphology via the alluvial fan (see Sections 3.2.1 and 8.6.3.3). Some sands near Willmann's Camp, however, are even redder (5 YR), which suggests a local origin. These sands were collected from basal dune parts (surface and down to 50 cm depth: nos. 13/00–15/00) in direct contact to well-preserved playa remnants. Chemical weathering is demonstrated by the altered heavy-mineral assemblages (see Section 7.2 and Table 10) and, additionally, by clay coatings (see Section 8.6.1). The strongly red colour (5 YR) was also observed at the southern end of the investigated draa at about 15 km farther SSE, within the otherwise only reddish (7.5 YR) draa. On the geological map, a shallow channel with fluvial deposits can be recognized. This channel enters the sand sea from the SSW, widens near Willmann's Camp and goes under the investigated draa north of the second cross-section (25°06'N, 25°41'30"E). Playa conditions in this topographic low may have extended from Willmann's Camp to the eastern draa. The red playa deposits (including sands) could have been blown onto the draa by westerly winds. Later, they could have been transported along the draa by northerly winds towards the southern tip. Meanwhile the lighter reddish sands (7.5 YR) from the north have reached the site of the second cross-section as cover sands. This situation would correspond to the observations at Regenfeld on the eastern transection (Besler, 1998).

It should be remembered that in the coring near the playa at Willmann's Camp (25°07'N, 25°37'E), a slightly brownish horizon was found within the reddish (7.5 YR) sand at depths of 1 and 1.5 m (see Section 5.1). Here again, clay coatings were observed under the SEM (see Section 8.6.1). A peculiarity is the fact that this sand – contrary to the shifted red sands – must have gained its hue *in situ*. The sand from a depth of 2 m was dated at 11.8 ka, which means that it was deposited on the eastern draa flank as a slip-face avalanche (see Section 4.3.1) before the Holocene humid period.

To sum up, a distinct reddening of sands in addition to the colour inherited from the sandstone seems to have occurred only in direct contact to playas. The red (5 YR) sands were blown out after desiccation and incorporated into the draa, whereas clays and silts were blown off as dust.

#### 6.2.2.2. The middle transection

Red sands (5 YR) do not occur along this transection, and the reddish surface sands (7.5 YR) only reach the third cross-section (24°55'N). A connection with fluvial deposits from the Gilf Kebir cannot be constructed because the interdraa corridors

have a bedrock floor. If the combined LANDSAT-TM and RADAR images in El-Baz et al. (2000) are interpreted, a fluvial system can be traced reaching below the sand sea from the southeast. In addition, the geological map shows patches of sands and gravels in this direction. Playa remnants could not be found in the relatively rugged terrain.

The Cretaceous bedrock is changing from place to place. Cross-sections 1–3 lie on the coastal Maghrabi Formation and cross-sections 4 and 5 ( $25^{\circ}05'N$ ) on the fluvial and aeolian Taref Sandstone, which to the north is followed by alternating facies of the Quseir Formation. The sandstones are of interest because of their different colours: Maghrabi with 10 YR, Taref with 7.5 YR and Quseir again with 10 YR. The eroded aeolianite of the Taref Formation could have provided reddish sands which, however, should not have been transported too far. Today, the reddish sands are found south of the underlying Taref Sandstone, but the geological map shows that exactly below the investigated draa a small tongue of Taref Sandstone extends towards the south. Under optimal conditions, the reddish sands had to be transported only 10 km southward while the lighter draa sands (10 YR), derived from an allogenic alluvial fan, were deposited on the Taref Sandstone (see Section 8.6.3). The granulometric analysis provided several indications for mixed sands of different origin in this area (see Section 4.2.4). It was already pointed out that, most probably, alluvial fans as well as underlying sandstones delivered source materials for the draa.

A completely different situation exists at the ninth cross-section ( $25^{\circ}25'N$ ), where a reddish sand (7.5 YR) below yellow sands was cored from a depth of 3.4 m on the eastern flank of the draa which was dated at 9.8 ka (no. 14/99, a minimum age, see Section 5.4). With regard to the geology, this site lies on the Quseir Formation (sandstones with 10 YR) and approximately 10 km south of the Dakhla Formation (sandstones with 10 YR). As the deposition occurred at the beginning of the Holocene humid period, the rubification was most probably generated in situ. Clay coatings were identified under the SEM (see Section 8.6.1). The topography shows no traces of a former playa. However, on the opposite side of the interdraa corridor, two archaeological sites were discovered on the lower draa slope. One of these was dated as Epipalaeolithic (7800–6700 cal BC = 9800–8700 cal BP); the other one has a mixed inventory and is not easy to date (Kindermann, pers. comm., 7 October 2003). A coring at this site ( $25^{\circ}24'N$ ,  $26^{\circ}36'E$ ) only yielded yellow sands (10 YR) which contained thin layers of greenish sands, a hint of reduction processes under wet conditions. Under the SEM, the sand from a depth of 2.5 m (no. 17/99) revealed the growth of calcite crystals, indicating a slow desiccation process. The surface sand at this site (no. 15/99) even contained traces of organic matter indicative of an aquatic environment (see Section 8.6.1).

This cumulative evidence – including the strong salinity mentioned in Section 6.1 – leads to the conclusion that a playa had existed at this locality, and that the playa deposits have been blown out completely. Again, the reddening of sands seems to have been related to the contact with playa conditions. In summary, along the middle transection, in situ reddening of sands as well as inherited red sands may be assumed.

### 6.2.2.3. The eastern transection

It should be mentioned first that, at the beginning of the investigations in the Great Sand Sea in 1996, the sampling was carried out less systematically and that a part of the samples had to be left in Egypt. Therefore, the sand-colour documentation is not complete along the eastern transection. Bagnold (1931), who crossed the sand sea starting from Ain Dalla proceeding to the west and southwest, already noticed a colour change to reddish brown south of 25°25'N. Following older literature on dune reddening (see Section 6.2.1), El-Baz (1982) observed that the “shifting dunes show reddening of the quartz grains as the transport distance increases”. However, the reddish sands (7.5 YR) in the southern part belong to the Holocene dunes, which there extend from the southern end of the draa (25°03'N) towards the south for some 60 km (Besler, 1997a, 1998, 2000a). As this migration of sands must have taken place after the Holocene humid period, their colour could have been inherited from the reddish interior draa sands cored at Regenfled (25°25'N), which were reactivated around 5 ka ago (see Section 5.4). Unfortunately, there exists a gap for several cross-sections in the colour documentation. However, some observations indicate that yellow sands are dominant between the northernmost (sampled) reddish surface sand (no. 12/96) at 24°44'N and the coring site. This will be discussed further in Section 6.2.2.4.

Like along the middle transection, the Cretaceous bedrock is rather differentiated. Unfortunately, it was not sampled here. It cannot be excluded, however, that the aeolianites of the Taref Sandstone there, too, have provided sands for draa and dunes. The southern end of the investigated draa with yellow sands rests on this formation, which has its southern limit between 24°55'N and 24°50'N. The reddish dune sands are found on the adjacent Maghrabi and Sabaya Formations in the south, comparable to the situation along the middle transection. In contrast to the situation in the latter transection, however, the sand transport along the eastern transection would have been over 35–40 km. On the other hand, the sand transport along silk dunes has a much stronger longitudinal component than transport due to helical vortices during draa formation. In addition, there is evidence of temporary sand transport in rapidly migrating barchan dunes (see Section 3.3.3; Besler, 1997a, 1998, 2000a).

Another possibility, which has originally been considered, is the migration of reddish sands out of the red draa body at Regenfled. After the investigation in 1996, archaeologists, using a dredger, made a 1.5 m deep trench in the base of the draa at Regenfled. Unfortunately, we could not take part in this field campaign. Therefore, only the observations of the archaeologists are discussed here (Fig. 51). The succession is described here, from top to bottom, according to Riemer (pers. comm., 25 September 2001).

1. Light-yellow blown sand, increasing in redness and consolidation with depth.
2. Pale reddish to red sand (7.5 YR 5/6 to 5 YR 5/6), slightly consolidated; many rootlets; increasing clay and silt content towards the playa in the east.
  - Cultural layer, dated at 6978 ± 38 BP (pottery, few stone artefacts).
3. Red sand (5 YR 5/6), strongly consolidated.
  - Cultural layer, dated at 7965 ± 48 BP (Epipalaeolithic).

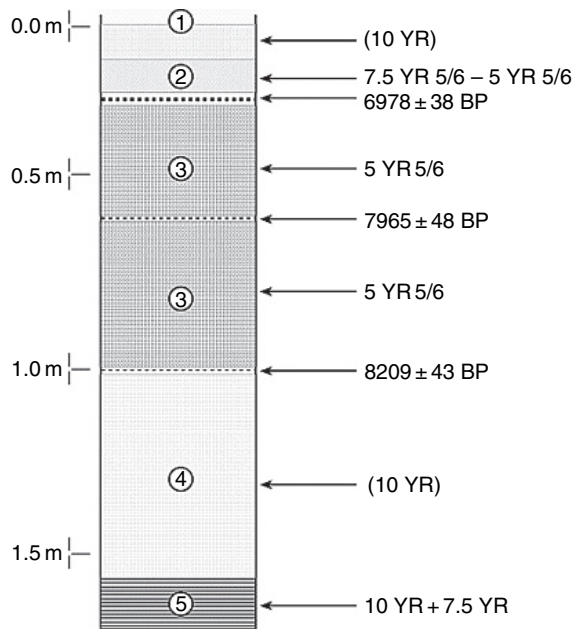


**Fig. 51** Stratigraphic profile in a dredged trench in the basal part of the draa next to the archaeological site at Regenfeld (on cross-section 11). Modified after Besler and Kuper (2001). See Section 6.2.2.3 for explanation.

3. Red sand (5 YR 5/6), increasingly grey towards the playa, horizontal upper boundary.
  - Cultural layer, dated at  $8209 \pm 43$  BP (no artefacts).
4. Light yellowish fine-grained sand (lighter than 1), relatively soft.
5. Layers of clay/silt (reddish, consolidated) alternating with sands (colour as 4, soft) at intervals of a few centimetres.

The  $^{14}\text{C}$  dates were obtained from charcoal of fire places in the two upper layers and from ostrich eggshells in the lower layer. For a better understanding of these data in the context of the Regenfeld history (as summarized in Section 5.4), these data have been converted to cal BP (see Section 5.4).

It thus appears that some decimetres of red sand have been deposited on top of the occupation remnants after 8209 BP ( $\sim 9300$  cal BP). As the sands in the bottom layers are yellowish like the modern blown sands along the draa, the red sands are supposed to have been blown out from the desiccating playa where they had got their clay/iron-oxide coatings by adhesion. The iron oxides then were increasingly reduced in amount towards the east, which may be interpreted as groundwater influence near the playa. After renewed human occupation, red sands were again deposited on top after 8000 BP ( $\sim 9000$  cal BP), without traces of groundwater presence. After a third human occupation, lighter reddish to red sands were deposited on top after 7000 BP ( $\sim 7900$  cal BP). Most probably, these sands

correspond to the sands cored at a depth of 2 m on the draa flank, which were OSL-dated at  $5 \pm 1$  ka. In the drilling succession perpendicular to the slope, the change to clay/silt-rich sediments towards the playa had also been noticed. These deposits are red (5 YR) to dark red (2.5 YR) and have also been found (with desiccation cracks) at the western base of the draa. They are not shown in the colour distribution map (Fig. 50) because they are not (purely) aeolian.

According to the stratigraphy in the trench, there seem to be red aeolian sands (5 YR) below the reddish (7.5 YR) sands. The former were not reached in the drillings, which were finished when the reddish draa core was met. These red sands (if they are present in the draa) should be older than 7000 BP ( $\sim 7900$  cal BP). According to the datings, the pale reddish sand layer belongs to the time of the final unit D at Regenfeld (see Section 5.4), whereas the two lower red sand layers fall into unit C, which seems to represent the time interval most favourable for human occupation (see Section 5.4). Their interfingering with cultural layers shows that arid-climate fluctuations, when playas dried up and deposits were blown out, also reigned within the Early Holocene humid phase. A dry spell at approximately 8400–8000 cal BP, corresponding to the last one in the sedimentary record at Regenfeld, is also mentioned by Hoelzmann et al. (2004), who stress, however, the existence of strong regional differences. Later, these red sands could have been transported with the southward advancing dunes after reactivation of the draa, before the yellow cover sands at Regenfeld arrived from the north. This possibility is discussed further in Section 6.2.2.4.

#### 6.2.2.4. Colour observations during the topographic surveys

Apart from the Munsell classification of the sand samples, field observations were made with regard to the optical impression of sand colours along the transections. On all transections, segments were found where particularly the dunes on the draa (in the southeast also dunes without draa) show a patchwork of yellowish and reddish sands (see Fig. 50). Obviously, red and yellow sands have been mixed incompletely. Usually, the dune crests are lighter, and the reddish patches occur on the dune flanks.

Along the western transection, these bi-coloured sands were found within the area of the reddish sands (7.5 YR) as well as in the area of the northward following yellowish sands (10 YR). Within the realm of reddish sands ending at  $25^{\circ}18'N$ , the patches are red (5 YR). The bedrock there is almost totally covered by gravels of the Gilf Kebir alluvial fan. Only in the far south near Willmann's Camp, the Taref Sandstone (7.5 YR and 5 YR) crops out and reaches until  $25^{\circ}15'N$ . The red patches could also be explained as blown-out playa deposits. According to the geological map, substantial playa deposits are still found at the latitude of the third cross-section ( $25^{\circ}12'N$ ) and can be expected even farther north because fluvial channels from the southwest are directed towards this area (see Section 6.2.2.1). The red sands could be a heritage of former playa deposits as well as of weathered Taref Sandstone in the interdraa corridors. This explanation cannot be used for the bi-coloured sands between  $25^{\circ}18'N$  and  $25^{\circ}36'N$  farther north (sixth cross-section). However, the sediment on the corridor floor (no. 16/00), which is fluvial (from clay to gravels) with a slight aeolian deflation according to the granulometry, is also red (5 YR). As the



northern boundary of the alluvial fan was assumed to be situated around  $26^{\circ}\text{N}$ , the reddish patches correlate well with northerly winds. Still farther north, the floor deposits are much lighter (10 YR). Unfortunately, the transition zone had not been sampled. On the whole, the distribution of red and reddish sands along the western transection cannot be used as an indicator to find a northern boundary of rubification. This leaves only the vicinity of Willmann's Camp as a locality where sands were reddened.

Along the middle transection, bi-coloured sands were met between  $24^{\circ}55'\text{N}$  (third cross-section) and  $25^{\circ}15'\text{N}$  (seventh cross-section). Contrary to the situation in the western transection, the sands at the southern end of the draa ( $24^{\circ}50'\text{N}$ ) were homogeneously reddish (7.5 YR). Until the fifth cross-section, the sands lie upon or south of the Taref Sandstone and could have inherited their reddish proportions (see Section 6.2.2.2). At the sixth and seventh cross-sections, the draa are developed on the Quseir Formation with light sandstones. The reddish sands were, however, found up to only 20 km south of the ninth cross-section, where reddish draa sands had been cored from the interior ( $25^{\circ}25'\text{N}$ ). The reddish surface sands in this case are an additional indicator of blown-out playa deposits.

Along the eastern transection, where the eastern and the western flanks of the draa were observed in 1996 and 1999, the bi-coloured sands were found between  $24^{\circ}47'\text{N}$  and  $24^{\circ}57'\text{N}$ . Contrary to the other transections, they only occur over a short distance (of about 20 km) and only in dunes without the underlying draa, which ends at  $25^{\circ}03'\text{N}$ . From there, it is a long way with only yellow surface sands to the cored reddish draa sands at Regenfild ( $25^{\circ}25'\text{N}$ ). This suggests that the reddish southern dune sands did not originate in the playa deposits at Regenfild. Indeed, all bi-coloured sands lie south of, or at the southern boundary of, the Taref Sandstone. Most probably, the yellow sands from the north and the reddish sands from the weathered local sandstone have not been properly mixed. Only the southernmost dune sands that have temporarily been migrating in barchans are well mixed and homogeneous in colour.

To sum up, reddish sands have been provided by the Gilf Kebir Sandstone and the Taref Sandstone in the southwest and by the latter in the south and southeast. Apart from these inherited colours, a locally restricted rubification of sands has occurred under playa conditions on all transections only south of  $25^{\circ}30'\text{N}$ . Outside the Great Sand Sea, the northernmost locality with reddening of sands was found south of the Farafra Sand Sea at  $25^{\circ}46'\text{N}$ . Therefore, it is assumed that humid conditions favourable for the rubification of sands reigned only south of approximately  $26^{\circ}\text{N}$ . The necessary moisture must have been provided by a monsoonal precipitation system coming from the south during the Holocene climatic optimum (Bubenzer and Besler, 2005).

## HEAVY-MINERAL ANALYSIS

### Contents

7.1. The Total Heavy-Mineral Content	145
7.2. The Heavy-Mineral Assemblages	148

For two reasons, the total heavy-mineral content and the heavy-mineral assemblages are discussed separately. First, the total content is available for almost all samples along the transections, whereas the assemblages were studied only at the coring sites and at additionally selected locations. Second, the total content and the assemblages partly provide clues to different problems.

### 7.1. THE TOTAL HEAVY-MINERAL CONTENT

Independent of the heavy-mineral assemblages, the total heavy-mineral content may provide valuable information about the aeolian history of sands (processes of accumulation, deflation and reactivation) and their sources. On all transections, the statistical mean of the total heavy-mineral content comes close to 0.5% (Table 10; for individual values, see Appendix 1). This seems to be representative for aeolian sands in many parts of the Sahara (Pfeiffer, 1991). Mainguet and Vimeux-Richeux (1981) mentioned a mean of 0.2% for aeolian sands in Niger. Comparably low heavy-mineral contents of <0.5% were found in the Kalahari Sands (Poldervaart, 1957). However, Petit-Maire and Riser (1983) found 4–7% of heavy minerals in ergs of the Taoudenni Basin in northern Mali. Comparably high heavy-mineral contents were mentioned by Anton (1983) for eastern Saudi Arabia, where the quartz content ranges from 90 to 99% in the Al Jafurah sand fields, amounts to 99% in the Dahna sand fields and to 97% in the northeastern Rub' al Khali. However, there may be low deviations from the mean, as in the Great Sand Sea, or broad ranges of individual values as, for example, in the Keriya region of the Taklamakan Sand Sea in China, where Pfeiffer (1991) calculated a mean of 2.75% with a range from 0.03 to 17.61% (50 samples). Qian Yibing et al. (1994) mentioned an average of 5% including various localities in the Taklamakan and also river and “underground” sands. Exceptionally high heavy-mineral contents were found in the Namib Erg with an average of 11.8% and a range from 1.03 to 31.29% (47 samples).

**Table 9** Comparative total heavy-mineral contents according to sampling locations

	<i>W</i> (weight %)	<i>Drilling sites only</i> <i>W slope E</i>		<i>Middle</i> (weight %)	<i>Drilling sites only</i> <i>W slope E</i>		<i>E</i> (weight %)	<i>Drilling sites only</i> <i>W slope E</i>
Dune	0.62			0.45			0.28	
Draa	0.44			0.44			0.62	
Longitudinal draa	0.46	0.27	0.50	0.59	0.54	0.56	0.69	1.00
Transverse draa	0.37	0.37		0.34	0.33		0.56	0.93
Draa surface	0.51			0.41			0.45	
Draa interior	0.42			0.46			0.84	

Generally, the heavy-mineral content decreases with augmenting numbers of sedimentary cycles. According to Fay and Herrmann–Degen (1984), rocks from the Nubian sandstone in the Dakhla Basin had their origin mainly in Palaeozoic sediments. The lower formations have experienced several sedimentary cycles and the upper ones most probably only one. A decrease in heavy minerals is only found, however, if the cycles include decay and re-deposition under humid conditions. The Namib sands, which are most probably in their third cycle, possess a high heavy-mineral content compared to the young Taklamakan sands because the reactivation of aeolianites occurred in a relatively dry environment. Here, the heavy-mineral content increases in the modern dune sands compared to the Tsondab Sandstone (their source). This transition by winnowing and aeolian entrainment of lighter grains could be studied in detail (Besler, 1995, 1996b; Besler and Pfeiffer, 1995). As this is also the case in the Great Sand Sea with regard to the underlying sandstones, it may be concluded that – if the sandstones have provided sands for the draa – this happened without a long history in a humid environment. There are, however, two exceptions: the aeolianite in the Gilf Kebir Sandstone (no. 1/00) reaches the average heavy-mineral value, and the sandstone in the Quseir Formation (no. 13/99) even surpasses it. The latter was found to be deflated (see Section 4.3.3). The Gilf Kebir aeolianite, obviously, experienced a wet cycle of weathering and re-deposition in alluvial fans. The aeolian reworking into draa consequently found less heavy minerals in the sands (compare Section 8.6.3.3).

A table of the spatial distribution of the total heavy-mineral contents, in analogy to the granulometric parameters, does not deliver comparably valuable information (Table 9). Nevertheless, it indicates some tendencies. The eastern transection cannot well be involved in this comparison because of too few samples. On the other transections, the interior sands of the draa are comparable. Their surface sands, however, show a remarkable difference: the heavy-mineral content is slightly higher in the western transection and lower than average in the middle transection. This difference accompanies another one, i.e. in their granulometry. This must be attributed to deflation of most surface sands on the western transection, which was not the case with the middle transection (see Section 4.3.1).

On all transections, the longitudinal draa contain more heavy minerals than the transverse draa. This may be due to different sand sources (see Section 8.6.3) or to different wind velocities during draa formation. In this case, the trade winds should have been stronger than the westerlies (see below). Another reason may have been different weathering environments, which will be discussed in Section 7.2.

The dunes tend to have more heavy minerals than the draa. This had already been found in the Namib Erg, where the heavy-mineral content increases in the dunes because the lighter grains are preferably entrained during the seasonal oscillations of the dune crests on the draa. The exceptionally low amount of heavy minerals in the dunes of the eastern transection is most probably due to the fact that the few samples were collected from dunes which had advanced southwards from the draa. During this progradation, the heavier grains were left behind. Poldervaart (1957) stated that young dunes from reworked sands in the Kalahari did not contain heavy minerals. This observation is not applicable to the Great Sand Sea.

The heavy-mineral contents at the drilling sites correspond to the average values in the longitudinal and in the transverse draa, apart from one exception. This is the site on the western slope of the longitudinal draa on the western transection ( $25^{\circ}42'N$ ), where the mean is particularly low. This is caused by a scarcity of heavy minerals in the upper layers and cannot be explained by a special granulometry or a different sand source. If the samples are observed under the SEM, it appears that the upper sand (no. 28/00) has undergone weathering processes in a high-energy environment at some time, whereas the lower sand (no. 33/00) has not (see Table 17).

Only few samples from the Great Sand Sea contain more than 1% of heavy minerals. According to their grain-size frequency distributions, most of these can be correlated with deflation processes (see Sections 4.3.1 and 4.3.2). Therefore, the tendency to higher values in the longitudinal draa may indicate that the trade winds during draa formation had been stronger than the westerlies during formation of the transverse draa. However, a comparison of all heavy-mineral contents on the middle transection shows a decrease around  $25^{\circ}30'N$ , already before the transition to transverse draa. In this section, the sands also possess diverging grain-size parameters (see Sections 4.2.2–4.2.4) which indicate different sand sources. Therefore, the parent material may be the reason for the different heavy-mineral contents. Indeed, the boundary between the Quseir Formation in the south and the Dakhla Formation in the north lies around  $25^{\circ}30'N$ . Sample no. 13/99 of the Quseir Formation has already been mentioned above as being rich in heavy minerals (0.75%). Sample no. 22/99 of the Dakhla Formation has a heavy-mineral content below the average (0.2%). Although these two samples are by no means representative for their geological formations, the difference between continental and marine facies may play a part (see Section 3.1). Moreover, at least north of  $26^{\circ}N$  the influence of a different sand source via an alluvial fan from the east can be expected. The parent material, most probably the Minqar el-Talh Sandstone (see Section 8.6.3.4), has an extremely low heavy-mineral content (0.07%).

Contrary to the Namib Erg (Besler and Pfeiffer, 1995) and to the Taklamakan Sand Sea (Besler, 1995), no statistical correlation between the total heavy-mineral content and the mean grain size exists in the Great Sand Sea. As a consequence, the granulometric sand types do not form clusters in a diagram of mean grain size and heavy-mineral content such as present in similar diagrams for the Tsondab Sandstone in Namibia. All granulometric sand types – with the exception of deflated sand-sheet sands – contain 0.4–0.5% of heavy minerals on the average. This lack of relationship between heavy-mineral content and grain-size distribution is an indication of various sand sources with originally different heavy-mineral contents, which did not allow the accumulation of comparable proportions of heavy minerals during their shared aeolian history. In the Keriya area of the Taklamakan, all sands have come from one alluvial source of the Kun Lun Shan Mountains. In the Namib Erg, one geological formation has been supposed to be the source. It seems that in the Great Sand Sea the absence of a regular pattern combining the granular and the mineralogical evolution of sands may indicate different sand sources even if the heavy-mineral assemblages show no significant differences (see Section 7.2).

In summary, the total heavy-mineral content indicates that different sources and various sandstones in different environments (humid and arid) have provided sands for draa formation. A higher content in draa-surface sands supports the hypothesis of stronger deflation in the western sand sea. The still higher concentration in dune-crest sands proves the active aeolian selection of lighter grains for long-distance transport.



## 7.2. THE HEAVY-MINERAL ASSEMBLAGES

The general spectrum of heavy minerals in the sands of the Great Sand Sea is not very differentiated (Table 10). The stable group is represented by zircon, tourmaline and rutile, and the unstable group comprises garnet, epidote, green hornblende and pyroxene. Staurolite, disthene, andalusite and sillimanite are placed between these groups because they are considered to be of medium stability according to Pfeiffer's great experience with aeolian sands from various deserts (Pfeiffer, 1991; Besler and Pfeiffer, 1992, 1995). Accessory heavy minerals include alterite, apatite, eudyalite, sapphirine, spinel and topaz. Opaque grains are not considered here. The spectrum seems to be broader along the eastern transection because green hornblende, pyroxene and topaz occur only there. This may be due to a drier cycle of sandstone decay and re-deposition than in other parts of the sand sea (see Sections 7.1 and 8.6.3).

The heavy-mineral spectra as well as the individual frequencies are rather similar. Therefore, nothing can be deduced with regard to different sand sources. Only the samples from the Siwa region in the north diverge from the general pattern (sandstone no. 40/96 and dune-crest sand no. 39/96). Extremely high zircon contents, together with conspicuously low values for staurolite and for epidote and, particularly, the presence of pyroxene and spinel (the latter occurs nowhere else and is not included in the table), indicate that the Moghra Sandstone was a sand source for the younger northern dunefield (see Section 3.3.3). Moreover,

**Table 10** Heavy-minerals (%) in sand samples (HM: heavy-mineral content; ZR: zircon; TO: tourmaline; RU: rutile; ST: staurolite; DI: disthene; AN: andalusite; SI: sillimanite; GA: garnet; EP: epidote; HB: green hornblende; PX: pyroxene; S/I: ratio of stable to unstable minerals; G/E: ratio of garnet to epidote.)

Sample no.	$\Sigma HM$	ZR	TO	RU	ST	DI	AN	SI	GA	EP	HB	PX	S/I	G/E
11/96	0.36	33	18	4.5	12	—	3	2	21	3	3	—	2.06	7.00
12/96	0.20	24	19	3	16	1	5	2	27	1	1	—	1.59	27.00
17/96	0.58	19	34	3	16	1	2	1	19	2	1	—	2.55	9.50
18/96	1.13	33	21	—	12	2	1	—	17	8	—	—	2.16	2.13
20/96	0.80	15	22	—	17.5	—	2.5	2.5	23	10	4	0.5	0.94	2.30
22/96	0.13	15	26	—	19.5	—	3	2	19.5	10.5	0.5	—	1.26	1.86
28/96	0.27	30	3.5	1.5	12.5	—	2	0.5	32.5	16	0.5	0.5	0.71	2.03
30/96	0.13	27.5	11	1.5	16	—	2	0.5	30	9.5	1	—	0.99	3.16
35/96	0.60	24	21	1	9	1	1.5	2	29	10	1	—	1.15	2.90
36/96	1.25	10	32	—	8	—	—	—	13	27	—	4	0.95	0.48
37/96	0.07	20	24	—	28	1	—	—	11	12	—	—	1.33	0.92
39/96	0.45	49	15	6.5	6.5	—	0.5	0.5	14	3	3	1	3.56	4.67
40/96	0.65	40	19	9.5	6	—	0.5	0.5	14.5	5	1	3	2.91	2.90
12/99	0.63	14	27	0.5	17	—	1	1.5	32.5	6.5	—	—	1.06	5.00
15/99	0.22	16	22	1	16	—	0.5	2	25	17.5	—	—	0.92	1.43
17/99	0.34	28.5	27	2.5	8	—	1.5	—	21	11.5	—	—	1.78	1.83
18/99	0.35	20.5	29	2	17	—	1	1	21.5	8	—	—	1.75	2.69
25/99	0.43	34.5	22	4.5	10	—	1.5	—	20.5	7	—	—	2.22	2.93
26/99	0.24	37.5	16.5	0.5	15	—	1.5	0.5	20.5	8	—	—	1.84	2.56
33/99	0.30	18.5	28.5	2	7.5	1.5	1.5	0.5	19.5	20.5	—	—	1.23	0.95
3/00	0.44	11	48.5	0.5	21	—	3	—	14	2	—	—	3.75	7.00
9/00	0.20	17	44.5	1	23	1	1	2	10	0.5	—	—	5.95	20.00
11/00	0.75	8	45	1	30	1	1	1	12	1	—	—	4.15	12.00
15/00	0.49	16	49	2	21	—	0.5	1.5	8.5	1.5	—	—	6.70	5.67
28/00	0.21	21	18.5	2.5	20.5	—	2.5	—	24.5	10.5	—	—	1.20	2.33
33/00	0.31	13	27	1	28.5	—	1	—	22.5	7	—	—	1.39	3.21
46/00	1.25	21	22	1.5	17	—	1.5	—	22	15	—	—	1.20	1.47
49/00	0.30	12.5	27	1	16	—	1.5	—	22.5	19.5	—	—	0.96	1.15
52/00	0.25	18.5	28	0.5	14	—	1.5	0.5	21	16	—	—	1.27	1.31

contrary to all other samples, these zircons are idiomorphic and angular to a high degree (Besler, 1998). This means that the Siwa Depression was not important for the sand supply before and during draa formation. Pyroxene is only found in one sample (no. 36/96) from the surface at the drilling site in the transverse draa of the eastern transection and not in the interior. However, the cover sands at the 17th cross-section (no. 28/96: 26°49'N) and even at Regenfeld (no. 20/96: 25°25'N) contain small amounts of pyroxene (0.5%), which reflects a considerable long-distance transport of blown sands along the draa by Holocene northerly winds (see Section 3.4).

If the heavy-mineral assemblages are considered separately for the aeolian generations of draa and dunes, significant differences exist in the proportions of rutile and epidote as well as in the ratios of garnet to epidote, respectively. Rutile, a stable heavy mineral and rare in the Great Sand Sea, is present in dunes twice as much as in the draa. Almost 50% of the unstable mineral epidote, on the other hand, has disappeared. The latter causes an increase of the garnet/epidote ratio in the dunes to more than the double of this ratio in the draa. This is a clear indication of weathering during cycles of humid and dry seasons. Under these conditions, garnet is covered by coatings more often than epidote. This slows down the weathering (Besler, 1998). Bellair (1940) already found garnet to be resistant to chemical weathering in Saharan sands. The weathering should have taken place before reactivation of the draa and dune formation. In this context, it is important to know that most analysed dune sands were sampled in the southern sand sea. Therefore, the differences in heavy-mineral proportions may be valid only for this part.

A very useful approach is the formation of sample clusters according to the individual drilling sites and the comparison of their means with regard to the various heavy minerals. Minerals with very rare occurrences are neglected in Table 11. In the discussion of this table, the southern end of the eastern transection is considered later, because no comparable dunes exist on the other transections. At the drilling site of Regenfeld in the eastern transection, a distinction between the yellow cover sands (nos. 20, 22/96) and the reddish sands (nos. 17, 18/96) is necessary because of their great differences in heavy-mineral proportions. This particularly concerns zircon and epidote, and therefore also the ratios of stable to unstable heavy minerals and of garnet to epidote. The yellow cover sands come close to the northern sands, which supports a possible sand transport from the north (see Section 8.6.1.2.1). With regard to zircon, the high percentages in the transverse draa in the middle transection (30.2%) and in the reddish sands at Regenfeld (26%) in comparison to an overall mean of 17.8% in the other parts are conspicuous. At Regenfeld, chemical weathering was caused by the playa environment which favoured a relative increase in the amount of stable zircon. In the transverse draa, weathering processes had occurred at different and earlier times according to SEM analysis (see Section 8.6.1). Apart from this, the sites in the transverse draa show a comparable pattern.

At Willmann's Camp in the south of the western transection, a large excess of the stable tourmaline (46.8%) in comparison to the mean of 23.9% (with a range from 17 to 28%) is found, whereas zircon is not enriched. Inheritance from the Gilf Kebir Sandstone cannot be excluded, and weathering may not be the sole reason. There exist cumulative exceptions, however, at both Willmann's Camp and

**Table 11** Mean heavy-mineral assemblages at drilling sites (S/I: ratio of stable to unstable minerals; G/E: ratio of garnet to epidote)

<i>Heavy minerals (%)</i>										
	<i>W transection</i>			<i>Middle transection</i>			<i>E transection</i>			
	<i>Transverse draa</i>	<i>Longitudinal draa</i>		<i>Transverse draa</i>	<i>Longitudinal draa</i>		<i>Transverse draa</i>	<i>Longitudinal draa (Regenfeld)</i>		<i>S</i>
	<i>N</i>	<i>W</i>	<i>E (Willmann's Camp)</i>	<i>N</i>	<i>W</i>	<i>E</i>	<i>N</i>	<i>yellow</i>	<i>red</i>	
	<i>(46–52)</i>	<i>(28 and 33)</i>	<i>(3–15)</i>	<i>(25–33)</i>	<i>(15 and 17)</i>	<i>(12 and 18)</i>	<i>(28–36)</i>	<i>(20 and 22)</i>	<i>(17 and 18)</i>	<i>(11 and 12)</i>
ZR	17.33	17.00	13.00	30.17	22.25	17.25	22.88	15.00	26.00	28.50
TO	25.67	22.75	46.75	22.33	24.50	28.00	16.88	24.00	27.50	18.50
RU	1.00	1.75	1.13	2.33	1.75	1.25	1.00	0.00	1.50	3.75
ST	15.67	24.50	23.75	10.83	12.00	17.00	11.38	18.50	14.00	14.00
GA	21.83	23.50	11.13	20.17	23.00	27.00	26.13	21.25	18.00	24.00
EP	16.83	8.75	1.25	11.83	14.50	7.25	15.63	10.25	5.00	2.00
S/I	1.14	1.30	5.14	1.76	1.35	1.41	0.95	1.10	2.36	1.83
G/E	1.31	2.77	11.17	2.14	1.62	3.85	2.13	2.08	5.80	17.00



Regenfeld. With only 11% at Willmann's Camp and 18% at Regenfeld, the unstable garnet is less abundantly present than in other localities, where it reaches an average of 23.3% (with a range from 20 to 27%). Epidote, even less resistant in alternately humid and dry environments, shows an extreme impoverishment at Willmann's Camp (1.25%) and at Regenfeld (5%) compared to the mean value of 12.2% (with a range from 7.3 to 16.8%) in the rest of the sand sea. The ratios of stable to unstable heavy minerals, which are between 1 and 2 everywhere else, reach values of 5 at Willmann's Camp and still 2.4 at Regenfeld. The ratios of garnet to epidote with  $>11$  at Willmann's Camp and 5.8 at Regenfeld are even more affected compared to  $<4$  at all other localities. In fact, the ratio elsewhere stays even below three with one exception, which is the eastern slope of the longitudinal draa in the middle transection ( $G/E = 3.85$ ). A slightly reddened draa sand was cored here (Section 5.1), and additional evidence for an ancient playa environment is provided by SEM analysis (Section 8.6.1.2).

These relations clearly indicate seasonally alternating humid and dry weathering conditions. It becomes also obvious that this type of weathering was even more intense and/or lasted longer at Willmann's Camp than at Regenfeld. The heavy-mineral proportions have not been inherited from the Gilf Kebir Sandstone, which can be deduced from the comparison with samples no. 28/00 and 33/00. They stem from the same alluvial fan (see Sections 4.2.1 and 7.1) and come close to the average of the sand sea. In this context, the extremely high proportion of tourmaline may also be a consequence of chemical weathering.

The dune sands from the southern end of the eastern transection (nos. 11, 12/96) show a comparable pattern with an excess of zircon (28.5%), an impoverishment of epidote (2%) and the highest ratio of garnet to epidote (17). The great mineralogical resemblance between these dune sands and the reddish sands at Regenfeld (nos. 17, 18/96) cannot be denied. Based on the colour analysis (see Section 6.2), these sands were related to the Taref Sandstone, which might indicate this unit as a possible source. However, the probability that the Taref Sandstone has passed on the same weathering phenomena in heavy minerals as the playa conditions at Regenfeld (on the boundary of the Quseir and Duwi Formations) is rather low. This means that a southward progression of weathered sands from Regenfeld cannot be excluded.

To sum up, the heavy-mineral assemblages indicate that the Siwa Depression in the north did not deliver sands for draa formation but only for the younger northern dunefield. Only the southern sand sea seems to have experienced a seasonally humid tropical climate before aeolian sand reactivation and dune formation. These weathering conditions occurred particularly where playas could form seasonally in the interdraa corridors during the Holocene climatic optimum. Therefore, the weathering of heavy minerals corresponds strongly to the rubification of quartz sands (see Section 6.2).

## SCANNING ELECTRON MICROSCOPY

### Contents

8.1. Brief History of the Development	153
8.2. How to Prevent a Biased Interpretation	154
8.3. General Properties of the Quartz Grains	155
8.4. Correlations with Dating	156
8.5. The Most Frequent Microstructures: Controversial Phenomena	160
8.6. Discussion of the Environmental Developments	164
8.6.1. Processes in the Holocene	164
8.6.2. Pre-Holocene processes in the Great Sand Sea	176
8.6.3. Major sand sources	181
8.7. The Question of Earlier Cycles of Draa/Dune Formation	193

### 8.1. BRIEF HISTORY OF THE DEVELOPMENT

Particularly the 1970s were the heyday of literature about the use of SEM in the study of quartz–sand grains and their depositional environments. In one of the earliest publications, Gees (1969), studying grains of 0.21–0.42 mm, found that – compared to dune sands – coastal sands had a higher grain–surface relief, which he ascribed to chemical etching controlled by the crystal structure. Hillefors (1971) stated that the grains had to be coated with copper (gold is commonly used today). In the same year, a contribution by Krinsley (Margolis and Krinsley, 1971) appeared, in which the frosting of quartz grain surfaces was studied. They found this to be a function of the formation of silica scales. These, in turn, were seen as the result of long-lasting and strong winds. In a short note for geographers, the authors stressed the role of the degree of magnification for the interpretation (Doornkamp and Krinsley, 1973). In the same year, the well-known atlas of quartz–sand surface textures by Krinsley and Doornkamp (1973) was published.

A substantial French monograph dealing with this topic (L'exoscopie) followed soon (Le Ribault, 1975). Le Ribault emphasized the importance of the assemblages of microfeatures on the grain surfaces. He stressed the point that the chronological history of a grain could be deduced by combining the various features found on the different parts of a grain. A later publication (Le Ribault, 1977) contains even more details and is particularly helpful because of its diagnostic tables of features and their occurrences in different environments. About 10 years later, a gap in the range of

surveyed environments was filled by Kowalkowski and Mycielska-Dowgiałło (1985), who investigated quartz grains in permafrost solonchaks (saline soils).

During the late 1970s and the early 1980s, the SEM analysis was applied to solve various problems. Goudie et al. (1979) used it for the observation of quartz grains in their experiments on the formation of silt from dune sand by salt-weathering processes. In his monograph on continental red beds, Turner (1980) used SEM to study the processes of infiltration, alteration and formation of clay minerals. El-Baz and Prestel (1982) applied SEM – including the use of a microprobe – for the identification of chemical elements in their study on sand grain coatings in Egypt.

On the whole, however, SEM analysis was rarely applied. The main reason may lie in the time-consuming procedures and the large amount of effort involved in the work at the microscope, as well as in the interpretation of paper photomicrographs. A new SEM atlas of sand grain surface textures and applications has appeared since (Mahaney, 2002). It should also be mentioned that some disagreement exists with Krinsley and Doornkamp (1973) in the German literature, concerning the interpretation of certain solution and precipitation features on quartz grains (Tietz, 1987, 2005).

In own investigations, SEM analysis was used to support the identification of different dune generations in Mali (Besler, 1991a). This was done in comparison with a morphoscopic analysis in order to find out the advantages and the weaknesses of both methods. In an investigation of aeolian sands from the Taklamakan Sand Sea in China (Besler, 1995), SEM analysis provided good results, particularly with regard to the different environmental histories of various sands, supporting a poly-genetic evolution of the sand sea.

## 8.2. HOW TO PREVENT A BIASED INTERPRETATION

Already knowing some facts about weathering processes in the Great Sand Sea, there was a great danger of prejudice or bias in the SEM analysis. One might easily see expected structures or interpret them in a favoured direction. The evaluation should, however, be as unbiased as possible. Therefore, special care was taken to separate the interpretation from the analysis. How this was achieved, is briefly described here.

A concentration of grains was selected from each sample for inspection at 100-fold magnification; it was photographed, and the general appearance was noted. Subsequently, the individual grains were scanned, particularly looking for shapes and structures and special microfeatures. When the latter were not abundant, additional grains were scanned. Everything of interest was documented by photography. These paper photomicrographs were the main subject of a desk study with magnifying glasses. As not all structures and microfeatures are visible or preserved on every grain, each individual photomicrograph of a grain or of just a detail was analysed separately. Moreover, a chronological sequence of partly overlapping microfeatures was deduced for each photo, but without any interpretation yet.

In the following step, a chronological sequence of features was synthesized from all photomicrographs of one sample. Up to 15 different microfeatures per sample could be identified. Then the sequence of microfeatures in the untreated part of the sample was combined with the sequence of grain microfeatures from the part of the sample that had been washed in hydrochloric acid. The former sequence usually added the most recent processes in this combination (e.g. coatings). This procedure was carried out with all samples. Only when the sequences for all samples had been determined, the interpretation began by comparing the observed features with the figures in the atlases of Krinsley and Doornkamp (1973), Le Ribault (1977) and Mahaney (2002). Thus, the processes causing the microfeatures were established. The greater details and the diagnostic tables in the Le Ribault (1977) atlas proved to be particularly helpful for the analysis. Frequently, several microfeatures associated with each other could be ascribed to processes in the same environment. In a last step, the longer sequences could thus be reduced to maximally eight environmentally different stages. An example of the entire, tedious procedure is given for sample no. 35/96 in the Appendix 2.

This very laborious analysis would have been too time-consuming to apply to all samples from the Great Sand Sea. Therefore, a selection of the most promising samples had to be made. They were chosen from the eight drilling localities, because the time of deposition might be found to be related to the genesis of the microfeatures. At each drilling site, the draa-surface sand and the dune-crest sand of the respective cross-section were also analysed. Additional samples were selected at Regenfeld on the eastern transection (the yellow cover sand no. 20/96) and at Willmann's Camp in the western transection (the sand immediately above the playa surface, no. 15/00).

### 8.3. GENERAL PROPERTIES OF THE QUARTZ GRAINS

On the survey photomicrographs with 100-fold magnification, which corresponds to the morphoscopic analysis, the majority of grains are subrounded. This is found in many ergs and dunefields. It was mentioned by Schultz (1927) from the Kara Kum in Central Asia, and by Norris and Norris (1961) from the Algodones dunes in California, where 60% of the sands are subrounded to subangular. In Peruvian barchan dunes, rounded grains were found to be the exception (Tricart and Mainguet, 1965). In the Simpson Desert in central Australia, Folk (1978) stated that 70–90% of the dune sands were even subangular to angular. Own investigations in the Namib Erg show that the majority of sand grains there are subangular (Besler, 1980). According to Mahaney and Andres (1996), subrounded grains dominate all five ergs studied in Algeria. This overview is important because Bagnold (1935) already thought that the grains become rounded by aeolian impacts. This assumption is still found in the literature. Indeed, some rounding processes are active to a certain degree in aeolian sands, but the major environments to generate overall roundness are beaches and streams. This will be discussed in more detail below.

With regard to the surface texture, most grains have a dull appearance, even after treatment with hydrochloric acid. Only four samples (nos. 18/96, 36/96, 15/99, 26/99) possess rather clear surfaces. The first one from Regenfled had experienced the beach environment of a playa (see Section 8.6.1). The other samples are surface sands which obviously have lost their roughness of adhering particles by strong aeolian impacts. Three untreated samples have particularly “dirty” surfaces (nos. 18/96, 14/99, 9/00), which turned out to be caused by clay coatings (see Section 8.6.1).

## 8.4. CORRELATIONS WITH DATING

As all luminescence data represent minimum ages referring to the last deposition, a correlation of the environmental sequences can only be achieved if the environmental changes are reconstructed going back in time step by step. An exception is Regenfled in the eastern transection, where a depositional phase that was dated as Holocene beyond any doubt had been a short aeolian interlude that did not leave any traces on the quartz grains (compare sample no. 18/96 in Table 12).

All other OSL ages (of draa) have to be ascribed to their last long-time desert environment, which for the northern transverse draa can be assumed between 10 and 20 ka ago, and for the southern longitudinal draa before 20 ka ago. The end-Pleistocene wind shift and re-deposition of sands on the eastern lee slopes of the longitudinal draa (9.8–11.8 ka ago) do not seem to have left additional traces on the quartz grains, because only one desert environment could be identified in the drillings at Willmann’s Camp (no. 9/00) and in the middle transection (no. 14/99). This, of course, corresponds to the time of draa formation. As the east-slope deposition seems to have been simultaneous with the last deposition in the transverse northern draa, the end phase of the respective last desert environment for all draa samples can be assumed to have occurred at more or less the same time. Only the beginning of this environment differs strongly between longitudinal and transverse draa. For this reason, a comparable chronology of the environmental developments, starting with the respective last long-time desert environment placed into the same time interval (>10 ka in the tables), is possible.

Tables 12–14 are adjusted according to this concept. All earlier and later environments are correlated on the basis of mutual resemblance. This does not mean that all sand transport by water currents occurred simultaneously. It is highly probable, however, that all transport happened within (the same) effective humid period and does not represent a singular or ephemeral event. This can already be inferred from their most likely spatial distribution. In any case, the last transport by water must have led to deposition in the wider area of the Great Sand Sea, whereas the first transport by water must have removed the sands from the region of their parent material (sedimentary rock or weathering mantles). If the sands have encountered two desert environments, they should have experienced the first one in a region outside the Great Sand Sea. Even the intercalated processes correlate relatively well. A great differentiation, however, is found in the Holocene after the end

**Table 12** Summarized environmental developments along the eastern transection. Explanation of SEM Tables 12 to 20: for each transection the coring sites are listed from south (left) to north (right) (WC=Willmann's Camp). The coordinates are given below. The headline shows the numbers and positions (including the coring depth) of the analysed samples. Blank fields indicate that along the line no equivalent features are found in the samples. Environments and processes are described and discussed in detail in the respective sections of Chapter 8

<i>No. 18/96 Regenfeld 2 m</i>	<i>No. 20/96 Regenfeld 1 m</i>	<i>No. 21/96 Regenfeld silk</i>	<i>No. 22/96 Regenfeld surface</i>	<i>No. 35/96 N: 4 m</i>	<i>No. 36/96 N: surface</i>	<i>Environment</i>
Pedogenesis, alteration	Pedogenesis, alteration	Pedogenesis, alteration	Pedogenesis, alteration	Pedogenesis, alteration	Pedogenesis, alteration	In sand-source areas
Transport by water				Transport by water	Transport by water	Out of sand-source areas
				Pedogenesis		
Long desert phase	Long desert phase	Long desert phase	Long desert phase	Long desert phase	Long desert phase	>10 ka
Beach environment						<10 ka
Beginning pedogenesis			Beginning pedogenesis	Beginning pedogenesis		
Chemical alteration	Chemical alteration		Chemical alteration	Chemical alteration	Chemical alteration	
	Short desert phase	Short desert phase	Short desert phase			
	Basic diagenesis			Basic diagenesis		
Beginning pedogenesis				Desiccation		
25°25'N–27°05'E				27°19'N–26°32'E		

**Table 13** Summarized environmental developments along the middle transection (for explanation see Table 12)

<i>No. 12/99 S: crest</i>	<i>No. 18/99 S: surface E</i>	<i>No. 14/99 S: E 3.4 m</i>	<i>No. 15/99 S: surface W</i>	<i>No. 17/99 S: W 2.5 m</i>	<i>No. 25/99 N: silk</i>	<i>No. 26/99 N: surface</i>	<i>No. 33/99 N: 4 m</i>	<i>Environment</i>
Pedogenesis, alteration	Pedogenesis, alteration	Pedogenesis, alteration	Pedogenesis, alteration	Pedogenesis, alteration	Pedogenesis, alteration	Pedogenesis, alteration	Pedogenesis, alteration	In sand-source area
Transport by water	Transport by water							Out of sand-source area
Pedogenesis	Pedogenesis							
Transport by water	Transport by water				Transport by water	Transport by water	Transport by water	Into sand-sea area
Long desert phase	Long desert phase	Long desert phase	Long desert phase	Long desert phase	Long desert phase	Long desert phase	Long desert phase	>10 ka
Chemical alteration	Chemical alteration	Chemical alteration	Chemical alteration	Chemical alteration	Chemical alteration	Chemical alteration	Chemical alteration	<10 ka
	Beginning pedogenesis	Beginning pedogenesis	Beginning pedogenesis	Beginning pedogenesis		Beginning pedogenesis	Beginning pedogenesis	
			Beach environment					
		Desiccation		Desiccation				
Short desert phase	Short desert phase		Short desert phase		Short desert phase			
25°25'N–26°36'E			25°24'N–26°36'E		27°12'N–26°02'E			

**Table 14** Summarized environmental developments along the western transection (for explanation see Table 12)

<i>No. 3/00 WC surface E</i>	<i>No. 9/00 WC 3 m E</i>	<i>No. 11/00 WC dune</i>	<i>No. 15/00 WC playa</i>	<i>No. 28/00 S: surface W</i>	<i>No. 33/00 S: 5 m W</i>	<i>No. 46/00 N: crest</i>	<i>No. 49/00 N: surface</i>	<i>No. 52/00 N: 4 m</i>	<i>Environment</i>
Pedogenesis, alteration	Pedogenesis, alteration	Pedogenesis, alteration	Pedogenesis, alteration	Pedogenesis, alteration	Pedogenesis, alteration	Pedogenesis, alteration	Pedogenesis, alteration	Pedogenesis, alteration	In sand-source area
				Transport by water			Transport by water	Transport by water	Out of sand-source area
	Pedogenesis						Pedogenesis	Pedogenesis	
Transport by water	Transport by water				Transport by water	Transport by water	Transport by water	Transport by water	Into sand-sea area
Pedogenesis			Pedogenesis	Pedogenesis		Pedogenesis	Pedogenesis		
Long desert phase	Long desert phase	Long desert phase	Long desert phase	Long desert phase	Long desert phase	Long desert phase	Long desert phase	Long desert phase	>10 ka
	Beginning chemical alteration			Beginning chemical alteration	Beginning chemical alteration	Beginning chemical alteration	Beginning chemical alteration	Beginning chemical alteration	<10 ka
Beginning pedogenesis	Beginning pedogenesis		Beginning pedogenesis	Beginning pedogenesis					
	Desiccation		Desiccation				Desiccation		
			Short desert phase						
25°07'N–25°37'E				25°42'N–25°40'E		26°51'N–25°36'E			



of the long desert phase ( $>10$  ka), which in the Great Sand Sea includes the reworking of draa during the transition from the Pleistocene to the Holocene.

In this context, it has to be remembered that the reactivation of draa sands occurred only a few thousand years ago, after the Holocene climatic optimum (Section 5.4). The present-day desert conditions have not lasted long enough yet to produce the characteristic microfeatures (desert smoothing, see Section 8.5) on the quartz grains.



## 8.5. THE MOST FREQUENT MICROSTRUCTURES: CONTROVERSIAL PHENOMENA

With regard to the environmental sequences, it should be stressed that the various sedimentary stages cannot yet be ascribed precisely to specific time intervals. In addition, it has to be kept in mind that processes active in the various environments did not necessarily alter the grains at their sampling sites, because there are distinct indications of repeated phases of sand transport by water. Comparing Tables 12–14, the southern part of the eastern transection shows a relatively short chronology. This might indicate that the sand sources have not been far away.

Independent of this aspect, almost all sequences start with strong chemical alteration or pedogenesis, as indicated by protruding contact surfaces and solution depressions (Le Ribault, 1977, his Fig. 94). This gives the grains a “knobby” appearance, which was found in more than 50% of the sands (Fig. 52). Samples with only few “knobby” grains were usually better rounded. In almost all cases, pedogenesis is supported by silica globules precipitated in an oriented, overlapping flow pattern (Fig. 53; Le Ribault, 1977, his Figs 22, 138: *pellicule siliceuse pédogénétique en coulées*) and sometimes by additional flower-shaped silica precipitations (Le Ribault, 1977: *fleurs de silice*). These microfeatures are ascribed by Le Ribault to the pedogenic B-horizon. The flow pattern resembles silica precipitation in the form of upturned plates following cleavage lines which, according to Krinsley and Doornkamp (1973, their Fig. 13), indicates diagenesis. They stress the point that weathering is excluded from their definition of diagenesis. This very common feature will be discussed further in Section 8.6.3.1. According to Mahaney (2002), upturned plates are cleavage scarps modified by solution and precipitation of silica in a desert environment. The latter processes are equivalent to the smoothing by the desert-dew cycles mentioned by Krinsley and Doornkamp (1973) and by Le Ribault (1977). On most grains from the Great Sand Sea, the smoothing is superimposed upon the other microfeatures mentioned so far (see Fig. 53). Krinsley and Doornkamp (1973, their Fig. 71) distinguish, however, between the small-scale desert smoothing modifying upturned plates (see below) and the original solution and precipitation along cleavage lines. Mahaney does not seem to see these larger-scale microfeatures as separate phenomena. Unfortunately, his Fig. 6.1A (mentioned as an example of upturned plates) shows another phenomenon also thought to be diagnostic for the aeolian environment (parallel ridges). Interestingly, these



**Fig. 52** Quartz grain from the surface sand at the coring site in the transverse draa on the eastern transection (sample no. 36/96). The overview shows many contact surfaces and solution depressions of earlier chemical weathering or pedogenesis. The latter is indicated by silica-flow structures to the right and to the left of the centre, the former by unoriented silica precipitation at the left bottom. Both microfeatures are smoothed by desert-dew cycles. A few aeolian crescents can be seen on the upper left part, and tiny etchings (holes and cracks) are visible mainly on the darker lower part.

grains came from a soil in Wyoming. These primary structures most probably are very old and have been inherited from the parent sedimentary rock or developed in its weathering mantle (see Section 8.6.3.1).

In many sequences, the following process is indicated by conchoidal fracture surfaces. This again is a microfeature which has to be discussed. In general, Krinsley and Doornkamp see it as diagnostic of the glacial environment. They found it also as a more recent feature on a high-energy beach, however (Fig. 50 in Krinsley and Doornkamp, 1973). In an earlier classification, Krinsley and Margolis (1971) listed conchoidal fracture surfaces of a smaller scale and a more uniform and regular pattern as diagnostic of the littoral environment. Gees (1969) found comparable structures in Californian beach sands. According to Le Ribault (1977), this feature can appear in grains of glacial, torrential and intertidal environments. In addition, he states that a better criterion for glacial grains are frictional features in the shape of striae combined with crescents or V-shapes aligned in rows (Figs 13 and 61 in Le Ribault: *frottement*). The latter are not mentioned by Krinsley and Doornkamp, and seem to be completely absent in the Great Sand Sea.

Mahaney again sees things differently. With his great experience in glacial deposits, all fracture faces (conchoidal or straight) in the quartz grains of Algerian ergs are supposed to be of glacial origin, passed on from the Ordovician glaciation via Devonian sandstones (Mahaney and Andres, 1996). Even without the existence

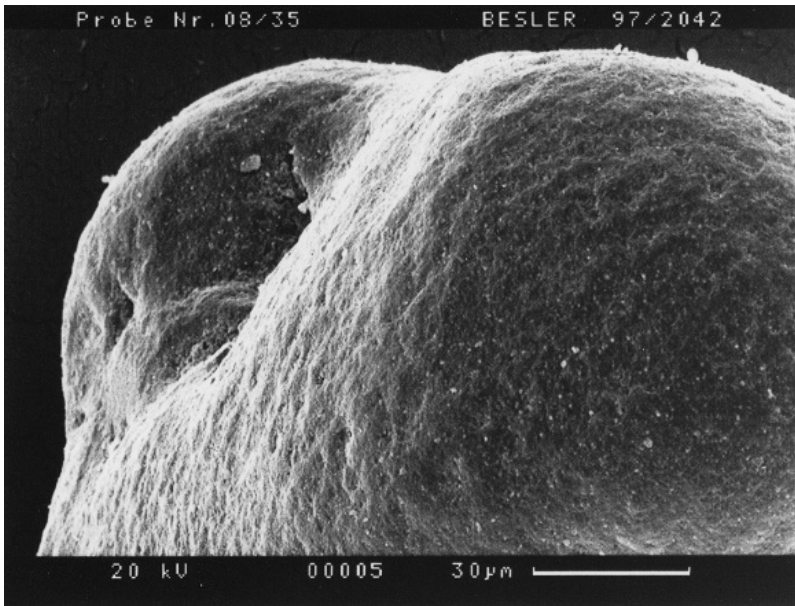


**Fig. 53** Detail of a quartz grain from 4 m depth of the coring in the transverse draa on the eastern transection (sample no. 35/96). The grain shows an old solution depression surrounded by well developed silica-flow patterns (vertical). The right half displays a well developed orange skin as the result of desert-dew cycles that have also smoothed the flow structure. The youngest microfeature is the small crack near the upper rim of the depression.

of younger sedimentary cycles in these regions, there must have been some fluvial transport into the basins where the ergs are found. On the other hand, Mahaney and Andres list many glacial features that are absent in the studied sands. In any case, the sedimentary rocks in the vicinity of the Great Sand Sea are much younger (Cretaceous to Tertiary) and have gone through several sedimentary cycles (Fay and Herrmann-Degen, 1984). For example, no fracture surfaces are found in the Gifl Kebir Sandstone sample (no. 1/00).

In this context it should be mentioned that Klitzsch (1983) identified fluvio-glacial deposits and even tillites (lithified deposits of till produced by the action of glaciers) below the Jurassic and Cretaceous sandstones in the stratigraphic record of the deeply incised Wadi Abd el Malik that drained the Abu Ras Plateau west of the Gifl Kebir and headed towards the Sarir Dalma. Because of Late Devonian trace fossils (Seilacher, 1983), a Devonian to Carboniferous age was assigned to the glacial sediments which are considered as deposited during a glacial epoch correlatable to the Dwyka Glaciation in South Africa. It may be that the one exception where fracture surfaces are the oldest structure in the quartz grains (no. 17/99, not in the tables) refers to this very old heritage. The traces here are almost obliterated and could not be identified as either glacial or turbulent-fluvial, a distinction which was possible in the Taklamakan Sand Sea in China, where the glacial microfeatures were found to show a more complex pattern than the more uniform and regular impact

fractures resulting from transport by water (Besler, 1995). For these reasons, the conchoidal fracture surfaces found in the sands of the Great Sand Sea which are younger and cut across the structures mentioned above, are assumed to be the result of transport by turbulent water.

The similarity between the various environmental sequences ends here. A strong differentiation of environmental stages begins after the first transport by water. Sooner or later, however, indications of a long time spent in a warm desert environment are found in all samples. These consist of micro-scale dissolution and re-precipitation of silica, at a much smaller scale than the features resulting from alteration or pedogenesis (see upturned plates above). The grains are completely covered by this skin, which annihilates minor relief structures (Fig. 53). This phenomenon is called “smoothing” by Krinsley and Doornkamp (1973) and is explained as the result of innumerable desert-dew cycles that start with micro-scale dissolution by dew charged with  $\text{CO}_2$  in the night. This process is accelerated by a soluble layer of disrupted lattice quartz created by aeolian abrasion (Mahaney, 2002). Evaporation during the day subsequently leads to redeposition of silica and smoothing. The same processes are described by Le Ribault (1977), who calls the result “amorphisation”.

Kuenen and Perdok (1962) already saw desert frosting as opposed to mechanical frosting and as a result of dew corrosion leading to a kind of “opalization”. Smoothing of aeolian grains was also mentioned by Hillefors (1971). Doornkamp and Krinsley (1973) stressed the necessity of a high magnification for the identification. A sand grain from the Libyan Desert with silica precipitations in an only 190-fold magnification would easily be interpreted as being pitted by aeolian abrasion. Strongly magnified surfaces resemble an orange skin. This was also found by Tsoar (1976) in sands of the Sinai Erg. According to Folk (1978) this orange skin, which he called “turtle skin” in the Simpson Desert, may develop directly on the quartz surface as well as on the clay/iron-oxide coatings. He stressed the small scale of this microfeature as being intermediate between frosted and polished surfaces. The formation of this skin requires a very long presence in a warm desert environment. In fact, this microfeature could not be found in the sands of the Taklamakan Sand Sea in China (Besler, 1995). Perhaps, it is commonly lacking in cold deserts. Most examples in the literature stem, indeed, from warm deserts. The few specimens from North American dunes and the one example from Antarctica shown by Krinsley and Doornkamp (1973) are very poorly smoothed. The smoothing subdues a minor relief in the grain surface and therefore increases the roundness of a grain. However, as this works only at a microscale, the overall sphericity will not be enhanced. If this were the case, the majority of quartz grains in warm deserts should be rounded. But this was found to be an exception (see Section 8.3).

Differences in the intensity of the smoothing process seem to be visible on the grains of the Great Sand Sea. It is of interest that particularly the samples from the southern end of the western transection near Willmann’s Camp (nos. 3, 9, 11, 15/00) show less smoothing, contrary to the samples from the drilling site farther north (nos. 28, 33/00). This seems to fit with the fact that the southwestern sands were deposited in a younger alluvial fan from the Gilf Kebir and spent less time in the desert environment. This would support the assumption of a southwards retreating,

fluvial deposition during increasing aridity deduced from the morphology of the area (see Section 3.2.1). On the other hand, the smoothing may have been destroyed by sub-recent processes (see Section 8.6.1).

In some cases, a second transport by water after the desert environment is indicated, partly by turbulent water (as indicated by fracture surfaces) and partly by more moderate transport. The latter type of transport is suggested by organic matter cemented by silica precipitation (Le Ribault: *débris organique*). The polishing by water, mentioned in the literature, cannot be expected to have survived the intense processes in subsequent environments. Most probably for the same reason, the V-shaped percussion cracks, also diagnostic of water transport according to the literature (e.g. Mahaney, 2002), are rarely found. This is of special interest where either two types of transport by water were active or where no transport by water (at all) can be deduced. This will be discussed in more detail in Section 8.6.3.

Because all samples were collected from draa or dunes, a second desert environment has to be expected after a second phase of sand transport by water currents, and this was, in fact, found in all cases. Sometimes, however, the processes of smoothing were less intense than in the first desert environment. The northwestern sands, for example, seem to have spent a much longer time in a first desert environment before reaching the area of the Great Sand Sea. In the summarizing tables, the first desert environment is not listed separately since it can only be deduced if older and younger fracture surfaces are compared, and this is possible only in few samples.



## 8.6. DISCUSSION OF THE ENVIRONMENTAL DEVELOPMENTS

### 8.6.1. Processes in the Holocene

All processes that affected the area after the last (long) desert environment (Tables 12–14) are considered to be of Holocene age. As a composite SEM analysis of this kind has been carried out for the first time to this extent, it is necessary to make the procedures of interpretation as transparent as possible. Therefore, and because the Holocene environmental history is particularly important, the Holocene parts of the successions are evaluated separately. Moreover, the processes, mentioned in the tables only in summarized form, are analysed underneath in detail with regard to the various microfeatures (Tables 15–17).

#### 8.6.1.1. The more common features

At all localities – and in almost all samples – evidence is present that chemical weathering processes or pedogenesis started after draa formation, most probably during the Holocene climatic optimum. The evidence is only lacking in two samples (Willmann's Camp no. 11/00 and Regenfeld no. 21/96). These two samples come from modern dunes on the draa. Probably these sands experienced aeolian transport and desert-dew cycles after the humid interval for several thousands of years, which resulted again in smoothing of the grain surfaces.

**Table 15** Holocene developments along the eastern transection (for explanation see Table 12)

<i>No. 18/96 Regenfeld 2 m</i>	<i>No. 20/96 Regenfeld 1 m</i>	<i>No. 21/96 Regenfeld silk</i>	<i>No. 22/96 Regenfeld surface</i>	<i>No. 35/96 N: 4 m</i>	<i>No. 36/96 N: surface</i>	<i>Environment</i>
SiO <sub>2</sub> scale clusters						Subaqueous
Clay scales			SiO <sub>2</sub> flow structure	SiO <sub>2</sub> desquamation SiO <sub>2</sub> flow structure Clay scales		Pedogenic
Holes + cracks	Holes + cracks		Holes + cracks	Holes + cracks	Holes + cracks	Chemical weathering
	Salt spalling		Salt spalling	Salt spalling	Salt spalling	Salt weathering
	SiO <sub>2</sub> chips in depressions	Aeolian crescents	SiO <sub>2</sub> chips in depressions			Aeolian
	Craters			SiO <sub>2</sub> crystal growth		High-energy chemical
Clay coatings				NaCl crystal growth and dissolution		Fluctuating desiccation
25°25'N–27°05'E				27°19'N–26°32'E		

**Table 16** Holocene developments along the middle transection (for explanation see Table 12)

<i>No. 12/99</i> <i>S: crest</i>	<i>No. 18/99</i> <i>S: surface E</i>	<i>No. 14/99</i> <i>S: E 3.4 m</i>	<i>No. 15/99</i> <i>S: surface W</i>	<i>No. 17/99</i> <i>S: W 2.5 m</i>	<i>No. 25/99</i> <i>N: silk</i>	<i>No. 26/99</i> <i>N: surface</i>	<i>No. 33/99</i> <i>N: 4 m</i>	<i>Environment</i>
Holes + cracks	Holes + cracks	Holes + cracks Shallow solutions	Holes + cracks	Tiny holes Shallow solutions	Holes + cracks	Holes + cracks	Holes + cracks Shallow solutions	Chemical weathering
		Scalings		Crevasses				High-energy chemical
	Clay scales in depressions	Clay coating	Thin clay cover	SiO <sub>2</sub> flow structures Clay scales		SiO <sub>2</sub> desquamation	SiO <sub>2</sub> flow structures Clay scales	Pedogenic
			Organic matter				Strange crystals	Subaqueous
	Salt spalling around clay							Salt weathering?
		Calcite precipitation		Calcite crystals Calcite precipitation				Desiccation
SiO <sub>2</sub> chips in depressions	SiO <sub>2</sub> chips in depressions		SiO <sub>2</sub> chips in depressions		SiO <sub>2</sub> chips in depressions			Aeolian
25°25'N–26°36'E			25°24'N–26°36'E		27°12'N–26°02'E			

**Table 17** Holocene developments along the western transection (for explanation see Table 12)

<i>No. 3/00 WC surface E</i>	<i>No. 9/00 WC 3 m E</i>	<i>No. 11/00 WC dune</i>	<i>No. 15/00 WC playa</i>	<i>No. 28/00 S: surface W</i>	<i>No. 33/00 S: 5 m W</i>	<i>No. 46/00 N crest</i>	<i>No. 49/00 N surface</i>	<i>No. 52/00 N: 4 m</i>	<i>Environment</i>
	Holes + cracks			Holes + cracks Shallow solution	Holes + cracks	Holes + cracks	Holes + cracks	Holes + cracks	Chemical weathering
	SiO <sub>2</sub> flow structures								Pedogenic
			Organic matter						Subaqueous
	Calcite crystals								Desiccation
Few clay scales	Clay scales		Clay scales	Clay scales					Pedogenic
	Clay/calcite coating		Clay/calcite coating				Calcite precipitation and solution		(Fluctuating) Desiccation
			Aeolian crescents						Aeolian
25°07'N–25°37'E				25°42'N–25°40'E		26°51'N–25°36'E			



The Regenfeld sample shows additional crescentic impacts, indicating the suggested strong aeolian transport. Many samples, however, possess tiny etchings like holes or cracks in the quartz surfaces. In more than 50% of the samples, these etchings appear as the first microfeature in the Holocene succession, and in almost all cases they resemble the early chemical weathering displayed in a dune sand from Australia (Fig. 82 in Krinsley and Doornkamp, 1973), but in less regular shapes (Fig. 54). They are found in interior draa sands as well as in surface sands, and even in three dune-crest sands (nos. 12/99, 25/99, 46/00) that most probably belong to the latest reactivated sands.

In several samples – mainly from the middle transection – scales and chips of silica are preserved as irregular clusters in depressions. According to Le Ribault (1977), this indicates aeolian sand transport with abrasion of the grain surfaces. Indeed, these are dune and surface sands, with the exception of the Holocene yellow cover sand from a depth of 1 m at Regenfeld (no. 20/96), which is assumed to have been blown southwards by Holocene winds (see Section 8.6.1.2.1). This feature was not found in the west.

The next microfeature, now in untreated samples, are scales or platelets of clay minerals usually found in surface depressions of the grains. They are observed in almost half of the samples, but only in three cases they form a complete coating of the grains. The latter are the reddish draa sands at Regenfeld (no. 18/96, Fig. 55), on the middle transection (no. 14/99) and at Willmann's Camp (no. 9/00). The clay minerals were identified with a microprobe indicating their chemical elements in the energy-dispersive X-ray spectra (Fig. 56). Most common, besides Si, are Al,

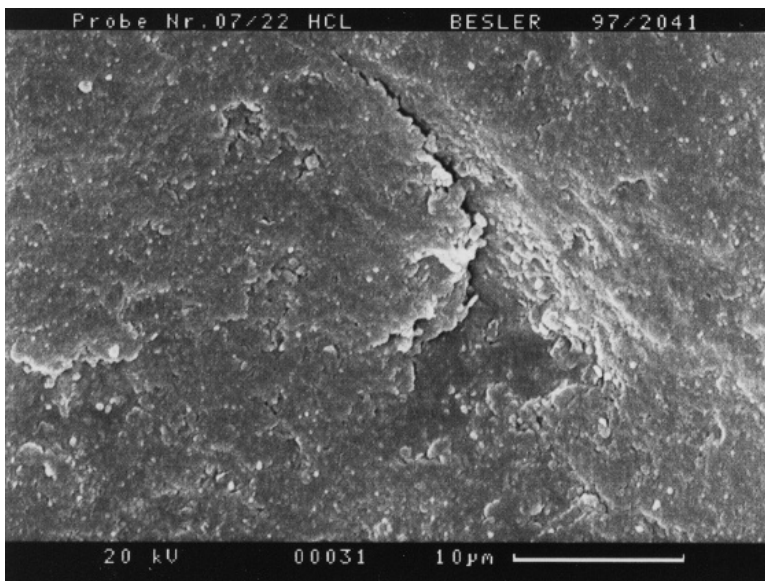


**Fig. 54** Detail of a quartz grain (treated with HCl) from the surface sand of the draa top at Regenfeld in the eastern transection (sample no. 22/96), showing early chemical weathering (crack) in a strongly smoothed surface.

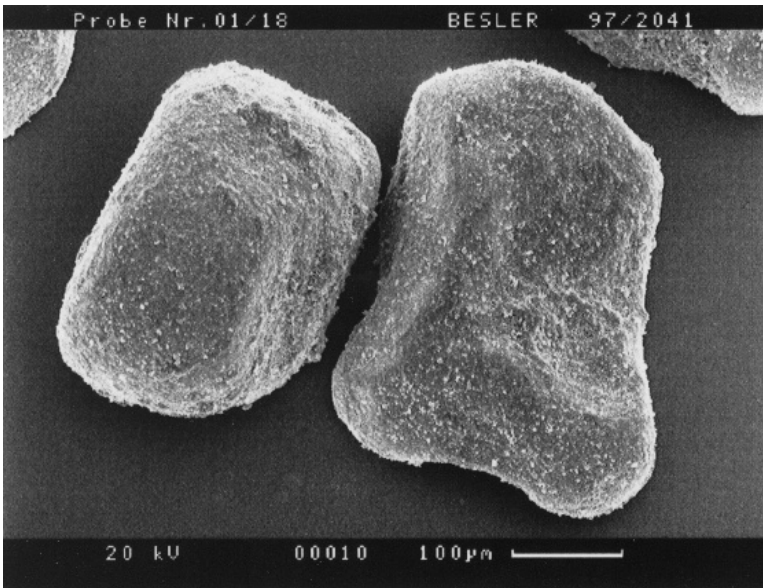


**Fig. 55** Two untreated quartz grains from the reddish draa sand at 2 m depth from the coring at Regenfeld in the eastern transection (sample no. 18/96). The clay/iron-oxide coatings blur surface features, but contact surfaces and shallow solution depressions can be detected in the right grain.

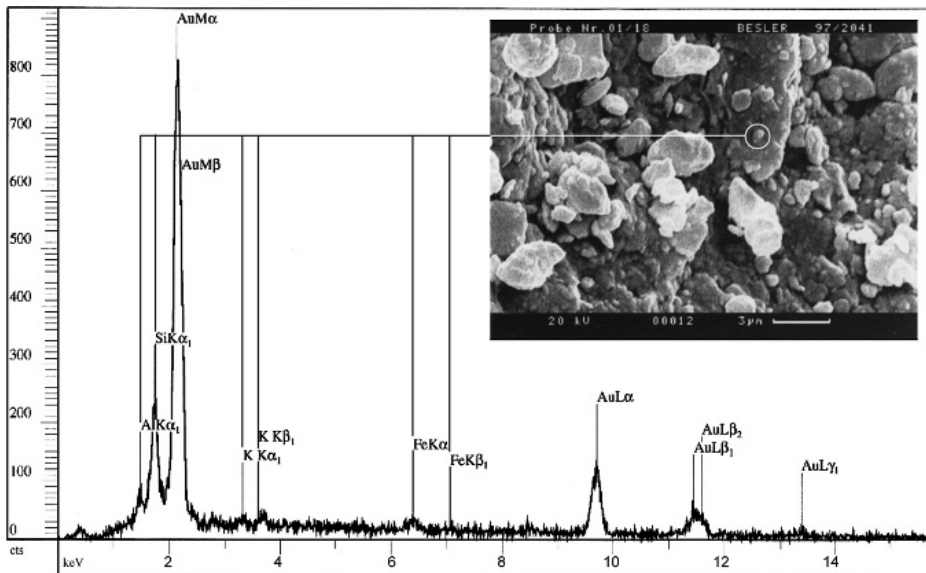


**Fig. 56** Detail of the right quartz grain in Fig. 55. The energy-dispersive X-ray spectrum indicates Al, K and Fe, and shows a low Si peak. The Au peaks result from sputtering with gold.

Fe and K, but Ca and Mg are also present. In about 30% of the samples, the youngest microfeatures are tiny isolated particles covering large parts of the grain surfaces (not shown in the tables). According to Le Ribault (1977), they indicate the final fossilization or immobilization of a sand. Any transport would abrade these particles, which are rarer along the eastern transection.

#### 8.6.1.2. The environments at the dating sites

With the exception of the western draa flanks on the western transection, all interior draa sands possess additional microfeatures and show a more differentiated environmental history. Therefore, the dating sites are discussed separately.

##### 8.6.1.2.1. *The eastern sites*

In four sands from the eastern transection (Table 15; nos. 20, 22, 35, 36/96), the usual early chemical weathering is associated with beginning desquamation of silica. At a small scale ( $<5\ \mu\text{m}$ ), this is caused by dissolution in the pedogenic A-horizon (Fig. 75 in Le Ribault, 1977); it was found in the interior sand of the eastern transverse draa (no. 35/96) and in the surface sand of the middle transverse draa (no. 26/99). The desquamation features in the four mentioned eastern sands are larger than  $10\ \mu\text{m}$ , however, and come closer to the scaling of cleavage plates (Fig. 89 in Krinsley and Doornkamp, 1973), which is diagnostic for a high-energy chemical environment. Whereas a chaotic pattern is displayed in the Krinsley and Doornkamp figure, only singular scalings – always situated in slight depressions – are observed in the sand-sea samples, however (Fig. 57). Fortunately, an experimental investigation into the formation of silt from quartz-dune sand by salt weathering in deserts (Goudie et al., 1979) includes a SEM analysis. Their plate 1(b) shows the very same feature as a circular crack passing shallowly under a spalling fragment of the grain surface. Goudie et al. (1979) mention dish-shaped concavities as the preferred location of this feature. The other features found by Goudie (current study) were not observed in the Great Sand Sea. In this context, it is interesting that the salt-induced spalling or scaling is found only in cover sands which could have been derived from the (interior) sands of the transverse draa, where sodium chloride (NaCl) crystals are found. Only on the eastern transection, all draa sands were found to be saline (see Section 6.1).

The reddish draa sand at Regenfled (no. 18/96), which was deposited around 5 ka ago, shows no traces of salt weathering but possesses isolated clusters of silica scales on the plain grain surfaces; these have been ascribed to a low-energy fluvial environment or to floodplain channels by Le Ribault (1977). Clay scales (Al, Fe, K) according to him indicate pedogenic processes. Only later the early chemical weathering, already mentioned above, seems to have affected these grains, which finally were completely covered by clay coatings (Al, Fe, K). This Holocene development is in accordance with the history discussed in Section 6.2.2.3: The blown sand in the interdraa corridor was subjected to chemical alteration in the large water-filled playa. When this fell dry, pedogenic processes and small-scale etching – also found in many other samples – started in the little moisture left behind. The perfect clay/iron-oxide coatings most probably formed by adhesion in

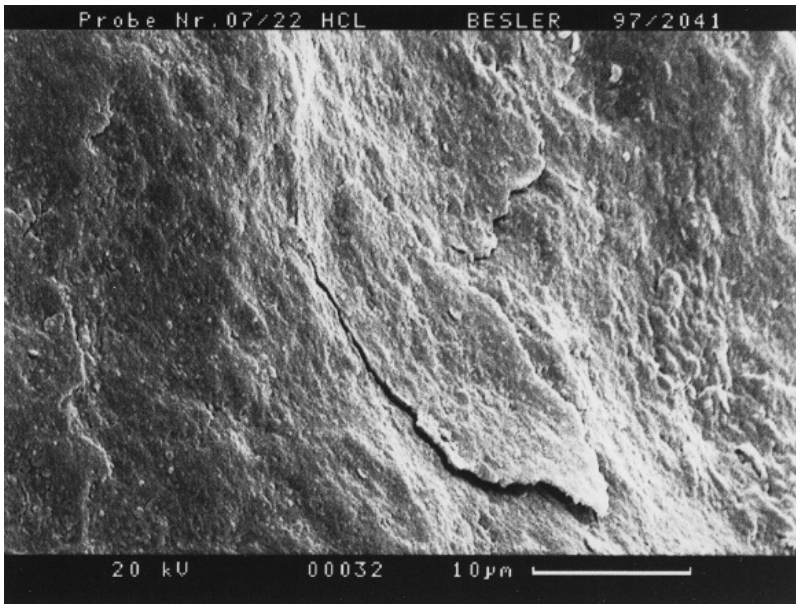


**Fig. 57** Detail of a quartz grain (treated with HCl) from the surface sand of the draa top at Regenfeld in the eastern transection (sample no. 22/96). Spalling of silica in a slight concavity is caused by salt weathering. Note the strong desert smoothing overlying pedogenic silica-flow structures which can still be seen to the right.

the desiccating playa. The coated, reddened sand grains were finally blown onto the draa.

The modern yellow cover sand from a depth of 1 m at the same site (no. 20/96) displays a different development. The first microfeatures on the smoothed grains are the widely distributed, early chemical weathering forms associated with those of salt weathering. In addition, silica scales and chips preserved in depressions indicate an aeolian environment (Le Ribault, 1977). Most conspicuous, however, are singular little eruption craters, which pushed scales and chips into an upright position. According to Krinsley and Doornkamp (1973, their Fig. 95), they are signs of subsurface weathering in the grain, perhaps of salt-crystal growth in a high-energy chemical environment. In this context it has to be remembered that this cover sand is supposed to have been transported southward from the northern draa (Besler, 1998).

The interior sand of the transverse draa on the eastern transection (no. 35/96) shows the small-scale features of desquamation in the pedogenic A-horizon (Fig. 75 in Le Ribault, 1977) and, in addition, younger layers of silica precipitated in the pedogenic flow pattern (see Section 8.5). After these processes and the development of clay scales (Al, Fe, K, Ca), small quartz crystals grew on the surface, even on clay-covered parts, and isolated large ones ( $<2\ \mu\text{m}$ ) could be verified by probing (only Si in the spectrum). This indicates diagenetic processes in the sediment. In addition, the microprobe identified crystals of NaCl on many grains, which

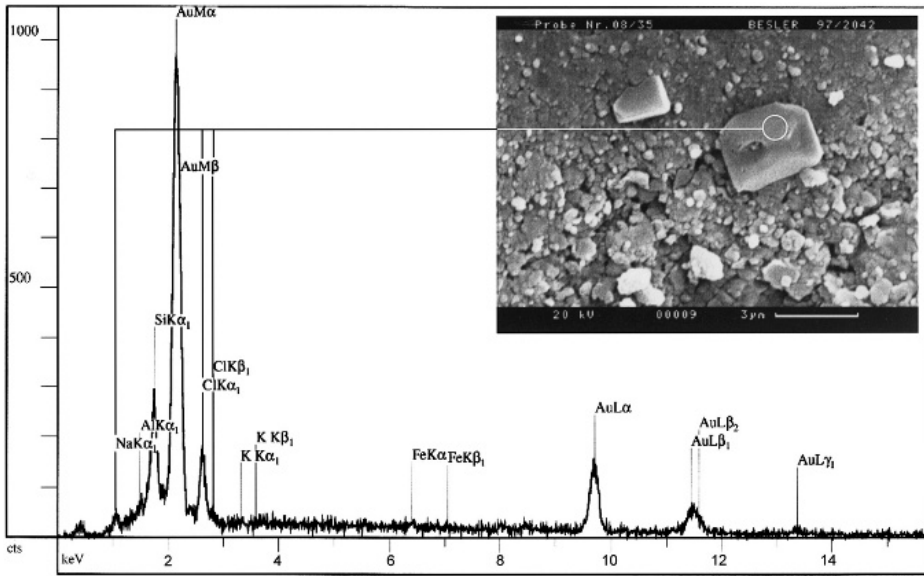


**Fig. 58** Detail of an untreated quartz grain from a core (4 m depth) from the transverse draa in the eastern transection (sample no. 35/96). The energy-dispersive X-ray spectrum indicates Na and Cl, and also shows a reduced Si peak. The NaCl crystal displays solution features. The smaller crystal at the upper left is pure quartz (high Si peak only). The background consists of clay scales (Si, Al, Fe and K indicated).

indicates a high-energy alkaline environment and also a slow desiccation of the sand (Fig. 58). Some NaCl crystals show signs of a subsequent solution. The moisture content seems to have fluctuated.

#### 8.6.1.2.2. *The sites in the middle*

On the middle transection (Table 16), the interior sands of the eastern (no. 14/99) and of the western slope (no. 17/99) of the longitudinal draa show a remarkably similar development. The older microfeatures of early chemical weathering are associated with small, shallow solution features in both samples. In both samples, microfeatures follow, which – according to Krinsley and Doornkamp (1973) – indicate a high-energy chemical environment. On the eastern slope, these are true scalings of cleavage plates in an initial stage (compare Fig. 89 in Krinsley and Doornkamp, 1973), which are found outside of depressions (Fig. 59). On the western slope, a high-energy chemical environment is indicated by isolated, conspicuous solution crevasses up to 60  $\mu$ m long, much larger than the common, tiny, cracks. They seem to be followed by the pedogenic flow pattern of silica precipitation (Fig. 53; see also Fig. 138 in Le Ribault, 1977). In both samples, clay deposits are found on quartz grains (Al, Fe, K, Ca), but in strongly varying amounts. Whereas only clay scales are present on the western slope, the grains from the eastern slope are completely – but thinly – coated, yielding a reddish sand

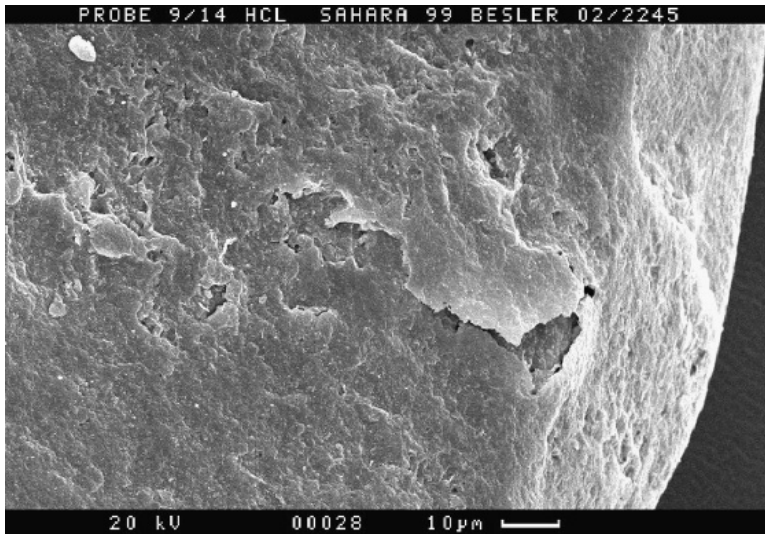


**Fig. 59** Detail of a quartz grain (treated with HCl) from 3.4 m depth in the coring on the eastern slope of the longitudinal draa on the middle transection (sample no. 14/99). Initial silica scaling on a smoothed convex grain surface indicates a high-energy chemical environment. Smoothed pedogenic silica-flow structures are seen on the right edge of the grain. Note the difference from salt spalling in Fig. 57.

(see Section 6.2.2.2). In both samples, the microprobe produced an extremely high peak of calcium in the energy-dispersive X-ray spectra, again with a quantitative difference. On the western slope, even calcite crystals ( $\sim 2 \mu\text{m}$ ) could be seen in depressions and verified by probing, followed by non-crystalline calcite precipitations, also present on the eastern slope (Fig. 60). This indicates a slower desiccation on the western slope, where remains of human occupation have been found (see Section 5.1).

The surfaces of these slopes are also interesting. Besides the early chemical weathering and a thin clay cover in some parts of the grains (Al, Fe, K), the surface sample from the western slope (no. 15/99) contains organic matter with a particle size of about  $6 \mu\text{m}$ , trapped in shallow depressions. According to Le Ribault (1977), this indicates low-energy fluvial transport or a beach environment. The latter is more plausible here because, after fluvial transport, organic matter is more cemented; in addition, it also occurs outside the depressions (see Section 8.6.2). Besides early chemical weathering and clay scales in depressions, the surface sample from the eastern slope (no. 18/99) shows typical salt cracks around clay scales. Contrary to the samples with salt-weathering features on the eastern transection, this sand is non-saline. Perhaps only cracks passing under spalling fragments of silica are diagnostic for salt weathering. On the other hand, the particles causing salinity may have been abraded in this surface sample. The interior draa sand of this site (no. 14/99) was found to be strongly saline (see Section 6.1). On the whole, the Holocene

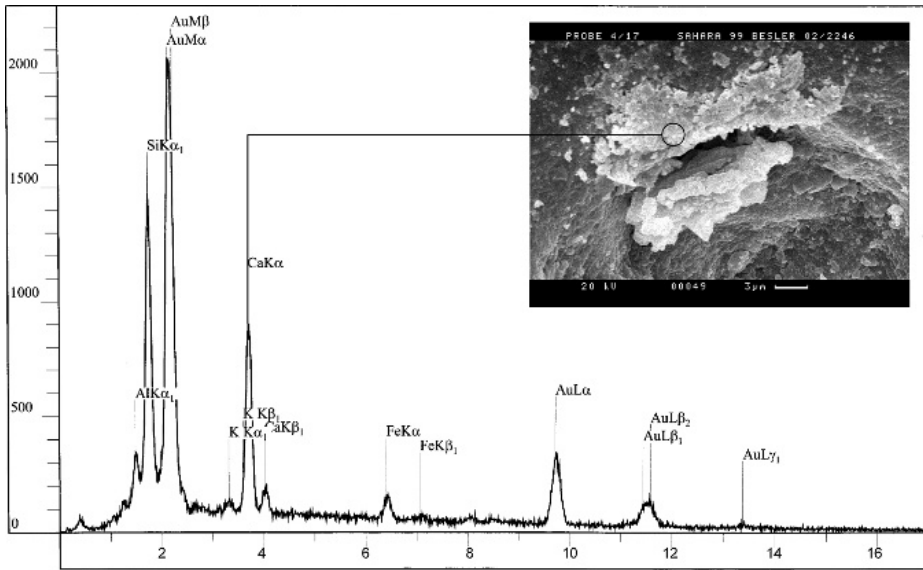


**Fig. 60** Detail of an untreated quartz grain from a core (2.5 m depth) from the western slope of the longitudinal draa in the middle transection (sample no. 17/99). An older etching hole in a smoothed surface contains white crystals and shows poorly crystallized precipitates on its rim. The energy-dispersive X-ray spectrum shows a high Ca peak beside Si, Al, Fe and K, indicating clay minerals. The spectrum of the larger crystals shows two very high Ca peaks, and very low Si and Al values.

developments in this place as deduced from SEM support the assumption of an ancient playa having existed here.

The interior sand from the transverse draa (no. 33/99) shows traces of early chemical weathering and of shallow solution. Beginning pedogenesis is indicated by the silica-flow pattern, and by a few clay platelets (Al, Fe, K, Ca, Mg, Ti). The presence of titanium is exceptional on quartz grains. The only mineral containing titanium in the Great Sand Sea is rutile ( $\text{TiO}_2$ ), which in this sample constitutes only 2% of the total heavy-mineral content. Perhaps the traces result from a former rutile solution, although it belongs to the more stable heavy minerals. Another curiosity was found in this sample. Incomplete crystals with diameters of 5–8  $\mu\text{m}$  and with solution features contain the clay elements Si, Al, Fe, K, Ca and Mg, but could not be identified by a specialized mineralogist. The crystals are covered by tiny pimples (high Si peak) which resemble the “globules siliceux épars” of Le Ribault (1977, his Fig. 81).

#### 8.6.1.2.3. *The western sites*

On the western transection (Table 17), the interior sands from the west slopes of longitudinal and transverse draa only show an average early chemical weathering. At Willmann’s Camp, however, interior samples show an exceptional development. In the interior draa sand (no. 9/00), the development starts with early chemical

weathering and with pedogenic flow structures (according to Le Ribault, 1977). Subsequently, calcite crystals ( $\sim 5\ \mu\text{m}$ ) grew in shallow surface depressions, which indicates a slow desiccation. Quartz and calcite are likewise covered by clay scales (Al, Fe, K, Ca), and the youngest features are clay/calcite coatings, most probably a sign of fast desiccation. Contrary to the middle transection, calcite is nothing special here, because the playa remnants still contain layers of calcareous sediments.

The conditions were different for the sand of sample no. 15/00, which was collected from the interior of a lee-side avalanche on the draa, spilling onto playa deposits. On the smoothed surface of one grain, a  $100\ \mu\text{m}$  long piece of organic material was cemented and covered by clay scales (Al, Fe, Ca). The calcium peak in the spectrum was extremely high, however, which indicates additional calcite precipitation. Clay/calcite coatings were also observed on other grains of this sample. The youngest microfeatures are crescentic aeolian impacts and a final cover with tiny particles. According to this sequence of features, the sand experienced a low-energy water transport, beginning pedogenic processes, followed by fast desiccation and a moderate aeolian transport, and became rather immobile at last. The youngest feature may indicate a rather slow encroachment of the slip face.

With regard to the question raised in Section 8.5 – whether the poor smoothing at Willmann's Camp resulted from desert environments with a relatively short duration or from the destruction of smoothing by sub-recent processes – it can be stated that the latter is only possible for the interior draa sand where chemical weathering and alteration of the grain surfaces occurred after deposition. The other samples were only subjected to processes that added various materials in certain places. When these were removed by the treatment with hydrochloric acid, the degree of smoothing could be discerned. This only leaves the option that the sands at Willmann's Camp indeed spent less time in their last desert environment.

### 8.6.1.3. The spatial pattern

There is evidence of a spatial pattern of the Holocene processes in the Great Sand Sea. In the transverse draa around  $27^\circ\text{N}$ , the indications of an aggressive, high-energy chemical environment after 12.5 ka ago increase towards the east. The influence of a fluctuating groundwater table cannot be excluded here because interdrea corridors are lacking. Salt weathering is found only in the interior eastern transverse draa and in cover sands on the longitudinal draa which could have been derived from the north.

According to various features, aeolian activity seems to have been more violent in the east. Only between the southern longitudinal draa, there is evidence of surficial water bodies. Reddening of quartz grains and humid environments can be traced as far north as  $25^\circ 25'\text{N}$  on the eastern and on the middle transections. Only in the vicinity of playas, clay (iron-oxide) coatings developed. Whereas they seem to have formed in a desiccating playa at Reginfeld in the east (later deposition on the draa), they have grown in situ within sands deposited around 9.8 ka ago in the middle and around 11.5 ka ago at Willmann's Camp. The influence of calcareous playa deposits, which are absent in the east, increases towards the west. This



may also explain the decreasing reddening of drilled sands in this direction, where clay/calcite coatings with less iron oxide prevail.

### 8.6.2. Pre-Holocene processes in the Great Sand Sea

The concept of the chronology going backward in time, as explained in Section 8.4, implies that the sands experienced their last significant desert environment in the Great Sand Sea during the Pleistocene (including the transition to the Holocene) and that they were brought into the Great Sand Sea by the last phase of water currents in the respective environmental sequences. If there are no indications that transport by water took place, it is assumed that all processes resulting in surface microfeatures occurred in or near the Great Sand Sea. All environments before the last transport by water should, however, have existed elsewhere, outside the Great Sand Sea. It can even not be excluded that earlier transport of the grains by water currents took already place during the Tertiary. This will be discussed in the next subsection, together with the sand sources (see Section 8.6.3). In the present section, only the processes between the last transport by water currents and the last presence in a long-time desert environment will be discussed. The pre-Holocene (including Pleistocene) processes, which resulted in various microfeatures, are listed in detail in Tables 18–20. It has to be kept in mind, however, that they also include environments outside the Great Sand Sea. The older Pleistocene microfeatures are less well preserved on the grains. For parts of some sequences, it is difficult to establish with reasonable certainty which of the microfeatures are older, and which are younger.

The most frequent microfeatures have already been introduced in Section 8.5. Transport by turbulent water is usually indicated by conchoidal fractures. In a strict sense, these are identified in five samples from longitudinal and transverse draa (nos. 12/99, 18/99, 28/00, 49/00, 52/00). In 12 cases, however, concave or dish-shaped fracture surfaces are smooth and younger, in some samples even cutting across older conchoidal surfaces (e.g. no. 12/99; Fig. 64). This feature is particularly frequent along the middle transection, but in four samples its presence is not certain. According to Krinsley and Doornkamp (1973, their Fig. 86), it is caused by aeolian fracturing in heavy sandstorms. This interpretation most probably results from the observation that the usual conchoidal pattern of upturned cleavage plates, enhanced by dissolution and precipitation of silica along cleavage lines, is absent on the fracture surfaces. The example given in the just-mentioned figure of Krinsley and Doornkamp (1973) stems from Antarctica, and the authors mention that the dish-shaped pattern is never this pronounced on desert sand grains. They seem to refer to smaller features with regard to aeolian processes. Similar dish-shaped forms are interpreted by Le Ribault (1977, his Fig. 110) as caused by impacts in a torrential environment. In the Great Sand Sea, however, the dimensions of these features are comparable to the conchoidal fractures with altered cleavage lines (striped fractures in the tables). Therefore, they are assumed to be the result of transport by water, but with a different subsequent history. Stronger chemical alteration of all older conchoidal fracture surfaces is indicated by dissolution and precipitation of silica along

**Table 18** Pre-Holocene developments along the eastern transection (for explanation see Table 12)

<i>No. 18/96 Regenfeld 2 m</i>	<i>No. 20/96 Regenfeld 1 m</i>	<i>No. 21/96 Regenfeld silk</i>	<i>No. 22/96 Regenfeld surface</i>	<i>No. 35/96 N: 4 m</i>	<i>No. 36/96 N: surface</i>	<i>Environment</i>
	Deep etching Tropical healing		Striped etching	Striped etching Tropical healing	Deep etching Tropical healing	Tropical
	SiO <sub>2</sub> flow structures		SiO <sub>2</sub> flow structures	SiO <sub>2</sub> flow structures	SiO <sub>2</sub> flow structures Silica flowers Clay coating	Pedogenic
Smooth fractures, polished surface				Smooth fractures	Polish, uncertain fractures	Younger fluvial
				SiO <sub>2</sub> flow structures		Pedogenic
Smoothing	Smoothing (few grains)	Smoothing, crescents (few grains)	Smoothing	Smoothing	Smoothing	Aeolian
25°25'N–27°05'E				27°19'N–26°32'E		

**Table 19** Pre-Holocene developments along the middle transection (for explanation see Table 12)

<i>No. 12/99</i> <i>S: crest</i>	<i>No. 18/99</i> <i>S: surface E</i>	<i>No. 14/99</i> <i>S: E 3.4 m</i>	<i>No. 15/99</i> <i>S: surface W</i>	<i>No. 17/99</i> <i>S: W 2.5 m</i>	<i>No. 25/99</i> <i>N: silk</i>	<i>No. 26/99</i> <i>N: surface</i>	<i>No. 33/99</i> <i>N: 4 m</i>	<i>Environment</i>
Deep V-etchings, striped etchings	Tropical healing		Tropical healing	Feldspar healing, tropical healing	Selective etching	Feldspar healing	Tropical healing	Tropical
	Silica flowers		Silica flowers					Pedogenic
Striped fractures	Striped fractures uncertain							Tropical fluvial
Silica flowers	SiO <sub>2</sub> flow structures			SiO <sub>2</sub> flow structures	Silica flowers	SiO <sub>2</sub> flow structures		Pedogenic
Smooth fractures	Smooth fractures	Polished edges			Smooth fractures	Smooth fractures, older organic material	Uncertain fractures	Younger fluvial
Smoothing	Smoothing, crescents	Smoothing	Smoothing	Smoothing	Smoothing	Smoothing	Smoothing	Aeolian
25°25'N–26°36'E			25°24'N–26°36'E		27°12'N–26°02'E			

**Table 20** Pre-Holocene developments along the western transection (for explanation see Table 12)

<i>No. 3/00 WC surface E</i>	<i>No. 9/00 WC 3 m E</i>	<i>No. 11/00 WC dune</i>	<i>No. 15/00 WC playa</i>	<i>No. 28/00 S: surface W</i>	<i>No. 33/00 S: 5 m W</i>	<i>No. 46/00 N: crest</i>	<i>No. 49/00 N: surface</i>	<i>No. 52/00 N: 4 m</i>	<i>Environment</i>
Deep selective etching, tropical healing	Feldspar healing, selective etching	V-etchings, deep hole		Deep etching, selective etching, "Gilf healing"	Feldspar healing, rectangular etching, selective etching	Feldspar healing, etching holes	Feldspar etching, feldspar healing, deep etching	Feldspar healing, V-etching	Tropical
SiO <sub>2</sub> flow structures, silica flowers				SiO <sub>2</sub> flow structures				SiO <sub>2</sub> flow structures	Pedogenic
				Striped fractures			Fractures and healing uncertain	Striped fractures	Tropical fluvial
	Polished smoothed clay						SiO <sub>2</sub> flow structures	Silica flowers	Pedogenic
Smooth fractures	Older organic material, clay polish				Smooth fractures uncertain	Smooth fractures uncertain	Smooth fractures	Smooth fractures, organic matter	Younger fluvial
SiO <sub>2</sub> flow structures			Unpolished smoothed clay	Unpolished smoothed clay		Unpolished smoothed clay	Unpolished smoothed clay		Pedogenic
Smoothing	Smoothing	Smoothing	Smoothing	Smoothing crescents	Smoothing crescents	Smoothing crescents	Smoothing crescents	Smoothing	Aeolian
25°07'N–25°37'E				25°42'N–25°40'E		26°51'N–25°36'E			

cleavage lines, in the sense of Krinsley and Doornkamp (1973). Generally, the smoother fracture surfaces seem to be younger. This will be discussed in more detail in Section 8.6.3. Additional indications of transport by currents are organic materials glued to the grain surface by old and strongly smoothed Al-Fe silicates (nos. 26/99, 9/00, 52/00).

Only in few samples, pedogenic processes that occurred after the last transport by a water current – and therefore in the sand sea – can be identified by the typical silica flow structure. These samples are the interior sands of the transverse draa in the east (no. 35/96) and the surface sand at Willmann's Camp in the southwest (no. 3/00). Other, more frequent indications of beginning pedogenesis are clay scales adhering to the grain surfaces in or outside depressions (Al, Fe, K, Ca, Ti) which obviously have been subjected to the same desert-smoothing processes as the quartz surfaces. This has been described by Folk (1978) for the Simpson Desert of Australia. It cannot be stated for sure, however, that all these features in the Great Sand Sea are younger than the last transport of the grains by a water current, because – at least in one case – the surface seems to have been polished by water. In addition, organic matter was trapped in the clay scales of this sample (no. 9/00), which also indicates a low-energy fluvial environment (according to Le Ribault, 1977).

It is interesting that one sand with the pedogenic flow structure and all five sands containing smoothed clay deposits come from the western transection, from both longitudinal and transverse draa (nos. 9, 15, 28, 46, 49/00). Only the polished clay scales are found in an interior draa sand. All other cases could represent pedogenic processes in the fluvial deposits that were present before draa formation. More moisture seems to have been available in the western sand sea. On the other hand, former clay deposits on the grains could have been abraded by stronger aeolian transport in the middle and eastern parts of the Great Sand Sea (see below). It is also of interest that in the pre-Holocene clay deposits on quartz grains, titanium is more frequent than in the Holocene clay scales. This could indicate stronger weathering of heavy minerals (rutile in this case, see Section 8.6.1.2.2) in the alluvial sediments before draa formation. This may, however, be just incidental, because the few samples do not allow a statistically significant conclusion.

All pre-Holocene sequences end with the desert smoothing of the grain surfaces, but to a varying degree. There is less final smoothing along the western transection. Nevertheless, also there large (10–20  $\mu\text{m}$ ) crescentic aeolian impacts indicate strong sand transport by heavy storms, but with the exception of Willmann's Camp. According to Le Ribault (1977: forte densité = haute énergie), the density of these crescents can be used as a measure of the aeolian energy. The density seems to be highest in the dune sand at Regenfeld (no. 21/96), where no pre-Holocene processes can be recognized that occurred before extreme smoothing took place.

To sum up, only few microfeatures are found on the quartz grains which result from processes between the fluvial transport into the region and the draa formation. Most probably, many features – such as the small dissolution holes and cracks – have been obliterated by the rather strong smoothing that is also present in the interior draa sands. The latter indicates that the quartz grains were subjected to aeolian surface processes and desert-dew cycles for a very long time during draa-formation

periods before their final burial, which corroborates the rather low growth rates of the draa (see Section 5.3.2).

### 8.6.3. Major sand sources

A very brief preliminary report on this investigation has already been published (Besler, 2006).

#### 8.6.3.1. Environments outside the Great Sand Sea

As already mentioned (see Section 8.3), the most frequent ancient structures on quartz grains of all samples are protruding contact surfaces and solution depressions, followed by upturned plates; these are both signs of chemical alteration or pedogenesis. In addition, in almost all samples the chemical weathering was more aggressive, resulting in deep surface etchings. These comprise deep angular to rounded pits with diameters of up to 40  $\mu\text{m}$  (compare Fig. 18 in Krinsley and Doornkamp, 1973), which are found in seven samples, mainly from the western transection (nos. 11/00, 28/00, 33/00, 46/00, 49/00) and particularly in the interior and surface sands of the western flank of the longitudinal draa, where pits exist with cubical and rounded shapes. Comparable pits in other transections were found only in the surface sand of the eastern transverse draa (no. 36/96) and in the cover sand at Reginfeld (no. 20/96). Other etchings are V-shaped and up to about 60  $\mu\text{m}$  large (compare Fig. 57 in Krinsley and Doornkamp, 1973). They are found in two samples from the western transection (nos. 11/00, 52/00) and in the dune sand from the longitudinal draa in the middle transection (no. 12/99). A third etching pattern consists of stripes or grooves of selective etching along cleavage lines (compare Figs 20, 33 and 86 in Krinsley and Doornkamp, 1973), which are very common: they are found in all samples, with the exception of three sands from Reginfeld in the east and the interior sand of the eastern flank in the middle transection.

These very old features most probably were generated in the weathering mantle of sedimentary rocks. However, they could also have developed in solid rock, because the photomicrographs of the Gilf Kebir Sandstone, sampled from a solid vertical wall along a dry-valley side, display similar solution patterns and particularly deep V-etchings. The only difference is that they are not blurred by younger features.

The deep and large etchings deserve special attention and a discussion because their interpretation by Krinsley and Doornkamp (1973) is challenged by Tietz (1987, 2005). Tietz studied lateritic sandstones in Nigeria and – for comparison – Tertiary quartz sands from the Franconian Alb (Fränkische Alb) in Germany. He claims that these microfeatures are not the result of etching, i.e. solution of quartz, particularly not if their rims include angular or straight sections. Tietz states that true solution features in quartz have always smoothed rims and that particularly all V-shaped etchings represent moulds of weathered feldspars. This is possible because in magmatic rocks quartz/feldspar intergrowth is common at the eutectic point. Striped patterns like parallel ridges or solution and precipitation along cleavage lines

are explained as the result of healing processes in the quartz after feldspar solution. According to Tietz, the healing processes depend strongly on a seasonally humid, tropical climate, which in his studies refers to the Tertiary.

With regard to the Great Sand Sea, this interpretation makes sense because the features discussed are found at the beginning of the environmental development. They refer to the source areas of the sands before the first transport by water. Indeed, the sample of the Early Cretaceous Gilf Kebir Sandstone shows features comparable to the photomicrographs of the Nigerian Late Cretaceous sandstone (Tietz, 1987). The transformation from the fresh V-shaped pits in the sandstone sample (no. 1/00, Fig. 61) to patterns where the healing process has taken place seems to be visible in the sample from the western flank of the western (no. 28/00) longitudinal dree, of course with a later smoothing (Fig. 62). Moreover, in five samples from the western transection (nos. 9/00, 33/00, 46/00, 49/00, 52/00), healing structures of diverging stripes resemble exactly the Figs 4 and 5 of plate 28 in Tietz (1987), which are interpreted as an advanced stage of quartz growth in a feldspar mould (Fig. 63, feldspar healing in the tables).

With regard to the climatic interpretation, in both cases (Krinsley and Doornkamp as well as Tietz), a chemically aggressive environment is needed. For Tietz, this is located in the groundwater zone. For Krinsley and Doornkamp, the process is diagenesis, wherever it takes place. Although the processes are different according to the authors (etching of quartz versus solution of feldspar), the diagnostic value of these microfeatures with respect to the environment is the same.

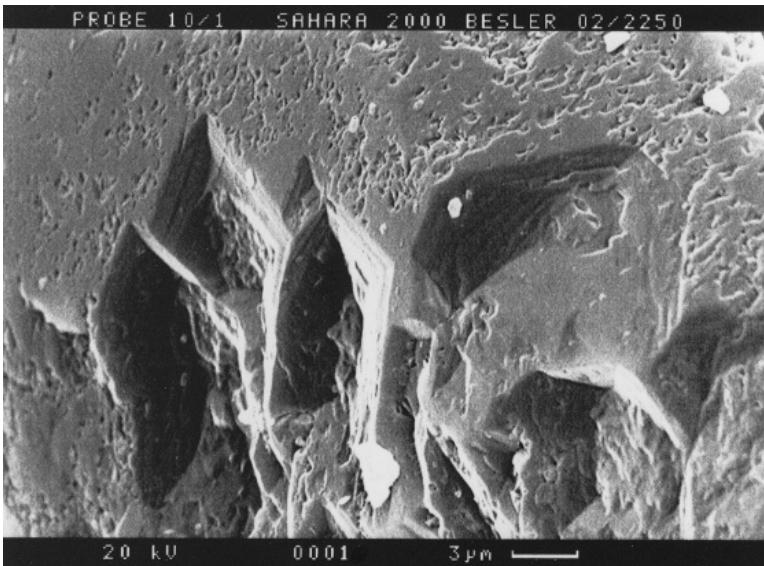


**Fig. 61** Detail of a quartz grain from the Gilf Kebir Sandstone sampled in Wadi Hamra (sample no. 1/00). Deep rhombohedral or V-etchings in the grain surface, with numerous smaller etchings, result from feldspar dissolution.

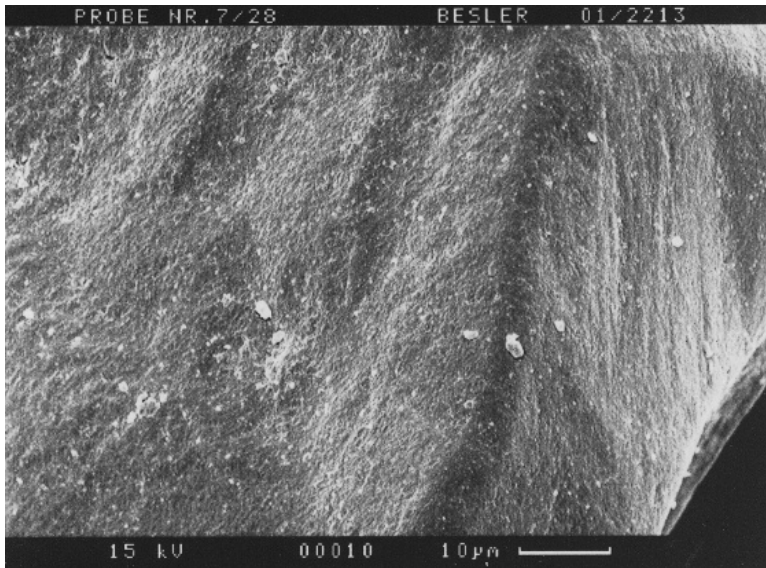


**Fig. 62** Detail of a quartz grain from the surface sand at the drilling site on the western flank of the longitudinal draa in the western transection (sample no. 28/00). The rhomboidal pattern of stripes was most probably generated by quartz growth in feldspar moulds, subsequently covered by silica precipitation and smoothed by desert-dew cycles.

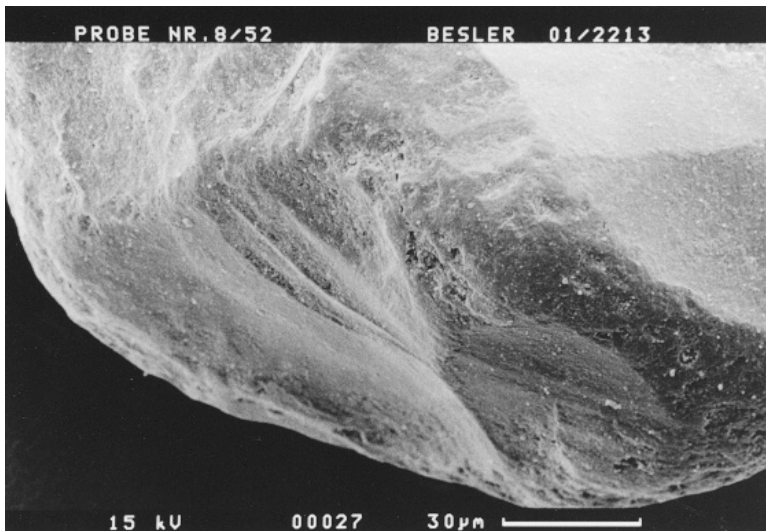


**Fig. 63** Detail of a quartz grain from 4 m depth from the drilling in the transverse draa in the western transection (sample no. 52/00). The striped triangle in the left centre represents the healing of an older feldspar solution pit by quartz growth. The pattern seems to be also present in the lower right and upper left parts. The short and wider stripes oriented towards the upper right are most probably remnants of an older conchoidal fracture surface with healing structures (compare Fig. 64). Smooth younger fracture surfaces cut across. Tiny etchings can be seen on the darker parts.



The question remains whether they have to be of Tertiary age, because in some samples from the Great Sand Sea, the same pattern of stripes appears on conchoidal fracture surfaces after the first transport by water (taking the grains away from their source area). Tietz did not examine younger sediments. It can therefore not be excluded that similar weathering conditions reigned in some parts of northern Africa at least locally during the Pleistocene pluvials (interglacials?). According to Krinsley and Doornkamp (1973), such “wounded” fracture surfaces are particularly vulnerable to solution and precipitation along the conchoidal lines. Tietz does not mention any fractures in quartz grains.

In the Great Sand Sea, this phenomenon is found in grains from the longitudinal draa in the middle (only surfaces: nos. 12/99, 18/99, Fig. 64) and in longitudinal and transverse western draa (nos. 28/00, 49/00, 52/00). With regard to the smoothed fracture surfaces without this pattern, it means different weathering conditions after the stages of transport by water. Obviously, the older fractures were subjected to weathering conditions that were comparable to those of the Tertiary environment. The younger fractures, however, have been chemically so little affected that all traces were subsequently obliterated by desert smoothing. The environment in this case seems to have been much more arid.

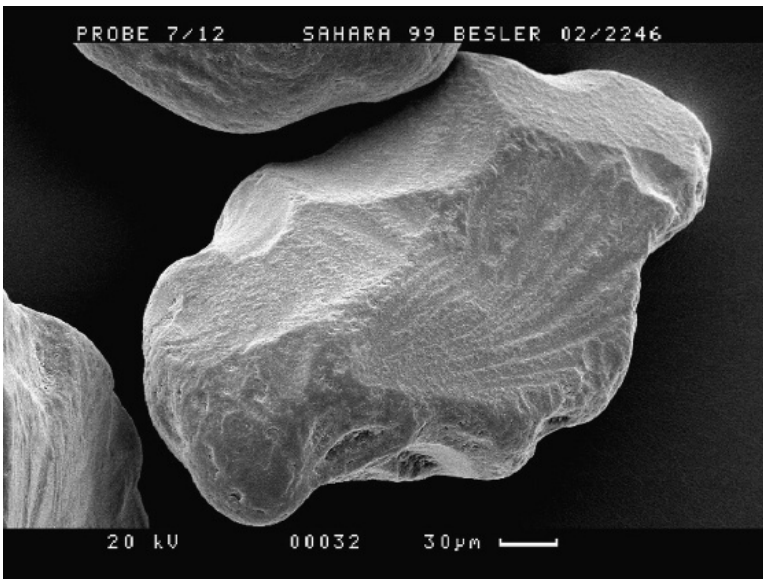


**Fig. 64** Quartz grain from the dune-crest sand on the draa at the drilling site in the longitudinal draa in the middle transection (sample no. 12/99). The oldest feature is the (dark) contact surface at the bottom. Several conchoidal fracture surfaces cut across and show silica dissolution and precipitation along cleavage lines. These are cut in turn by younger smooth fracture surfaces. Only the smaller concavity at the middle bottom is comparable in size to aeolian fracturing in heavy sandstorms. A few silica flowers seem to be present beneath the overall smoothing (upper right).

In a few samples both types of transport by water – the older one with, and the younger one without strong chemical weathering in their wake – can be distinguished. This refers to the western transverse draa (nos. 49/00, 52/00) and to two surface sands from the longitudinal draa in the middle (nos. 12/99, 18/99, the latter uncertain). Between these transport phases, the sands spent a long time in a desert environment because all conchoidal fracture surfaces with silica solution and precipitation along cleavage lines are extremely smoothed.

Before the first desert environment, the healing features on the breakage surfaces indicate a (tropical) seasonally humid climate after deposition, however. Supporting evidence for strong weathering or pedogenesis at this time are silica precipitations in the flow structure found on some fracture surfaces in the western transverse draa (nos. 49/00, 52/00) and on surface-sand grains from the longitudinal draa (no. 18/99) in the middle transection. In addition, silica-flower precipitation occurred in some samples after the healing along the conchoidal lines (nos. 12/99, 52/00). According to Le Ribault (1977), both features are diagnostic for the pedogenic B-horizon.

A strange curiosity, found in the surface sand at Willmann's Camp (no. 3/00), deserves to be mentioned. A well rounded and smoothed quartz grain shows 70–80  $\mu\text{m}$  long scratches on the surface with pushed-up flakes at one end. The peaks in the X-ray spectra diagnose only Fe, Cr, Ni in the flakes and only Si in the surroundings. The associated features resemble an oblique micro-impact of an extraterrestrial body. Perhaps this – like the silica glass in the area – represents a legacy of the Tertiary event referred to in Section 3.3.1 (Fig. 65).

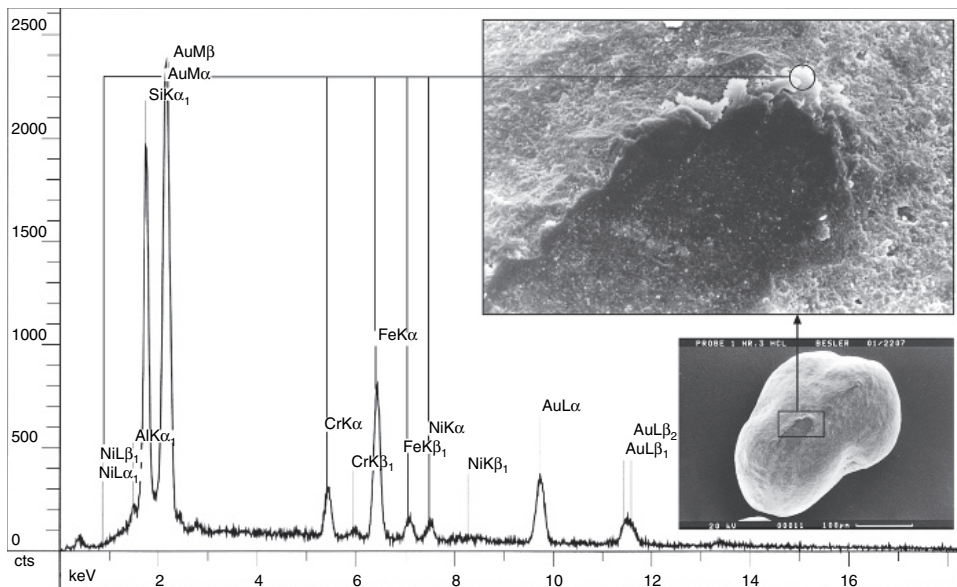


**Fig. 65** Quartz grain (treated with HCl) with a detail from the surface sand at the coring site at Willmann's Camp in the western transection (sample no. 3/00). The energy-dispersive X-ray spectrum indicates Si, Fe, Cr and Ni in the pushed-up flakes, and elsewhere only Si.

### 8.6.3.2. Major differences

The sands along the western transection underwent the heaviest early chemical alteration – tropical according to Tietz (1987, 2005) – before the transport by water. The healing of feldspar moulds, resembling strongly the solution pits in the Gilf Kebir Sandstone, is visible in the surface sand from the western slope of the longitudinal draa of the western transection ( $25^{\circ}42'N$ ). This provides additional evidence of a southwestern alluvial fan and its northern extent. The healing features in the western transverse draa are different.

Early stages of transport by water, with subsequent healing of fracture surfaces under tropical climatic conditions, can be identified in the interior of the western transverse draa and on surface sands of the middle longitudinal draa, in both cases with traces of additional pedogenesis. The surface sands are less significant, because they may partly have been transported over longer distances by winds during the Holocene. Where only early transport by water is identified, it may be assumed that these sands reached the wider area of the Great Sand Sea earlier than the other sands. This refers to the sands from the southern part of the western transection, where the healing structures of feldspar solution in the Gilf Kebir Sandstone were found.

Sands indicating exclusively later transport by water, with only desert smoothing on the fracture surfaces, are more widely distributed and found in longitudinal and transverse draa.

### 8.6.3.3. The southwestern sand source

There is abundant evidence of a southwestern sand source in the Gilf Kebir Plateau and adjacent highlands. Important indications are the topography and morphology of the southwestern sand sea (channels, broad irregular interdraa corridors with gravel deposits: Sections 3.1 and 3.2), the highest sand budget (Section 3.4), and the granulometry of draa sands (negative skewness: Section 4.2.3). The heritage of the aeolianite facies in the Gilf Kebir Sandstone is particularly obvious in the granulometry: the smallest mean grain size occurs in dunes and draa (Section 4.2.1), the best sorting in dune and draa sands (Section 4.2.2), leptokurtosis is present in draa sands (Section 4.2.4), and the granulometric types of (in)active crest sands in the draa (Section 4.3.1), are the same as in the sandstone (Section 4.3.3). Additional evidence is provided by the reddish colour (7.5 YR) of draa and dune sands (Section 6.2.2.1) and by the characteristic healing structures of feldspar moulds that exist in quartz grains of the aeolianite (Section 8.6.3.1). A Gilf Kebir river running towards the area of the sand sea was already suggested by Kröpelin (1993) and Embabi (1998), and can now be taken for sure. Pachur and Altmann (2006) even assume that Miocene streams from the Gilf Kebir and the adjacent Abu Ras Plateau have been the major sand source for the entire Great Sand Sea. There exists, however, evidence that contradicts this assumption (see Sections 8.6.3.4 and 8.6.3.5).

Even the size and extent of the alluvial fan related to this river can now be reconstructed. With regard to the southward transport of sands during draa and, particularly, dune formation, the cumulative evidence indicates that the fan reached at least  $26^{\circ}$ – $26^{\circ}30'N$ . The evidence is formed by the irregular corridors (Section 3.2:  $26^{\circ}10'N$ ), the northernmost transverse dunes indicating a positive budget of fine sands (Section 3.3.2:  $25^{\circ}48'N$ ), a sudden increase in mean grain size towards

the north (Section 4.2.1: 26°06'N), the granulometric type of old barchan sands north of 26°N (Section 4.3.2), the granulometric type of ridge sands in the corridor (Section 4.3.2: 26°25'36''N), reddish sands extending to 25°18'N (Section 6.2.2.1), and bi-coloured sands to 25°36'N (Section 6.2.2.4). Moreover, the healing structures of feldspar moulds in quartz grains were identified at the drilling site (25°42'N) in the western transection (Section 8.6.3.1). Additional support comes from the radiocarbon dating of Pleistocene humid environments by Pachur (Pachur and Braun, 1986; Pachur et al., 1987; Pachur, 1993), and – most important – Pachur and Altmann (2006). As already mentioned in Section 5.4, their lacustrine deposits cluster at two localities and cover the time span of 33–19 ka in the southwest, and of 36–20 ka in the east. The southwestern concentration of dated deposits (between 25°30'N, 26°E and 25°53'N, 26°08'E) is situated close to the northeastern margin of the reconstructed alluvial fan (see Fig. 66) and gives support to the following scenario: the younger discharge from the Gilf Kebir occurred in the subsurface as a groundwater stream in the alluvium. This would even have been possible below already existent draa. The groundwater stream reached the surface where the deposits are thinning out, and a nearby impermeable bedrock led to the formation of lakes. In fact, comparable processes can be observed in the Taklamakan Sand Sea today, where the marginal oases are not directly fed by the meltwater streams from the Kun Lun Shan Mountains, but by groundwater outflow below the dunes at the distal end of the huge alluvial fans (Hövermann and Hövermann, 1991).

From the low proportion of blown sand in the Pleistocene lacustrine deposits, Pachur and Altmann (2006) conclude that the lakes possessed a reed belt and/or that the draa were vegetated. They would have preferred a Holocene age of these lakes and therefore suggest a possible contamination by calcareous dust blown out of Tertiary sediments. Indeed, these sites most probably were also suitable for the formation of wetter islands during the Holocene climatic optimum. This opens the door for a third possibility that cannot be excluded according to Pachur and Altmann, i.e. that the deposits were rejuvenated by younger rhizomes.

With regard to age and history of the alluvial deposits, at least reasonable assumptions can be made. Sands were provided several times during a long time span. The supply started at a time when healing of feldspar moulds in quartz grains and healing along conchoidal lines of fracture surfaces was still possible after deposition in a tropical climate with dry and rainy seasons (no. 28/00). The sand supply went on after aridization, when the fracture surfaces of the sand grains were only smoothed and perhaps subjected to beginning pedogenesis (no. 3/00). Support for earlier fluvial deposits also comes from the total heavy-mineral content (Section 7.1), indicating a wet cycle of decay and redeposition.

This corroborates the Oligocene/Miocene age suggested by Embabi (1998) or the Middle to Late Tertiary age assumed by Kröpelin (1993), as well as the Miocene age assumed by Pachur and Altmann (2006). At that time, rubification processes could already have reddened the sands after their deposition. In this context, the morphoscopic analysis is valuable because – contrary to what can be observed from SEM photographs – colours are visible; about a hundred grains per sample were observed this way. The scanned sands from the longitudinal draa in the western transection and a few of the draa in the middle transection bear red stains of iron

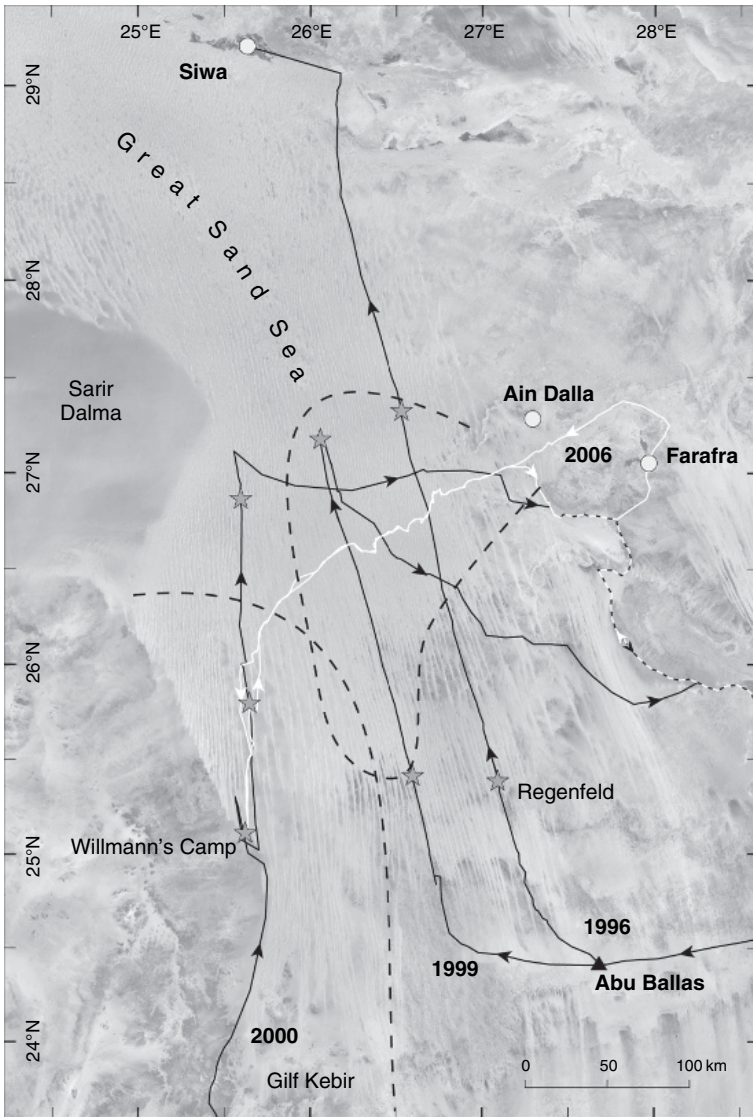


**Fig. 66** Tentative reconstruction of alluvial fans: broken lines indicate their minimum extent according to a combination of data from sedimentary analysis.

oxides, particularly in depressions, which could be the residue of thicker coatings. Only the sands from Willmann's Camp, however, have an additional yellow hue. The conclusion is therefore justified that the stains were inherited from the sandstone and that the yellowish hue developed in the alluvial deposits. Comparable situations have been observed in the Namib Erg (Besler, 1980; see also Section 6.2.1).

One should keep in mind, however, that this does not exclude later deposition during humid time intervals of the Pleistocene (Section 8.6.3.1). The alluvial fan seems to have been active for a long time, during which the climate became more arid. Evidence is provided by the lateral and vertical inversion of gradation usually observed during aridization (Section 3.2). This also explains why the same granulometry as that of the Gilf Kebir aeolianite is found in the southwestern draa. The abundance of fine-grained sands in the southwest must have resulted from fan regression when the area became more arid. This could also explain the negative skewness in the draa sands (Section 4.2.3).

It has to be mentioned that the tentative reconstruction of alluvial fans from sedimentary evidence (Fig. 66) had been completed long before the map of potential drainage systems (Fig. 18) was contributed to Chapter 3 by Bubenzer and Bolten. Regarding the eastern boundary of the alluvial fan, a remarkable similarity exists between the sedimentary reconstruction and the palaeo-watershed derived from digital elevation data. The northern sedimentary boundary of the fan (minimum extent) is not found on the drainage map. This is most probably due to the fact that the sands were transported southward during draa and dune formation.

#### 8.6.3.4. The eastern sand source

The evidence of an eastern alluvial fan is less extensive than for the southwestern sand source. Nevertheless, some evidence is provided by the second highest sand budget in the eastern transverse draa (Section 3.4) and by the coarsest mean grain size in this region (Section 4.2.1). In addition, the positive statistical correlation between draa width and geographical latitude along the middle transection indicates a northern sand source in the area of the transverse draa (Section 3.2.1, see below).

Surface features are not easily detected in the eastern sand sea. However, on LANDSAT 5 images (Fig. 66), a sandy, delta-shaped valley can be seen east of the Great Sand Sea, south of Ain Dalla. In the exact prolongation of its left (southeastern) bank into the sand sea (direction of 220°), the bare corridors of the south change fairly abruptly into sandy corridors. This line, which could represent the margin of an ancient alluvial fan, reaches the middle transection around 26°N. It is even more obvious on respective sheets of the geological map 1:500 000 (Klitzsch et al., 1986–87). The mean grain size of the transverse draa in the middle transection, which is still coarser than in the west (Section 4.1.1), indicates that the eastern sands reached at least 26°E. In this context, it is very interesting that the eastern cluster of Pleistocene lacustrine deposits with ages between 36 and 20 ka on the map by Pachur and Altmann (2006) is situated between 26°21'N, 26°16'E and 26°45'N, 26°32'E. This location represents the distal centre of the reconstructed alluvial fan. The same process of groundwater flow and outlet as for the southwestern fan (see Section 8.6.3.3) can be assumed here. In addition, the fluctuating groundwater table deduced from NaCl crystallization and dissolution found only in the drilling in the transverse draa on the eastern transection (see Section 8.6.2) may be related to this groundwater course.

Southeast of the valley, the approximately 150 m high plateau of El Quss Abu Said consists of Tertiary formations; these are mainly limestones comparable to the Tertiary and Cretaceous formations in the neighbourhood. In the southwestern part of the plateau, however, remnants of the post-Miocene Minqar El-Talh Formation

are found; according to the Geological Map of Egypt (Klitzsch et al., 1987), this is a continental to lacustrine sandstone. Erosion remnants of this sandstone are shown on the map also farther south ( $26^{\circ}$ – $26^{\circ}30'N$ ) and farther north, directly bordering the sand sea (around  $28^{\circ}N$ ). During the survey, small outcrops were even found in the corridor of the eastern transection (Section 3.1). The scattered remnants show that this sandstone once has covered a large area. As the last (upper) unit of the Tertiary succession, it was most probably eroded rather early.

Supporting evidence for this sandstone as a source rock comes from comparison between the granulometric type of ridge sands in the eastern and central draa on the one hand, and that in the sandstone on the other hand (Sections 4.3.1 and 4.3.3). Moreover, the sandstone contains the same heavy-mineral assemblage as the draa sands (Besler, 1998). The area of the Siwa Depression in the north can be excluded as an ancient sand source because the various heavy minerals of its local sandstone are found only in younger dunes (Section 7.2).

Compared to the southwest, the sands of the eastern alluvial fan were deposited later, at a time when chemical weathering was not very strong and when the climate was more arid. This is obvious from the smoothed fracture surfaces that do not show much chemical alteration (Section 8.5.3.1). The same fractures exist in all samples from the transverse draa in the middle transection, which supports the western extent that was deduced from the mean grain size. The assumption is corroborated by the total heavy-mineral content, which is conspicuously lower in the sandstone than in the draa sands, indicating a “dry” cycle of decay and re-deposition (Besler, 1995, 1996b; Besler and Pfeiffer, 1995, in Section 7.1). Of course, transport from the highlands took place by currents, but the weathering may have been dominated by mechanical disintegration of the sandstone. Thus, the conditions may have been comparable to the situation found in the Namib Erg (Besler, 1980).

The boundaries of the eastern alluvial fan according to sedimentary evidence (Fig. 66) are supported by the palaeo-watersheds on the digital drainage map (Fig. 18), at least in the middle part of the sand sea. Between Ain Dalla and El Quss Abu Said, however, the drainage on the latter map is directed towards Farafra which means a reversal of drainage orientation in the proximal part of the fan. In this context it has to be born in mind, that the reconstruction of drainage systems by digital elevation data reflects the gradients (immediately) before draa formation, and in the case of bare interdraa corridors even the gradients before alluvial deposition. The deposition of the fan material, however, must have started at a time when the high El Quss Abu Said Plateau was still covered by the Minqar El-Talh Sandstone, and the whole area east of the later sand sea was not eroded yet. A reorientation of channels and changes in gradients of alluvial fans after primary deposition are quite common. Many thousand years may have passed between the fluvial deposition of the sands and the draa formation.

#### 8.6.3.5. The western sand source

Geomorphological evidence for a western alluvial fan is provided by the gravel plain (Sarir Dalma) extending tongue-like from the west (Section 3.1), the eastward following uniform sand plateau (Section 3.2.2) and the gravel patches in grooves between the transverse draa in the west (Section 5.1). Additional support comes

from the amount of sand, which is higher in the west than in the middle sand sea (Section 3.4). Most important is that here two phases of current activity are recorded in the sands (nos. 49/00, 52/00). They are also found in the southern middle transection (nos. 12/99, 18/99), but only in the less indicative surface sands that could have been transported southward by northerly Holocene winds (see evidence along the eastern transection in Sections 7.2 and 8.6.1.2.1).

This leaves the western sand source as the one with the longest history. The particularly pronounced surface etching of quartz grains including healing structures of advanced stages (Section 8.6.3.1), already mentioned for the southwestern sand source, is also present here. It indicates a sedimentary rock source that was subjected to tropical weathering. The first transport of the sand grains by currents generated conchoidal fracture surfaces which show etching and healing features along the conchoidal lines. The latter indicates a still tropical climate after the first deposition. Chemical weathering in this sediment is also shown by pedogenic features. After the exposure to pedogenesis, a long time of desert conditions prevailed, which the sands spent somewhere outside the Great Sand Sea. This explains the leptokurtosis in the sands, which was surprising at first (Section 4.2.4). Before reaching the Great Sand Sea (Sarir Dalma and western sands) with the second phase of current activity, these sands had been pre-sorted in an aeolian environment. Meanwhile, in spite of the current activity, the climate must have become more arid, as indicated by the smoother fracture surfaces.

To answer the question of where these sands originated, several works of Pachur are of interest. In all these works, Pachur is mainly interested in the Early Holocene climatic optimum, but he assumes that the Holocene run-off most probably followed older discharge patterns which had already been established during the Late Tertiary. In 1993, he suggested a discharge from the northeastern Tibesti Mountains via the Kufrah Oases into the Sarir Dalma, where drainage lines running approximately south–north can be detected on Earth Resources Technology Satellite (ERTS) imagery (photo 2 in Pachur, 1982). Large-scale deposition along this route should have left traces like gravel plains or *serir/sarir* (the Arabic term) from where the sands could have been blown out in their first (long-time) desert environment. On some maps, a *Serir Chiapo* is mentioned south of the Kufrah Oases.

A more plausible alternative can be reconstructed following Pachur's (1974) investigation of the Sarir Tibesti. In an earlier investigation (Fürst, 1966), the Sarir Tibesti had been characterized as a horseshoe-shaped gravel and sand plain north of the Tibesti Mountains, with a gradient of 0.1% towards the northeast. The deposits were supplied by streams from the Tibesti Mountains and the Egheï Mountains in the southeast, and later reworked in an aeolian environment. The influence of the latter and the quartz content in the sands increase towards the north. Pachur distinguished between oldest, older and younger alluvial deposits. He assumed the oldest, rubified deposits to be of post-Late Eocene age. The older deposits, unfortunately not dated, reached the Serir Calanscio. On the map by Pachur et al. (1987), the wadi Behar Belama, originating in the Tibesti Mountains, is heading northeast, crossing the Serir Calanscio and ending close to the Calanscio Sand Sea.

With regard to the source sands of the Great Sand Sea, the following history is suggested. This transport from the Tibesti/Egheï Mountains into the Sarir



Calanscio by water could have been the first phase of current activity while tropical weathering affected the coarser deposits in the Sarir Calanscio and the finer sands in the area of the Calanscio Sand Sea. After aridization, a long aeolian phase reworked the sands into the older draa or dunes of the Calanscio Sand Sea. According to Hecht et al. (1964), aeolian and subaqueous sands alternate repeatedly below the Calanscio Sand Sea, and three aeolian cycles are suggested. A Pleistocene wet phase may have resulted in the second phase of currents transporting sands into the Sarir Dalma and adjacent parts of the Great Sand Sea. Fossil drainage lines beneath the present Calanscio Sand Sea, that support this hypothesis, have been mentioned (Pachur, 1974). Although they are heading in northern directions in Pachur's (1974) Fig. 9, the author mentions a gradient towards the northeast in his text. During the last long phase of desert conditions, the sands were incorporated in the draa of the Great Sand Sea by the trade winds and by subsequent strong extratropical westerlies. In the recently published book by Pachur and Altmann (2006), a whole subsection (Section 2.4.3.3.6) is dedicated to the formation of the Sarir Dalma. Although the main interest again focuses on the Holocene processes, terrace remnants of a former alluvial cover of the Sarir Dalma are surmised to be of Late Pleistocene age. These remnants, as well as the terraces near the Jabal Dalmah in the south, are covered by gravels that – according to their size and their imbricate bedding – were deposited in a high-energy current. A long-distance transport is concluded from the results of a thin-section analysis. Suggested sand-source areas are the East Kufrah rise and lastly the Tibesti Mountains. The sandstones of Jabal Dalmah are considered as a possible additional source. The lack of draa and dunes in the Sarir Dalma, that is almost completely surrounded by sand seas, is explained as the result of flooding which has washed away the blown sands.

Thus, in both scenarios, the Tibesti Mountains play a vital role, whether the sands were transported by water currents via the Sarir Tibesti and the Sarir Calanscio to the Sarir Dalma or via the East Kufrah rise to the Sarir Dalma.

The drainage pattern on the map of potential drainage systems (Fig. 18) includes the area around the Sarir Dalma and adds it to the southwestern alluvial fan from the Gilf Kebir. On the other hand, however, the drainage lines depict the convex shape of the sarir surface since they run from the centre to the edge and all along the eastern margin. It may well be that an older drainage pattern directed from the Sarir Dalma towards the east has been captured by the channels from the Gilf Kebir.

There is a striking series of gravel plains and sand seas alternating from west to east around 27°N: Sarir Calanscio, Calanscio Sand Sea, Sarir Dalma, Great Sand Sea. On satellite imagery, this looks as if the sand seas represent the downwind areas of the respective gravel plains, supporting strong westerlies (see Section 3.2.2). Contrary to the other sand sources, however, there is no clear evidence for the origin of the western sands.

#### 8.6.3.6. Sand sources for the southern middle sand sea

The large proportions of platykurtic sands in the interior draa of the middle transection (Section 4.2.4) indicate a poor mixing of sands from various sources, not yet adjusted to the aeolian environment. According to Table 4 in Section 4.2.1, this is also true for the northern transverse draa. Here, an overlap of alluvial fans

from the west and from the east seems most probable (see Sections 8.6.3.4 and 8.6.3.5). The sorting, however, is much poorer in the longitudinal than in the transverse draa (the eastern longitudinal draa are not considered because of too few samples). In the southern middle sand sea, indications exist that alluvial material from the western and the eastern sand sources as well as local sandstones contributed to the sands contained in the longitudinal draa.

There is no clear evidence of the contribution of the southwestern sand source (see also Fig. 18). The evidence for a western source is less convincing because the evidence of two phases of current activity was found only in surface samples (nos. 12/99, 18/99) from the eastern slope (Section 8.6.2.2), which could have been blown southwards by northerly Holocene winds. A contribution of the eastern sand source seems reasonable because the fan margin can be seen on satellite imagery to almost reach this area (Section 8.6.3.4). Moreover, the total heavy-mineral content decreases here towards the north (Section 7.1), which is in agreement with the extremely low value in the Minqar el-Talh Sandstone.

On the other hand, there are indications that local sandstones have contributed material. This could also be a reason for the mentioned differences in the total heavy-mineral content (Section 7.1). In addition, at least part of the reddish sands seem to have been inherited from the red Taref Sandstone (Sections 6.2.2.2 and 6.2.2.4).

The individual contributions of the various sand sources to the southern middle sand sea cannot be traced with certainty. However, overlapping alluvial fans (after the rather low palaeo-watershed had been buried) and local sandstones were most probably involved in the sand supply.

## 8.7. THE QUESTION OF EARLIER CYCLES OF DRAA/DUNE FORMATION

The environmental developments of the Great Sand Sea so far have been reconstructed without considering the possibility of repeated earlier cycles of draa/dune formation and intercalated humid periods or pluvials. The existence of several phases of sand transport by currents, as deduced from the SEM analysis, may, however, indirectly imply this possibility.

Several cycles of subaqueous and aeolian deposition are known from other sand seas (e.g. the Wahibah Sands in Oman: Juyal et al., 1998). In the Sahara, the Awbariy and Murzuq Sand Seas in Libya are good examples. Four pluvials have been dated in lacustrine carbonates with the  $^{230}\text{Th}/\text{U}$  thermal ionization mass spectrometry (TIMS) method: they occurred between 500 and 90 ka ago (Thiedig, 2005). Each of them started several thousands of years before the end of a glacial and ended during the maximum of the subsequent interglacial, when aeolian transport became dominant and dunefields (draa?) were built up. The author emphasizes that landslides occurred and even boulders were fluvially transported (Thiedig, 2005).

A topographic comparison shows the different situation of the Murzuq Basin, which is surrounded by high mountain ranges. The Great Sand Sea is only bordered

by relatively low terrain – especially in the western part – and therefore the explanation of grain-surface microfeatures as a result of repeated turbulent-flow features here would be difficult. It is therefore assumed that these features were generated somewhere else.

Theoretically, the younger fluvial activity could have bevelled the already existing draa or dunes, because the features of earlier tropical weathering are much more smoothed by desert-dew cycles than the younger fracture surfaces. In the case of two phases of sand transport by water currents, this was supposed to have happened in a desert environment outside the Great Sand Sea. These samples are, however of subordinate importance. On the other hand, smoothing in concavities is normally less strong than on the grain edges. The possibility that repeated fluvial input from the Gilf Kebir and adjacent highlands occurred during different pluvials with a long dune-building phase in between, has also to be considered. This could not explain, however, that older and younger fractures are found in the same grains. The possibility that the younger fractures are the result of a fluvial revival of drainage patterns in the area without a renewed input can be excluded, because the current would not have been turbulent. Only remnants of organic matter indicating a low-energy fluvial environment would suit this scenario. Unfortunately, such occurrences are very rare.

As already mentioned in Section 5.3.1, no direct traces of older draa patterns were found during the field work. In this context, it is important to have a closer look at the consolidated yardang sediment in the interdrea valley of the Desert Glass Area (see Section 4.4). The small-scale cross-bedding and the granulometric type of inactive crest sands are evidence for an aeolian deposit. The rather high clay/silt content can be ascribed to pedogenic processes, which seem to be indicated by a grey and aggregated upper horizon. Moreover, a minimum in the fraction of the finest sand (63–125  $\mu\text{m}$ ) shows that the clay/silt content was not present at the time of aeolian deposition. On the other hand, the upper horizons could also be the legacy of an old playa that existed on top of this sediment. This seems possible because playa remnants at the base of the eastern draa have the same level as the grey yardang top. Could this be a relict of older draa or dunes, perhaps even corresponding to the indurated dune sands mentioned by Pachur and Röper (1984)? Unfortunately, the granulometric type of inactive crest sands is found in draa as well as in dunes. It could also belong to the present-day draa which here, in the southwest, seem to have been cut off along a straight line by fluvial erosion. The response diagram reveals, however, the great similarity between this sediment and the Taref Sandstone (see Section 4.4). The Gilf Kebir Sandstone seems unlikely to be the parent material. Comparable yardang-like deposits in the southern sand sea north of the Gilf Kebir Plateau are described as psammitic–pelitic playa sediments by Pachur and Altmann (2006; their Fig. 2.6.80).

Taken all together, there is no clear evidence of older draa/dune generations. Two possibilities remain: first, tiny remnants could be hidden beneath the present-day draa; second, they may be found below the northwestern sand sea, where several hundreds of metres of sands fill a bedrock depression (see Section 3.1). According to Pachur and Altmann (2006), the stratigraphic record in the mentioned test well shows alternating aeolian and fluvial clastics.

## THE HISTORY OF THE GREAT SAND SEA COMPARED TO THAT OF OTHER ACTIVE ERGS

### Contents

9.1. Sand Sources and Their Influence	195
9.2. Draa Patterns and Draa Formation	197
9.3. Time Slices of Draa Formation and Reworking	202
9.4. Conditions During the Holocene Climatic Optimum	206
9.5. The Final Aridization	208

### 9.1. SAND SOURCES AND THEIR INFLUENCE

Aufrère (1932) has presented three hypotheses concerning the sand sources of ergs. According to his hypothesis of “dune ingression”, ergs are sedimentary basins of allochthonous aeolian sands. According to the hypothesis of “dune cycles”, in situ weathering of rocks and detritus in depressions play the major part. The hypothesis of “dune transgression” was based on observations of the Great Western Erg in Algeria, which is intruding into the Wadi Saoura, and of the “Libyan Erg”, which was supposed to house dunes composed of sands from the Qattara Depression near the Egyptian coast. Although the Qattara Depression lies in a (palaeo-) upwind direction of the Great Sand Sea, there is not the slightest evidence for this source. Not even the closer Siwa Depression in the north seems to have contributed sands during the Pleistocene (see Section 7.2). In situ decay of sandstones, however, played a minor part (Section 8.6.3.6).

Most authors (a.o. Wilson, 1971, 1973) agree that alluvial fans of large endorheic stream systems are a source. Gautier (1950) saw the Great Eastern Erg in Algeria as the legacy of the Wadi Irharrhar from the Hoggar Mountains, and the Great Western Erg as the heritage of the Wadi Saoura from the Atlas Mountains. In fact, the sands of the latter have their origin in the Jurassic and Cretaceous sandstones of the Sahara Atlas (Callot, 1998). No large streams reached the area of the later Great Sand Sea. In this respect, its position resembles more the Idhan Murzuq, where several smaller channels from the surrounding mountainous areas enter the almost closed depression, which is tectonically induced (Capot-Rey, 1947). As already mentioned, however, the highlands around the Great Sand Sea are much lower and only border it to the east and to

the southwest, from where numerous palaeo-channels have been mentioned by El-Baz et al. (2000). Indeed, sand sources from both directions have supplied alluvial material for the area of the later sand sea. This happened at different times, beginning in the Late Tertiary or during Early Pleistocene pluvials with a quasi-tropical climate. It occurred again during more humid time intervals in the later Pleistocene and ended during the Holocene climatic optimum.

In the southwest, the Gilf Kebir and adjacent highlands were parent regions of earliest to latest sediment input, which changed from pebbles to very fine sands, along with the decreasing fluvial transport capacity through time. A large proportion of the sands was derived from the aeolianites of the Gilf Kebir Sandstone. In comparison to the other sand sources, the nature and extent of these alluvial deposits are documented well (Section 8.6.3.3).

The alluvial input from the eastern highlands seems to have occurred later, under more arid conditions, and seems to have ceased earlier, already before the Holocene. Most probably, the major parent rock was the post-Miocene Minqar el-Talh Sandstone that was eroded in most places. The traces of a former alluvial fan can be tracked up to the middle part of the sand sea (Section 8.6.3.4).

At more or less the same time, large amounts of alluvial particles were supplied by a western source. These sand-sized particles had spent a long time in an aeolian environment elsewhere before reaching the area of the later sand sea. Their original source is assumed to have been far away, perhaps in the Tibesti region (Section 8.6.3.5).

Detailed investigations of the sand sources of ergs are rather rare. In this context, a comparison between the Namib Erg (northern part) and the Wahibah Sands in Oman, that look very similar on satellite images, is of interest. In the Namib Erg, all three major possibilities of sand supply play a role: marine sands near the coast, sandstone weathering (aeolianites) mainly in the east and alluvial fans of channels reaching the central part from the Great Escarpment (Besler, 1980, 1984a). The main source, however, seems to have been the aeolianite of the Tsondeb Sandstone (Besler and Pfeiffer, 1995; Besler, 1996b; Bubenzer et al., 2007a). In the Wahibah Sands, on the other hand, most sands seem to have been derived from marine sources in the south. Materials from the mountains were brought by streams to the coast before entering the erg. Apart from later cycles, obviously, reworking of aeolianites played a minor part here (Allison, 1988).

The largest sand sea of the world, the Rub' al Khali in Arabia that covers 600 000 km<sup>2</sup>, represents one giant alluvial fan sloping ENE from the Al-Hijaz Plateau in the west. Most sands stem from Palaeozoic and Mesozoic sandstones (Chapman, 1978; McClure, 1978). Edgell (2006) has stated that alluvium (frequently carbonate material) from the once dried up or shrunken Arabian Gulf was blown southwards. This is most probably true for the northeastern Rub' al Khali, where subangular sands from the Oman Mountains were additionally incorporated (Besler, 1982). Nevertheless, Edgell described gravel plains surrounding the southwestern Rub' al Khali and gravel strips entering the sand sea, which supports the hypothesis of supply from an alluvial fan in the west (McClure, 1978).

The other extreme seems to be represented by the Taklamakan Sand Sea in China. Topographically situated in an almost closed tectonic basin with the high Kun Lun Shan Ranges to the south and the Tian Shan Mountains to the north, it resembles the Idhan Murzuq. Numerous channels provide material from almost all

directions, and the sand sea in the depression consists of quite a number of separate draa/dunefields of different ages (Jäkel, 1991; Besler, 1995). Again, sandstones are important sources.

Considering all mentioned sand seas together, sandstones of Palaeozoic (e.g. Rub' al Khali) to Tertiary age (e.g. Namib Erg) seem to be their major sand source. In most cases, the sands were transported by streams and deposited on alluvial fans. The Great Sand Sea in Egypt fits well into this frame. Only the Wahibah Sands in Oman seem to be an exception.

The different source materials influenced the subsequent aeolian modelling of the Great Sand Sea to varying degrees. This legacy is strongest in the southwest, where not only the particular draa pattern and the sand colour are a result, but even the Holocene dunes – via the granulometry – still bear part of the heritage.

The importance of the source material for the later aeolian topography was already stressed by Capot-Rey (1970), referring to Bagnold: a high proportion of coarse sand, after deflation of the fine-grained component, results in sandy undulations, later called “zibar” (Cooke and Warren, 1973). Zibar in a strict sense (in dune corridors) are not found in the Great Sand Sea. Most probably, the sands are not sufficiently coarse-grained. There are, however, giant undulations on the draa perpendicular to the major modern winds (see Sections 3.2 and 3.3.4). According to Wilson (1973), the thickness of the former sand cover is related to the heights of draa and partly to their wavelength. In this context, the sand cover does not seem to have been very thick in the area of the Great Sand Sea, particularly not where the interdraa corridors are bare. As already stated (Section 3.2.1), however, the draa have usually been flattened by processes under different subsequent climatic conditions. With regard to the wavelength, it seems to be rather the grain size (gravels) that caused a disruption in the uniform draa pattern in the southwest (see Sections 3.1 and 3.2.1).



## 9.2. DRAA PATTERNS AND DRAA FORMATION

All larger sand seas of the world consist of draa, which are always of Pleistocene age. In the more recent literature, the term “megadunes” is commonly applied instead (a.o. Warren, 1988). In older literature, no distinction was made between draa and dunes. Therefore, confusing interpretations result, or the bedforms cannot be explained at all. In most cases, however, dimensions and spacings are mentioned, allowing some conclusions as to whether draa or dunes are referred to.

Aufrère (1932) already stated that the parallel sand ridges in the western Sahara normally follow the direction of the trade winds. In the Erg Chech in Algeria and in the Erg Ouarane in Mauritania, the widely spaced “dunes” run ENE–WSW (Brosset, 1939). The area west of the Erg Ouarane in Mauritania was investigated by Lancaster et al. (2002) more recently. They differentiate between NE-directed large degraded linear ridges, NNE-aligned moderate-sized linear dunes with active crests, and N-running small linear dunes. The smaller forms are superimposed on the larger ones. According to their dimensions, at least the first generation consists

of draa (spacings of 1–3 km). The direction (NE) is not exactly the same as farther to the east (ENE) as mentioned by Brosset; both directions are, however, consistent with the trade winds. Michel (1977) already called the sand ridges in southern Mauritania that had blocked the Senegal River “large dunes of the trade winds”. He stated that they consist of colluvial to alluvial material that has not been transported far by the wind, which is consistent with the helical-vortex model (Section 3.2).

In the Great Western Erg in Algeria, the parallel ridges run NW–SE in the northern part and NE–SW in the southern part (Capot-Rey, 1945). They follow, nevertheless, the wind directions according to this author. It should be mentioned that modern westerly winds are dominant here during the winter. A more recent and detailed investigation of this sand sea by Callot (1998) corroborates the directions, but also indicates that a N–S direction becomes more dominant in the middle part towards the west. Because the N–S direction is partly superimposed on the other directions, these are assumed to belong to an older erg. Indeed, the rows of sand domes in the northeastern sand sea, veering from NW–SE to N–S, show spacings of around 3 km on a SPOT image (see Fig. 3 in Callot, 1998), thus representing draa of Pleistocene age. Unfortunately, Callot (1998) did not mention any dimensions of the other “dune” types. At least the eastern part of the NE–SW–running sand ridges in the south seem to carry superimposed dunes as well, and may have draa dimensions. Callot suggested a Plio-Pleistocene age for the larger aeolian structures and stated that their stability cannot be explained.

Although the Great Eastern Erg, because of its mostly sand-free corridors, is much more accessible than the Great Western Erg, it has not been the subject of a general investigation of draa and dunes. The sand domes or star dunes (Arabic term: ghourd or rhourd), which possess dimensions and wavelengths at the draa scale, are most spectacular. They are approximately 1 km wide, have spacings of approximately 4 km and are aligned preferably NW–SE in the northern part and N–S in the southern part. Between 30°N and 30°30'N, both directions overlap, resulting in a network pattern with high nodes. The ghourds here are not single star-shaped complexes but resemble double stars connected by a linear roof-like ridge. These short ridges are always aligned W–E, which means almost in the draa direction in the north, but perpendicular to it in the south. The following hypothesis has been put forward as a tentative explanation (Besler, 1987a): already in the Pleistocene, strong winds from westerly and northerly directions, i.e. the extratropical westerlies and the trade winds, alternated with the seasons. Each of the winds led to the formation of longitudinal helical vortices. This must have occurred each time during the same year because otherwise the feedback mechanism mentioned in Section 3.2 would have prevented the alteration of a linear draa system once it had been established. Only a seasonal change in the vortex system could have built the high nodes of the network over a longer time-span. This means that the westerlies seasonally reached as far south as 28°30'N.

In the central Sahara, Kanter (1943) found major sand ridges trending NE–SW in the eastern part, and N–S in other parts of the Idhan Murzuq, but W–E-aligned ridges in the Idhan Awbari (around 27°N). He could not understand this “disorientation” – as he called it – with regard to the trade-wind direction. Bellair (1951) found the trend to be WSW–ENE in the southern Awbari sand sea. McKee

and Tibbitts (1964), who investigated the Zallaf Sand Sea, which is an eastern extension of the Awbari erg, described sand ridges with approximately W–E directions and very wide corridors. Capot-Rey (1947) mentioned NE–SW-oriented sand ridges in the northern, ENE–WSW-aligned “dunes” in the eastern and WNW–ESE-aligned corridors and ridges in the western and southwestern parts of the Idhan Murzuq. Hagedorn, who unfortunately investigated only the western margin of the Murzuq sand sea, presented an air photo of these ridges (Fig. 1 in Hagedorn, 1979), which he called “giant transverse dunes”. The wavelength of 3–4 km and the wide dune-free corridors (1.5–2 km) identify this pattern as longitudinal draa in an approximate W–E direction. Indeed, the northern slopes are flattened nowadays, and the southern margins show small advancing dunes. This reworking is due, however, to the present-day trade winds. Hagedorn’s photo shows an area around 25°N. Even at this latitude, strong westerlies thus seem to have modelled longitudinal draa.

The 1:3 000 000 satellite-image map of the eastern Sahara in Pachur and Altmann (2006) offers a splendid overview of all sand seas and their draa in this region. Even the reworking of draa displayed on Hagedorn’s air photo can be identified. Moreover, in the northwestern part of the Idhan Murzuq, a small area of isolated star dunes or ghourd of draa dimensions, comparable to the Great Eastern Erg, is clearly recognizable. Their occurrence was already noticed in the remote-sensing investigation of the Libyan Sahara by Linsenbarth (1996), who called these features “pyramidal sand ridges”. If the hypothesis regarding their genesis is transferred to the Idhan Murzuq, it means that the efficacy of strong westerlies alternating with trade winds reached as far south as 25°30′N. The W–E-oriented draa at the western margin change to WNW–ESE directions farther south (as already mentioned by Capot-Rey, 1947). Although deviations from the trade-wind directions in the Idhan Murzuq occur only along the western margin, they occur in the Idhan Murzuq as far south as 24°N.

In this context, the observations of oriented features formed due to wind erosion in exposed solid rock during field trips in Algeria, Mali and Niger are of interest (Besler, 1987b). Westerly directions (SW–WNW) have been observed north of a line crossing Algeria from 30°N near Morocco in ESE direction to around 5°E, where the line bends southward to the Hoggar Mountains at around 24°N, from where it runs eastward. It should be mentioned, however, that the number of mapped abrasion features is rather small in relation to the vast area and that they are consistent with present-day meteorological data (i.e. winter winds).

The Idhan Awbari on the mentioned satellite-image map is dominated by longitudinal draa in the trade-wind direction. A W–E alignment, mentioned by Kanter (1943), is present only in the middle southern part. In his remote-sensing study, Linsenbarth (1996) called these sand ridges “longitudinal” and mentioned interdraa corridors of 1.2–1.6 km width. Towards the west, he observed dunes crossing the corridors obliquely, thus creating a grid pattern.

The Rebiana (Rabyanah) Sand Sea in southern Libya has been described by Klitzsch (1967) as consisting of sand ridges trending SW with spacings of 0.5–1.5 km, and by Kanter (1973) as possessing ridges and corridors – up to 3 km wide – in a NNE–SSW direction. Without any difficulty, these draa directions can be ascribed to the trade winds. The pattern is corroborated by the remote-sensing study of Linsenbarth (1996) and by the satellite-image map of Pachur and Altmann (2006).



In the Calanscio Sand Sea (eastern Libya), which covers an area at the same latitudes as the Great Sand Sea, the sand ridges are aligned NNE–SSW in the south and in the middle. The northern part is dominated by irregular dunes (Hecht et al., 1964) that are partly related to outcrops. These irregular dunes are, most probably, not draa, although no dimensions were given by Hecht et al. (1964). On satellite images (LANDSAT 5), the change from NNE–SSW structures to irregular patterns occurs around 27°N. A great variety of draa/dune directions and types was mapped from remote-sensing analysis by Linsenbarth (1996), who, unfortunately, called the Calanscio Sand Sea the Great Sand Sea. He differentiated between sand ridges (formed by helical vortices = draa) and dunes. In the description of the sand-sea morphology, however, he did not follow this distinction and mainly used the term “dunes”. This is also the case for the northern part of the Calanscio Sand Sea. Remarkably though, he described a drastic change in the sand-ridge pattern around 27°N. North of this latitude, the “dunes”/draa have an asymmetrical cross-section and are spaced at 1.5–3 km; south of it the spacing is larger (>3 km) and they seem to be symmetrical (a similar change as in the Great Sand Sea).

To sum up, there are only few regions where draa are found that do not follow the direction of trade winds. These are the utmost northeastern part of the Great Western Erg north of 31°N with rows of dome-shaped draa with a NW–SE orientation, the ghourd in the northern part of the Great Eastern Erg aligned approximately NW–SE north of 30°30′N, and the W–E-directed ridges in the southern Idhan Awbari and along the western margin of the Idhan Murzuq as far south as 24°N. Today, these regions are exposed to winter winds from westerly directions. According to the draa alignment, strong extratropical westerlies can be assumed to have been active here, also in the Pleistocene.

The marginal occurrence of longitudinal W–E draa in the Awbari Sand Sea (southern margin) and in the Idhan Murzuq (western margin) can be explained on the basis of the retreat of alluvial fans towards their proximal parts (as in the Great Sand Sea) during a less humid interval later in the Pleistocene. In this case, the younger fluvial deposits, merely reaching the edges of the basins that already contained the older trade-wind draa, could have been modelled by extratropical westerlies. Linsenbarth (1996), who also tried to explain the different draa directions, assumed that the formerly existing trade-wind ridges were partly destroyed by the pluvial activity that added the marginal alluvial sands. A pluvial obliteration of the pattern would, however, take an exceedingly long time. Many examples show that a once established draa pattern is not easily erased. The vegetated draa (“savane arbustive”) along the southern margin of the Sahara (e.g. in southern Mali and Burkina Faso) are 16 000–20 000 years old (Chamard and Courel, 1981). This region receives an annual precipitation of around 500 mm, and the draa are still very pronounced landform elements. Even the sand ridges that have been drowned in the Lake Mega Chad for several thousand years are still clearly visible after the retreat of the lake level, as the map of “dune” types by Grove and Warren (1968) shows.

The coincidence of dome draa and star-shaped draa of the same alignment in several ergs provokes the conclusion that the tentative model of seasonally shifting strong Pleistocene wind systems developed for the Great Eastern Erg may also be applied to the Great Western Erg and to the northwestern edge of the Idhan Murzuq.

The sand budgets, however, are very different. Whereas the corridors in the Great Eastern Erg are mostly bare – which seems to be also the case in the Idhan Murzuq – the dome draa in the Great Western Erg are much lower and arise from a thick sand cover with relatively small deflation depressions. Obviously, the draa-forming processes ended earlier here, whereas they went on in the Great Eastern Erg until all sands were eventually incorporated into the draa.

The Wahibah Sands in Oman are a good example of the rule that larger bedforms cannot be replaced by smaller bedforms but only modified (Warren, 1988): in the High Sands, the NE–SW-oriented mega-ridges with wavelengths of 1.4–3.3 km carry longitudinal meso-ridges with spacings of about 500 m on their flanks. It has to be pointed out that not the trade winds but dry monsoonal SW winds are supposed to have been the generating force here. On the mega-ridges, however, two types of transverse megadunes – with spacings of 500 m and 1 km, respectively – have been described. Even in the less conspicuous Low Sands, transverse megadunes with a wavelength of 1 km have been mentioned. The genesis and development of this very complex sand sea is not yet understood. Possibly, a more systematic investigation of the Saharan ergs may lead to the discovery of even more transverse draa.

In the northern Rub' al Khali (Chapman, 1978), transverse and longitudinal sand ridges occur, whereas straight longitudinal ridges with sharp crests and broad corridors are dominant in the centre and the western part. McClure (1978) stated that the sandy bedforms were mainly shaped *in situ*. According to Bagnold (1951), the longitudinal ridges can reach a width of 3 km (2 miles) at their base. On aerial photographs, the NE–SW-oriented ridges show wavelengths of 2–3 km. The sharp crests belong, of course, to superimposed Holocene dunes. Edgell (2006) stated that the “uruq” (the local name for draa) are remarkably uniform, but that the secondary dunes comprise different types. There is no clear evidence whether the NE trade winds or the SW monsoons – as in the Wahibah Sands – have shaped the draa in the southern Rub' al Khali. Bagnold mentioned that their SW ends are wide and look like rear sides.

In the northeastern Rub' al Khali, giant pyramidal or star dunes occur. Linked megabarchans are described as the highest dunes in this part of the Rub'. Complex barchanoid ridges form a great arc-shaped “dunefield” around the Liwa Oases (Edgell, 2006). According to investigations by the present author, these ridges are ancient longitudinal draa, most probably following winds around an anticyclonic pressure cell above the Oman Mountains. They were shaped into transverse barchanoid ridges by subsequent northerly winds. This is indicated by the regular, wide corridors, which are not present in transverse draa (Besler, 1982; see also Section 3.3.2). Interestingly, the local name of these ridges is also “uruq”, as for the straight longitudinal draa in the southwestern Rub' al Khali. Embabi (1991), who analysed “dune” types and patterns in the United Arab Emirates, using LANDSAT TM data, described these draa as “clustered megabarchans” with wavelengths of 0.8–2.3 km. They are overridden by faster moving small modern barchans that are fed by sands from the megaforms. Embabi suggested that the megabarchans have reached a state of equilibrium under the present wind system. Glennie (1991) even stated that a southward migration of the major slip faces in the large Al-Liwa “dunes” is not obvious.

Contrary to Arabia, there is evidence of trade winds having caused the formation of longitudinal draa in the Namib Erg, because the various alluvial sands of rivers ending in the sand sea have been subjected to aeolian transport towards the north. The draa with spacings of about 2 km run straight north in the northern part and NE in the southern part (Besler, 1980, 1984a). Whereas no break in slopes between draa and dunes is found in the north, the south looks very similar to the Great Sand Sea at comparable latitudes (Bubenzer et al., 2007). The transverse dunes along the coast, however, have a wavelength of about 1 km (particularly in the northern part) and could be regarded as draa resulting from strong southwesterly winds. This has not been investigated yet.

Among all ergs discussed above, the draa in the Taklamakan in China are most subdued. Draa as well as corridors are so extensively covered by modern dunes that in some parts they cannot be detected at all on aerial photographs. Also here, however, they are spaced at about 2 km. Their major directions are NE–SW, N–S in the east and NW–SE in the central southern part (Besler, 1991b, 1995). As already mentioned (Section 9.1), this sand sea consists of various draa fields of different ages, and nothing can be said about the palaeo-winds. Today, local winds play a major part. In any way, the position between 37°N and 41°N makes a comparison with the Great Sand Sea difficult as regards the wind systems involved.

The Great Sand Sea belongs in its southern part to the Saharan (even African) ergs of Pleistocene trade winds. A unique feature in the Sahara, so far, are the northern transverse draa of Pleistocene extratropical westerlies. At comparable latitudes, however, equivalent longitudinal draa directions exist in the Sahara. Up to now, transverse draa have been described only from the Wahibah Sands in Oman. In the Namib Erg, they are only interpreted as such on the basis of their wavelengths.



### 9.3. TIME SLICES OF DRAA FORMATION AND REWORKING

Direct datings of aeolian deposits are scarce because the luminescence-dating techniques were developed only during the last decades. The ages of aeolian sediments can be inferred indirectly if they are intercalated between materials that are datable by the radiocarbon method, such as the reddish aeolian sands between cultural layers at Regengefeld (see Section 6.2.2.3). Recently, these data were compiled for the whole Sahara and converted to BP cal ages by Swezey (2001), who used the calibration program CALIB 3.0.3c (detailed description in Stuiver and Reimer, 1993). Only very few cases, however, are connected with sand seas, because most investigations were carried out in environments more favourable for human occupation.

In Mauritania, the oldest generation of much degraded NE–SW ridges yielded OSL ages of 24–15 ka (Lancaster et al., 2002; see Table 21). The NNE-aligned younger ridges – which, according to their wavelength, lie around the threshold between draa and dunes (~900 m), but are also described as degraded and indurated – yielded OSL ages of 13–10 ka. This corroborates the assumption

**Table 21** Time slices of draa formation and reworking in selected active ergs

	<i>Draa</i>		<i>Reference</i>
	<i>Formation</i>	<i>Formation or reworking</i>	
Mauritania	>24–15 ka	13–10 ka	Lancaster et al., 2002
Erg Chech/Algeria	>21 ka	>11 ka	Swezey, 2001
Great Sand Sea/Egypt			Besler, 2002a
Longitudinal draa	>23–20 ka	12–10 ka	
Transverse draa	>20–12 ka		
Farafra Sand Sea/Egypt	>35–28 ka	~13 ka	Bubbenzer and Besler, 2005
Rub' al Khali/Arabia			
SW	>36 ka 17–9 ka		McClure, 1978
NE	>26 ka	>12 ka	Lancaster et al., 2003 (in Edgell, 2006)
Wahibah Sands/Oman	22–18 ka	13.5–10 ka	Goudie et al., 2000
S Namib Erg/Namibia	>24–17 ka	10–8.5 ka	Preusser et al., 2002 Bubbenzer et al., 2007a

of Michel (1977), who ascribed the “large dunes of the trade winds” in Mauritania to the Late Glacial (20–15 ka ago). Data comparable to the younger time interval of Lancaster et al. stem from the northern margin of the Erg Aouker in southern Mauritania, where aeolian sand was found intercalated between a lacustrine limestone underneath and a silty limestone on top. Diatomites of the lacustrine limestone were  $^{14}\text{C}$ -dated around 10 ka ago (Swezey, 2001). Unfortunately, this type of deposit in general cannot be correlated with draa-modelling time slices, even if it seems to fit into the time interval. Possibly, it was a single small dune invading a lake basin.

No direct datings exist for the Erg Chech in Algeria. Two data from aeolian deposits intercalated between datable units, however, are mentioned by Swezey (2001). They come from the wells of Kadda, where aeolian sand is overlain by lacustrine carbonates that were  $^{14}\text{C}$ -dated at around 21 and 11 ka. Although data from carbonates are not very reliable and tend to be too young (see Section 5.4), the coincidence with the time intervals found by OSL dating in Mauritania is remarkable.

No data are available for the Great Western Erg and the Great Eastern Erg. OSL datings from Tunisia exist, but these have been obtained from the southern margin of the Chott-Rharsa Basin, which is situated north of the Chott el Jerid and has no connection to the Great Eastern Erg. The series covers >86 to 5 ka and consists of aeolian sandstones alternating with lacustrine sandstones (Swezey, 2001). The Pleistocene cycles of alternating fluvial and aeolian sediments at the northern margin of the Murzuq Sand Sea (Thiedig, 2005) are much older, the youngest pluvial phase reaching 165–89 ka.

It is remarkable that the draa ages from the western and the eastern extremes of Saharan sand seas, i.e. Mauritania and Egypt, are fairly well comparable. In Mauritania, strong trade winds modelled longitudinal draa >15 ka ago and in the Great Sand Sea in Egypt >20 ka ago. In both regions, a change in the wind system

is noticeable. In Mauritania, the direction changed from NE–SW to NNE–SSW, still forming longitudinal draa 13–10 ka ago. In Egypt, a pronounced change from approximately N–S to approximately W–E took place 12–10 ka ago, when the westerlies pushed south and reworked the longitudinal draa. Directions and wind systems cannot be inferred from the data for the Erg Chech, but the ages of 21 and 11 ka fit well into this pattern. The older data are assumed to be connected with the Last Glacial Maximum and the younger data with the Younger Dryas cold event (Lancaster et al., 2002; 12 800–11 500 BP cal according to Swezey, 2001). It should be kept in mind that the OSL datings in Mauritania were obtained from investigations carried out south of the tropics, and in Egypt north of it, which explains the different change in wind directions. The Younger Dryas event obviously led to a southward displacement of wind systems. Therefore, the sands in Mauritania were reworked by winds from more northerly directions, corresponding to the zone where the trade winds are evolving. (This explanation is not provided by Lancaster et al., 2002.) In Egypt, where the N–S alignment of the draa is due to this zone of evolving trade winds, the draa were reworked by extra-tropical westerlies.

Both data sets – which give minimum ages – are supported by the investigation of the Farafra Sand Sea, a smaller sand sea east of the Great Sand Sea in Egypt, which also consists of longitudinal draa of the trade winds. The transverse draa are missing here because the Farafra Sand Sea does not extend into the area north of 27°N. Sampling for luminescence dating was conducted in 2002. A western draa slope yielded OSL ages of 35–28 ka and the eastern slope ages of around 13 ka. Thus, everything seems to be a little older than in the Great Sand Sea. A possible reason is revealed by the granulometry, because the sands in the Farafra Sand Sea were already heavily deflated during or between the depositional intervals, which results in higher ages at comparable depths (Bubenzer and Besler, 2005). This is corroborated by the calculation of the net-accumulation rate that is much lower in the Farafra Sand Sea (14 cm/1000 years). Considering time intervals with a lack of radiocarbon data, Kröpelin (1993) already concluded that the Last Glacial Maximum and also the “Ogolien” (>11 ka, covering the Younger Dryas) were characterized by an extreme aridity.

In the southwestern Rub’ al Khali, a draa-formation time interval must have occurred between the deposition of lake beds that have been <sup>14</sup>C-dated at 36–17 ka BP (uncalibrated) and pedogenesis and dune induration that took place 9–6 ka BP (McClure, 1978). Remnants of the Pleistocene lake beds are found as low terraces in the interdraa corridors, which supports erosional corridor formation according to the helical-vortex model. On the other hand, lakes and swamps are supposed to have existed between the draa. This implies an even older draa-formation time interval before 36 ka BP and a younger one between 17 and 9 ka BP. Edgell (2006) provided an “attempt at Quaternary palaeoclimate reconstruction” for the Rub’ al Khali. As his older data are, however, mainly derived from speleothems in a limestone cave several hundred kilometres farther north, they are not very reliable. OSL data exist only for the northeastern Rub’ al Khali, where the draa pattern is much more complex and not well understood. Apart from earlier intervals, sand accumulations were dated at 40, 26 and 12 ka (Lancaster et al., 2003 – in

Edgell, 2006). The latter ages again point to the Last Glacial Maximum and the Younger Dryas, as in Africa. The arid spell of the Younger Dryas is also corroborated by Goudie et al. (2000), who obtained OSL ages between 13.5 and approximately 10 ka.

The Wahibah Sands in Oman are the most thoroughly investigated erg in Arabia. Apart from older draa-formation intervals with intercalated pluvial events (Preusser et al., 2002), the youngest aeolian interval in the Pleistocene has been OSL-dated at 22–18 ka, thus covering the Last Glacial Maximum.

On the southern hemisphere, a comparative study using the same approach as in the Great Sand Sea was carried out in Namibia, in the southern Namib Erg, in 2004 (Bubenzer et al., 2007a). The results of OSL dating show a great similarity to the Great Sand Sea with formation of longitudinal draa by trade winds during the Last Glacial Maximum (24–17 ka) and their subsequent alteration by strong westerlies around 10–8.5 ka ago. The latter date, however, cannot be connected with the Younger Dryas.

Only one (uncertain)  $^{14}\text{C}$  age is available for comparable time intervals in the Taklamakan Sand Sea in China. Calcareous material below the oldest field of longitudinal draa east of the Keriya river yielded an age of 28.7 ka BP (uncalibrated), which marks the earliest possible draa formation (Hövermann and Hövermann, 1991). First results of OSL dating in the Taklamakan area have been published recently (Yang et al., 2006). Unfortunately, however, the obtained ages cannot be used to deduce draa-formation intervals because either the dated materials are comparatively thin aeolian layers intercalated between lacustrine deposits without any connection to the draa fields or they are sediments from outside the sand sea. The only sands sampled from the draa for dating were collected close to the surface of a dome-shaped draa in the flood-out of the Keriya river, and therefore they represent the modern dune cover (of a few hundred years old). In fact, this is the type locality where the granulometric type of dome sands was first determined (Besler, 1996a). As already explained (see Section 4.3), this type indicates the aeolian input of finest sands from nearby runoff sources into older dunes.

Up to the present, no corings reached the innermost parts of draa. Therefore, all data obtained represent minimum ages of draa formation. This makes the correlation of luminescence ages with the Last Glacial Maximum somewhat doubtful, and this doubt is fed by the OSL age (35 ka) of the Farafra Sand Sea. Draa formation seems to have been interrupted by a lake phase in the Rub' al Khali (McClure, 1978) and by pluvial events with calcrete formation in the Wahibah Sands (Preusser et al., 2002). However, if the Farafra Sand Sea and the Great Sand Sea in Egypt are compared with regard to the granulometry of their draa sands, they seem to belong to the same draa-formation interval, because the older sands have not been reached in the corings in the Great Sand Sea.

The Younger Dryas, on the other hand, was characterized by aeolian accumulation between around 13 and 10 ka ago in almost all sand seas discussed above. At least in Mauritania and in Egypt, the aeolian activity during the Younger Dryas is also morphologically distinguishable from the earlier draa formation due to a change in wind directions, caused by a southward shift of the atmospheric circulation systems.

## 9.4. CONDITIONS DURING THE HOLOCENE CLIMATIC OPTIMUM

A wealth of radiocarbon data exists for the Holocene. Only few data are, however, obtained from archaeological sites within sand seas, such as Regenfeld in the Great Sand Sea. Nevertheless, it is beyond the scope of this book to discuss the archaeological literature. Therefore, the compilation by Swezey (2001) is used for additional information on the climatic conditions. Only the  $^{14}\text{C}$  datings derived from organic matter are considered here, whereas datings from calcareous materials are neglected.

Michel (1977) has already concluded that the climate in southern Mauritania was much more humid than today, leading to soil formation and shrub savannahs on the draa, and to lake formation at their base between 11 and 8 ka ago. Lancaster et al. (2002) describe the surface of the Pleistocene draa in their study area ( $18^{\circ}30' - 20^{\circ}30'\text{N}$ ) as “littered with Neolithic stone artefacts and pottery, bounding a bioturbated, slightly indurated red–brown sand enriched in silt and clay”, which is interpreted as a palaeosol. For the inland part of the Akchar Erg within their study area, a humic sand overlying aeolian sands yielded  $^{14}\text{C}$  ages between 10.8 and 6.2 ka BP cal ( $21^{\circ}05'\text{N}$ ,  $13^{\circ}16'\text{W}$ ). Organic material in calcretes underlying aeolian sands was dated between 5.6 and 4.5 ka BP cal ( $21^{\circ}05'\text{N}$ ,  $13^{\circ}16'\text{W}$ ; Swezey, 2001). According to these data, the aeolian activity seems to have ended around 10 ka ago, which goes well together with the last OSL ages of sand accumulation in draa (Lancaster et al., 2002). The aeolian activity seems to have started again after 4.5 ka ago.

Only one  $^{14}\text{C}$  dating is available from within the Erg Chech between Bou Bernou and Nebkha ( $27^{\circ}20'\text{N}$ ,  $03^{\circ}04'\text{W}$ ), where a black organic-rich soil yielded an age between 7.5 and 7.1 ka BP cal (Swezey, 2001). The situation is the same for the Great Western Erg, as only one dating exists there, from a marginal part ( $32^{\circ}06'\text{N}$ ,  $03^{\circ}10'\text{E}$ ) where ostrich eggshells in aeolian sands between layers of silts were dated between 8.4 and 8.1 ka BP cal. From the Great Eastern Erg – also a marginal part ( $31^{\circ}59'\text{N}$ ,  $06^{\circ}29'\text{E}$ ) – an ash-rich sand in an archaeological level yielded 6.9–6.5 ka BP cal. No data have been compiled by Swezey for the Libyan sand seas.

Data from Egypt are abundant (a.o. Kuper, 2006; Kuper and Kröpelin, 2006), however; many stem from oases with artesian groundwater or with Nile water and, therefore, are not significant for climatic conditions in the Great Sand Sea (Bubenzer et al., 2007b). The well-documented archaeological site Regenfeld was occupied from 10.6 to 7.3 ka BP cal, which has been deduced from numerous radiocarbon datings and artefact classifications (see Section 5.4). A climatic boundary seems to have divided the Great Sand Sea during the Holocene climatic optimum. Monsoonal summer rains from the south brought 50–100 mm/year (Section 6.1), and reached approximately  $26^{\circ}\text{N}$ . The draa were flattened and slightly consolidated. Runoff and percolating water seeping out at their base led to playa formation in the rocky interdraa corridors. In their moist vicinity, heavy minerals weathered (Section 7.2) and sands were rubified (Section 6.2). Humid conditions are corroborated by pedogenic processes, and clay and calcite precipitation (Section 8.6.1). At least herbs and grasses allowed some faunal life (Section 5.4). These places were favourable for occupation by hunter-gatherers, but they experienced dry spells within the humid phase as well (Section 5.4). In the southwestern part, runoff

from the Gifl Kebir most probably added moisture for even longer-lasting better conditions.

According to the literature (Arz et al., 2003; Bubenzer et al., 2007b), the northern cyclonic winter rains also increased during the Holocene climatic optimum. In the Great Sand Sea, however, no traces of human occupation were found north of 27°N. Most probably, the lack of corridors in the transverse draa pattern did not allow the formation of surficial water bodies and dwelling sites. On the contrary, a seasonally raised groundwater table may have led to fluctuating saline waters (Section 8.6.1).

Although the dating localities in Mauritania lie south of the tropic whereas the dating sites in Algeria lie much farther north (~30°N) than the Great Sand Sea, all <sup>14</sup>C ages converge in the same time interval. Younger ages are mentioned only from the Akchar Erg in Mauritania (5.6–4.5 ka). If Willmann's Camp in the Great Sand Sea is included; however, the youngest date (5 ka, see Section 5.4) once more corresponds to the Mauritanian ergs. The large latitudinal variation, however, is reflected in the different processes of palaeosol formation. Whereas in Mauritania red–brown soils developed on the draa, a slight rubification in the Great Sand Sea occurred only in the vicinity of playas, and only south of 26°N. The black soil mentioned from the Erg Chech at a latitude that is roughly comparable (Swezey, 2001) may have been a local hydromorphic formation in a water-logged position.

From the southwestern Rub' al Khali in Arabia, McClure (1978) described a “sub-pluvial” characterized by Holocene lake beds of the playa type and Neolithic artefacts on the Pleistocene draa that show weak pedogenesis and carbonate- or gypsum-cemented sands. This interval was dated at 9–6 ka BP (uncalibrated), and the southwestern Rub' al Khali is assumed to have been a semi-arid grassland. Neolithic sites have also been dated by Zeuner (1954 – cited in Edgell, 2006) from 5.5 to 5.0 ka ago. From the arid intervals dated with OSL techniques in the northeastern Rub' al Khali (Lancaster et al., 2003 – in Edgell, 2006), a humid interval without aeolian activity may be inferred at 12–6 ka ago. According to Juyal et al. (1998), who conducted IRSL dating in the Emirates and in Oman, the Holocene humid phase began 10 ka ago and continued at least to about 6 ka ago. This indicates that comparable ages of the Holocene climatic optimum were obtained for the Wahibah Sands in Oman. Lakes in corridors existed around 9 ka ago (Warren, 1988); they have been dated from abundant fresh-water gastropods (Radies et al., 2005 – cited in Edgell, 2006). According to Glennie (1998), the earliest-known signs of humans in southeast Arabia seem to date from about 8–7 ka ago. Many more data for the Holocene semi-arid interval are given by Edgell (2006, his Fig. 20.5). However, only ages derived from within the sand seas are considered here. Although these Arabian sand seas are situated south of the tropics – comparable to the Mauritanian ergs – they show the same time interval of more humid conditions as the Great Sand Sea.

In the southern Namib Erg – where comparable time intervals for draa formation have been obtained (Bubenzer et al., 2007a) – the aeolian accumulation seems to have ceased around 8.5 ka ago. However, no evidence of human occupation



could be found, although remnants of ancient pans do exist. The lack of human occupation is explained by the poorly consolidated underlying sandstone, but most of all by the fact that better conditions were found not far away, e.g. along the coast, around the southern inselbergs and in the eastern highlands.

Summarizing, the onset of the Holocene climatic optimum occurred around 10–9 ka ago in all sand seas mentioned above. With regard to their large latitudinal range, this gives additional support for the assumption of a rather rapid northward advance of the monsoonal circulation system with summer rains (Nicholson and Flohn, 1980; Gasse and Van Campo, 1994; Pachur and Wünnemann, 1996; Hoelzmann et al., 2004).

## 9.5. THE FINAL ARIDIZATION

In Mauritania, Holocene OSL ages of dune formation concentrate in a youngest group of less than 5 ka ago and reach present-day times (Lancaster et al., 2002). The Holocene data compiled by Swezey (2001) only refer to coastal areas and do not imply an erg reactivation. According to Michel (1977), southern Mauritania became dryer around 2 ka ago, which implies a slower retreat of the monsoon front. No Holocene data are given by Swezey for the Algerian and Libyan ergs.

In the Great Sand Sea in Egypt, continuous reactivation of aeolian sands took most probably place after 5 ka ago (see Sections 3.3 and 5.4). Once more, the coincidence with the OSL ages from Mauritania is striking, in spite of the great latitudinal difference.

In the southwestern Rub' al Khali, the onset of dryer conditions can be inferred from the end of the lake phase around 6 ka BP (McClure, 1978). In the northeastern Rub' al Khali, an arid interval is documented by OSL ages of 6–4 ka (Lancaster et al., 2003 – cited in Edgell, 2006). In the Al Liwa draa field of southern Abu Dhabi (draa transverse to modern winds), 72 m of aeolian sands were cored. A constant sedimentation rate of 470 cm/1000 years has been calculated for the interval between 6.8 and 3 ka ago (Bray and Stokes, 2003). This accumulation rate is comparable to Pleistocene slip-face avalanches dated in the Farafra Sand Sea (Egypt) and in the Namib Erg (data not published yet). Intervening less arid intervals have been mentioned; they are documented only, however, from outside the Arabian sand seas, or they are inferred from the dating of single dunes (Edgell, 2006). Therefore, it can be assumed that the general trend of aridization was going on. Edgell (2006) also has stressed that the Rub' al Khali is still a region of strong aeolian activity and changing dune patterns.

Preusser et al. (2002) have dated the reactivation of Pleistocene palaeo-dunes in the Wahibah Sands in Oman at 2 and 0.7 ka ago. Once more, a trend of continual aridization is likely, because small active dunes of the sif type cover the whole sand sea (Warren, 1988).

Nothing is really known about the beginning reactivation of the Namib Erg. However, a difference in draa/dune topography between the northern and the southern Namib Erg possibly implies different times of beginning reactivation. In the south, where the investigations for OSL dating were carried out, rather low and

flat whalebacks carry several rows of silk, and draa and dunes can be distinguished relatively easily. This distinction is not possible north of approximately 25°S, because there is no break in the slopes, and the higher draa are completely covered by younger secondary dunes and their large slip faces. In this area, the reactivation seems to have started earlier than in the south. Only recently, first results of OSL dating in the northern Namib Erg have been published (Bristow et al., 2007). They were obtained from a longitudinal dune extending northward from a draa. The situation is comparable to the southward progradation of dunes on the eastern transection in the Great Sand Sea. Remarkably, the oldest (bottom) part of the dune was dated at around 5.7 ka ago, an age comparable to that of the Great Sand Sea. The reactivation of draa, however, may have occurred earlier since this part of the dune does not lie immediately north of the draa, and the sands may have needed some time to reach this latitude.

With regard to the Holocene dune pattern, the Great Sand Sea seems to be very homogeneous. Only comparatively few dunes of the longitudinal silk type top the draa, apart from in the southwestern part where abundant fine-grained sands and transverse dunes are found. The Mauritanian ergs (Lancaster et al., 2002: small linear dunes), the southern Namib Erg and the Farafra Sand Sea in Egypt seem to be comparable. The Farafra Sand Sea, however, comprises huge transverse dunes at its southern margin.

Although the Wahibah Sands show the most complex draa (and mesodune) pattern, the active Holocene dunes are small sif as well. As already explained (Section 3.3.3), these are linked sif elements forming silk. Peripheral to the Low Sands, barchanoid transverse dunes and aklé (network) patterns have also been mentioned (Warren, 1988). A comparable variety of Holocene dune types is found in the northeastern Rub' al Khali (Besler, 1982; Edgell, 2006), whereas the silk type seems to dominate in the southwestern Rub' al Khali (McClure, 1978). The assessment of dune patterns from the literature is not easy if no aerial images or air photos are supplied, because the texts most commonly do not distinguish between draa and dunes. In this respect, the detailed remote-sensing case study from the Libyan Sahara by Linsenbarth (1996) is no exception. Although this author differentiated between sand ridges (formed by helical vortices = draa) and dunes, he did not stick to this distinction in the characterization of the sand-sea morphology, and mainly used the term “dune”. Therefore, his descriptions of the sand seas within the borders of Libya are not very helpful. In general, it seems that the variety of dune types increases with greater directional changes of the Holocene winds. As the example of Egypt shows, however, the sand supply plays an important part, too.

Compared to the ergs discussed in this section, the Great Sand Sea today is the most arid one, and in fact hyperarid. Hyperaridity is defined by a ratio of precipitation (P) to potential evaporation (PET) lower than 0.05 ( $P/PET < 0.05$ ; Arnold, 1992). Contrary to most other sand seas, the Great Sand Sea is completely void of vegetation. Only one small spot with green herbs was discovered during the last crossing in 2006, but this vegetation may have been human-induced because traces of an oil change in vehicles were found nearby. Perhaps, some water had been spilled as well. The exodus of people from the Great Sand Sea started around 7–6 ka ago (Kuper, 2006; Bubenzer et al., 2007b). Together with other inhabitants of

the Western Desert in Egypt, they are supposed to have become the ancestors of the Pharaonic kingdom in the Nile valley. The aridization driving people out of the Western Desert, however, at the same time reduced the Nile swamps and made the large Nile valley inhabitable. Herodotus stated that Egypt was a gift of the Nile. The concentration of people necessary for the dawn of a cultural empire was only possible, however, because of the climatic deterioration. Referring to Herodotus, Kuper (1999) put forward the question: Is not Egypt also a gift of the desert?

## **LIST OF SAMPLES AND THEIR INVESTIGATED PARAMETERS**

<i>Number</i>	<i>Position</i>	<i>Sample from</i>	<i>Depth (cm)</i>	<i>Colour</i>			<i>Mz (mm)</i>	<i>So (<math>\varphi</math>)</i>	<i>Sk (<math>\varphi</math>)</i>	<i>K (<math>\varphi</math>)</i>	<i>Granulometric type</i>	<i>Response diagram</i>	<i>Salinity <math>\mu\text{S/cm}</math></i>	<i>HM content %</i>
10/96	24°29'N 27°20'E	Dune	0	7.5	YR	6/6	0.2948	0.8575	0.2222	0.9421	7	Stable	86	–
11/96	24°31'N 27°20'E	Dune	0	7.5	YR	6/6	0.2563	0.4935	0.4171	1.4495	6	Stable	90	0.36
12/96	24°44'N 27°17'E	Dune	20	7.5	YR	6/6	0.2768	0.6360	–0.0040	1.0306	5	Stable	417	0.20
17/96	25°25'N 27°05'E	Corridor	0	2.5	YR	4/4	0.0862	0.9749	–0.7287	0.8617	10	Fluvial	5580	0.58
18/96	25°25'N 27°05'E	Draa	210	7.5	YR	5/8	0.3115	0.9494	0.1249	0.9387	10	Stable	182	1.13
19/96	25°25'N 27°05'E	Corridor	0	5.0	YR	5/6	0.3014	0.9583	0.1675	0.8996	10	Stable	1276	–
20/96	25°25'N 27°05'E	Draa	110	10.0	YR	6/5	0.2941	0.7981	0.1233	1.0037	7	Stable	122	0.80
21/96	25°25'N 27°05'E	Dune	0	10.0	YR	6/5	0.2473	0.5533	0.1682	1.0246	5	Stable	96	–
22/96	25°25'N 27°05'E	Draa	0	10.0	YR	6/5	0.3565	1.2635	–0.1939	0.7649	10	Stable/ residual	121	0.13
24/96	25°25'N 27°05'E	Draa	0	10.0	YR	6/5	0.3903	1.1358	0.2508	0.8367	10	Residual	144	–
25/96	25°25'N 27°05'E	Corridor	20	2.5	YR	4/4	0.0523	0.3036	–0.2788	2.1227	Not aeolian 3	Mobile	1941	–
27/96	26°49'N 26°41'E	Dune	0	10.0	YR	7/4	0.2073	0.3817	0.0157	1.0344		Mobile	129	–
28/96	26°49'N 26°41'E	Draa	0	10.0	YR	6/4	0.3643	1.1220	0.3277	0.7789	9	Residual	139	0.27
29/96	26°49'N 26°41'E	Dune	0	10.0	YR	7/4	0.2412	0.3459	0.1592	0.9841	5	Mobile	79	–
30/96	26°49'N 26°41'E	Draa	0	10.0	YR	7/4	0.3194	1.3723	0.1135	0.6933	9	Stable	120	0.13
33/96	27°19'N 26°32'E	Draa	200	10.0	YR	6/4	0.3133	0.8851	0.0803	0.9278	10	Stable	795	–
35/96	27°19'N 26°32'E	Draa	400	10.0	YR	7/4	0.3469	0.8712	0.1445	0.8556	10	Stable	351	0.60

36/96	27°19'N 26°32'E	Draa	0	10.0	YR	7/4	0.4125	1.0980	0.0701	0.8223	10	Residual	110	1.25
37/96	27°29'N 26°30'E	Sandstone	–	10.0	YR	7/6	0.1920	1.0084	0.1597	1.0046	10	Stable	633	0.07
39/96	29°00'N 26°10'E	Dune	0	10.0	YR	7/4	0.2056	0.5019	0.0732	0.9592	5	Stable	180	0.45
40/96	29°12'N 25°31'E	Sandstone	–	10.0	YR	8/6	0.1331	1.4378	–0.5571	0.6865	Sub-aqueous	Fluvial	11160	0.65
1/99	24°46'N 26°46'E	Dune	0	7.5	YR	6/6	0.2328	0.4194	0.2664	0.9883	5	Mobile	73	0.35
2/99	24°53'N 26°43'E	Dune	0	7.5	YR	6/6	0.2453	0.4153	0.3475	1.0517	5	Mobile	65	0.48
3/99	24°50'N 26°44'E	Dune/draa	0	7.5	YR	6/6	0.3379	1.0973	0.2562	0.9492	9	Stable	105	0.81
4/99	24°50'N 26°44'E	Sandstone	–	10.0	YR	6/6	0.0950	0.7077	–0.1929	1.0161	2	Mobile	267	0.39
5/99	24°55'N 26°43'E	Dune	0	7.5	YR	6/6	0.2413	0.4097	0.2976	1.0238	5	Mobile	78	0.58
6/99	25°00'N 26°42'E	Dune	0	10.0	YR	6/6	0.2629	0.3340	0.2404	1.1730	6	Mobile	68	0.63
7/99	25°00'N 26°42'E	Sandstone	–	7.5	YR	5/8	0.1172	0.6502	0.3733	0.9436	4	Mobile	234	0.32
8/99	25°05'N 26°41'E	Dune	0	10.0	YR	6/6	0.3019	0.4179	0.1622	1.2429	6	Stable	56	1.49
9/99	25°10'N 26°40'E	Dune	0	10.0	YR	7/6	0.2724	0.4487	0.2346	1.1805	6	Stable	64	0.53
10/99	25°15'N 26°38'E	Dune	0	10.0	YR	7/4	0.2398	0.3747	0.2128	0.9785	5	Mobile	67	0.09
11/99	25°20'N 26°37'E	Dune	0	10.0	YR	7/4	0.2753	0.4547	0.2589	1.3100	6	Stable	68	0.55
12/99	25°25'N 26°36'E	Dune	0	10.0	YR	7/4	0.2132	0.3884	0.0538	0.9471	3	Mobile	97	0.63
13/99	25°25'N 26°36'E	Sandstone	–	10.0	YR	7/4	0.1194	0.7716	0.3670	0.7877	5	Fluvial	552	0.75
14/99	25°25'N 26°36'E	Draa	340	7.5	YR	6/6	0.3214	1.0597	–0.0551	0.9030	10	Stable	1103	0.77

(Continued)

<i>Number</i>	<i>Position</i>	<i>Sample from</i>	<i>Depth (cm)</i>	<i>Colour</i>			<i>Mz (mm)</i>	<i>So (<math>\varphi</math>)</i>	<i>Sk (<math>\varphi</math>)</i>	<i>K (<math>\varphi</math>)</i>	<i>Granulometric type</i>	<i>Response diagram</i>	<i>Salinity <math>\mu\text{S/cm}</math></i>	<i>HM content %</i>
15/99	25°24'N 26°36'E	Draa	0	10.0	YR	6/4	0.4419	1.2661	0.2983	0.7582	10	Residual	70	0.22
16/99	25°24'N 26°36'E	Draa	200	10.0	YR	7/4	0.3833	1.1364	0.0915	0.8012	10	Residual	86	1.07
17/99	25°24'N 26°36'E	Draa	250	10.0	YR	7/4	0.3547	0.9068	0.2378	0.8921	10	Residual	183	0.34
18/99	25°25'N 26°36'E	Draa	0	10.0	YR	7/4	0.3018	0.8104	0.1347	1.0238	7	Stable	70	0.35
19/99	25°30'N 26°34'E	Dune	0	10.0	YR	7/4	0.2219	0.3676	0.0491	0.9467	3	Mobile	95	0.59
20/99	25°40'N 26°32'E	Dune	0	10.0	YR	7/4	0.2028	0.3810	-0.0475	1.0764	3	Mobile	83	0.16
21/99	26°00'N 26°25'E	Dune	0	10.0	YR	7/4	0.2209	0.3970	0.1014	0.9672	5	Mobile	112	0.06
22/99	26°06'N 26°24'E	Sandstone	-	10.0	YR	6/6	0.0976	0.8308	-0.3076	0.8505	2	Fluvial	4680	0.20
23/99	26°43'N 26°11'E	Dune	0	10.0	YR	7/4	0.4706	0.6738	0.4615	1.2928	Mega-ripple	Residual	58	0.13
24/99	26°57'N 26°06'E	Dune	0	10.0	YR	7/4	0.3366	0.7119	0.2554	1.2350	6	Stable	97	0.05
25/99	27°12'N 26°03'E	Dune	0	10.0	YR	7/4	0.2782	0.9544	0.2460	0.8351	7	Stable	117	0.43
26/99	27°12'N 26°02'E	Draa	0	10.0	YR	7/4	0.3228	1.1153	-0.0348	0.9064	10	Stable	154	0.24
27/99	27°12'N 26°02'E	Draa	100	10.0	YR	7/4	0.3114	0.9989	0.2361	0.8314	10	Stable	82	0.50
28/99	27°12'N 26°02'E	Draa	150	10.0	YR	7/4	0.3584	0.8713	0.4658	0.9228	10	Residual	98	0.42
29/99	27°12'N 26°02'E	Draa	200	10.0	YR	7/4	0.3714	0.8334	0.4108	0.8895	10	Residual	212	0.15
30/99	27°12'N 26°02'E	Draa	250	10.0	YR	7/4	0.3667	0.8551	0.3109	0.8620	10	Residual	202	0.50
31/99	27°12'N 26°02'E	Draa	300	10.0	YR	7/4	0.3108	0.9927	0.2108	0.8294	10	Stable	276	0.26

32/99	27°12'N 26°02'E	Draa	350	10.0	YR	7/4	0.3234	0.9648	0.1380	0.8551	10	Stable	99	0.28
33/99	27°12'N 26°02'E	Draa	400	10.0	YR	7/4	0.3303	0.8528	0.0553	0.8755	10	Stable	173	0.30
1/00	23°54'N 25°28'E	Sandstone	–	2.5	YR	6/2	0.2015	0.5149	0.0163	1.2062	3	Mobile/ stable	249	0.51
2/00	24°16'N 25°39'E	Dune	0	7.5	YR	6/6	0.1733	0.3769	0.0400	1.1151	3	Mobile	49	0.97
3/00	25°07'N 25°37'E	Draa	0	7.5	YR	6/6	0.3387	0.8196	−0.1508	0.7223	10	Stable	49	0.44
4/00	25°07'N 25°37'E	Draa	50	7.5	YR	6/6	0.1849	0.2674	−0.0050	1.0155	3	Mobile	29	0.41
5/00	25°07'N 25°36'E	Draa	100	7.5	YR	6/6	0.2237	0.5805	−0.2944	1.3926	3	Stable	86	0.49
6/00	25°07'N 25°36'E	Draa	150	7.5	YR	6/6	0.2233	0.5481	−0.1166	1.0429	5	Stable	78	0.81
7/00	25°07'N 25°36'E	Draa	200	7.5	YR	6/6	0.2788	0.7830	−0.1560	1.0082	5	Stable	105	0.60
8/00	25°07'N 25°36'E	Draa	250	7.5	YR	6/6	0.2585	0.6345	−0.1672	1.0180	5	Stable	107	0.58
9/00	25°07'N 25°36'E	Draa	300	7.5	YR	6/6	0.2368	0.6058	−0.2000	1.0858	5	Stable	127	0.20
10/00	25°07'N 25°36'E	Draa	350	7.5	YR	6/6	0.2032	0.3070	−0.0678	1.1008	3	Mobile	109	0.39
11/00	25°07'N 25°36'E	Dune	0	7.5	YR	6/6	0.1751	0.1878	−0.0214	0.9755	3	Mobile	63	0.75
12/00	25°07'N 25°36'E	Draa	400	7.5	YR	6/6	0.2408	0.3920	−0.0301	1.0028	5	Mobile	117	0.54
13/00	25°06'N 25°37'E	Draa	0	5.0	YR	6/6	0.3089	0.8385	−0.4248	0.7015	10	Stable	62	0.46
14/00	25°06'N 25°37'E	Draa	30	5.0	YR	6/6	0.2294	0.4248	−0.0887	1.0304	3	Mobile	44	0.52
15/00	25°06'N 25°37'E	Draa	50	5.0	YR	6/6	0.2045	0.5131	0.0017	1.1205	3	Mobile	498	0.49
16/00	25°06'N 25°37'E	Corridor	40	5.0	YR	6/4	0.2343	1.9228	0.1912	1.2305	Fluvial/ aeolian	Stable	2270	0.54

(Continued)



Number	Position	Sample from	Depth (cm)	Colour			Mz (mm)	So ( $\varphi$ )	Sk ( $\varphi$ )	K ( $\varphi$ )	Granulometric type	Response diagram	Salinity $\mu\text{S/cm}$	HM content %
17/00	25°10'N 25°34'E	Corridor	40	5.0	YR	6/5	0.1697	0.7663	0.2731	1.1761	5	Fluvial	172	0.36
19/00	25°18'N 25°34'E	Sandstone	–	5.0	YR	4/4	0.1676	0.9608	0.1012	1.0963	4	Fluvial	908	0.18
20/00	25°00'N 25°42'E	Draa/dune	0	5.0	YR	5/6	0.3954	0.9778	0.3614	0.8782	10	Residual	26	0.95
21/00	25°00'N 25°42'E	Dune	0	5.0	YR	5/8	0.2811	0.5417	0.0412	0.9901	5	Stable	44	0.70
22/00	25°06'N 25°42'E	Dune	0	7.5	YR	6/6	0.2224	0.2902	0.0917	1.1186	3	Mobile	51	1.36
23/00	25°12'N 25°41'E	Dune	0	7.5	YR	6/6	0.2032	0.2871	0.0456	1.0753	3	Mobile	66	0.34
24/00	25°18'N 25°46'E	Dune	0	7.5	YR	6/7	0.2136	0.3307	0.0175	1.0200	3	Mobile	58	0.52
25/00	25°24'N 25°39'E	Dune	0	10.0	YR	7/4	0.1665	0.2434	0.0296	0.9763	3	Mobile	65	0.30
26/00	25°36'N 25°39'E	Dune	0	10.0	YR	7/4	0.1916	0.3051	0.0317	1.0703	3	Mobile	47	0.55
27/00	25°42'N 25°41'E	Dune	0	10.0	YR	7/4	0.1978	0.2965	0.0271	1.0918	3	Mobile	54	0.46
28/00	25°38'N 25°40'E	Draa	0	10.0	YR	7/4	0.2177	0.5627	0.1767	1.1898	3	Stable	120	0.21
29/00	25°42'N 25°40'E	Draa	100	10.0	YR	7/4	0.3466	0.5060	0.0236	0.9945	6	Stable	78	0.20
30/00	25°42'N 25°40'E	Draa	200	10.0	YR	7/4	0.2650	0.7955	0.3233	0.8982	5	Stable	134	0.27
31/00	25°42'N 25°40'E	Draa	300	10.0	YR	7/4	0.2459	0.4223	0.1882	1.0020	5	Mobile	212	0.18
32/00	25°42'N 25°40'E	Draa	400	10.0	YR	7/4	0.2618	0.7099	0.2371	0.9599	5	Stable	235	0.46
33/00	25°42'N 25°40'E	Draa	500	10.0	YR	7/4	0.2707	0.5229	0.0700	1.0302	5	Stable	246	0.31
34/00	25°48'N 25°38'E	Dune	0	10.0	YR	7/4	0.2128	0.3798	0.0252	0.9601	3	Mobile	68	1.03

35/00	25°54'N 25°37'E	Dune	0	10.0	YR	7/4	0.2106	0.3779	0.0386	1.0221	3	Mobile	84	0.54
36/00	25°00'N 25°36'E	Dune	0	10.0	YR	7/4	0.2542	0.3193	0.1431	0.9996	5	Mobile	66	0.56
37/00	26°12'N 25°41'E	Draa	0	10.0	YR	7/4	0.2684	1.0752	0.1221	0.6776	Mega-ripple	Stable	134	0.61
38/00	26°12'N 25°35'E	Dune	0	10.0	YR	7/4	0.2764	0.3685	0.1296	1.0659	6	Mobile/ stable	48	0.59
39/00	26°19'N 25°36'E	Draa	0	10.0	YR	7/4	0.2859	0.8844	0.1424	0.9111	7	Stable	137	0.58
40/00	26°24'N 25°37'E	Dune	0	10.0	YR	7/4	0.2782	0.2943	0.1461	1.2760	6	Mobile	67	0.34
41/00	26°30'N 25°37'E	Dune	0	10.0	YR	7/4	0.2713	0.3065	0.1720	1.2202	6	Mobile	74	0.46
42/00	26°36'N 25°35'E	Dune	0	10.0	YR	7/4	0.2673	0.3185	0.1189	1.0980	6	Mobile	68	0.39
43/00	26°26'N 25°36'E	Corridor	140	10.0	YR	8/3	0.5052	1.1404	0.1895	1.0448	10	Residual	277	0.55
44/00	26°26'N 25°36'E	Corridor	40	7.5	YR	8/2	0.4099	1.1133	0.0604	1.1269	10	Residual	74	0.38
45/00	26°42'N 25°35'E	Dune	0	10.0	YR	7/4	0.2223	0.3511	0.0252	0.9807	3	Mobile	71	0.21
46/00	26°48'N 25°36'E	Dune	0	10.0	YR	7/4	0.2696	0.3711	0.2164	1.1704	6	Mobile	83	1.25
47/00	26°54'N 25°36'E	Dune	0	10.0	YR	7/4	0.3127	0.3291	0.0886	1.2768	6	Stable	76	0.38
48/00	26°51'N 25°36'E	Draa	100	10.0	YR	7/4	0.3181	0.8714	0.0640	0.8853	10	Stable	279	0.37
49/00	26°51'N 25°36'E	Draa	0	10.0	YR	7/4	0.3408	1.2557	0.0278	0.9155	10	Stable	82	0.30
50/00	26°51'N 25°36'E	Draa	200	10.0	YR	7/4	0.3282	0.6365	0.0519	1.1355	6	Stable	268	0.43
51/00	26°51'N 25°36'E	Draa	300	10.0	YR	7/3	0.3310	0.8034	0.0523	1.0088	10	Stable	78	0.49
52/00	26°51'N 25°36'E	Draa	400	10.0	YR	7/4	0.3303	0.7615	0.0281	0.9431	10	Stable	195	0.25

This page intentionally left blank

**PROCEDURE OF SEM FEATURE ANALYSIS  
AND ENVIRONMENTAL COMPOSITION EXEMPLIFIED  
FOR SAMPLE No. 35/96**

16.8  
 Probe 35/16 (ungewaschen)

E Traverse N: 4m Tiefe

- 1: Detail von Rosenkorn! in 4 rechts oben im Zentrum
  - ① Budel + Lösungsbedeutung
  - ② Drupt. plates  $\hat{=}$  flow structure
  - ③ smoothing
  - ④ Rinne in Vertiefungsin, wobei  
Spektrum: nur Si  $\rightarrow$  SiO<sub>2</sub>
- 2: anderes Korn mit Kante (in 4 rechts unten)
  - ① Krümelkorn vorhanden, upt. plate, ②
  - ③ flache konkave Fläche fast identisch wie bei 13 von HCl-Probe  
K + D 86
  - ④ ~~andere~~ smoothing
  - ⑤ kl. Rinne  
unbis den erst. relativ alter Hohlraum mit unvollkommen  
oben fröhen! etc.
3. Detail von 2: flache Bruchfläche  
ist nicht sehr glatt:
  - ① Platz 139; couleur (aber etwas größer!)  
115: näherungsweise (passt besser v. Größe)
  - ② herauswachsende Kristalle  
Spektrum: Na ① } NaCl  
Si niedrig Cl ② }
  - ③ rechts davon scheint anderer Kristall schon wieder gelöst
4. überblick 6 Körner: Rosenk. 1 K. wie gelüftet!!  
Krümelk. 3 (wie bei Probe 18)
- 5: detail von anderem Korn, in 4 im Zentrum
  - ① Rosenkorn
  - ② ~~upt. plate~~ i pellicule p.d.
  - ③ smoothing sehr stark!
  - ④ in Lösungsbuchst Riss
6. detail von anderem Korn:
  - ① Kontaktfläche erhalten
  - ② darauf smoothing
  - ③ im Lösungsbuchst Schuppen
  - Spektrum: Al ① } Tonminerale  
Ca ② }
  - Si niedrig! Fe ③ sehr wenig
7. anderes Korn: geriffelt, detail  
Spektrum: nur Si  $\rightarrow$  SiO<sub>2</sub>
- ① relative Atmung, darüber smoothing ②
8. Gesamtkorn von 7  
Sowas keine Bearbeitung erkennbar!

- 2 -

9. : Detail von and. Korn mit Kristallen  
schuppiger Hintergrund

① nach Ril Größ. Schuppen Desquamation  
② " kleinere " precipitation

Kristalle:

Spektrum: Al ① Hintergrund: Tonbeläge }  
K ③

Si niedrig Fe ②

④ Spektrum vom rechten Kristall: Na ② } NaCl  
Si niedrig Al ①

③ Spektrum vom linken Kristall: nier Si  
→ SiO<sub>2</sub>

⑤ Kristalle wieder aufgelöst!

10. : überivert: Ate mulde mit 9

umgebung sehr smooth, platter als äolisch!!  
pellicule silic.?

11. : anderes Detail von 10: linker Rand d. Mulde

④ Dreieck-Kristall:

Spektrum: Na ③

Al ②

Si niedrig Al ①

Fe ④ (sehr schwarz)

NaCl + Hintergrund mit Tonbelag

Abfolge : 1. Kontaktflächen und Lösungsrücken  
2. upturned plates  $\hat{=}$  flow structures  
3. Starkes Smoothing  $\rightarrow$  relative itzung  
4.

5. aeolian breakage!  $\rightarrow$  water!

6. ~~neogene~~ Desquamation, Risse

7. precipitation + Tonbeläge

8. Neogene

9. Quarz-Kristalle

10. NaCl-Kristalle

11. NaCl-Kristall-Lösung

No. 9  
Probe 35/96 (im HCl geätzt)

E-Transverse N: 4m Tiefe

Probeaufnahmen (alle Nr. 26)

- 1.: Übersicht 5 Körner (u. viele Kerne) (100µm)
  - 1 Rosette.
  - 2 Knubbel.
  - 1 gerundete K.
  - 1 rel. kantige K.
2. Übersicht 3 Körner (+ viele Details) (100µm)
  - 1 Rosette.
  - 1 Knubbel.
  - 1 rel. kantige K.
3. Einzelkorn: rel. glatte Oberfl. (100µm)
  - Strömung
4. Rosettenkorn aus 1. Mitte: (30µm)
  - ⊗ Kontaktpf. + Lösungsrücken
  - ⊗ Upt. plates
  - ⊗ Smoothing
5. Detail von 4 rechts unten: (30µm)
  - Fläche mit Strömung für Abtrag unregelmäßig
  - ⊗ evtl. lokale Bruchfläche mit solut. + precip. an Lösungslinien unregelmäßig!
  - ↳ links zur linken Fluss-Struktur
6. Detail von anderem Korn mit Bruchflächen
  - ⊗ sehr schön korrosiv, mehrere  $\downarrow$  isocelllement en faisceaux
  - ⊗ Strömung mit upt. plates + smoothing
  - ⊗ Restbruch erhalten
  - ↳ Körne. wie bei K + D 108:
  - ↳ viele äol. Marken ohne smoothing!
  - ↳ oder kl. Ätzungen? bzw. nach smoothing!
7. Detail von anderem Korn:
  - ⊗ Bruch u. Lösungsrücken
  - ⊗ Upt. plates
  - ⊗ leicht korrosive Fläche mit Strömung
  - ⊗ + smoothing
  - ↳ auf Bruch wie bei 6: viele äol. Marken nach smoothing
8. Detail von 3: Strömung
  - ⊗ isocelllement en faisceaux
  - ↳ darüber upt. plates
  - ⊗ + smoothing

- Refuge:
1. Kontakflächen u. Lösungsrücken
  2. upt. plates
  3. isocelllements
  4. solution + precip along cleavage lines
  5. smoothing
  6. äol. Impakte (Luft!) nach smoothing

Probe 35/96 (in HCl gewaschen)

E-Transverse N: 4cm Tiefe

12: Detail von Rosenkorn

- ① Kontaktflächen u. Lösungsbuchten
- ② upturned plates + flow structure
- ④ kl. Abköder
- ③ smoothing

13: Detail von Korn mit Kanten:

- ① <sup>Poröse</sup> up<sub>1</sub> plates
- ③ smoothing
- Abbl. fläche: viel glatter
- ④ K + D 26: conchoidal breakage + up<sub>1</sub> plates  
↳ aeolian! sandkorpus! → aber viel größer!  
darauf: wenig smoothing! > 100µm
- ⑤

14:

- ↳ anderes Korn = knübelkorn
- ① Kontaktfl. + Lösungsbuchten
  - ② up<sub>1</sub> plates
  - ③ smoothing
  - ④ kl. Risse

- Abfolge:
1. Kontaktflächen u. Lösungsbuchten
  2. upturned plates + flow structure
  3. smoothing
  4. aeolian breakage → zu groß!
  5. wenig smoothing
  6. kl. Abkungen

Σ Abfolge gewaschen + ungewaschen + Probeaufnahmen

1. Kontaktflächen u. Lösungsbuchten
  2. upturned plates + flow structure
  5. relative Ätzung
  6. starker smoothing
  7. aeolian breakage
  8. wenig smoothing
  9. Desquamation, Risse, kl. Abkungen
  10. SiO<sub>2</sub>-Abcheiden + Tonbeläge (Al, Fe, K+Ca)
  11. Neogenese
  12. Quarz-Kristallwachstum
  13. NaCl-Kristallwachstum
  14. NaCl Lösung
3. Circaillement  
4. S.Olat. + prec. cleavage flow structure!  
heftige äol. Impulse zu groß: fluvial!



Milieu (Probe 35/96)Ribault

1. 94: alternation, pédogenèse
2. 138: coulée: pédogenèse
3. 51: cassure conchoidal
- 4.
- 5.
6. viele desert dew cycles
- 7.
8. langer Wüstenaufenthalt
9. 75: desquamation
10. a)  $SiO_2$ -Körner: pellicule silic.  
b) Tonbeläge Al, Fe, K+Ca: Pedogenese
11. 119: néogenèse
12.  $SiO_2$ -Kristallwachstum
13. NaCl - "
14. NaCl - Lösung

K & D.

- 96: solution + precip. on llways  
 20: deep surface etching selective  
 86: aedician breakage } mud  
 108: wind machine: 20 bills / h } <sup>sun</sup> <sub>shade</sub>  
 82: bes. chem. weathering

Fazit: Milieu & Prozesse

1. Verwitterung, Pedogenese
2. Pedogenese (B-Horiz.)
3. turbulenter Wärmetransport
4. high-energy chem. + Pedogen.
5. Diagenese
6. langer Wüstenaufenthalt
7. Sandstürme
8. langer Wüstenaufenthalt
9. Pedogenese (A-Horiz.)  
bes. chem. Verwitterung
10. a) Pedogenese (B-Horiz.)  
b) " "
11. Diagenese
12. Diagenese
13. Austrocknung, langsam
14. Befeuchtung

Konkrete Abfolge (Probe 35/96)

1. alte Pedogenese (B-Horiz.)
2. turbulenter Wärmetransport
3. Diagenese / Pedogenese
4. langer Aufenthalt in heißer Wüste mit Sandstürmen
5. bes. chem. Verwitterung + Pedogenese (sepen fürde woeniger!)
6. Diagenese, bas Milieu
7. langsame Austrocknung
8. erneute Ref. Befeuchtung (zsh gering!)

## REFERENCES

- Abrams, M., 2000: The advance spaceborne thermal emission and reflection radiometer (ASTER): data products for the high spatial resolution imager on NASA's Terra platform. *Int. J. Remote Sens.*, **21**, 847–859.
- Adamiec, G., 2000: Variations in luminescence properties of single quartz grains and their consequences for equivalent dose estimation. *Radiat. Meas.*, **32**, 427–432.
- Adamiec, G., and M. J. Aitken, 1998: Dose-rate conversion factors: update. *Ancient TL*, **16**(2), 37–50.
- Agnew, C., 1988: Soil hydrology in the Wahiba sands. In: Dutton, R. W. (Ed.), *The Scientific Results of The Royal Geographical Society's Oman Wahiba Sands Project 1985–1987*. Journal of Oman Studies, Special Report, Vol. 3, Diwan of the Royal Court, Muscat, Oman, pp. 191–200.
- Aitken, M. J., 1985: *Thermoluminescence Dating*. Academic Press, London, 359 pp.
- Aitken, M. J., 1998: *An Introduction to Optical Dating – The Dating of Quaternary Sediments by the Use of Photon-stimulated Luminescence*. Oxford University Press, Oxford, 267 pp.
- Alaily, F., 1996: Carbonate, Gips und lösliche Salze. In: Blume, H. P., Felix-Henningsen, P., Fischer, W. R., et al. (Eds), *Handbuch der Bodenkunde*. ecomed, Landsberg/Lech, pp. 1–8.
- Alimen, M. H., 1957: Sables quaternaires du Sahara nord-occidental. Publications du Service de la Carte Géologique de l'Algérie, Nouvelle Série, *Bulletin*, **15**, 1–207, Alger.
- Allison, R. J., 1988: Sediment types and sources in the Wahiba Sands, Oman. In: Dutton, R. W. (Ed.), *The Scientific Results of The Royal Geographical Society's Oman Wahiba Sands Project 1985–1987*. Journal of Oman Studies, Special Report, Vol. 3, Diwan of the Royal Court, Muscat, Oman, pp. 161–168.
- Almeida-Filho, R., F. R. S. Moreira, and C. H. Beisl, 2005: The Serra da Cangalha astrobleme as revealed by ASTER and SRTM orbital data. *Int. J. Remote Sens.*, **26**, 833–838.
- Anton, D., 1983: Modern eolian deposits of the Eastern Province of Saudi Arabia. In: Brookfield, M. E., and Ahlbrandt, T. S. (Eds), *Eolian Sediments and Processes, Developments in Sedimentology*, Vol. 38, Elsevier, Amsterdam, pp. 365–378.
- Arnold, E. (Ed.), 1992: *World Atlas of Desertification*. UNEP, London, 69 pp.
- Arz, H. W., F. Lamy, J., Pätzold, et al., 2003: Mediterranean moisture source for an early-Holocene humid period in the Northern Red Sea. *Science*, **300**, 118–121.
- Aufrère, L., 1932: Morphologie dunaire et météorologie saharienne. *Bulletin de l'Association de Géographes Français*, **56**, 34–48.
- Aufrère, L., 1934: Les dunes du Sahara algérien. *Bulletin de l'Association de Géographes Français*, **83**, 130–142.
- Bagnold, R. A., 1931: Journeys in the Libyan Desert 1929 and 1930. *Geogr. J.*, **78**, 13–19, 78, 524–535.
- Bagnold, R. A., 1935: The movement of desert sands. *Geogr. J.*, **85**, 342–370.
- Bagnold, R. A., 1938: Grain structure of sand dunes and its relation to their water content. *Nature*, **142**, 403–404.

- Bagnold, R. A., 1941: *The Physics of Blown Sand and Desert Dunes*. Methuan, London, 265 pp.
- Bagnold, R. A., 1951: Sand formations in southern Arabia. *Geogr. J.*, **117**, 78–88.
- Bagnold, R. A., 1953: The surface movement of blown sand in relation to meteorology. *Res. Council Israel, Spec. Publ.*, **2**, 89–93.
- Bagnold, R. A., 1954: The physical aspects of dry deserts. In: Cloudsley-Thompson, J. L. (Ed.), *Biology of Deserts*. Institute of Biology, London, pp. 7–13.
- Baker, R. A., 1968: Kurtosis and peakedness. *J. Sediment. Petrol.*, **38**, 679–681.
- Ball, J., 1927: Problems of the Libyan Desert. *Geogr. J.*, **70**, 21–38, 105–129, 209–225.
- Beadnell, L., 1910: The sand dunes of the Libyan Desert. *Geogr. J.*, **35**, 379–395.
- Becker R. E., 1979: Die tertiäre und quartäre Entwicklung im Bereich der Kufrah-Oasen (Zentrale Sahara) unter besonderer Berücksichtigung aktualistischer Vorgänge. *Geologische Rundschau*, **68**, 584–621.
- Behrmann, W., 1932: Beobachtungen am Rande der Wüste. *Geographische Zeitschrift*, **38**, 321–334, 399–412.
- Bellair, P., 1940: Les sables de la Dorsale Saharienne et du Bassin de l'oued Rhir. Bulletin du Service de la Carte Géologique de l'Algérie, 5. serie : Péetrographie 5, Alger, pp. 1–80.
- Bellair, P., 1951: La ramla des Daouada (Fezzân). Travaux de l'Institut de Recherches Sahariennes 7, Université d'Alger, pp. 69–86.
- Bergmann, F., 2000: Wetterbeobachtungen auf fünf Forschungsreisen in der Libyschen Wüste 1996–2000 (Ägypten/Sudan). *Staatsexamensarbeit, Universität zu Köln*, 101 pp. (unpubl.).
- Besler, H., 1975: Messungen zur Mobilität von Dünenansenden am Nordrand der Dünen-Namib (Südwestafrika). *Würzburger Geographische Arbeiten*, **43**, 135–147.
- Besler, H., 1977a: Untersuchungen in der Dünen-Namib (Südwestafrika); Vorläufige Ergebnisse des Forschungsaufenthaltes 1976. *J. SWA Sci. Soc.*, **31**, 33–64.
- Besler, H., 1977b: Fluviale und äolische Formung zwischen Schott und Erg. In: Meckelein, W. (Ed.), *Geographische Untersuchungen am Nordrand der tunesischen Sahara*. *Stuttgarter Geographische Studien*, Vol. 91, Geographisches Institut, Universität Stuttgart, pp. 19–81.
- Besler, H., 1979: Salinitätsmessungen an Sanden als Hilfsmittel zur Rekonstruktion fossiler Gewässernetze in ariden Räumen. *Zeitschrift für Geomorphologie, Neue Folge*, **23**, 192–198.
- Besler, H., 1980: Die Dünen-Namib: Entstehung und Dynamik eines Ergs. *Stuttgarter Geographische Studien*, **96**, 241 pp.
- Besler, H., 1982: The north-eastern Rub' al Khali within the borders of the United Arab Emirates. *Zeitschrift für Geomorphologie, Neue Folge*, **26**, 495–504.
- Besler, H., 1983: The response diagram: distinction between aeolian mobility and stability of sands and aeolian residuals by grain-size parameters. *Zeitschrift für Geomorphologie, Neue Folge, Suppl.*, **45**, 287–301.
- Besler, H., 1984a: The development of the Namib dunefield according to sedimentological and geomorphological evidence. In: Vogel, J. C. (Ed.), *Late Cainozoic Palaeoclimates of the Southern Hemisphere*. Balkema, Rotterdam, pp. 445–453.
- Besler, H., 1984b: Verschiedene Typen von Reg, Dünen und kleinen Ergs in der algerischen Sahara. *Die Erde*, **115**, 47–79.
- Besler, H., 1986: The Toshka-Canal dune: analysis of development and dynamics. In: Nickling, W. G. (Ed.), *Aeolian Geomorphology. The Binghamton Symposia in Geomorphology. International Series*, Vol. 17, Allen & Unwin, Boston, pp. 113–130.
- Besler, H., 1987a: Entstehung und Dynamik von Dünen in warmen Wüsten. *Geographische Rundschau*, **39**, 422–428.
- Besler, H., 1987b: Windschliffe und Windkanter in der westlichen Zentral-Sahara. *Palaeoecol. Afr.*, **18**, 217–228.

- Besler, H., 1987c: Äolische Dynamik am Rande der Sahara. In: Vogg, R. (Ed.), *Forschungen in Sahara und Sahel I, Stuttgarter Geographische Studien*, Vol. 106, Geographisches Institut, Universität Stuttgart, pp. 161–223.
- Besler, H., 1989: Dünenstudien am Nordrand des Großen Östlichen Erg in Tunesien. *Stuttgarter Geographische Studien*, **100**, 221–246.
- Besler, H., 1991a: Dünengenerationen in Nord-Mali unter dem Raster-Elektronenmikroskop. In: Blümel, W. D. (Ed.), *Forschungen in Sahara und Sahel II. Stuttgarter Geographische Studien*, Vol. 116, Geographisches Institut, Universität Stuttgart, pp. 45–68.
- Besler, H., 1991b: The Keriya Dunes: first results of sedimentological analysis. In: Jäkel, D., and Zhu, Z. (Eds), *Reports on the 1986 Sino-German Kunlun Shan-Taklimakan-Expedition*. Gesellschaft für Erdkunde zu Berlin, Die Erde, Ergänzungsheft 6, pp. 73–88.
- Besler, H., 1992: Geomorphologie der ariden Gebiete. *Erträge der Forschung*, Vol. 280, Wissenschaftliche Buchgesellschaft, Darmstadt, 189 pp.
- Besler, H., 1995: The Keriya Dunes in the Taklimakan Sand Sea: sedimentological evidence for a polygenetic evolution. *Die Erde*, **126**, 205–222.
- Besler, H., 1996a: Granulometrische Sandtypen im Wüstenvergleich (Häufigkeitsverteilungen als Informationsträger). *Zeitschrift für Geomorphologie, Neue Folge*, **40**, 23–46.
- Besler, H., 1996b: The Tsondab Sandstone in Namibia and its significance for the Namib Erg. *South Afr. J. Geol.*, **99**, 77–87.
- Besler, H., 1997a: Aktuelle und Paläoformung in der Großen Sandsee Ägyptens (Erste Ergebnisse aus dem Kölner SFB 389). *Zeitschrift für Geomorphologie, Neue Folge, Suppl.*, **111**, 1–16.
- Besler, H., 1997b: Eine Wanderdüne als Soliton? *Physikalische Blätter*, **53**, 983–985.
- Besler, H., 1998: Periods of aeolian activity and stability in the Great Sand Sea in Egypt. *Zentralblatt für Geologie und Paläontologie*, Teil 1, 1997, pp. 23–39.
- Besler, H., 2000a: Modern and palaeo-modelling in the Great Sand Sea of Egypt (Initial results from the Cologne Cooperative Research Project 389). In: Kröpelin, S., and Petit-Maire, N. (Eds), *Palaeomonsoon Variations and Global Change during the Late Quaternary*. Global and Planetary Change, Vol. 26, Elsevier, Amsterdam, pp. 13–24.
- Besler, H., 2000b: Dünen als Klimaarchive – Beispiele aus der Taklamakan (China) und der Großen Sandsee (Ägypten). *Geographische Rundschau*, **52**, 30–36.
- Besler, H., 2002a: The Great Sand Sea (Egypt) during the Late Pleistocene and the Holocene. *Zeitschrift für Geomorphologie, Neue Folge, Suppl.*, **127**, 1–19.
- Besler, H., 2002b: Complex barchans in the Libyan Desert: dune traps or overtaking solitons? *Zeitschrift für Geomorphologie, Neue Folge, Suppl.*, **126**, 59–74.
- Besler, H., 2002c: The formation of artefact-stabilized dunes near Lower Wadi Howar (Sudan). In: Kuper, R. (Ed.), *Tides of the Desert – Gezeiten der Wüste*. Africa Praehistorica, Vol. 14, Heinrich-Barth-Institut, Köln, pp. 389–398.
- Besler, H., 2005: The granulometric evolution of aeolian sands – an empirical and statistical approach. In: Garcia-Rojo, R., Herrmann, H. J., and McNamara, S. (Eds), *Powders and Grains 2005*, Vol. II, Balkema, Leiden, pp. 973–976.
- Besler, H., 2006: Sand sources of the Great Sand Sea (Egypt) according to sedimentological analysis. *Zentralblatt für Geologie und Paläontologie*, Teil 1, 2004, pp. 69–83.
- Besler, H., and S. Gut, 1997: Untersuchungen zum Feuchtegehalt in Dünen am Beispiel der Namib/Namibia. *Kölner Geographische Arbeiten, Sonderfolge Afrika*, **13**, 39–47.
- Besler, H., and K. Kuper, 2001: Regionale Klimaentwicklung und menschliche Besiedlung zwischen Niltal und Zentralsahara. In: Sonderforschungsbereich 389 (Ed.), *Kultur- und Landschaftswandel im ariden Afrika – Entwicklungsprozesse unter ökologischen Grenzbedingungen. Ergebnisbericht für die Jahre 1998/2-2001*. Universität zu Köln, pp. 3–64.

- Besler, H., and L. Pfeiffer, 1992: Sand encroachment at Oursi (Burkina Faso): reactivation of fixed dunes or deflation of Mare sands? *Zeitschrift für Geomorphologie, Neue Folge, Suppl.*, **91**, 185–195.
- Besler, H., and L. Pfeiffer, 1995: The Tertiary proto-erg of the Namib: depositional environment of the Tsondab sandstone in Namibia. *J. Namibia Sci. Soc.*, **44**, 7–24.
- Binda, P. L., 1983: On the skewness of some eolian sands from Saudi Arabia. In: Brookfield, M. E., and Ahlbrandt, T. S. (Eds), *Eolian Sediments and Processes, Developments in Sedimentology*, Vol. 38, Elsevier, Amsterdam, pp. 27–39.
- Blumberg, D. G., 2006: Analysis of large aeolian (wind-blown) bedforms using Shuttle Radar Topography Mission (SRTM) digital elevation data. *Remote Sens. Environ.*, **100**, 179–189.
- Blume, H. P., F. Alaily, U. Smettan, and J. Zielinski, 1984: Soil types and associations of southwest Egypt. In: Klitzsch, E., Said, R., and Schrank, E. (Eds), *Research in Egypt and Sudan. Berliner Geowissenschaftliche Abhandlungen*, Vol. A50, Reimer, Berlin, pp. 293–302.
- Blume, H. P., U. Smettan, E. Kalk, and H. Lange, 1987: Mineralbestand typischer Böden der hyperariden Wüste Südwest-Ägyptens. In: *Berliner Geowissenschaftliche Abhandlungen*, Vol. A78, Reimer, Berlin, pp. 117–126.
- Blume, H. P., W. G. Vahrson, and H. Meshref, 1985: Dynamics of water, temperature, and salts in typical arid soils after artificial rainstorms. *Catena*, **12**, 343–362.
- Bolten, A., in press: Geomorphometrische Analysen zur Rekonstruktion holozäner Nutzungspotentiale ausgewählter Standorte in der Western Desert (Ägypten). Dissertation, Universität zu Köln.
- Bolten, A., 2001: Cluster-Analyse von Sanddaten aus der Großen Sandsee (Ägypten) und anderen Ergs. Staatsexamensarbeit, Universität zu Köln, 83 pp. (unpubl.).
- Bolten, A., and O. Bubbenzer, 2006: New elevation data (SRTM/ASTER) for geomorphological and geoarchaeological research in arid regions. *Zeitschrift für Geomorphologie, Suppl.* **142**, 265–279.
- Bötter-Jensen, L., 1997: Luminescence techniques: instrumentation and methods. *Radiat. Meas.*, **27**, 749–768.
- Bötter-Jensen, L., and G. A. T. Duller, 1992: A new system for measuring OSL from quartz samples. *Nucl. Tracks Radiat. Meas.*, **20**, 549–553.
- Bötter-Jensen, L., G. A. T. Duller, A. S. Murray, and D. Banerjee, 1999: Blue light emitting diodes for optical stimulation of quartz in retrospective dosimetry and dating. *Radiat. Prot. Dosim.*, **84**, 335–340.
- Bötter-Jensen, L., S. W. S. McKeever, and A. G. Wintle, 2003: *Optically Stimulated Luminescence Dosimetry*. Elsevier, Amsterdam, 404 pp.
- Bray, H. E., and S. Stokes, 2003: Chronologies for Late Quaternary barchan dune reactivation in the southern Arabian Peninsula. *Quaternary Sci. Rev.*, **22**, 1027–1033.
- Breed, C. S., S. C. Fryberger, S. Andrews, et al., 1979: Regional studies of sand seas using Landsat (ERTS) imagery. In: McKee, E. D. (Ed.), *A Study of Global Sand Seas*. United States Geological Survey Professional Paper, Vol. 1052, US Government Print Office, Washington D.C., pp. 305–398.
- Brezina, J., 1980: Sedimentological interpretation of errors in size analysis of sands. In: International Association of Sedimentologists, 1<sup>st</sup> European Meeting, Abstracts, Bochum 1980, pp. 9–11.
- Briem, E., 1977: Beiträge zur Genese und Morphodynamik des ariden Formenschatzes unter besonderer Berücksichtigung des Problems der Flächenbildung (aufgezeigt am Beispiel der Sandschwemmebenen in der östlichen zentralen Sahara). *Berliner Geographische Abhandlungen*, Vol. 26, Appendix. Freie Universität Berlin, pp. 1–89.

- Brinkmann, P. J., and M. Heintz, 1986: Numerical groundwater model. In: Thorweihe, U. (Ed.), *Impact of climatic variations on East Saharian groundwaters – Modelling of large scale flow regimes*. Berliner Geowissenschaftliche Abhandlungen, Vol. A72, Reimer, Berlin, pp. 135–155.
- Bristow, C. S., G. A. T. Duller, and N. Lancaster, 2007: Age and dynamics of linear dunes in the Namib Desert. *Geology*, **35**, 555–558.
- Brookes, I. A., 2001: Aeolian erosional lineations in the Libyan Desert, Dakhla Region, Egypt. *Geomorphology*, **39**, 189–209.
- Brookes, I. A., 2003: Geomorphic indicators of Holocene winds in Egypt's Western Desert. *Geomorphology*, **56**, 155–166.
- Brookfield M. E., and T. S. Ahlbrandt, (Eds), 1983: Eolian sediments and processes. *Developments in Sedimentology*, Vol. 38, Elsevier, Amsterdam, pp. 1–660.
- Brosset, D., 1939: Essai sur les ergs du Sahara occidental. *Bulletin de l'Institut Français d'Afrique Noire*, **1**, 657–690.
- Brown, R. A., 1983: The flow in the planetary boundary layer. In: Brookfield, M. E., and Ahlbrandt, T. S. (Eds), *Eolian Sediments and Processes, Developments in Sedimentology*, Vol. 38, Elsevier, Amsterdam, pp. 291–310.
- Brunt, D., 1937: Natural and artificial clouds. *Q. J. R. Meteorol. Soc.*, **63**, 277–288.
- Brunt, D., 1951: *Experimental cloud formation. Compendium of Meteorology*, American Meteorological Society, Boston, pp. 1255–1262.
- Bubenzer, O., 2000: Abu Muharik – Nord-Süd-Wandel und Genese eines 500 km langen ägyptischen Dünenzuges. In: Abstracts 26. AK Geomorphologie 4.-7.10. 2000, Universität Trier, pp. 12–14.
- Bubenzer, O., 2001: Manual coring equipment for the collection of stratified samples from dry sand dunes. *Ancient TL*, **19**, 1–3.
- Bubenzer, O., and H. Besler, 2005: Human occupation of sand seas during the early and mid-Holocene, examples from Egypt. *Zeitschrift für Geomorphologie, Neue Folge, Suppl.*, **138**, 153–165.
- Bubenzer, O., H. Besler, and A. Hilgers, 2007b: Filling the gap: OSL data expanding <sup>14</sup>C chronologies of Late Quaternary Environmental change in the Libyan Desert. *Quaternary Int.*, 175, 41–52.
- Bubenzer, O., O. Bödeker, and H. Besler, H., 2007a: A transcontinental comparison between the southern Namib Erg (Namibia) and the Southern Great Sand Sea (Egypt). *Zentralblatt für Geologie and Paläontologie I*, **2006**, 7–23.
- Bubenzer, O., and A. Bolten, in press: The use of new elevation data (SRTM/ASTER) for the detection and morphometric quantification of Pleistocene megadunes (draa) in the eastern Sahara and the southern Namib. *Geomorphology*.
- Bubenzer, O., and H. Riemer, 2007: Holocene climatic change and human settlement between the Central Sahara and the Nile Valley: archaeological and geomorphological results. *Geoarchaeology*, **22**, 607–620.
- Cailleux, A., 1952: Morphoskopische Analyse der Geschiebe und Sandkörner und ihre Bedeutung für die Paläoklimatologie. *Geologische Rundschau*, **40**, 11–19.
- Cailleux, A., 1972: Contribution de la morphoscopie des sables à la géomorphologie de l'URSS et du Nord-Ouest de la Chine. In: Hövermann, J., and Oberbeck, G. (Eds), *Hans-Poser-Festschrift, Göttinger Geographische Abhandlungen*, Vol. 60, Erich Goltze KG, Göttingen, pp. 39–63.
- Callot, Y., 1998: Aeolian forms and climatic changes in the Great Western Erg, Algerian Sahara. In: Alsharhan, A. S., Glennie, K. W., Whittle, G. L., et al. (Eds), *Quaternary Deserts and Climatic Change*. Balkema, Rotterdam, pp. 251–259.
- Capot-Rey, R., 1945: Dry and humid morphology in the Western Erg. *Geogr. Rev.*, **35**, 391–407.

- Capot-Rey, R., 1947: L'Edeyen de Mourzouk. *Travaux de l'Institut de Recherches Sahariennes*, Vol. 4, Université d'Alger, pp. 67–109.
- Capot-Rey, R., 1970: Remarques sur les ergs du Sahara. *Annales de Géographie*, **79**, 2–19.
- Capot-Rey, R., A. Cornet, and B. Blaudin de Thé, 1963: Glossaire des principaux termes géographiques et hydrogéologiques sahariens. *Institut de Recherches Sahariennes*, Alger, 82 pp.
- Capot-Rey, R., and M. Grémion, 1964: Remarques sur quelques sables sahariens. *Travaux de l'Institut de Recherches Sahariennes*, Vol. 23, Université d'Alger, pp. 153–163.
- Chamard, P. C., and H. T. Courel, 1981: De l'autochthonie des dépôts superficiels du Liptako Nigero-Voltaïque. *Revue de Géomorphologie Dynamique*, **30**, 11–20.
- Chapman, R. W., 1978: Geomorphology. In: Al-Sayari, S. S., and Zötl, J. G. (Eds), *Quaternary Period in Saudi-Arabia. 1. Sedimentological, Hydrogeological, Hydrochemical, Geomorphological and Climatological Investigations in Central and Eastern Saudi-Arabia*. Springer, Wien, pp. 19–30.
- Chrintz, T., and L. B. Clemmensen, 1993: Draa reconstruction, the Permian Yellow Sands, northeast England. *Special Publications of the International Association of Sedimentologists*, **16**, 151–161.
- CGIAR–CSI (Consortium for Spatial Information), 2007: *Consultative Group for International Agriculture Research (CGIAR)*. <http://www.csi.cgiar.org> (accessed, June 6th, 2007).
- Clarke, M. L., H. M. Rendell, and Wintle, A. G., 1999: Quality assurance in luminescence dating. *Geomorphology*, **29**, 173–185.
- Clayton, P. A., and M. A. Spencer, 1932: Silica glass from the Libyan Desert. *J. Miner. Soc.*, **23**(137), 501–508.
- Cooke, R. U., and A. Warren, 1973: *Geomorphology in Deserts*. Batsford, London, 374 pp.
- Corbett, I., 1993: The modern and ancient pattern of sandflow through the southern Namib deflation basin. *Int. Assoc. Sedimentol. Spec. Publ.*, **16**, 45–60.
- Cuartero, A., A. M. Felicismo, and F. J. Ariza, 2005: Accuracy, reliability, and depuration of SPOT HRV and Terra ASTER digital elevation models. *IEEE Trans. Geosci. Remote Sens.*, **43**, 404–407.
- Czegka, W., and S. Braune, 2005. SRTM-90 m Höhendaten und ihre Verwendbarkeit in Geoinformations-Systemen in Hinblick auf Anwendungsmöglichkeiten in den Geo- und Umweltwissenschaften. *Zeitschrift für Geologische Wissenschaft Berlin*, **33**, 199–208.
- De Michele, V. (Ed.), 1997: Silica '96. *Proceedings Centro Studi Luigi Nero, Pyramids*. Segrate, Milano, 158 pp.
- Dikau, R., 1989: Application of a digital elevation model to landform analysis in geomorphology. In: Raper, J. (Ed.), *Three Dimensional Application in Geographic Information Systems*. Tylor & Francis, London, pp. 51–77.
- Donner, J., and N. S. Embabi, 2000: The significance of yardangs and ventifacted rock outcrops in the reconstruction of changes in the late Quaternary wind regime in the Western Desert of Egypt. *Quaternaire*, **11**(3–4), 179–185.
- Doornkamp, J. C., and D. H. Krinsley, 1973: Chronicles in grains of sand. *Geogr. Mag.*, **45**, 633–635.
- Duller, G. A. T., 2004: Luminescence dating of Quaternary sediments: recent advances. *J. Quaternary Sci.*, **19**, 183–192.
- Duller, G. A. T., L. Bøtter-Jensen, and A. S. Murray, 2000: Optical dating of single sand-sized grains of quartz: sources of variability. *Radiat. Meas.*, **32**, 453–457.
- Edgell, H. S., 2006: *Arabian Deserts – Nature, Origin, and Evolution*. Springer, Dordrecht, The Netherlands, 592 pp.
- El-Baz, F., 1982: Genesis of the Great Sand Sea, Western Desert of Egypt. In: International Association of Sedimentologists (Ed.), 11th International Congress of Sedimentology, Hamilton 1980. Abstracts of Papers, Hamilton, p. 68.

- El-Baz, F., 1998: Sand accumulation and groundwater in the eastern Sahara. *Episodes*, **21**, 147–151.
- El-Baz, F., 2007. Radar images and geoarchaeology of the Eastern Sahara. In: Wiseman, J., and El-Baz, F. (Eds), *Remote Sensing in Archaeology*. Springer, New York, pp. 47–69.
- El-Baz, F., M. Mainguet, and C. Robinson, 2000: Fluvio-aeolian dynamics in the north-eastern Sahara: the relationship between fluvial/aeolian systems and ground-water concentration. *J. Arid Environ.*, **44**, 173–183.
- El-Baz, F., and D. Prestel, 1982: Coatings on sand grains from southwestern Egypt. In: El-Baz, F., and Maxwell, T. A. (Eds), *Desert Landforms of Southwest Egypt: A Basis for Comparison with Mars*. Scientific Technical Information Bureau, NASA, Washington, DC, pp. 175–188.
- El-Baz, F., and R. W. Wolfe, 1982: Wind patterns in the Western Desert In: El-Baz, F., and Maxwell, T. A. (Eds), *Desert Landforms of Southwest Egypt – A Basis for Comparison with Mars*. Scientific Technical Information Bureau, NASA, Washington, DC, pp. 119–139.
- Embabi, N. S., 1991: Dune types and patterns in the United Arab Emirates using LANDSAT TM data. In: *Proceedings of the Twenty-fourth International Symposium on Remote Sensing of Environment*. Vol. II, Rio de Janeiro, Brazil, pp. 895–909.
- Embabi, N. S., 1998: Sand seas of the Western Desert of Egypt. In: Alsharhan, A. S., Glennie, K. W., Whittle, G. L., et al. (Eds), *Quaternary Deserts and Climatic Change*. Balkema, Rotterdam, pp. 495–509.
- Embabi, N. S., 2000: Sand dunes in Egypt. In: Soliman, S. M. (Ed.), *Sedimentary Geology of Egypt, Applications and Economics*. Ain Shams University, Cairo, pp. 45–87.
- Embabi, N. S., 2004: The geomorphology of Egypt. *Landforms and Evolution Vol. I: The Nile Valley and the Western Desert*. The Egyptian Geographical Society Special Publication, Cairo, 447 pp.
- EOS DG, 2007: Earth Observing System Data Gateway. *Land Processes – Distributed Active Archive Center*. <http://edcimswww.cr.usgs.gov/pub/imswelcome> (accessed June 9th, 2007).
- Farr, T. G., P. A. Rosen, E. Caro, et al., 2007: *The Shuttle Radar Topography Mission*. *Reviews of Geophysics*, Vol. 45, doi:10.1029/2005RG000183.
- Fay, M., and W. Herrmann-Degen, 1984: Mineralogy of Campanian/Maastrichtian sand deposits and a model of basin development for the Nubian Group of the Dakhla Basin (Southwest Egypt). In: Klitzsch, E., Said, R., and Schrank, E. (Eds), *Research in Egypt and Sudan. Berliner Geowissenschaftliche Abhandlungen*, Vol. A50, Reimer, Berlin, pp. 99–115.
- Fenwick, G. A., 1991: Grain size and easterly wind influences on dunes of the north central Namib desert. *Zeitschrift für Geomorphologie, Neue Folge*, **35**, 283–292.
- Folk, R. L., 1971: Longitudinal dunes of the northwestern edge of the Simpson Desert, Northern Territory, Australia. 1. Geomorphology and grain size relationships. *Sedimentology*, **16**, 5–54.
- Folk, R. L., 1978: Angularity and silica coatings of Simpson Desert sand grains, Northern Territory, Australia. *J. Sediment. Petrol.*, **48**, 611–624.
- Folk, R. L., and W. C. Ward, 1957: Brazos River Bar: a study on the significance of grain size parameters. *J. Sediment. Petrol.*, **27**, 3–26.
- Friedman, G. M., 1961: Distinction between dune, beach, and river sands from their textural characteristics. *J. Sediment. Petrol.*, **31**, 514–529.
- Friedman, G. M., 1962: On sorting, sorting coefficients, and the lognormality of the grain-size distribution of sandstones. *J. Geol.*, **70**(6), 737–753.
- Friedman, G. M., 1967: Dynamic processes and statistical parameters compared for size frequency distribution of beach and river sands. *J. Sediment. Petrol.*, **37**, 327–354.
- Fürst, M., 1966: Bau und Entstehung der Serir Tibesti. *Zeitschrift für Geomorphologie, Neue Folge*, **10**, 387–418.



- Gabriel, A., 1934: Beobachtungen im Wüstengürtel Innerpersiens. *Mitteilungen der Geographischen Gesellschaft Wien*, **77**, 53–77.
- Garbrecht, J., J. Campbell, and L. Martz, 2004: TOPAZ User manual. Grazinglands Research Laboratory Miscellaneous Publication. Available: <http://www.ars.usda.gov/Research/docs.htm?docid=7837> (accessed June 9th, 2007).
- Gasse, F., and E. van Campo, 1994: Abrupt Post-glacial Climate Events in West Asia and North Africa Monsoon Domains. *Earth Planet. Sci. Lett.*, **126**, 435–456.
- Gautier, E. F., 1950: *Le Sahara* (3rd Edition), Payot, Paris, 231 pp.
- Gees, R. A., 1969: Surface textures of quartz sand grains from various depositional environments. *Beiträge zur Elektronenmikroskopischen Direktabbildung von Oberflächen*, Vol. 2, Münster, pp. 283–297.
- Gehlen, B., K. Kindermann, J. Linstädter, and H. Riemer, 2002: The Holocene occupation of the Eastern Sahara: regional chronologies and supra-regional developments in four areas of the absolute desert. *Africa Praehistorica*, Vol. 14, Heinrich-Barth-Institut, Köln, pp. 85–116.
- Gesch, D. B., and K. S. Larson, 1996: Techniques for development of global 1-kilometer digital elevation models. *Pecora Thirteen Human Interactions with the Environment – Perspectives from Space*, 20–22. Available: <http://edc.usgs.gov/products/elevation/topo30/papers/geschd3.html> (accessed June 9th, 2007).
- Gläser, B., 1984: Quantitative Untersuchungen zur Morphogenese und Mobilität des Altdünen-Komplexes in der Provinz Weisser Nil. In: Mensching, H. G. (Ed.), *Beiträge zur Morphodynamik im Relief des Jebel-Marra-Massivs und in seinem Vorland (Darfur/Republik Sudan)*. Akademie der Wissenschaften in Göttingen, pp. 202–217.
- GLCF, 2007: *Global Land Cover Facility*. <http://glcf.umiacs.umd.edu/data/srtm> (accessed June 9th, 2007).
- Glennie, K. W., 1991: Sand dunes in the Emirates. *Tribulus*, **1.1**, 14–17.
- Glennie, K. W., 1998: The desert of southeast Arabia: A product of Quaternary climatic change. In: Alsharhan, A. S., Glennie, K. W., Whittle, G. L., et al. (Eds), *Quaternary Deserts and Climatic Change*. Balkema, Rotterdam, pp. 279–291.
- Godfrey-Smith, D. I., D. J. Huntley, W.-H. Chen, 1988: Optical dating studies of quartz and feldspar sediment extracts. *Quaternary Sci. Rev.*, **7**, 373–380.
- Goudie, A. S., A. Colls, S. Stokes, et al., 2000: Latest Pleistocene and Holocene dune construction at the north-eastern edge of the RubAl Khali. United Arab Emirates. *Sedimentology*, **47**, 1011–1021.
- Goudie, A. S., R. U. Cooke, J. C. Doornkamp, 1979: The formation of silt from quartz dune sand by salt-weathering processes in deserts. *J. Arid Environ.*, **2**, 105–112.
- Grove, A. T., and A. Warren, 1968: Quaternary landforms and climate on the south side of the Sahara. *Geogr. J.*, **134**, 194–209.
- Grün, R., 1989: Die ESR-Altersbestimmungsmethode. *Reihe: Hochschultext*. Springer, Berlin-Heidelberg, 132 pp.
- Gut, S., 1988: *Untersuchungen zum Feuchtehaushalt in den Dünen der zentralen Namib (Namibia/Südwestafrika)*. Diplomarbeit, Universität Zürich, 125 pp. (unpubl.).
- Hagedorn, H., 1979: Das Verbreitungsmuster der Dünen am Westrand des Murzuk-Beckens (Zentrale Sahara). In: Hagedorn, H., and Wagner, H. G. (Eds), *Natur- und wirtschaftsgeographische Forschungen in Afrika*. Würzburger Geographische Arbeiten, Vol. 49, Geographisches Institut, Universität Würzburg, pp. 103–123.
- Hanna, S. R., 1969: The formation of longitudinal sand dunes by large helical eddies in the atmosphere. *J. Appl. Meteorol.*, **8**, 874–883.
- Harris, S. A., 1958: Probability curves and the recognition of adjustment to depositional environment. *J. Sediment. Petrol.*, **28**, 151–163.

- Haynes Jr., C. V., 1982: Great Sand Sea and Selima Sand Sheet, Eastern Sahara: geochronology of desertification. *Science*, **217**, 629–633.
- Hecht, F., M. Fürst, and E. Klitzsch, 1964: Zur Geologie von Libyen. *Geol. Rundsch.*, **53**, 413–470.
- Hellwig, D. H. R., 1974: Evaporation of water from sand. 5. The effect of evaporation on the concentration of salts dissolved in the water stored in sand. *J. Hydrol.*, **21**, 101–110.
- Herrmann, H. J., 2005: Spuren im Sand – Die Physik der Dünen. *Physik J.*, **4**(8/9), 57–60.
- Hilgers, A., E. Gehrt, A. Janotta, and U. Radtke, 2001a: A contribution to the dating of the northern boundary of the Weichselian loess belt in Northern Germany by luminescence dating and pedological analysis. *Quaternary Int.*, **76/77**, 191–200.
- Hilgers, A., A. S. Murray, N. Schlaak, and U., Radtke, 2001b: Comparison of quartz OSL protocols using Lateglacial and Holocene dune sands from Brandenburg, Germany. *Quaternary Sci. Rev.*, **20**, 731–736.
- Hillefors, A., 1971: Deep weathered rock material and sand grains under the scanning electron microscope. *Lund Stud. Geogr.*, **A49**, 138–164.
- Hirano, A., R. Welch, and H. Lang, 2003: Mapping from ASTER stereo image data: DEM validation and accuracy assessment. *ISPRS J. Photogramm. Remote Sens.*, **57**, 356–370.
- Hoelzmann, P., F. Gasse, L. M. Dupont, et al., 2004: Palaeoenvironmental changes in the arid and the subarid belt (Sahara-Sahel-Arabian Peninsula) from 150 kyr to present. In: Batterbee, R. W., Gasse, F., and Stickley, C. E. (Eds), *Past Climate Variability through Europe and Africa, Developments in Palaeoenvironmental Research*, Vol. 6, Springer, Dordrecht, pp. 219–256.
- Hövermann, J., and E. Hövermann, 1991: Pleistocene and Holocene geomorphological features between the Kunlun Mountains and the Taklimakan Desert. In: Jäkel, D., and Zhu, Z. (Eds), *Reports on the 1986 Sino-German Kunlun Shan Taklimakan-Expedition*, Die Erde, Ergänzungsheft 6, pp. 51–72.
- Huntley, D. J., and M. R. Baril, 1997: The K content of K-feldspars being measured in optical and thermoluminescence dating. *Ancient TL*, **15**, 11–13.
- Inman, D. L., 1952: Measures for describing the size and distribution of sediments. *J. Sediment. Petrol.*, **22**, 125–145.
- Ivanovich, M. and R. S. Harmon (Eds), 1982: Uranium series disequilibrium: Applications to environmental problems. Oxford University Press, Oxford, 571 pp.
- Jäkel, D., 1991: The evolution of dune fields in the Taklimakan Desert since the Late Pleistocene. Notes on the 1:2 500 000 map of dune evolution in the Taklimakan. In: Jäkel, D., and Zhu, Z. (Eds), *Reports on the 1986 Sino-German Kunlun Shan-Taklimakan-Expedition*, Gesellschaft für Erdkunde zu Berlin, Die Erde, Ergänzungsheft 6, pp. 191–198.
- Jäkel, D., 2002: The importance of dunes for groundwater recharge and storage in China. *Zeitschrift für Geomorphologie, Neue Folge, Suppl.*, **126**, 131–146.
- Jäkel, D., and H. Rückert, 1998: Recent rainfall distribution patterns of the Republic of Sudan as a model for rainfall variations in the past and climate-induced geomorphological processes in Sahelian countries. *Palaeoecol. Afr.*, **25**, 101–120.
- JPL, 2007: Jet Propulsion Laboratory, NASA. California Institute of Technology <http://www2.jpl.nasa.gov/srtm/instr.htm> (accessed June 9th, 2007).
- Juyal, N., A. K. Singhvi, and K. W. Glennie, 1998: Chronology and palaeoenvironmental significance of Quaternary desert sediment in southeastern Arabia. In: Alsharhan, A. S., Glennie, K. W., Whittle, G. L., et al. (Eds), *Quaternary Deserts and Climatic Change*. Balkema, Rotterdam, pp. 315–325.
- Kääb, A. C., F. P. Huggl, and R. Wessels, 2002: Glacier monitoring from ASTER imagery: accuracy and applications. *EARSeL Proceedings LIS-SIG Workshop*, Bern (March 11–13), pp. 43–53.

- Kádár, L., 1934: A study of the sand sea in the Libyan Desert. *Geogr. J.*, **83**, 470–478.
- Kanter, H., 1943: Der Fezzan als Beispiel innersaharischer Becken. In: Krebs, N. (Ed.), *Sitzungsberichte der Zusammenkunft Europäischer Geographen in Würzburg* 16. bis 19. März 1942. Quelle und Meyer, Leipzig, pp. 403–463.
- Kanter, H., 1973: Der Südosten und Osten des Libyschen Raumes. In: Schiffers, H. (Ed.), *Die Sahara und ihre Randgebiete*, Vol. 3, Weltforum, München, pp. 370–423.
- Karátson, D., and G. Timár, 2005: Comparative volumetric calculations of two segments of the Carpathian Neogene/Quaternary volcanic chain using SRTM elevation data: implications to erosion and magma output rates. *Zeitschrift für Geomorphologie, Neue Folge, Suppl.*, **140**, 19–35.
- Kindermann, K., O. Bubenzer, F. Darius, et al., 2006: Palaeoenvironment and Holocene land use of Djara, Western Desert of Egypt. *Quaternary Sci. Rev.*, **25**, 1619–1637.
- Klitzsch, E., 1967: Bericht über eine Ost–West–Querung der Zentralsahara. *Zeitschrift für Geomorphologie, Neue Folge*, **11**, 62–92.
- Klitzsch, E., 1983: Paleozoic formations and a Carboniferous glaciation from the Gilf Kebir–Abu Ras Area in southwestern Egypt. *J. Afr. Earth Sci.*, **1**, 17–19.
- Klitzsch, E., F. K. List, and G. Pöhlmann, 1986–1987: *Geological Map of Egypt 1:500 000*. The Egyptian General Petroleum Corporation, Cairo.
- Knetsch, G., 1950: Beobachtungen in der libyschen Sahara. *Geol. Rundsch.*, **38**, 40–60.
- Kowalkowski, A., and E. Mycielska-Dowgiałło, 1985: Weathering of quartz grains in the liquefied horizon of permafrost solonchaks in the arid steppe zone, central Mongolia. *Catena*, **12**, 179–190.
- Krbetschek, M. R., U. Rieser, L. Zöller, and J. Heinicke, 1994: Radioactive disequilibria in palaeodosimetric dating of sediments. *Radiat. Meas.*, **23**, 485–489.
- Krinsley, D. H., and J. C. Doornkamp, 1973: *Atlas of Quartz Sand Surface Textures*. University Press, Cambridge, 91 pp.
- Krinsley, D., and S. Margolis, 1971: Quartz sand grain surface textures. In: Carver, R. E. (Ed.), *Procedures in Sedimentary Petrology*. Wiley & Sons, New York, pp. 151–180.
- Kröpelin, S., 1993: Geomorphology, Landscape Evolution and Paleoclimates of Southwest Egypt. In: Meissner, B., and Wycisk, P. (Eds), *Geopotential and Ecology – Analysis of a Desert Region, Catena Supplement*, Vol. 26, Catena, Cremlingen-Destedt, pp. 31–65.
- Krumbein, W. C., 1934: Size frequency distribution of sediments. *J. Sediment. Petrol.*, **4**, 65–77.
- Krumbein, W. C., 1936: Application of logarithmic moments to size frequency distribution of sediments. *J. Sediment. Petrol.*, **6**, 35–47.
- Krumbein, W. C., and F. J. Pettijohn, 1938: *Manual of Sedimentary Petrography*. D. Appleton–Century, New York, 549 pp.
- Kubiena, W., 1957. Neue Beiträge zur Kenntnis des planetarischen und hypsometrischen Formenwandels der Böden Afrikas. In: Wilhelmy, H. (Ed.), *Hermann Lautensach-Festschrift*. Stuttgarter Geograph. Studien, Vol. 69, 50–64.
- Kuenen, P. H., and W. G. Perdok, 1962: Experimental abrasion: 5. Frosting and defrosting of quartz grains. *J. Geol.*, **70**, 648–658.
- Kuhlman, H., 1959: On identification of blown sand. An example from the salt-marsh area at Tonder. *Geografisk Tidsskrift*, **58**, 182–196.
- Kuper, R., 1989: The Eastern Sahara from North to South: data and dates from the B.O.S. Project. In: Krzyzaniak, L., and Kobusiewicz, M. (Eds), *Late Prehistory of the Nile Basin and the Sahara*. Studies in African Archaeology, Vol. 2, Archaeological Museum Poznań, pp. 197–203.
- Kuper, R., 1995: Prehistoric Research in the Southern Libyan Desert. A brief account and some conclusions of the B. O. S. project. In: Actes de la VIIIe conférence Internationale des Études Nubiennes (Lille 11.17.09. 1994), Cripel 17, Université Lille 3, pp. 123–140.

- Kuper, R., 1999: Auf den Spuren der frühen Hirten. *Archäologie in Deutschland*, **2**, 12–17.
- Kuper, R., 2006: After 5000 BC: The Libyan Desert in transition. *Comptes Rendus Palevol*, **5**, 409–419.
- Kuper, R., and S. Kröpelin, 2006: Climate-controlled Holocene occupation in the Sahara: motor of Africa's evolution. *Science*, **313**, 803–807.
- Lancaster, N., 1983: Controls of dune morphology in the Namib sand sea. In: Brookfield, M. E., and Ahlbrandt, T. S. (Eds), *Eolian Sediments and Processes, Developments in Sedimentology*, Vol. 38, Elsevier, Amsterdam, pp. 261–290.
- Lancaster, N., 1989: *The Namib Sand Sea*. Balkema, Rotterdam, 180 pp.
- Lancaster, N., 1998: Dune morphology, chronology, and Quaternary climatic change. In: Alsharhan, A. S., K. W. Glennie, G. L. Whittle, et al. (Eds), *Quaternary Deserts and Climatic Change*. Balkema, Rotterdam, pp. 339–349.
- Lancaster, N., G. Kocurek, A. Singhvi, et al., 2002: Late Pleistocene and Holocene dune activity and wind regimes in the western Sahara Desert of Mauritania. *Geology*, **30**, 991–994.
- Lang, G., 1994: *Quartäre Vegetationsgeschichte Europas*. Fischer, Jena, 462 pp.
- Le Ribault, L., 1975: *L'exoscopie. Méthode et applications. Notes et Mémoires*, 12, 230 pp. Total, Paris.
- Le Ribault, L., 1977: *L'exoscopie des quartz*. Masson, Paris, 150 pp.
- Leroux, M., 1991: Paléométéorologie de la région de Taoudenni. In: Petit-Maire, N. (Ed.), *Paléoenvironnements du Sahara*. Centre National de la Recherche Scientifique Paris, pp. 197–233.
- Levin, N., H. Tsoar, L. P. Maia, et al., 2007: Dune whitening and inter-dune freshwater ponds in NE Brazil. *Catena*, **70**, 1–15.
- Lian, O. B., and R. G. Roberts, 2006: Dating the Quaternary: progress in luminescence dating of sediments. *Quaternary Sci. Rev.*, **25**, 2449–2468.
- Lillesand, T. M., R. W. Kiefer, and J. W. Chipman, 2004: *Remote Sensing and Image Interpretation*. Wiley, New York, 784 pp.
- Linsenbarth, A., 1996: A remote sensing approach to geomorphological investigations of sand desert areas. Libyan Sahara case study. *Proceedings of the Institute of Geodesy and Cartography*, **93**, 255 pp., Warszawa.
- List, F. K., B. Meissner, and G. Pöhlmann, 1990: Application of remote sensing and satellite cartography in preparing new geological map 1:500 000. In: Said, R. (Ed.), *Geology of Egypt*. Balkema, Rotterdam, pp. 27–44.
- Livingstone, I., 1987: Using the response diagram to recognise zones of aeolian activity: a note on evidence from a Namib dune. *J. Arid Environ.*, **13**, 25–30.
- Livingstone, I., 1989: Applying Besle's response diagram: a comment. *Zeitschrift für Geomorphologie, Neue Folge*, **33**, 499–502.
- Livingstone, I., and D. S. G. Thomas, 1993: Modes of linear dune activity and their palaeoenvironmental significance: an evaluation with reference to southern African examples. *Geol. Soc. Spec. Publ.*, **72**, 91–101.
- Madigan, C. T., 1936: The Australian Sand-Ridge Deserts. *Geogr. Rev.*, **26**, 205–227.
- Mahaney, W. C., 2002: *Atlas of Sand Grain Surface Textures and Applications*. University Press, Oxford, 237 pp.
- Mahaney, W. C., and W. Andres, 1996: Scanning electron microscopy of quartz sand from the north-central Saharan desert of Algeria. *Zeitschrift für Geomorphologie, Neue Folge, Suppl.*, **103**, 179–192.
- Mainguet, M., 1976: Propositions pour une nouvelle classification des édifices sableux éoliens d'après les images des satellites LANDSAT I, GEMINI, NOAA 3. *Zeitschrift für Geomorphologie, Neue Folge*, **20**, 275–296.

- Mainguet, M., and Y. Callot, 1978: Lèrg de Fachi-Bilma (Tchad-Niger). Contribution à la connaissance de la dynamique des ergs et des dunes des zones arides chaudes. *Mémoires et Documents. Nouvelle Série*, **18**, 1–184.
- Mainguet, M., and M. C. Chemin, 1983: Sand seas of the Sahara and Sahel: an explanation of their thickness and sand dune type by the sand budget principle. In: Brookfield, M. E., and Ahlbrandt, T. S., (Eds), *Eolian Sediments and Processes, Developments in Sedimentology*, Vol. 38, Elsevier, Amsterdam, pp. 353–363.
- Mainguet, M., and M. Vimeux-Richeux, 1981: Autochthonie et allochthonie des sables éoliens. Etude des minéraux lourds de la couverture du Niger. *Comptes Rendus de l'Académie de Sciences, Paris, Série II*, **292**, 1437–1440.
- Margolis, S. V., and D. H. Kinsley, 1971: Submicroscopic frosting on eolian and subaqueous quartz sand grains. *Geol. Soc. Am. Bull.*, **82**, 3395–3406.
- Mason, C. C., and R. L. Folk, 1958: Differentiation of beach, dune and aeolian flat environments by size analysis, Mustang Island, Texas. *J. Sediment. Petrol.*, **28**, 211–226.
- Mayhew, S., and A. Penny, 1992: *The Concise Oxford Dictionary of Geography*. University Press, Oxford, 250 pp.
- McCauley, J. F., G. G. Schaber, C. S. Breed, et al., 1982: Subsurface valleys and geoarchaeology of the Eastern Sahara revealed by shuttle radar. *Science*, **218**, 1004–1020.
- McClure, H. A., 1978: Ar Rub' al Khali. In: Al Sayary, S., and Zötl., J. G., (Eds), *Quaternary Period in Saudi Arabia*. Springer, Wien, pp. 252–263.
- McCoy, J., K. Johnston, 2001. *Using ArcGIS Spatial Analyst*. ESRI press, Redlands, 236 pp.
- McKee, E. D., 1983: Eolian sand bodies of the world. In: Brookfield, M. E., and Ahlbrandt, T. S. (Eds), *Eolian Sediments and Processes, Developments in Sedimentology*, Vol. 38, Elsevier, Amsterdam, pp. 1–25.
- McKee, E. D., and G. C. Tibbitts, 1964: Primary structures of a seif dune and associated deposits in Libya. *J. Sediment. Petrol.*, **34**, 5–17.
- Mejdahl, V., 1979: Thermoluminescence dating: Beta-dose attenuation in quartz grains. *Archaeometry*, **21**, 61–72.
- Mendelsohn, J., A. Jarvis, and C. Roberts, 2002: *Atlas of Namibia. A portrait of the land and its people*. David Philip Publishers, Cape Town, 200 pp.
- Michel, P., 1977: Geomorphologische Forschungen in Süd- und Zentral-Mauretarien (Probleme der Lateritmäntel, Eisenpanzer, Kalkkrusten, der Einfluss von Klimaschwankungen). *Mitteilungen der Basler Afrika-Bibliographien*, **19**, 81–108.
- Miliaresis, G. C., and C. V. Paraschou, 2005: Vertical accuracy of the SRTM DTED level I of Crete. *International Journal of Applied Earth Observation and Geoinformation*, **7**, 49–59.
- Möckel, A., 2004: *Granulometrischer Vergleich mitteleuropäischer Binnendünen mit aktuellen Wüstendünen*. Diplomarbeit, Universität zu Köln, 107 pp. (unpubl.).
- Moiola, R. J., and D. Weiser, 1968: Textural parameters: an evaluation. *J. Sediment. Petrol.*, **38**, 45–53.
- Müller, G., 1964: *Sediment-Petrologie Teil I: Methoden der Sediment-Untersuchung*. Stuttgart, 303 pp.
- Müller, H. D., 1981: *Die Entwicklung des Oasengebietes von Al-Kharga (Ägypten) als Resultat ökologischer Bedingungen und sozioökonomischen Wandels*. Diplomarbeit, Universität Göttingen, 142 pp. (unpubl.)
- Munyikwa, K., 2005: The role of dune morphogenetic history in the interpretation of linear dune luminescence chronologies: a review of linear dune dynamics. *Prog. Phys. Geogr.*, **29**, 317–336.
- Murray, A. S., and J. M. Olley, 1999: Determining sedimentation rates using luminescence dating. In: Bruns, P., and Haas, H. C. (Eds), *Determination of Sediment Accumulation Rates*. GeoResearch Forum, Vol. 5, Trans Tech Publications, Switzerland, pp. 121–144.

- Murray, A. S., and A. G. Wintle, 2000: Luminescence dating of quartz using an improved single-aliquot regenerative-dose protocol. *Radiat. Meas.*, **32**, 57–73.
- Neumann, K., 1989a: Vegetationsgeschichte der Ostsahara im Holozän: Holzkohlen aus prähistorischen Fundstellen. In: Kuper, R. (Ed.), *Forschungen zur Umweltgeschichte der Ostsahara. Africa Praehistorica*, Vol. 2, Heinrich-Barth-Institut, Köln, pp. 13–182.
- Neumann, K., 1989b: Holocene vegetation of the eastern Sahara: charcoals from prehistoric sites. *Afr. Archaeol. Rev.*, **7**, 97–116.
- Nicholson, S., and H. Flohn, 1980: African environmental and climatic changes and the general circulation in late Pleistocene and Holocene. *Clim. Change*, **2**, 313–348.
- Nishimori, H., M. Yamasaki, and K. H. Anderson, 1998: A simple model for the various pattern dynamics of dunes. *Int. J. Modern Phys.*, **B12**, 257–272.
- Norris, R. M., and K. S. Norris, 1961: Algodones dunes of southeastern California. *Geol. Soc. Am. Bull.*, **72**, 605–620.
- Olley, J. M., Murray, A. S. and R. G. Roberts, 1996: The effects of disequilibria in the uranium and thorium decay chains on burial dose rates in fluvial sediments. *Quaternary Science Reviews*, **15**, 751–760.
- Olley, J. M., R. G. Roberts, and A. S. Murray, 1997: Disequilibria in the uranium decay series in sedimentary deposits at Allen's Cave, Nullarbor Plain, Australia: Implications for dose rate determinations. *Radiat. Meas.*, **27**, 433–443.
- Otto, G. H., 1939: A modified logarithmic probability graph for the interpretation of mechanical analyses of sediments. *J. Sediment. Petrol.*, **9**, 62–76.
- Pachur, H. J., 1966: Untersuchungen zur morphoskopischen Sandanalyse. Berliner Geographische Abhandlungen 4, pp. 1–32. Freie Universität Berlin.
- Pachur, H. J., 1974: Geomorphologische Untersuchungen im Raum der Serir Tibesti (Zentralsahara). Berliner Geographische Abhandlungen, 17, pp. 1–62. Freie Universität Berlin.
- Pachur, H. J., 1982: Das Abflußsystem des Djebel Dalmar—eine Singularität? *Würzburger Geographische Arbeiten*, 56, 93–110.
- Pachur, H. J., 1993: Paläodrainagesysteme im Sirte-Becken und seiner Umrahmung. *Würzburger Geographische Arbeiten*, 87, 17–34.
- Pachur, H. J., 1999: Paläo-Environment und Drainagesysteme der Ostsahara im Spätpleistozän und Holozän. In: Klitzsch, E., and Thorweihe, U. (Eds), *Nordost-Afrika: Strukturen und Ressourcen – Ergebnisse aus dem SFB 69 Geowissenschaftliche Probleme in ariden und semiariden Gebieten*. Weinheim, Wiley-VCH, pp. 366–445.
- Pachur, H. J., and N. Altmann, 2006: *Die Ostsahara im Spätquartär*. Springer, Berlin, 662 pp.
- Pachur, H. J., and G. Braun, 1980: The paleoclimate of the central Sahara, Libya and the Libyan Desert. *Palaeocol. Afr.*, **12**, 351–363.
- Pachur, H. J., and G. Braun, 1986: Drainage systems, lakes and ergs in the eastern Sahara as indicators of Quaternary climatic dynamics. In: Thorweihe, U. (Ed.), *Impact of climatic variations on east Saharian groundwaters – Modelling of large scale flow regimes*. Berliner Geowissenschaftliche Abhandlungen, Vol. A72, Reimer, Berlin, pp. 3–16.
- Pachur, H. J., and P. Hoelzmann, P., 1998: Zur Paläoökologie der Ostsahara. *Berliner Geographische Abhandlungen*, Vol. 63, Freie Universität Berlin, pp. 27–34.
- Pachur, H. J., and H. P. Röper, 1984: The Libyan (Western) Desert and Northern Sudan during the Late Pleistocene and Holocene. In: Klitzsch, E., Said, R., and Schrank, E. (Eds), *Research in Egypt and Sudan*. Berliner Geowissenschaftliche Abhandlungen, Vol. A50, Reimer, Berlin, pp. 249–284.
- Pachur, H. J., H. P. Röper, S. Kröpelin, and M. Goschin, 1987: Late Quaternary hydrography of the eastern Sahara. In: Klitzsch, E., and Schrank, E. (Eds), *Research in Egypt and Sudan. Hydrogeology, Hydrology, Palaeoclimate, Quaternary Geology, Pedology*. Berliner Geowissenschaftliche Abhandlungen, Vol. A75.2, Reimer, Berlin, pp. 331–384.

- Pachur, H. J., and B. Wünnemann, 1996: Reconstruction of the palaeoclimate along 30°E in the eastern Sahara during the Pleistocene/Holocene transition. *Palaeocol. Afr.*, **24**, 1–32.
- Petit-Maire, N., 1994: Natural variability of the Asian, Indian and African monsoons over the last 130 ka. In: Desbois, M., and Désalmand, F. (Eds), *Global Precipitations and Climate Change. NATO, ASI Series*, Vol. 1(26), Springer, Berlin, pp. 3–26.
- Petit-Maire, N., and J. Riser, 1983: *Sahara ou Sahel? Quaternaire Récent du Bassin de Taoudenni (Mali)*. Paris, 473 pp.
- Pfeiffer, L., 1991: Schwermineralanalysen an Dünen sanden aus Trockengebieten mit Beispielen aus Südsahara, Sahel und Sudan sowie der Namib und der Taklamakan. *Bonner Geographische Abhandlungen*, **83**, 235.
- Poldervaart, A., 1957: *Kalahari Sands. Proceedings of the 3. Panafrican Congress on Prehistory, Livingstone, 1955*. London, pp. 106–114.
- Prescott, J. R., and J. T. Hutton, 1994: Cosmic ray contribution to dose rates for luminescence and ESR dating: large depths and long-term variations. *Radiat. Meas.*, **23**, 497–500.
- Prescott, J. R., and J. T. Hutton, 1995: Environmental dose rates and radioactive disequilibrium from some Australian luminescence dating sites. *Quaternary Science Reviews*, **14**, 439–448.
- Preusser, F., B. G. Andersen, G. H. Denton, and C. Schlüchter, 2005: Luminescence chronology of Late Pleistocene glacial deposits in North Westland, New Zealand. *Quaternary Sci. Rev.*, **24**, 2207–2227.
- Preusser, F., D. Radies, and A. Matter, 2002: A 160 000-year record of dune development and atmospheric circulation in southern Arabia. *Science*, **296**, 2018–2020.
- Price, W. A., 1962: Stages of oxidation coloration in dune and barrier sands with age. *Geol. Soc. Am. Bull.*, **73**, 1281–1284.
- Pye, K., and H. Tsoar, 1990: *Aeolian Sand and Sand Dunes*. Unwin Hyman, London, 396 pp.
- Qian, Y., Z. Wu, and T. Ishii, et al., 1994: A Study on the Sand Source of the Taklimakan Desert. *Chin. J. Arid Land Res.*, **7**, 123–131.
- Rabus, B. M., A. R. Eineder, and R. Bamler, 2003: The shuttle radar topography mission – a new class of digital elevation models acquired by spaceborne radar. *ISPRS J. Photogram. Remote Sens.*, **57**, 241–262.
- Radtke, U., A. Janotta, A. Hilgers, and A. S. Murray, 2001: The potential of OSL and TL for dating Late Glacial and Holocene dune sands tested with independent age control of the Laacher See-tephra (12 880 a) at the section ‘Mainz-Gonsenheim’. *Quaternary Sci. Rev.*, **20**, 719–724.
- Riemer, H., 2003: The ‘Re-conquest’ of the Great Sand Sea. In: Hawass, Z., and Pinch Brock, L. (Eds), *Egyptology at the Dawn of the Twenty-first Century. Proceedings of the Eighth International Congress of Egyptologists Cairo 2000*. American University in Cairo Press, Cairo, pp. 408–415.
- Riemer, H., 2004a: Holocene game drives in the Great Sand Sea of Egypt? Stone structures and their archaeological evidence. *Sahara*, **15**, 31–42.
- Riemer, H., 2004b: News about the Clayton Rings: long distance desert travellers during Egypt’s Predynastic. In: Hendrickx, S., Friedman, R. F., Ciałowicz, K. M., and Chłodnicki, M. (Eds), *Egypt at its Origins. Studies in Memory of Barbara Adams*. Orientalia Lovaniensia Analecta, Vol. 138, Peeters Publisher, Leuven, pp. 972–989.
- Riemer, H., 2005: Pastoralism and the ‘absolute’ desert. A view from the southern Great Sand Sea, Egypt. In: Barich, B. E., Tillet, T., and Striedter, K. H. (Eds), *Hunters vs. Pastoralists in the Sahara: Material Culture and Symbolic Aspects. BAR International Series*, Vol. 1338, Oxford, pp. 57–65.
- Riemer, H., and R. Kuper, 2000: ‘Clayton rings’: enigmatic ancient pottery in the Eastern Sahara. *Sahara*, **12**, 91–100.

- Ritter, M., 2005: *Die neue Klimastation des SFB 389 in Balat (Oase Dakhla, Ägypten)*. Diplomarbeit, Universität zu Köln, 118 pp. (unpubl.).
- Rognon, P., 1989: *Biographie d'un désert*. Plon, Paris, pp. 262–263.
- Rohlfs, G., 1871: *Von Tripolis nach Alexandria*. Hinricus Fischer, Norden.
- Rohlfs, G., 1875: *Drei Monate in der Libyschen Wüste*. Cassel. Reprinted In: *Africa Explorata*, Vol. 1, Heinrich-Barth-Institut, Köln 1996, pp. 1–340.
- Ruck, A., U. Schneider, and K. Stahr, 1987: Water balance of irrigated virgin desert soils of the Selima Sand Sheet (SW-Egypt) and related biomass production. In: Klitzsch, E., and Schrank, E. (Eds), *Research in Egypt and Sudan. Hydrogeology, Hydrology, Palaeoclimate, Quaternary Geology, Pedology*. Berliner Geowissenschaftliche Abhandlungen, Vol. A 75.2, Reimer, Berlin, pp. 545–574.
- Sahu, B. K., 1964: Depositional mechanisms from the size analysis of clastic sediments. *J. Sediment. Petrol.*, **34**, 73–83.
- Schlösser, S., 1995: *Praktische Untersuchungen und theoretische Überlegungen zu Leitfähigkeit und Ionengehalten am Beispiel von Sanden aus der Taklamakan (Tarim-Becken/Sinkiang/China)*. Staatsexamensarbeit, Universität zu Köln, 133 pp. (unpubl.).
- Schmullius, C., W. Flugel, K. Frotscher, et al., 2000: The Shuttle Radar Topography Mission (SRTM) and applications in Europe, Afrika and Siberia. *Photogrammetrie Fernerkundung Geoinformation*, **5**, 361–366.
- Schultz, A., 1927: Morphologische Beobachtungen in der östlichen Kara-Kum-Wüste. *Zeitschrift für Geomorphologie*, **3**, 249–294.
- Schwämmle, V., and H. J. Herrmann, 2003: Solitary wave behaviour of sand dunes. *Nature*, **426**, 619–620.
- Seilacher, A., 1983: Upper Paleozoic trace fossils from the Gilf Kebir–Abu Ras area in southwestern Egypt. *J. Afr. Earth Sci.*, **1**, 21–34.
- Siehl, A., 1996: Grundlagen und geowissenschaftliche Aspekte der Umweltradioaktivität. In: Siehl, A. (Ed.), *Umweltradioaktivität. Geologie und Ökologie im Kontext*. Reihe Geologie und Ökologie im Kontext, Ernst & Sohn, Berlin, pp. 1–30.
- Singhvi, A. K., A. Bluszcz, M. D. Bateman, et al. 2001: Luminescence dating of loess–palaeosol sequences and coversands: methodological aspects and palaeoclimatic implications. *Earth-Sci. Rev.*, **54**, 193–211.
- Smettan, U., and H. P. Blume, 1987: Salts in sandy desert soils, southwestern Egypt. *Catena*, **14**, 333–343.
- Smith, H. T. U., 1968: Nebraska dunes compared with those of North Africa and other regions. In: Schultz, C. B., and Frye, J. C. (Eds), *Loess and related eolian deposits of the world. Proceedings of the VII Congress of the International Association for Quaternary Research USA 1965*, Vol. 12, University Press. Lincoln, Nebraska, pp. 29–47.
- Sonntag, C., U. Thorweihe, and J. Rudolph, et al., 1980: Isotopic identification of Saharan groundwaters, groundwater formation in the past. *Palaeocol. Afr.*, **12**, 159–171.
- Steele, R. P., 1983: Longitudinal draa in the Permian Yellow Sands of north-east England. In: Brookfield, M. E., and Ahlbrandt, T. S. (Eds), *Eolian Sediments and Processes, Developments in Sedimentology*, Vol. 38, Elsevier, Amsterdam, pp. 543–550.
- Steffan, E. M., 1983: *Untersuchungen zur Morphologie und Genese der aeolischen Akkumulationsformen der Otsahara mit Hilfe der Fernerkundung*, Berliner Geowissenschaftliche Abhandlungen, Vol. A45, Reimer, Berlin, 137 pp.
- Stokes, S., 1999: Luminescence dating applications in geomorphological research. *Geomorphology*, **29**, 153–171.



- Stokes, S., Maxwell, T. A., Haynes Jr., C. V., and Horrocks, J. 1998: Latest Pleistocene and Holocene sand-sheet construction in the Selima Sand Sea, Eastern Sahara. In: Alsharhan, A. S., Glennie, K. W., Whittle, G. L., and Kendall, C. G. St. C. (Eds), *Quaternary deserts and climatic change*. Balkeman, Rotterdam, pp. 175–183.
- Stokes, S., D. S. G. Thomas, and P. S. Shaw, 1997: New chronological evidence for the nature and timing of linear dune development in the southwest Kalahari Desert. *Geomorphology*, **20**, 81–93.
- Stokes, S., D. S. G. Thomas, and R. Washington, 1997: Multiple episodes of aridity in southern Africa since the last interglacial period. *Nature*, **388**, 154–158.
- Stuiver, M., and P. Reimer, 1993: Extended  $^{14}\text{C}$  database and revised CALIB 3.0  $^{14}\text{C}$  calibration program. *Radiocarbon*, **35**, 215–230.
- Survey of Egypt, 1941–1945: Egypt, 1:500 000. Survey of Egypt, Giza.
- Swezey, C., 2001: Eolian sediment responses to late Quaternary climate changes: temporal and spatial patterns in the Sahara. *Palaeogeogr. Palaeoclimatol. Palaeoecol.*, **167**, 119–155.
- Szabo, B. J., C. V. Haynes Jr., and T. A. Maxwell, 1995: Ages of Quaternary pluvial episodes determined by uranium-series and radiocarbon dating of lacustrine deposits of Eastern Sahara. *Palaeogeogr. Palaeoclimatol. Palaeoecol.*, **113**, 227–242.
- Thiedig, F., 2005: Ein großes quartäres Binnendelta in der Zentral-Sahara. In: Tietz, G. F. (Ed.), *Geowissenschaftliche Afrikaforschung – ein Abenteuer. Jahrestagung der Afrikagruppe deutscher Geowissenschaftler 2005, Abstracts*. Universität Hamburg, p. 50.
- Thomas, D. S. G., 1986: The response diagram and ancient desert sands – a note. *Zeitschrift für Geomorphologie, Neue Folge*, **30**, 363–369.
- Thorweihe, U., 1988. Das Grundwasser des Nubischen Aquifersystems der Ostsahara. Herkunft, Bewegung, Nutzungsmöglichkeiten. Habilitationsschrift. Technische Universität Berlin 1989, 116 Blätter.
- Thorweihe, U., 1990a: Nubian aquifer system. In: Said, R., (Ed.), *The Geology of Egypt*. Balkema, Rotterdam, pp. 601–611.
- Thorweihe, U., 1990b: Das Grundwasser der Ostsahara. *Geowissenschaften*, **8**(8), 211–220.
- Thorweihe, U., M. Schneider, and C. Sonntag, 1984: New aspects of hydrogeology in southern Egypt. In: Klitzsch, E., Said, R., and Schrank, E. (Eds), *Research in Egypt and Sudan. Sonderforschungsbereich 69: Results of the Special Research Project Arid Areas, Period 1981–1984*. Berliner Geowissenschaftliche Abhandlungen, Vol. A50, Reimer, Berlin, pp. 209–216.
- Tietz, G. F., 1987: Lösung und Ausheilung tropisch verwitterter Quarze aus einem Oberkreide-Sandstein (SW-Nigeria). *Facies*, **17**, 267–276.
- Tietz, G. F., 2005: Auflösung oder Weiterwachsen auf Quarzkörnern – was wir von afrikanischen Lateriten lernen. In: Tietz, G. F. (Ed.), *Geowissenschaftliche Afrikaforschung – ein Abenteuer. Jahrestagung der Afrikagruppe deutscher Geowissenschaftler 2005, Abstracts*. Universität Hamburg, p. 51.
- Toutin, T., and P. Cheng, 2002: Comparison of automated digital elevation model extraction results using along-track ASTER and across-track SPOT stereo images. *Opt. Eng.*, **41**, 2102–2106.
- Trask, P. D., 1932: *Origin and Environment of Source Sediments of Petroleum*. Gulf Publication Company, Houston.
- Tricart, J., 1958: Méthode améliorée pour l'étude des sables. *Revue de Géomorphologie Dynamique*, **9**, 43–54.
- Tricart, J., and M. Mainguet, 1965: Caractéristiques granulométriques de quelques sables éoliens du désert péruvien, aspects de la dynamique des barkhanes. *Revue de Géomorphologie Dynamique*, **15**, 110–122.

- Tsoar, H., 1976: Characterization of sand dune environments by their grain size, mineralogy and surface texture. In: Amiran, D. H. K. (Ed.), *Geography in Israel. A Collection of Papers Offered to the 23rd International Geographical Congress USSR, July–August 1976*. Israel National Committee, International Geographical Union, Jerusalem, pp. 327–343.
- Turner, P., 1980: Continental red beds. *Developments in Sedimentology*, Vol. 29, Elsevier, Amsterdam, 562 pp.
- Uhden, R., 1932: Beckenformen und Dünengebiete der Libyschen Wüste. In: Seebass, F. (Schriftleitung), *Festschrift für Carl Uhlig: zum Sechzigsten Geburtstag von seinen Freunden und Schülern dargebracht*. Hohenlohesche Buchhandlung F. Rau, Öhringen, pp. 106–131.
- Van Neer, W., and H. P. Uerpmann, 1989: Palaeoecological significance of the Holocene Faunal Remains of the B.O.S. Missions. In: Kuper, R. (Ed.), *Forschungen zur Umweltgeschichte der Ostsahara, Africa Praehistorica*, Vol. 2, Heinrich-Barth-Institut, Köln, pp. 307–341.
- Van Zinderen Bakker, E. M., 1982: African Palaeoenvironments 18 000 Yrs BP. *Palaeoecol. Afr.*, **15**, 77–99.
- Vincent P., 1985: Some Saudi Arabian dune sands: a note on the use of the response diagram. *Zeitschrift für Geomorphologie, Neue Folge*, **29**, 117–122.
- Vincent, P., 1988: The response diagram and sand mixtures. *Zeitschrift für Geomorphologie, Neue Folge*, **32**, 221–226.
- Vossmerbäumer, H., 1974: Grain-size data of some aeolian sands: Inland dunes in Franconia (southern Germany), Algeria and Iran, a comparison. *Geologiska Föreningens i Stockholm Förhandlingar*, **96**, 261–274.
- Wackernagel, H., 2003: *Multivariate Geostatistics: An Introduction with Applications*. Springer, Berlin, 403 pp.
- Walger, E., 1964: Zur Darstellung von Korngrößenverteilungen. *Geol. Rundsch.*, **54**, 976–1002.
- Walker, T. R., 1967: Formation of red beds in modern and ancient deserts. *Geol. Soc. Am. Bull.*, **78**, 353–368.
- Wallinga, J., A. S. Murray, G. A. T. Duller, and T. E. Tornqvist, 2001: Testing optically stimulated luminescence dating of sand-sized quartz and feldspar from fluvial deposits. *Earth Planet. Sci. Lett.*, **193**, 617–630.
- Wang, X., Z. Dong, J. Qu, et al., 2002: Dynamic processes of a simple linear dune – a study in the Taklimakan Sand Sea, China. *Geomorphology* **52**, 233–241.
- Warren, A., 1988: The dunes of the Wahiba Sands. In: Dutton, R. W. (Ed.) *The Scientific Results of the Royal Geographical Society's Oman Wahiba Sands Project 1985–1987*. Journal of Oman Studies, Special Report, Vol. 3, Diwan of the Royal Court, Muscat, Oman, pp. 131–160.
- Wendorf, F., and R. Schield, 1980: *Prehistory of the Eastern Sahara*. Academic Press, New York, 414 pp.
- Wiese, Ch., 1995: *Untersuchungen an Wüstensanden zur Siebmethodik bei Korngrößenanalysen: Der Einfluss von Probenteiler und Siebsätzen auf die Ergebnisse*. Diplomarbeit, Universität zu Köln, 132 pp. (unpubl.).
- Wilkinson, J. C., 1977: *Water and Tribal Settlement in South-East Arabia*. Clarendon Press, Oxford, 276 pp.
- Williams, C., and D. H. Yaalon, 1977: An experimental investigation of reddening in dune sand. *Geoderma*, **17**, 181–191.
- Wilson, I. G., 1971: Desert sandflow basins and a model for the development of ergs. *Geographical J.*, **137**, 180–199.
- Wilson, I. G., 1972: Sand waves. *New Sci.*, **53**, 634–637.
- Wilson, I. G., 1973: Ergs. *Sediment. Geol.*, **10**, 77–106.

- Wilson, J. P., and J. C. Gallant, 2000: *Terrain Analysis: Principles and Applications*. New York, Wiley, 479 pp.
- Wintle, A. G., 1997: Luminescence dating: Laboratory procedures and protocols. *Radiation Measurements*, **27**, 769–817.
- Wippermann, F., 1969: The orientation of vortices due to instability of the Ekman-Boundary Layer. *Beiträge zur Physik der Atmosphäre*, **42**, 225–244.
- Wippermann, F., 1973: The orientation of vortices due to instability of the Ekman-Boundary Layer. *Annalen der Meteorologie, Neue Folge*, **7**, 260–279.
- Wipplinger, O., 1958: *The Storage of Water in Sand*. Southwest Africa Administration, Water Affairs Branch Windhoek, 107 pp.
- Yamaguchi, Y., H. Kahle, T. K. Tsu, and M. Pniel, 1998: Overview of advanced spaceborn thermal emission and reflection radiometer (ASTER). *IEEE Trans. Geosci. Remote Sens.*, **36**(4): 1062–1071.
- Yang, X., F. Preusser, and U. Radtke, 2006: Late Quaternary environmental changes in the Taklamakan Desert, western China, inferred from OSL-dated lacustrine and aeolian deposits. *Quaternary Sci. Rev.*, **25**, 923–932.
- Zech, W., and G. Hintermaier-Erhard, 2002: *Böden der Welt – ein Bildatlas*. Spektrum, Heidelberg, 120 pp.
- Zimmerman, D. W., 1971: Thermoluminescence dating using fine grains from pottery. *Archaeometry*, **13**, 29–52.

# INDEX

- Abu Ballas, 2, 7, 20, 68, 71, 100, 126, 137, 188  
Abu Dhabi, 130, 208  
Abu Minqar, 2, 100, 126, 137  
Acacia sp., 126  
Acheulean, 37, 123  
active crest sands *see* granulometric sand types  
additive dose method, 30, 106, 109  
aeolian abrasion, 163  
aeolian age, 73, 81  
aeolian environment, 28, 80, 81, 82, 160, 171, 191, 192, 196  
aeolian erosion cycle, 50  
aeolian pre-sorting, 82  
aeolian sand evolution, 79, 83  
aeolian sand fraction, 25  
aeolian terrace sands *see* granulometric sand types  
aeolianite, 82, 94, 95, 140, 141, 146, 186, 189, 196  
Ain Dalla, 2, 7, 24, 57, 71, 100, 137, 141, 188–90  
Akchar Erg, 206, 207  
aklé dunes, 209  
Al Jafurah, 145  
Al Khufrah, 1, 2, 70, 131  
Al Liwa, 130, 201, 208  
Algodones dunes, 155  
aliquot, 29–30, 105–11  
alluvial fan, 50, 57, 64, 71, 93, 94, 122, 124, 125, 139, 140, 143, 144, 146, 147, 152, 163, 186–97, 200  
alluvial sands, 37, 39, 51, 82, 83, 86, 202  
alpha particles, 112  
alpha radiation, 27, 112  
Ammonite Hill Escarpment, 35, 44, 52, 61, 62, 63, 65  
Ammonite-Hill Member, 34, 35, 95  
anomalous fading, 110  
Antarctica, 163, 176  
archaeological finds, 126  
archaeological investigations, 40  
archaeological unit (Regenfeld), 125–6  
arid phase, 54, 118  
aridic soil, 130, 133  
aridization, 50, 58, 127, 187, 189, 192, 195, 208–10  
artefact, 39, 97, 103, 104, 123, 141, 142, 206, 207  
artefact assemblage, 20  
artefact-stabilized dunes, 104  
artesian groundwater, 124, 206  
artificial irradiation, 106, 110  
ASTER, 9–19, 41, 44  
Aterian, 124  
Atlas Mountains, 54, 195  
Australia, 80, 138, 155, 168, 180  
  
background radiation, 27  
bedrock, 19, 24, 34–9, 43, 44, 51, 59, 66, 68, 71, 103, 122, 134, 141, 143, 187, 194  
bedrock relief, 8, 17, 19, 41–5, 46, 48  
bedrock topography, 33–46, 54, 57, 65, 68  
Ben Afen Beds, 34  
beta radiation, 27  
bleaching, 28, 29, 139  
Bou Bernous, 206  
bromoform, 26  
  
Calanscio Sand Sea, 56, 191–2, 200  
calcareous crust, 124–5  
calcite precipitation, 166, 167, 173, 175, 206  
calcrete, 48, 114, 205, 206  
California, 155, 161  
capillary action, 129, 130  
capillary motion, 130  
capillary rise, 130  
capping inversion, 50  
carbonaceous lake chalk, 124  
carbonaceous sediment, 124  
carbonate, 35, 106, 114, 124, 131, 134, 193, 196, 203, 207  
catchment, 19, 39, 41, 43, 44, 46  
Central Asia, 155  
Central Australia, 155  
<sup>14</sup>C data, 54, 123–7, 142, 203–7  
charcoal, 124, 126, 127, 142  
chemical alteration, 157–60, 170, 176, 181, 186, 190  
chemical analysis, 26

- chloride, 131, 134, 170  
 Chott el Jerid, 203  
 Chott Rharsa, 203  
 clay/calcite coating, 167, 175, 176  
 clay coating, 136, 139, 140, 156, 165, 166, 170, 177  
 clay/iron-oxide coating, 25, 26, 142, 163, 169, 171  
 clay minerals, 135, 154, 168, 174  
 cleavage plates, 170, 172, 176  
 climatic change, 1, 6, 31, 116, 135–6, 144, 151, 182, 185, 187, 189–91, 196, 204, 206  
 cock's-comb dunes, 62–4, 103  
 conductometer, 27  
 coring, 20, 26, 35, 62, 84, 99, 102–4, 117, 133, 139, 140, 141, 145, 161, 162, 169, 173, 185, 205  
 cosmic rays, 27, 112, 115  
 cover sands, 88, 99, 102–4, 123, 131, 134, 139, 143, 150, 170, 175  
 cross-bedding, 35, 95, 97, 194  
 cross ripples, 62  
 cross section, 6, 9, 26, 36, 51–64, 67, 68, 71, 72, 76, 92, 100, 102–5, 121, 131, 137, 139, 140–4, 150, 155, 200  
 cross section sequence, 21–3, 51, 52, 56, 59, 71  
 crossings (sand sea), 1, 24, 60, 125, 191, 199, 209  
 crystal lattice, 27, 106, 112  
 crystal structure, 135, 153  
 cultural layer, 141, 142, 143, 202
- Dahna, 145  
 Dakhla Basin, 146  
 Dakhla Formation, 34, 35, 95, 140, 147  
 Dakhla Oasis, 2, 31, 69  
 date palms, 130  
 dating error, 118  
 deflated sands *see* granulometric sand types  
 deflation, 5, 6, 39, 79, 80, 82, 86, 104, 118, 119, 120, 124, 143, 145–8, 197, 201  
 deflation gap, 62, 63  
 density separation, 106  
 desert-dew cycle, 160–4, 180, 194  
 desert frosting, 163  
 desert pavement, 38, 85, 86  
 detritus model, 138
- Devonian, 161, 162  
 diagenesis, 136, 138, 157, 160, 182  
 diagenetic material, 94, 97  
 digital elevation data, 8–10, 39–1, 46, 189, 190  
 Digital Elevation Model (DEM), 5, 8, 9, 11, 12–16  
 dome sand *see* granulometric sand types  
 dose rate ( $D_0$ ), 28–9, 99, 105, 107, 112–14, 115, 117  
 dose value, 28, 30, 109  
 draa:  
 accumulation rate, 118  
 ages, 118–19  
 and-groove pattern, 55, 57, 59  
 concept, 46–9  
 consolidation, 58, 61, 103, 122, 123, 141  
 dome, 200, 201, 205  
 dynamics, 46, 49, 57, 62, 68, 75, 93, 94  
 formation, 46, 48, 50–2, 55, 61, 68, 71, 80, 82, 86, 95, 118, 121, 124, 125, 130, 141, 147, 148, 150, 151, 156, 164, 180, 190, 195, 197–207  
 ghourd, 63, 198–200  
 growth, 50  
 growth rate, 119–21  
 height, 50–2  
 history, 85  
 longitudinal, 49–52, 55–9, 60–6, 68, 71–2, 75–82, 86–90, 93, 96, 100–1, 118–23, 127, 130, 132, 134, 141, 146, 147, 151, 156, 172–5, 181–7, 193, 199–205  
 net-accumulation rate, 119–20, 126  
 reactivation, 122, 127, 160, 209  
 reworking, 99, 121–2, 160, 199  
 sand, 71, 75–82, 86, 87, 92–8, 118–19, 121–3, 130–1, 134–5, 140, 141, 145, 151, 160, 168–70, 173–5, 180, 186, 189–90, 205  
 stabilization, 120, 127  
 transverse, 52–60, 63, 65, 71–2, 75, 76, 78, 80–2, 86–8, 90–6, 101–5, 118–21, 125, 127, 131, 134, 146, 147, 150, 156, 161, 162, 170–2, 174–6, 180, 181, 183, 185–6, 189, 190, 192, 201–7  
 undulation, 55–6, 61, 63, 65, 103, 197  
 wavelength, 50, 53  
 width, 56, 189

- drilling (site), 86, 100, 105, 118, 140, 146, 147, 150, 155, 163, 183, 184, 187
- dry cycle of deposition, 190
- dune
- ages, 6, 65
  - barchan, 47, 64, 67, 74, 84, 85, 89, 97, 141, 155
  - cycle hypothesis, 193–4
  - dynamics, 75
  - evolution, 84, 89, 93, 95
  - extension, 33, 44, 46, 51, 65, 67, 68, 72, 89, 126, 199
  - formation, 6, 50, 51, 60, 64, 84, 85, 150, 151, 153, 156, 189, 193–4, 208
  - generations, 33, 154, 194
  - height, 60, 76, 79
  - hooked, 62, 63, 93
  - ingression hypothesis, 195
  - length, 60
  - linear, 58, 197, 209
  - longitudinal, 48
  - migration, 6, 84, 141, 201
  - progradation, 60, 65, 67, 68, 147, 209
  - pyramidal, 199, 201
  - reddening, 135–9
  - sand, 79, 117
  - sief, 58
  - sif, 58, 64, 68, 89, 209
  - silk, 66, 92, 141
  - star, 62, 198, 199, 201
  - tear drop, 62, 65
  - transgression hypothesis, 195
  - transverse, 63–6, 71, 76, 84, 91, 92, 104, 186, 199, 202, 209
- Duwai Formation, 34, 35, 151
- effective winds, 5, 6, 93
- Eghei Mountains, 191
- El Quss Abu Said, 2, 44, 189, 190
- electrical charge, 27, 28
- electrical conductivity, 27
- endorheic river, 50, 82
- energy-dispersive X-ray spectrum, 169, 172, 185
- ephemeral flood, 124
- Epipalaeolithic, 140, 141
- equivalent dose ( $D_e$ ), 28–30, 99, 105–9
- erg, 1
- Erg Akchar, 206, 207
- Erg Aouker, 203
- Erg Chech, 1, 197, 203, 204, 206, 207
- Erg Ouarane, 197
- evaporation, 27, 129, 130, 163, 209
- evaporation depth, 129, 130
- evaporation rates, 130
- extratropical westerlies, 54, 119, 121, 122, 192, 198, 200, 202, 204
- Fachi-Bilma Erg, 67, 136
- Farafra Sand Sea, 2, 145, 203–5, 208–9
- fauna, 126, 206
- feldspar, 27–9, 106, 110, 112, 113, 115, 178
- feldspar mould, 182, 183, 186, 187
- feldspar solution, 182, 183, 186
- fesh–fesh, 131
- Fezzan, 48, 134
- fission track, 113
- flow accumulation, 15–17
- flow direction, 15, 16, 17, 66
- fluvial environment, 170, 180, 194
- fluvial transport capacity, 196
- Franconian Alb (Fränkische Alb), 181
- frictional deviation, 39, 69, 70
- frosting of quartz grains, 153
- gamma radiation, 27
- garnet/epidote ratio, 149, 150, 151
- geostrophic wind, 47, 49, 57
- Gilf-Kebir (Plateau), 1, 22, 37, 39, 44, 50, 65, 66, 95, 124, 136, 186, 194
- Gilf-Kebir river, 39, 50, 82, 186
- glacial environment, 161
- glacials, 48, 184
- Glass Area, 22, 37, 39, 104, 123, 194
- goethite, 135
- grain coating, 138, 154
- grain shapes, 25, 135
- grain-size distribution:
- cumulative, 73
  - double-logarithmic, 74
  - first-differential, 82
  - frequency, 6, 25, 74, 75, 82, 83, 86, 88–94, 134, 147
  - logarithmic, 75
- grain-size parameters, 6, 24, 25, 60, 73–5, 77, 81, 96, 147
- granulometric analysis, 24, 37, 56, 73–98

- granulometric evolution, 82, 89, 93  
 granulometric sand types:  
   active crest sand, 82–5  
   aeolian terrace sand, 82–3  
   deflated sand, 81, 83, 85, 89, 148  
   dome sand, 80, 83, 84, 95, 97, 205  
   inactive crest sand, 82–97  
   old barchan sand, 83–97  
   plinth sand, 83–91  
   ridge sand, 83–7, 93, 95–7  
   sand-sheet sand, 83, 85–7  
   young dune sand, 81, 83–4, 95, 97  
 granulometry, 6, 24, 51, 72, 105, 131, 139,  
   143, 146, 147, 186, 189, 197, 204, 205  
 gray, 28  
 Great Eastern Erg, 48, 63, 68, 135, 195,  
   198–206  
 Great Western Erg, 47, 48, 195, 198, 200,  
   203  
 grinding stone, 99, 126  
 grooves, 55–7, 181, 190  
 ground check, 6, 8, 57  
 groundwater recharge, 54, 118, 125  
 groundwater (table), 130, 138, 175, 189,  
   207  
 growth curves, 30, 108, 109  
 GTOPO 30, 9, 17  
 gypsum, 131, 136, 207
- hand axe, 123  
 healing processes in quartz, 182  
 hematite, 136  
 heavy minerals:  
   assemblage, 6, 26, 72, 139, 139, 145,  
     148–51, 190  
   content, 6, 26, 115, 145–8, 174, 187,  
     190, 193  
 helical vortices, 48, 49, 141, 198, 200, 209  
 Herodotus, 210  
 high-energy chemical environment, 170–3  
 Hoggar Mountains, 195, 199  
 Holocene:  
   climatic optimum, 3, 127, 139, 145, 151,  
     160, 164, 187, 191, 195, 196, 206–8  
   microfeatures on quartz grains, 153–4  
   processes, 164–70  
   winds, 68, 79, 168, 191, 193, 209  
 human occupation, 103, 124, 126–8, 142,  
   143, 173, 202, 207
- humid conditions, 6, 27, 123, 124, 127,  
   134, 136, 145, 146, 206, 207  
 humid period, 58, 129–35, 136–44,  
   156, 193  
 hyper-aridity, 129
- Idhan Awbari, 55, 198, 199, 200  
 Idhan Murzuq, 55, 76, 195, 196, 198–200  
 inactive crest sands *see* granulometric sand  
   types  
 infiltration experiment, 133  
 infiltration test, 133  
 instability waves, 53, 118, 120  
 interdriaa corridor, 50, 53, 55, 56, 60, 64,  
   72, 98, 122, 125, 139, 140, 151, 170,  
   175, 176, 190, 197
- Kadda, 203  
 Kalahari, 20, 145, 147  
 kaolinite, 136  
 Kara Kum, 155  
 Keriya, 64, 145, 148, 205  
 Khufrah, 1, 2, 70, 131  
 Koichab Depression, 133  
 Kun Lun Shan, 148, 187, 196  
 kurtosis, 73, 76, 81–2, 86, 88, 95,  
   186, 191
- lacustrine deposits, 125, 187, 189, 205  
 Last Glacial Maximum (LGM), 125, 187,  
   189, 205  
 leaching, 125, 187, 189, 205  
 lee dune, 65, 66, 68  
 leptokurtosis, 76, 78, 81–2, 86, 95, 126,  
   186, 191  
 Libya, 1, 2, 34, 76, 193, 199, 200, 209  
 Liwa Oases, 130, 201  
 Lobo, 126  
 loess, 98, 135, 232, 238  
 luminescence age, 29, 99, 105, 107, 110,  
   111, 114–17, 124, 125, 205  
 luminescence dating, 5–7, 20, 22, 27–9, 37,  
   68, 99, 102, 104–28, 133, 202, 204
- Maghrabi Formation, 35, 95, 141  
 Mali, 49, 82, 85, 145, 154, 199, 200  
 marginal dune, 65  
 Mauritania, 48, 197, 198, 202–9

- mean grain size, 73, 75, 76, 79–81, 91, 92, 96, 98, 120, 121, 148, 186, 189, 190
- mechanical frosting, 163
- mega-ridges, 201
- mega-ripple sand, 214, 217
- megabarchans, 201
- megadunes, 1, 3, 5, 6, 8, 19, 20, 26, 33, 36, 39, 46, 55, 130, 197, 201
- meso-ridges, 201
- mesodunes, 55
- meteoritic impact, 37
- microfeatures of quartz grains, 153–5, 160–2, 164, 170–2, 175–6, 180–2, 194
- microprobe, 26, 154, 168, 171, 173
- Minqar El-Talh Formation, 34, 37, 94, 101
- Moghra Formation, 34, 37, 95
- moisture budget, 133
- moisture content, 113, 114, 117, 129, 133, 172
- monsoonal rains, 126, 145, 201, 206, 208
- Morocco, 199
- morphoscopic analysis, 25, 26, 154, 155, 187
- Munsell classification, 143
- Munsell colour, 143
- Namib Erg, 19, 24, 25, 27, 48, 49, 51, 55, 58, 71, 74, 129, 131, 133, 134, 136, 138, 145, 147, 148, 155, 188, 190, 196, 197, 202, 203, 205, 207–9
- Naqb Formation, 34, 37
- narrow-band filters, 106
- Nebkha, 206
- Neolithic, 97, 134, 206, 207
- neutron activation analysis, 29
- Niger, 85, 136, 145, 181, 182, 199
- Nigeria, 181, 182
- Nile Valley, 210
- North America, 48, 136, 163
- Nubian aquifer, 119
- old barchan sand *see* granulometric sand types
- Oman, 34, 49, 55, 133, 136, 193, 196, 197, 201, 202, 203, 205, 207, 208
- Oman Mountains, 136, 196, 201
- optically stimulated luminescence (OSL), 28
- Ordovician glaciation, 28
- organic matter, 138, 140, 164, 166, 167, 173, 179, 180, 194, 206
- OSL age, 99, 105, 111, 114–21, 123, 127, 128, 156, 202, 204, 205, 206, 208
- ostrich eggshell, 54, 126, 142, 206
- Oued Saoura, 195
- palaeo:
- channel, 72, 196
  - drainage (system), 8, 17, 33, 40, 41, 43
  - pan, 35, 37
  - soil, 207
  - watershed, 189, 190, 193
- Palaeozoic, 146, 196, 197
- peakedness, 81
- pedogenesis, 120, 123, 130, 136, 157–64, 174, 180, 181, 185–7, 191, 204, 207
- pedogenic features, 103, 191
- perched aquifer, 130
- permafrost, 154
- Peruvian dunes, 155
- Pharaonic Kingdom, 210
- photomicrograph, 26, 154, 155, 181, 182
- Planetary Boundary Layer, 46–50, 55, 118, 122
- platykurtosis, 82, 86, 88, 95
- playa, 36–8, 40, 54, 98, 99, 102, 103, 122, 123, 127, 131, 134, 135, 138, 139, 141–3, 150–1, 155, 156, 159, 167, 170, 171, 174, 175, 179, 194, 206, 207
- Pleistocene:
- microfeatures on quartz grains, 160–3, 168, 169, 170, 176, 180
  - winds, 76, 79
- plinth, 51, 52, 58, 83, 85–7, 89, 91, 92, 118, 134
- plinth sand *see* granulometric sand types
- pottery, 39, 126, 141, 206
- pre-Holocene processes, 153, 176, 180
- precipitation (event), 1, 54, 114, 116, 118, 119, 122, 124, 126, 129–34, 136, 138, 139, 145, 154, 160, 161, 163, 164, 166, 167, 172, 173, 175, 176, 181, 183–5, 200, 206, 209
- prehistoric site, 20, 22, 99, 103, 104
- probability paper, 25, 73



- Qattara Depression, 1, 2, 195
- quartz:
- geodes, 35
  - grain microfeatures:
    - conchoidal fracture (surfaces), 161, 163, 176, 183, 184, 185, 191
  - contact surfaces, 160, 161, 169, 181
  - craters, 165, 171
  - crescentic impacts, 168
  - crystal growth, 165, 171
  - deep etching, 177, 179
  - desert smoothing, 160, 171, 180, 184, 186
  - desquamation, 165, 166, 170, 171
  - etching holes, 179
  - etchings, 161, 168, 178, 179, 181–3
  - feldspar (mould) healing, 182, 183, 186, 187
  - orange skin, 162, 163
  - organic matter, 138, 140, 164, 166, 167, 173, 179, 180, 194, 206
  - polished surfaces, 163, 177
  - scaling, 166, 170, 172, 173
  - selective etching, 178, 179, 181
  - silica-flow pattern, 162, 174
  - silica flowers, 177, 178, 179, 184
  - smooth fracture (surfaces), 177, 178, 179, 184
  - solution crevasses, 172
  - solution depressions, 138, 160, 161, 169, 181
  - spalling, 165, 166, 170, 171, 173
  - striped fracture (surfaces), 176, 178, 179
  - turtle skin, 163
  - upturned plates, 160, 163, 181
  - V-etching, 178, 179, 181, 182
  - sand surface textures, 153
- Quseir Formation, 34, 35, 95, 103, 140, 145, 146, 147
- radar rivers, 19, 41
- radiocarbon age, 54, 123, 124, 127
- radiocarbon dating, 124, 127, 187, 206
- radioisotopes, 112, 114, 115
- Rebiana Sand Sea, 199
- red beds, 135, 154
- reed growth, 125
- reed moulds, 125
- regenerative dose method, 108, 110
- Regenfeld, 7, 20, 35, 36, 86, 98–100, 102, 123, 125–7, 131, 134–40, 142–3, 150–1, 155–7, 164–5, 168–71, 175, 177, 180, 181, 188, 202, 206
- remote sensing, 8, 13, 49, 50, 59, 61, 62, 65, 93, 136, 199, 200, 209
- reptation, 28
- response diagram, 73, 74, 95–8, 194, 212, 214, 216
- ridge sand *see* granulometric sand types
- rolling sands, 57, 59
- Rub'al Khali, 25, 130, 136, 145, 196, 197, 201, 203–9
- rubification, 123, 129, 135–9, 140, 145, 151, 187, 207
- Sabaya Formation, 34, 35, 141
- Sahara, 1, 2, 46, 47, 50, 51, 54, 61, 74, 85, 125, 129, 138, 145, 193, 195, 197, 198, 199, 200, 202, 209
- Sahara Atlas, 195
- Sahel, 20, 136
- saline horizon, 131–4, 139
- salinity, 5, 6, 24, 27, 51, 129–36, 140, 173, 212, 214, 216
- salt precipitation, 133
- salt weathering, 165, 166, 170, 171, 173, 175
- saltation, 28, 131, 138
- sample partitioner, 24
- sand:
- accretion, 129
  - accumulation, 9, 61, 118, 204, 206
  - budget, 33, 64, 65, 71–2, 75, 186, 189, 201
  - colour, 24, 136, 138, 141, 143, 197
  - deflation, 5, 6, 39, 62, 63, 79, 80, 82, 86, 104, 118–20, 124, 143, 145–8, 197, 201
  - domes, 198
  - drift potential, 49, 69
  - encroachment, 129, 175, 227
  - reddening, 136, 138, 139, 140, 141, 145, 175, 176
  - sheet, 40, 41, 44, 83, 85–7, 133, 148
  - sheet sands *see* granulometric sand types
  - shield, 57, 59, 85, 89, 134

- sources, 5, 6, 34, 44, 46, 72, 73, 76, 79–81, 94, 95, 125, 135, 147, 148, 153, 160, 176, 181, 192, 193, 195–7
- supply, 48, 51, 64, 65, 150, 187, 193, 196, 209
- transport, 5, 6, 46, 50, 60, 61, 69, 71, 73, 76, 91, 94, 141, 150, 156, 160, 164, 168, 180, 193, 194
- sandstones, 6, 24, 34–6, 73, 75, 82, 94, 95, 97, 138, 140, 145, 146, 148, 161, 162, 181, 192, 193, 195–7, 203
- Sarir Calanscio, 191, 192
- Sarir Dalma, 34, 46, 55, 72, 137, 162, 188, 190–2
- Sarir Tibesti, 191, 192
- Saudi Arabia, 80, 145
- scanning-electron microscopy (SEM), 26, 153–81
- scarps, 35–7, 51, 52, 68, 69, 160
- secondary dunes, 20, 49, 58, 84, 201, 209
- secondary flow (Planetary Boundary Layer), 47, 50, 121
- Senegal river, 198
- shadow dune, 35, 36, 68
- “short shine” luminescence signal, 108, 111
- short-shine normalization, 108, 111
- sieving machine, 24
- silt formation, 27, 35, 82, 94, 95, 97, 98, 119, 131, 139, 141–4, 154, 170, 194, 203, 206
- Simpson Desert, 80, 138, 155, 163, 180
- single aliquot, 29–30, 105–11
- Siwa Oasis, 2, 19, 34, 68, 95, 131
- skewness, 73, 80–1, 186, 189
- slope gradient, 20
- sodium polytungstate, 26, 106
- soil moisture content, 113–17, 129, 131, 133–4, 145, 170, 172, 180, 207
- soliton, 74
- solubility succession, 134
- sorting, 73, 74, 79–82, 86, 96–8, 114, 186, 193
- SRTM, 9, 12–14, 44
- SRTM-3, 11–19, 41
- stable heavy minerals, 150, 151, 174
- stone implements, 37, 104
- stone tools, 126
- stratigraphic analysis, 8
- stratigraphic record, 37, 124, 162, 194
- stream-flow chart, 60, 69, 70, 86
- surface roughness, 44, 46, 57
- survey procedure, 20
- suspension, 27, 28
- Taklamakan (Sand Sea), 136, 145, 148, 154, 162, 163, 187, 196, 205
- Tamarix sp, 126
- Taoudenni Basin, 145
- Tarawan Formation, 34
- Taref Formation, 34, 35, 95, 140
- Tarim Basin, 136
- Taylor–Görtler Motion, 48, 49
- Ténééré, 85
- TerraSAR-X, 46
- thermoluminescence (TL), 28
- threshold velocity, 69
- threshold wavelength, 49
- Tian Shan Mountains, 196
- Tibesti Mountains, 191, 192
- tillite, 162
- time resolution (of OSL), 127, 128
- time slices, 99, 123, 125, 127, 128, 195, 202–5
- topographic survey, 5–6, 19, 143
- torrential environment, 176
- trade winds, 49, 56, 60, 68, 86, 120, 121, 127, 147, 192, 197–205
- transection, 19–24, 31, 34–9, 44, 50–68, 71–2, 75–6, 79–82, 86–92, 94–8, 99, 102–5, 118–24, 130–43, 145–8, 150–1, 155–63, 165–87, 189–92, 209
- transport capacity, 50, 65, 196
- tropical climate, 136, 151, 182, 187, 191, 196
- Tsondab Sandstone, 135, 146, 148, 196
- United Arab Emirates, 136, 201
- unstable heavy minerals, 148, 173, 174
- vector resultant, 58, 64, 68
- ventifact, 54
- vertical gradation, 50
- Wadi El-Bakht, 136
- Wadi Hamra, 40, 44, 50, 95
- Wadi Irharhar, 195
- Wadi Saoura, 195

- Wahibah Sands, 34, 49, 55, 133, 193,  
196–7, 201–9
- water:
- content, 113, 115–18, 120
  - infiltration, 27
  - percolation, 138
  - storage, 113, 130
  - vapour, 130
- west jet, 54
- westerlies (extratropical), 33, 52–7, 60, 86,  
92, 119, 121–3, 127, 147, 192,  
198–205
- wet cycle of deposition, 146, 187
- wet sieving, 24
- whaleback (dune), 47, 52, 58, 61, 65, 85,  
124, 209
- Willmann's Camp, 7, 22, 24, 37, 38, 41,  
44, 57, 64, 88, 95, 96, 104, 121, 123,  
126, 127, 137, 139, 143, 145, 150–1,  
155–6, 163, 164, 168, 174, 175, 180,  
185, 188, 207
- wind field, 1, 6, 31, 52, 60, 94
- wind velocity, 31, 60, 69
- winds, 76, 79, 156, 200
- Wyoming, 161
- y-junction, 56
- Yardang, 54, 97, 194
- young dune sands *see* granulometric sand  
types
- Younger Dryas, 204–5
- Zallaf Sand Sea, 34, 199
- zeroing event, 28, 29
- zibar, 197